

1-1-2016

# Combustion, Ionization And Sporadic Pre-Ignition In A Turbocharged Gasoline Direct Injection Engine.

Shenouda Mekhael  
*Wayne State University,*

Follow this and additional works at: [http://digitalcommons.wayne.edu/oa\\_dissertations](http://digitalcommons.wayne.edu/oa_dissertations)



Part of the [Mechanical Engineering Commons](#)

---

## Recommended Citation

Mekhael, Shenouda, "Combustion, Ionization And Sporadic Pre-Ignition In A Turbocharged Gasoline Direct Injection Engine."  
(2016). *Wayne State University Dissertations*. Paper 1464.

This Open Access Dissertation is brought to you for free and open access by DigitalCommons@WayneState. It has been accepted for inclusion in Wayne State University Dissertations by an authorized administrator of DigitalCommons@WayneState.

**COMBUSTION, IONIZATION AND SPORADIC PRE-IGNITION IN A TURBOCHARGED  
GASOLINE DIRECT INJECTION ENGINE.**

by

**SHENOUDA MEKHAEL**

**DISSERTATION**

Submitted to the Graduate School

of Wayne State University,

Detroit, Michigan

in partial fulfillment of the requirements

for the degree of

**DOCTOR OF PHILOSOPHY**

2016

MAJOR: MECHANICAL ENGINEERING

Approved By:

Naiem A. Henein

Advisor

Date

Nabil Chalhoub

Leela Arava

Steven Salley

Akram Zahdeh

**@ COPYRIGHT BY**

**SHENOUDA MEKHAEL**

**2016**

**All Rights Reserved**

## **ACKNOWLEDGEMENTS**

I would never have been able to finish my dissertation without the help, love and support of my mother, Linda. She has always shown me compassion and patience, and always motivates me to solve the issues I face. My mother has spent many days encouraging me and pushing me to reach my maximum potential. Linda has given me her best care and guidance. She has always been there to cheer me up and has stood by me through the good times and bad. I can't forget my mother for the beautiful love and care she has given me since I was born. She has helped me become the successful man that I am, who can fight in the dark to arrive at his goals.

I attribute this success to my mother.

I would also like to express my deepest gratitude to my advisor, Dr. N. Henein, for his excellent guidance, care, patience, and for providing me with an excellent atmosphere for doing research as well as correcting my writing and financially supporting my research. Dr. N. Henein gave me the full opportunity to experience, learn, and strengthen my knowledge on my research with the new expanding technology that was provided to me and practical issues beyond the textbooks.

I would like to acknowledge the continuous support of Dr. A. Zahdeh in this investigation. This research could not have been progressed without his efforts and guidance in the endless hours he spent in the lab.

In addition, I would like to thank David Daavettila for his help and instruction in running the engine. Thanks to Dr. T. Singh and Dr. M. Jansons for their help during my research. Special thanks to Dr. Chalhoub, who was willing to participate in my final defense committee at the last moment.

Finally, I would like to thank Omkar Atre, Samuel Ayad, Prateek Fandot, Paul Payatuvilla and Bishoy Fahmy for their contribution in getting the test cell ready for the experimental test.



Andrew Watchorn and Renato Yapaulo from National Instrument for their continuous support in the hardware and software. My sincerest thanks are extended to my friends Nabila Bishay and Ramy Yacoub – you were always there with a word of encouragement or listening ear.

It is a humbling experience to acknowledge those people who have, mostly out of kindness, helped along the journey of my PhD. I am indebted to so many for encouragement and support

## TABLE OF CONTENTS

<b>Acknowledgments</b>	III
<b>List of Tables</b>	VIII
<b>List of Figures</b>	XX
<b>Abbreviations</b>	XXI
<b>Chapter 1 “Introduction”</b>	
1. I Ionization characteristics	1
1. II Burning velocity in GDI engine	1
1. III Pre-Ignition in GDI engine	2
1. IV Cyclic variability in GDI engine	2
<b>Chapter 2 “literature review”</b>	4
2.1. Combustion ionization in internal combustion engine	4
2.1.I Ionization in spark ignited gasoline engines, experimental investigation	4
2.1.II Ionization in spark ignited gasoline engines, simulation work	7
2.2. Sporadic pre-ignition in spark ignited gasoline engines	9
2.2.1 Introduction to pre-ignition	9
2.2.2 Pre-Ignition induced by hot surfaces and by oil droplets	10
2.2.3. Pre-Ignition due to deposits peeling from combustion chamber walls	11
2.2.4. Effect of Engine operating parameters	14
2.2.4. 1. Effect of induction manifold angles on pre-Ignition	14
2.2.4. 2. Effect of compression ratio	15
2.2.4. 3. Effect of injection strategy	15
2.2.4 .4. Effect of Inlet air pressure and inlet air temperature	17
2.2.4 .5. Effect of EGR	18
2.2.4 .6. Effect of engine coolant temperature	19
2.2.5. Fuel octane and volatility effects on pre-Ignition	20
2.2.6. Fuel impact of lubricant composition on LSPI	22
2.2.7. Effect of intake valve diameter on pre-ignition	23
2.2.8. Summary of sporadic pre-ignition in spark ignited gasoline engines	24
2.3 Cycle to cycle variation in spark ignited gasoline engines	25

2.3.1. Effect of access air on cycle to cycle variation.	25
2.3.2. Effect of EGR on cycle to cycle variation	26
2.3.3. Effect of load on cycle to cycle variation	27
2.3.4. Effect of ignition and injection characteristics cycle variation	28
2.3.5. Effect of engine speed on cycle variation	30
2.3.6 Summary of cycle to cycle variation in spark ignited gasoline engines	36

### **Chapter 3 “Experimental Setup and Instrumentation”**

3.1 Introduction	37
3.2 Test facility description	38
3.3 Torque and speed measurement and control	38
3.4 Engine Specifications	38
3.5 Crankshaft Encoder and the TDC determination	39
3.6 High-speed data acquisition	42
3.7 In-cylinder pressure measurement	43
3.8 Manifold intake air temperature and pressure measurement	45
3.9 Cylinder # 1 Intake air temperature and pressure measurement.	46
3.10 Cooling system.	47
3.11 After cooler system.	48
3.12 Engine coolant measurement	49
3.13 Exhaust temperature and pressure measurement	49
3.14 Air mass flow rate measurement	50
3.15 Fuel mass flow rate measurement system	50
3.16 Common rail pressure measurement	52
3.17 Cylinder # 1 injection pressure measurement	52
3.18 Soot measurement	53
3.19 NOx measurement	54
3.20 Summary of experimental setup and instrumentation	54

### **Chapter 4 “Engine Control Unit Development”**

4.1 Introduction to engine control unit development	55
4.2 The Developed ECU	55
4.2.1 The engine synchronizer	56

4.2.2 Data acquisition	56
4.2.3 The ignition control	57
4.2.4 The injection module	58
4.2.5 The throttle module	60
4.3. Summary of engine control unit development	60
<b>Chapter 5 “Ionization characteristics in turbocharged gasoline direct injection engine”</b>	
5.1 Introduction	61
5.2 Sources of the Ion current in hydrocarbon-air flames	61
5.3 Characteristics of Ion Current Signals	62
5.4 Sensors location in the combustion chamber	66
5.5 Ionization in the combustion chamber	68
5.6 Summary	70
<b>Chapter 6 “Burning Velocity in GDI engine”</b>	
6.1 Introduction to burning velocity in turbocharges direct injection engine	71
6.2 Ionization part in the combustion chamber	72
6.3 Effect of Speed and Load on Burning Velocity	75
6.4 Effect of injection timing and spark timing on Burning Velocity	76
6.5 Summary Burning Velocity in GDI engine	79
<b>Chapter 7 “Cycle to Cycle variation Investigation”</b>	
7.1 Introduction cycle to cycle variation investigation	80
7.2 Cyclic variation experimental test matrix	80
7.3 Parameters represent the cyclic variability	83
7.4 Effect of early flame development (CA0% - CA10%) on cycle to cycle variation.	83
7.5 Effect of valve overlap period and trapped mass in the cylinder	86
7.6 Effect of Spark timing on combustion stability	88
7.7 Effect of injection timing on combustion stability	89
7.8 Effect of intake port pressure and temperature on combustion stability	90
7.9 Effect of instantaneous piston speed on combustion stability	92
7.10 Effect of exhaust pressure and temperature on combustion stability	92
7.11 Effect of injection command characteristics on combustion stability	94
7.12 Results of 100 consecutive cycles at 1000 rpm and 1.5 IMEP	96

7.13 Results of 100 consecutive cycles at 1000 rpm and 3.9 IMEP	100
7.14 Results of 100 consecutive cycles at 1000 rpm and 5.2 IMEP	103
7.15 Results of 100 consecutive cycles at 1250 rpm and 1.5 IMEP	107
7.16 Summary of cycle to cycle variation investigation	110
<b>Chapter 8 “Pre-Ignition Investigation”</b>	
8.1 Introduction to pre-ignition investigation	111
8.2 Major Problem in GTDI engine	111
8.3 Main objective of pre-ignition investigation	111
8.4 Test cell preparation for pre-ignition test	111
8.5 Characteristics of the ion signal from spark plug with the ignition command	114
8.6 Pre-ignition prediction	115
8.7 Pre-Ignition Test results with single and double injection and synthetic oil	115
8.8 Pre-Ignition test with signal injection with standard oil with normal additives	133
8.9. Summary of pre-ignition investigation	146
<b>Chapter 9 “3D CFD Combustion Analysis”</b>	
9.1 Introduction to 3D CFD Combustion Analysis	147
9.2 Model setup	148
9.3 Model convergence	148
9.4 Single cylinder and multi-cylinders engine modeling	149
9.5 Boundary condition for the 3D CFD Converge model setup	152
9.6 Burning Velocity calculated from 3d CFD simulation	155
9.7 Summary of 3D CFD Combustion Analysis	158
<b>Chapter 10 “knock detection and combustion diagnoses using ionization”</b>	
10.1 Introduction	159
10.2 Ion current signal from the spark plug and fuel injector	159
10.2 Knock detection using ion signal from fuel injector	160
10.3 Knock detection using ion signal from spark plug	164
10.4 Combustion diagnoses using ionization	166
10.5 Injector functionality diagnoses using ion signal from fuel injector	168
10.6 Summary	169
<b>Chapter 11 “Conclusions and suggestions for further work”</b>	
11.1 Conclusions	171

11.2 Recommendations	173
<b>References</b>	<b>174</b>
<b>Abstract</b>	<b>185</b>
<b>Autobiographical Statement</b>	<b>187</b>

## LIST OF TABLES

Table 2.1: Engine specification and test conditions	10
Table 2.2: Engine specifications and Operating conditions	12
Table 2.3: Engine specifications and Operating conditions	22
Table 3.1: T-GDI engine Specifications used in the current investigation.	39
Table 3.2 Technical data of spark plug pressure transducer.	43
Table 7.1 Cyclic variability test matrix.	82
Table 8.1 Pre-Ignition test matrix using the production ECU and pump fuel	116
Table 8.2 Pre-Ignition test matrix using the production ECU and pump fuel.	117
Table 8.3 Chemical properties p of the standard oil with reduced additive and synthetic oil	133
Table 8.4 Pre-ignition test results of 2000 rpm and WOT condition using the standard oil with normal additives 5W-30 and single injection with based ECU ignition timing.	134
Table 9.1 Simulation setup data for single cylinder engine cycle simulation.	148
Table 9.2 Boundary conditions for the 3D CFD Converge model setup.	152
Table 9.3 Test matrix of three cases with different operating conditions	153

## LIST OF FIGURES

Figure 2.1: Three consecutive cycles for the cold start up [1]	4
Figure 2.2: Typical ion current and cylinder gas pressure traces in a spark ignition engine at speed = 1300 rpm, torque = 20 Nm and $\lambda = 0.89$ [5]	5
Figure 2.3: Cylinder Gas Pressure and its bandpass filtered output while knocking [3]	6
Figure 2.4: Ionization Current and its bandpass filtered output while knocking [3]	6
Figure 2.5: Ion signal obtained at 1000 RPM and 3000 RPM for different values of $\phi$ [2]	7
Figure 2.6: The 6 reactions used in the three zone ionization model [9]	8
Figure 2.7: Ion current measured and simulated results considering non- chemi-ionization and equilibrium thermo-ionization [9]	9
Figure 2.8: Pressure traces for regular combustion and pre-ignition [70]	10
Figure 2.9: Cylinder pressure of LSPI [69]	11
Figure 2.10: Typical occurrence of pre-ignitions in an intermittent sequence [70]	12
Figure 2.11: Effect of coolant temperature on pre-ignition frequency [70]	13
Figure 2.12: Spatial distribution of fuel droplets at the end of injection, lateral view [70]	14
Figure 2.13: Effect of equivalence ratio on the pre-ignition resistance for various induction manifold angles [97]	14
Figure 2.14: Effect of compression ratio on the pre-ignition resistance for various induction manifold angles [97]	15
Figure 2.15: Comparison of single and double injection [97]	16
Figure 2.16: GDI Injection timing effects on LSPI [86]	17
Figure 2.17: Influence of Manifold Pressure on Pre-ignition [97]	17
Figure 2.18: Effect of Intake Manifold Temperature on Pre-ignition [97]	18
Figure 2.19: Effect of Cooled-EGR Effects on LSPI [84]	18
Figure 2.20: Effect of Cooling on Pre-ignition [97]	19
Figure 2.21: SPI frequency for different fuels from Dahnz study [83]	20
Figure 2.22: Boiling curves of fuels used during fuel variations from Dahnz study [83]	20



Figure 2.23: Comparison of Research Octane Number (RON) to SPI events from Zahdeh study [67]	21
Figure 2.24: Influence of Oil on Pre-ignition [67]	22
Figure 2.25: Proposed pent roof design to reduce the intake side knock propensity found from experiments, Offset spark plug towards the intake side. [65]	23
Figure 2.26: Turbocharged PFI combustion effects of various piston designs (piston/piston ring assembly) including varying the number of compression rings (heat flux and oil control effects) and fuel quality. 7000 rev/ min, 200 kPa MAP, CR = 10, 12° BTDC spark timing. [65].	24
Figure 2.27: COV <sub>imep</sub> versus excessive air ratios [98]	26
Figure 2.28: CoV <sub>imep</sub> versus EGR ratio and hydrogen fraction	27
Figure 2.29: Rate of change of COV of cylinder pressure during compression for GDI	28
Figure 2.30: COV map in an engine using an injector of type A at an engine speed of 1200 rpm, 100% load, and a compression ratio of 14,1	29
Figure 2.31: Effect of BMEP on COV in an engine using an injector of type A at a compression ratio of 16,1 or 14,1, an engine speed of 1200 rpm and an optimal injection and ignition timings [99]	30
Figure 2.32: Effect of engine speed on COV in an engine using an injector of type A at a compression ratio of 16,1 or 14,1, 100% load, and an optimal injection and ignition timings [99]	33
Figure 2.33: Illustrations of start of fuel variations at 0.4 ms after SOI from two different fuel injectors (Four different injection cycles) [100]	31
Figure 2.34: Coefficient of variation as a function of excess ratio at 1500 rpm, BMEP of 262 kPa, and MBT spark timing [101]	32
Figure 2.35: COV of $T_{max}$ and $T_{av}$ as a function of COV of IMEP at 1500 rpm, BMEP of 262 kPa, and MBT spark timing [101]	32
Figure 2.36: COV of IMEP as a function of COV of $T_{max}$ and COV of $T_{ave}$ for different spark timing values at 1500 rpm, BMEP = 262 kPa, and $k = 1.00$ [101]	33
Figure 2.37: COV of IMEP as a function of COV of $T_{max}$ and COV of $T_{av}$ for different injection timing at 1500 rpm, BMEP of 393 kPa, $k = 1.10$ and MBT spark timing [101]	33
Figure 2.38: Cycle-to cycle variation of $P_{max}$ for gasoline and methanol at different intake air temperatures	34
Figure 2.39: CoV in maximum pressure at various excess air ratios at 0.55 MPa BMEP	35

Figure 2. 40: CoV in IMEP at various excess air ratios at 0.55 MPa BMEP. (A) $\lambda = 1.3, 1.5$ (B) $\lambda = 1.4, 1.6$	35
Figure 2.41: Variation of coefficient of variation in indicated mean effective pressure with relative air–fuel ratio	36
Figure 3.1: The schematic diagram for the test cell	37
Figure 3.2: the ACCU crankshaft encoder	40
Figure 3.3: the output signals waveform diagrams from the encoder, (Image source, NI 9411 Encoder setup manual)	41
Figure 3.4: The TDC determination using the encoder waveforms and the motoring pressure (Image source, NI 9411 Encoder setup manual)	42
Figure 3.5: AVL high Speed data acquisition system (Image source, AVL INDISET manual)	42
Figure 3.6: Kistler spark plug pressure transducer for in-cylinder pressure (Image source, Kistler pressure transducer manual)	44
Figure 3.7: Kistler charge amplifier type 4603B for the pressure transducer (Image source, Kistler pressure transducer manual)	44
Figure 3.8: Omega Pressure transducer model PX209-060G5V, for MAP measurement (Image source, Omega MAP manual)	45
Figure 3.9: the intake manifold, with the locations of the pressure and temperature sensors.	46
Figure 3.10: Image for the water to water HEX to control the engine coolant temperature	47
Figure 3.11: Image of the water to air cooled after-cooler	48
Figure 3.12: Location of the exhaust manifold equipped by the pressure transducer and the thermocouple	50
Figure 3.13: The AVL fuel mass flow meter	51
Figure 3.14, schematic diagram for the primary and secondary fuel measurement system.	51
Figure 3.15: Measuring chain of pressure transducer at the injector of cylinder #1.	52
Figure 3.16: schematic diagram for the injection pressure measurement	53
Figure 3.17: Continental fast response sensor for Nox measurement (Image source, NI Nox fast sensor)	54
Figure 4.1: Connecting a Differential Device to the NI 9411 (Image source, National Instrument NI 9411 Manual)	56

Figure 4.2: NI PXI 6123 high speed data acquisition card and BNC 2110 analog/digital data acquisition (Image source, National Instrument NI PXI 6123 Manual)	56
Figure 4.3: Connecting ignition coils to the driver module. (Image source, National Instrument NI PXI 6123 Manual)	58
Figure 4.4: GDI injection profile	59
Figure 4.5: Connecting direct-injectors to the driver module (Image source, National Instrument injector driver control Manual)	59
Figure 4.6: Module terminal connections to a single electronic throttle body (Image source, National Instrument throttle body control Manual)	60
Figure 5.1: Electric circuit for ion current measurement in Spark plug	63
Figure 5.2: Sample of cylinder gas pressure, ignition command, and the ion current signal from the spark plug, zoomed in traces at 1500 rpm, 175 N. m (11.0 BMEP)	64
Figure 5.3: Electric circuit for use of the injector as an ion current sensor	65
Figure 5.4: Sample of cylinder gas pressure and the ion current signal from the fuel injector. Zoomed in traces at 1500 rpm, 175 N.m (11.0 BMEP)	65
Figure 5.5: Picture of the cylinder head showing the locations of the MSFI and spark plug	66
Figure 5.6: Cycle-resolved traces for the ignition command, MSFI signal, spark plug ion current, injection command and cylinder gas pressure	67
Figure 5.7: Zoomed in traces at 1500 rpm and 175 N.m (11.0 BMEP)	68
Figure 5.8: Piston locations at key points of Figure	69
Figure 6.1: Zoomed in traces at 1500 rpm and 175 N.m (11.0 BMEP)	73
Figure 6.2: Piston locations at key points of Figure	73
Figure 6.3: cycle to cycle variation of 100 consecutive cycles	74
Figure 6.4: The effect of engine load on burning velocity at different engine	76
Figure 6.5: Effect of engine speed on burning velocity at different engine load	76
Figure 6.6: Effect of ignition timing on burning velocity at 1750 rpm and 50 N.m	77
Figure 6.7: Effect of injection timing on burning velocity at 1750 rpm and 50 N.m	77
Figure 6.8: Effect of engine speed on burning velocity at different engine load	78

Figure 7.1: Inputs and outputs parameters from cylinder # 1	82
Figure 7.2: In-Cylinder gas pressure of 100 consecutive cycles at 1000 rpm and 5.79 IMEP	84
Figure 7.3: Zoomed traces of In-Cylinder gas pressure of 100 consecutive cycles at 1000 rpm and 5.79 IMEP.	85
Figure 7.4: Effect of valve overlap period on the COV % at 1000 rpm and different loads	86
Figure 7.5: Effect of valve overlap period on the COV % at 1250 rpm and different loads	87
Figure 7.6: Effect of valve overlap period on the COV % at 1500 rpm and different loads	87
Figure 7.7: Effect of valve overlap period on the COV % at 1750 rpm and different loads	88
Figure 7.8: Effect of valve overlap period on the COV % at 2000 rpm and different loads	88
Figure 7.9: Effect of injection timing on the COV % at 1000 rpm and 95 N.m	89
Figure 7.11: MAP of 100 consecutive cycles at 1000 rpm and 5.79 IMEP	91
Figure 7.12: Instantaneous engine speed distribution of 100 consecutive cycles at 1000 rpm and 5.79 IMEP at the intake port of cylinder # 1	92
Figure 7.13: Instantaneous temperature pressure distribution of 100 consecutive cycles at 1000 rpm and 5.79 IMEP at the intake port of cylinder # 1	93
Figure 7.14. Instantaneous Exhaust pressure distribution of 100 consecutive cycles at 1000 rpm and 5.79 IMEP at the intake port of cylinder # 1	93
Figure 7.15: Injection command of 100 consecutive cycles at 1000 rpm and 5.79 IMEP	94
Figure 7.16: Instantaneous Injection Pressure distribution of 100 consecutive cycles at 1000 rpm and 5.79 IMEP at the intake port of cylinder # 1	95
Figure 7.17: Zoomed traces of In-Cylinder gas pressure of 100 consecutive cycles at 1000 rpm and 1.5 IMEP.	96
Figure 7.18: Instantaneous Injection Pressure distribution of 100 consecutive cycles at 1000 rpm and 1.5 IMEP at the intake port of cylinder # 1	97
Figure 7.19: Injection command of 100 consecutive cycles at 1000 rpm and 1.5 IMEP	97
Figure 7.20: Intake manifold absolute pressure of 100 consecutive cycles at 1000 rpm and 1.5 IMEP	98
Figure 7.21. Exhaust manifold absolute pressure of 100 consecutive cycles at 1000 rpm and 1.5 IMEP at the intake port of cylinder # 1	98

Figure 7.22. Exhaust manifold absolute temperature of 100 consecutive cycles at 1000 rpm and 1.5 IMEP at the intake port of cylinder # 1	99
Figure 7.23. Instantaneous engine speed distribution of 100 consecutive cycles at 1000 rpm and 1.5 IMEP at the intake port of cylinder # 1	99
Figure 7.24: In-Cylinder gas pressure of 100 consecutive cycles at 1000 rpm and 3.9 IMEP.	100
Figure 7.25: Instantaneous Injection Pressure distribution of 100 consecutive cycles at 1000 rpm and 3.9 IMEP at the intake port of cylinder # 1	100
Figure 7.26: Injection command of 100 consecutive cycles at 1000 rpm and 3.9 IMEP	101
Figure 7.27: Intake manifold absolute pressure of 100 consecutive cycles at 1000 rpm and 3.9 IMEP	101
Figure 7.28. Exhaust manifold absolute pressure of 100 consecutive cycles at 1000 rpm and 3.9 IMEP at the intake port of cylinder # 1	102
Figure 7.29. Exhaust manifold absolute temperature of 100 consecutive cycles at 1000 rpm and 3.9 IMEP at the intake port of cylinder # 1	102
Figure 7.30. Instantaneous engine speed distribution of 100 consecutive cycles at 1000 rpm and 3.9 IMEP at the intake port of cylinder # 1	103
Figure 7.31: Zoomed traces of In-Cylinder gas pressure of 100 consecutive cycles at 1000 rpm and 5.2 IMEP.	103
Figure 7.32: Instantaneous Injection Pressure distribution of 100 consecutive cycles at 1000 rpm and 5.2 IMEP at the intake port of cylinder # 1	104
Figure 7.33: Injection command of 100 consecutive cycles at 1000 rpm and 5.2 IMEP	104
Figure 7.34: Intake manifold absolute pressure of 100 consecutive cycles at 1000 rpm and 5.2 IMEP	105
Figure 7.35. Exhaust manifold absolute pressure of 100 consecutive cycles at 1000 rpm and 5.2 IMEP at the intake port of cylinder # 1	105
Figure 7.36. Exhaust manifold absolute temperature of 100 consecutive cycles at 1000 rpm and 5.2 IMEP at the intake port of cylinder # 1	106
Figure 7.37. Instantaneous engine speed distribution of 100 consecutive cycles at 1000 rpm and 5.2 IMEP at the intake port of cylinder # 1	106
Figure 7.38: Zoomed traces of In-Cylinder gas pressure of 100 consecutive cycles at 1250 rpm and 5.2 IMEP.	107

Figure 7.39: Instantaneous Injection Pressure distribution of 100 consecutive cycles at 1250 rpm and 1.5 IMEP at the intake port of cylinder # 1	107
Figure 7.40: Injection command of 100 consecutive cycles at 1250 rpm and 1.5 IMEP	108
Figure 7.41: Intake manifold absolute pressure of 100 consecutive cycles at 1250 rpm and 1.5 IMEP	108
Figure 7.42. Exhaust manifold absolute pressure of 100 consecutive cycles at 1250 rpm and 1.5 IMEP at the intake port of cylinder # 1	109
Figure 7.43. Exhaust manifold absolute temperature of 100 consecutive cycles at 1250 rpm and 1.5 IMEP at the intake port of cylinder # 1	109
Figure 7.44. Instantaneous engine speed distribution of 100 consecutive cycles at 1250 rpm and 1.5 IMEP at the intake port of cylinder # 1	110
Figure 8.1: Image for the water to water HEX to control the engine coolant temperature	112
Figure 8.2: Image of the water to air cooled after-cooler	113
Figure 8.3: The features of the ion current signal with the ignition command	114
Figure 8.4: In-cylinder gas pressure for pre-ignition cycle (red), cycle before PI (blue) and cycle after PI (black) at 1230 rpm and 148 N.m, cylinder # 1	118
Figure 8.5: Zoomed traces for In-cylinder gas pressure for pre-ignition cycle (red), cycle before PI (blue) and cycle after PI (black) at 1230 rpm and 148 N.m, cylinder # 1	119
Figure 8.6: Ion signal from spark plug for pre-ignition cycle (red), cycle before PI (blue) and cycle after PI (black) at 1230 rpm and 148 N.m, cylinder # 1	119
Figure 8.7: Ion signal from spark plug and RHR for pre-ignition cycle (red) and cycle before PI (blue) at 1230 rpm and 148 N.m, cylinder # 1	121
Figure 8.8: Zoomed traces for Ion signal from spark plug and ignition command for pre-ignition cycle (red) cycle after PI (black) at 1230 rpm and 148 N.m, cylinder # 1	122
Figure 8.9: Engine performance parameters (CA50, IMEP, SOC and PP) for pre-ignition cycle (red), cycle before PI (blue) and cycle after PI (black) at 1230 rpm and 148 N.m, cylinder # 1	123
Figure 8.10: In-cylinder gas pressure for pre-ignition cycle (red), cycle before PI (blue) and cycle after PI (black) at 1205 rpm an 12 bar IMEP, cylinder # 1	124
Figure 8.11: Ion signal from spark plug for pre-ignition cycle (red), cycle before PI (blue) and cycle after PI (black) at 1205 rpm an 12 bar IMEP, cylinder # 1	125

Figure 8.12: Zoomed traces for In-cylinder gas pressure for pre-ignition cycle (red), cycle before PI (blue) and cycle after PI (black) at 1205 rpm an 12 bar IMEP, cylinder # 1	125
Figure 8.13: Zoomed traces for the Ion signal from spark plug for pre-ignition cycle (red), cycle before PI (blue) and cycle after PI (black) at 1205 rpm an 12 bar IMEP, cylinder # 1	126
Figure 8.14: Zoomed traces for the Ion signal from spark plug and RHR for pre-ignition cycle (red), cycle before PI (blue) at 1205 rpm and 12 bar IMEP, cylinder # 1	127
Figure 8.15: Zoomed traces for Ion signal from spark plug and ignition command for pre-ignition cycle (red) and cycle before PI (blue) at 1205 rpm an 12 bar IMEP, cylinder # 1.	128
Figure 8.16: Engine performance parameters (CA50, IMEP, SOC and PP) for pre-ignition cycle (red), cycle before PI (blue) and cycle after PI (black) at 1205 rpm an 12 bar IMEP, cylinder # 1	128
Figure 8.17: In-cylinder gas pressure for pre-ignition cycle (red), cycle before PI (blue) and cycle after PI (black) at 2000 rpm and 388 N.m, cylinder # 1	129
Figure 8.18: Zoomed traces for In-cylinder gas pressure for pre-ignition cycle (red), cycle before PI (blue) and cycle after PI (black) at 2000 rpm and 388 N.m, cylinder # 1	130
Figure 8.19: Zoomed traces for the Ion signal from spark plug for pre-ignition cycle (red), cycle before PI (blue) and cycle after PI (black) at 2000 rpm and 388 N.m, cylinder # 1	130
Figure 8.20: Zoomed traces for Ion signal from spark plug and RHR for pre-ignition cycle (red) and cycle before PI (blue) at 2000 rpm and 388 N.m, cylinder # 1	131
Figure 8.21: Zoomed traces for Ion signal from spark plug and ignition command for pre-ignition cycle (red) and cycle before PI (blue) at 1205 rpm an 12 bar IMEP, cylinder # 1	132
Figure 8.22: Figure 8.22. In-cylinder gas peak pressure and peak pressure location of 2000 rpm and WOT condition using the standard oil with normal additives 5W-30 and single injection with based ECU ignition timing.	135
Figure 8.23: In-cylinder gas peak pressure and peak pressure location of 2000 rpm and WOT condition using the standard oil with normal additives 5W-30 and single injection with based ECU ignition timing.	136
Figure 8.23-a: In-cylinder gas peak pressure and peak pressure location of 2000 rpm and WOT condition. Shows the normal combustion cycle, Nock cycle, sporadic PI and the PI due to knock,	137
Figure 8.24: In-cylinder gas pressure an ion signal from spark plug for 2-consecutive cycles (Cycle 191 & Cycle 192) at 2000 rpm and WOT condition using the standard oil with normal additives 5W-30 and single injection with based ECU ignition timing.	138

Figure 8.25: In-cylinder gas pressure of 24 consecutive cycles at 2000 rpm and WOT condition using the standard oil with normal additives 5W-30 and single injection with based ECU ignition timing, cylinder 1.	140
Figure 8.26: Zoomed traces of In-cylinder gas pressure of 24 consecutive cycles at 2000 rpm and WOT condition using the standard oil with normal additives 5W-30 and single injection with based ECU ignition timing.	141
Figure 8.27: Integrated RHR of 24 consecutive cycles at 2000 rpm and WOT condition using the standard oil with normal additives 5W-30 and single injection with based ECU ignition timing.	142
Figure 8.28: Integrated RHR and the ion signal from spark plug for 2-consecutive cycles (Cycle 191 & Cycle 192) at 2000 rpm and WOT condition using the standard oil with normal additives 5W-30 and single injection with based ECU ignition timing.	144
Figure 8.29: In-cylinder gas pressure and ion signal from spark plug for 2-consecutive cycles (Cycle 191 & Cycle 192) at 2000 rpm and WOT condition using the standard oil with normal additives 5W-30 and single injection with based ECU ignition timing.	145
Figure 9.1: Layout of the single cylinder engine GTDI model	149
Figure 9.2: shows the convergence curve of the GTDI model around the Lambda 1.02 (Converge CFD v2.2)	150
Figure 9.3: shows the convergence curve of the GTDI model around the Lambda 1.02 (Converge CFD v2.2)	150
Figure 9.4: shows the convergence curve of the GTDI model around the Lambda 1.02 (Converge CFD v2.2)	151
Figure 9.5: Effect of actual air flow in to cylinder on cycle to cycle variation. (Converge CFD v2.2)	152
Figure 9.6: Effect of tumble-X and tumble-Y on cycle to cycle variation. (Converge CFD v2.2)	153
Figure 9.7: In-cylinder gas pressure (MPa) for 7 consecutive cycles for 1000 rpm, Spark 20 dBTDc and 40 mg of fuel, (Simulation done by Converge CFD v2.2)	154
Figure 9.8: In-cylinder gas pressure (MPa) for 7 consecutive cycles for 1250 rpm, Spark 15 dBTDc and 20 mg of fuel, (Simulation done by Converge CFD v2.2)	154
Figure 9.9: In-cylinder gas pressure (MPa) for 7 consecutive cycles for 1500 rpm, Spark 15 dBTDc and 20 mg of fuel, (Simulation done by Converge CFD v2.2)	155
Figure 9.10: Iso Surface for the flame in the combustion chamber at the spark timing (Simulation conducted by Converge CFD v2.2)	156



Figure 9.11: Iso Surface for the flame in the combustion chamber at the time when the flame started (Simulation conducted by Converge CFD v2.2)	156
Figure 9.12: Iso Surface for the flame in the combustion chamber at the time when the flame arrived at the fuel injector (Simulation conducted by Converge CFD v2.2)	157
Figure 10.1: Zoomed-in traces for the two ion current signals from the spark plug and fuel injector at 1500 rpm and 175 N.m (11.0 BMEP)	160
Figure 10.2: Figure 10.2 Zoomed-in traces for the ion current signal from the fuel injector and the in-cylinder gas pressure at 2000 rpm and 300 n.m	161
Figure 10.3: Figure 10.3 Detailed zoomed-in traces for the ion current signal from the fuel injector and the in-cylinder gas pressure for the period 10 to 20 degrees aTDC at 2000 rpm and 300 n.m	162
Figure 10.4: Figure 10.4 Detailed zoomed-in traces for the ion current signal from the fuel injector and the signal from the knock sensor at 2000 rpm and 300 n.m	163
Figure 10.5: Figure 10.5 Detailed zoomed-in traces for the ion current signal from the fuel injector and the signal from the knock sensor for the period 10 to 35 degrees aTDC at 2000 rpm and 300 n.m	164
Figure 10.6: Figure 10.6 Zoomed-in traces for the ion current signal from the spark plug and the signal from the knock sensor at 2000 rpm and 300 n.m	165
Figure 10.7: Figure 10.7 Detailed zoomed-in traces for the ion current signal from the spark plug and the signal from the knock sensor for the period 10 to 35 degrees aTDC at 2000 rpm and 300 n.m	166
Figure 10.8: Figure 10.8 Sample of cylinder gas pressure, ignition command, and the ion current signal from the spark plug, zoomed in traces at 1500 rpm, 175 N. m (11.0 BMEP).	167
Figure 10.9: Figure 10.9 Sample of cylinder gas pressure and the ion current signal from the fuel injector. Zoomed in traces at 1500 rpm, 175 N.m (11.0 BMEP)	168
Figure 10.10: Figure 10.10 the injector command and the ion current signal from fuel injector	169

## **ABBREVIATIONS**

AFR:	Air-to-Fuel Ratio
BTDC:	Before Top Dead Center
BV:	Burning Velocity
COV:	Coefficient Of Variation
CTCV	Cycle to Cycle variation
DISI	Direct Injection Spark Ignition
EOI:	End of Injection
EVO	Exhaust Valve Open
EVC	Exhaust valve Close
GDI:	Gasoline Direct Injection
GTDI	Gasoline Turbocharged direct injection
T-GDI	Turbocharged Gasoline Direct Injection
ICE:	Internal Combustion Engine
IMEP:	Indicated Mean Effective Pressure
IVO	Intake Valve Open
IVC	Intake Valve Close
ECU:	Engine Control Unit
EGR:	Exhaust Gas Recirculation
EOI:	End of Injection
LPDI:	Low Pressure Direct Injection
LSPI	Low Speed Pre-Ignition
MAP	Manifold Absolute Pressure
MAT	Manifold Absolute Temperature

MBT:	Minimum spark advance for Best Torque
MFB:	Mass Fraction Burned
NI	National Instrument
OVL	Overlap Period
PCP:	Peak Cylinder Pressure
PFI:	Port Fuel Injection
PI	Pre-Ignition
P-V:	Pressure-Volume
RPM:	Revolution per Minute
SI:	Spark Ignited
SPI	Sporadic Pre-Ignition
SOC	Start of Combustion
SOI:	Start of Injection
TDC:	Top Dead Center

## CHAPTER 1 INTRODUCTION

Most of the research on combustion ionization in gasoline engines has been conducted on port fuel injection (PFI) engines. It has been used to detect engine misfire, incomplete combustion (or partial-burn), knock, MBT (Maximum Brake Torque) spark timing and combustion instability. This research is focused on gasoline direct injection (GDI) engines which are currently replacing PFI engines for higher power density, more efficient and controllable engines. This introduction gives an overview of the main topics covered in this research.

In this research, the GDI engine combustion determined using two in-cylinder ion current sensors. The fuel injector was used as an ion current sensor, in addition to the spark plug. The fuel injector signal was correlated to the combustion characteristics determined from the rate of heat release. The spark plug signal was used to determine the start of combustion and the location of the peak pressure and end of combustion near the spark plug, Mekhael [100]

Many approaches have been taken to determine the burning velocity in internal combustion engines. Experimentally, the burning velocity has been determined in optically accessible gasoline engines by tracking the propagation of the flame front from the spark plug to the end of the combustion chamber. These experiments are costly as they require special imaging techniques and major modifications to the engine structure. Another approach to determine the burning velocity is from 3D CFD combustion simulation models. These models require basic information about the mechanisms of combustion which are not available for distillate fuels in addition to many assumptions that have to be made to determine the burning velocity. Such models take long periods of computational time for execution and have to be calibrated and validated through experimentation. In this investigation the burning velocity was determined from the ion current signals developed by the spark plug and the fuel injector.

Applying GDI with a high compression ratio and turbo-supercharging in a light duty passenger vehicle allows for a downsized and more fuel-efficient gasoline engine to perform as well as a much larger

naturally aspirated engine. Compared to a port fuel injected gasoline engine, the GDI engine has higher thermal efficiency caused by its higher compression ratio and higher specific power density caused by its higher volumetric efficiency. GDI's evaporative spray cooling of the hot compressed air charge contributes to the high volumetric efficiency of the GDI engine. However, the increase in the peak power of the GDI is limited by sporadic pre-ignition which mainly happens at low engine speeds (LSPI). Pre-ignition produces fairly high peak cylinder gas pressures and rates of pressure rise that can damage the piston and other moving parts. Prediction of pre-ignition would be of great value to control the engine to avoid the consequences of the severe high pressure and pressure rates that could damage the engine. In this investigation, research will be conducted to determine if such a prediction can be achieved.

Several approaches have been used to investigate the factors that affect cycle-to-cycle variations in internal combustion engines. It is widely recognized that the reduction of cycle-to-cycle variations would correspond to either a proportional increase in engine power output or a proportional reduction in engine fuel consumption and engine-out emissions. Therefore, a clear understanding of the origins and possible causes of such a high level of cyclic fluctuations would be of great interest to engine designers. In this investigation, experiments were conducted at different speeds and loads and the effect of variations in eight engine operating parameters on the cycle to cycle variation was investigated. These parameters are the intake pressure, injection pressure, injection characteristics, ignition characteristics, and instantaneous engine speed, and intake temperature, exhaust gas temperature and exhaust gas pressure.

The ion signal from the spark plug and the ion signal from the fuel injector have characteristics that can be used as an indication of the characteristics of the mass burned fraction calculated from the rate of heat released. The information gathered from the ion current signal has been used as a feedback signal to a developed engine control unit to control the engine on a dynamic control bases. A closed loop control has been developed using the characteristics of the two ion current signals. The signals from the two ion

current sensors as clear enough to capture all the information from the combustion process to control the engine

## CHAPTER 2 LITERATURE REVIEW

### 2.1. Combustion ionization in internal combustion engine

#### 2.1.1. Ionization in Spark Ignited Gasoline Engines, Experimental work:

Yinbo Cao and Liguang Li used the Ion current signal produced by the spark plug to detect misfire events and to control the engine at the cold start up for preventing the engine from misfiring [1]. The experiments were performed on a two cylinders gasoline direct injection engine with compression ratio of 11.5. A 100 voltage was used to generate the ion current and in order to filter it, a capacitance is connected between the ignition coil and the spark plug to obtain an accurate signal to show the misfire. Using the ion current signal and the time transferred by crank angle and engine speed the ion integral was obtained. They found that the integral of the ion current signal is better in control than the peak value. They activated the spark again to reignite with a second strike to ignite the mixture, as shown in Figure 2.

1. The use of that technique helped the engine to start up faster in the cold start up.

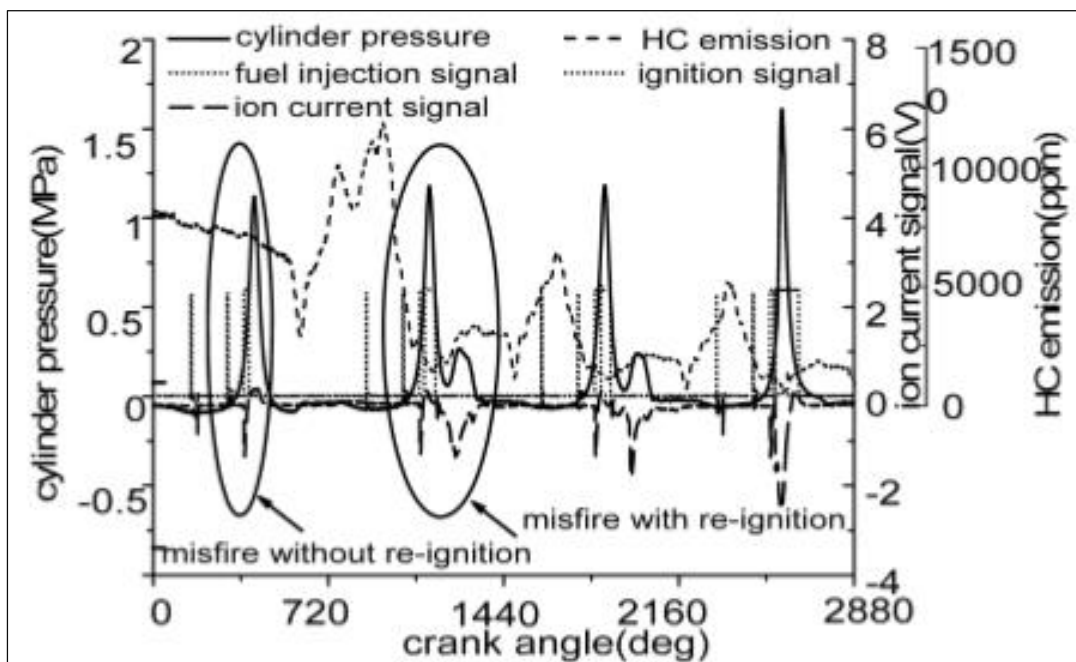


Figure 2.1. Three consecutive cycles for the cold start up [1]

Henein and Bryzik [35] compared the ion current signals produced in a single cylinder gasoline engine, a single cylinder diesel engine, an optically accessible diesel engine and an HCCI engine. The spark plug was used as the ion current sensor in the gasoline engine and a modified glow plug was used as the second sensor an ion current sensor in the diesel engine.

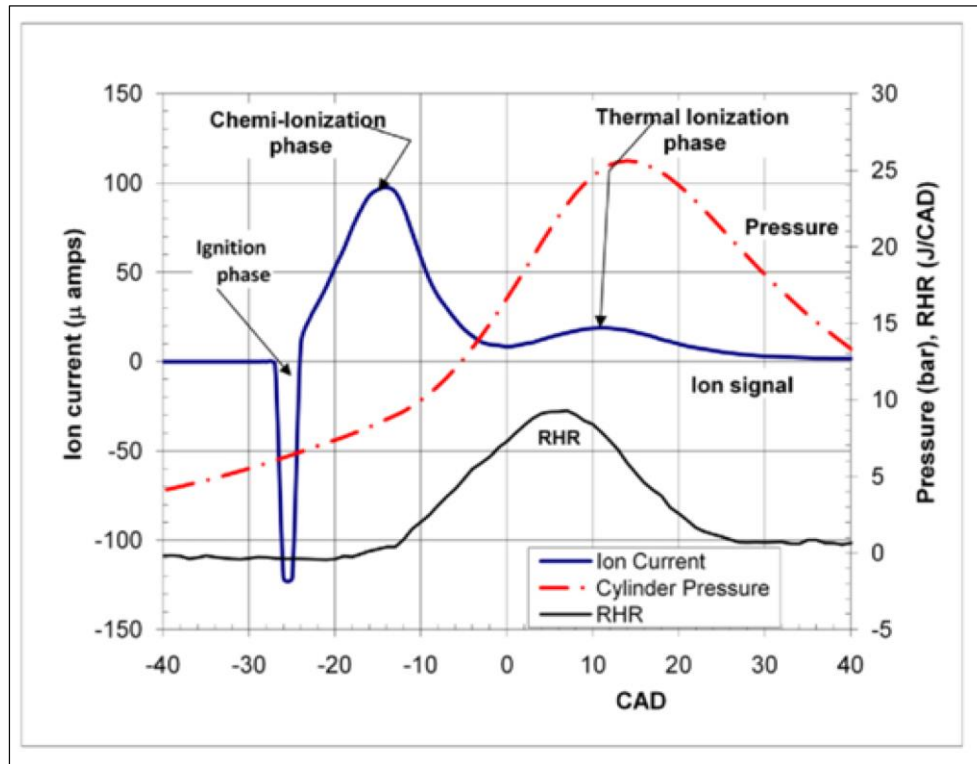


Figure 2.2, Typical ion current and cylinder gas pressure traces in a spark ignition engine at speed = 1300 rpm, torque = 20 Nm and  $\lambda = 0.89$ . [35]

Figure 2.2 shows typical ion current and cylinder gas pressure traces in a spark ignition engine at speed of 1300 rpm and engine load 20 N.m [35]. The ion signal has two peaks. The first is due to, high chemical reaction at the spark plug which called chemi-ionization where the  $\text{CHO}^+$  and  $\text{H}_3\text{O}^+$  ions are dominant. The second peak in the signal is due to thermal ionization caused by an increase in temperature of the gases in the rea around the speak plug gap. This increase in the local gas temperature around the spark plug is because of the high rise in the cylinder pressure. The thermal ionization is mainly due to NO.



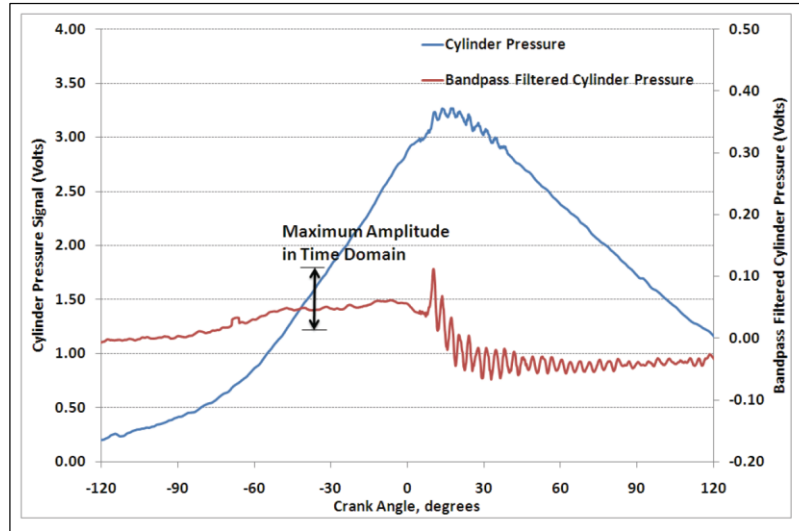


Figure 2.3, Cylinder Gas Pressure and its bandpass filtered output while knocking. [3]

The ion current signal from the spark plug was used to detect the engine knock. Davinder Kumar et. al. [3] conducted experiments on a single cylinder spark ignition engine. Figure 2. 3 shows traces for the ion current and cylinder gas pressure with a signal that filtered to show the oscillation of the knock. They measured the ion current signal with respect to crank angle and in case of engine knocking. The ion current signal showed oscillation close to the oscillation from the pressure trace which represents the response

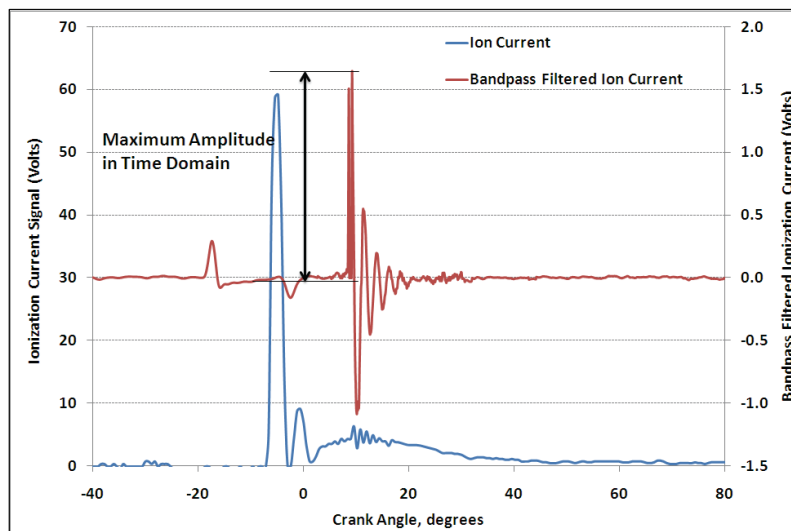


Figure 2.4, Ion current and its bandpass filtered output while knocking [3]

Furthermore, the ion current signal has been used to detect the air to fuel ratio and use the data from this signal to control the air to fuel ratio. Abhijit et al [2] conducted experiments on a 2.0L inline 4 cylinder spark ignited engine with compression ratio 10. Air to fuel ratio sensor used in each cylinder and the current signal shown in Figure 2. 5 showed a variation with the air to fuel ratio. Results were taken for the ion current signal at different operating conditions. It was found that both peaks increase at higher values of equivalence ratio. Results were plotted for the amplitude of 1st and 2nd peaks against the equivalence ratios for all the engine cylinders. The data from the experimental work showed a good agreement for the correlation between the ion current signal and air to fuel ratio.

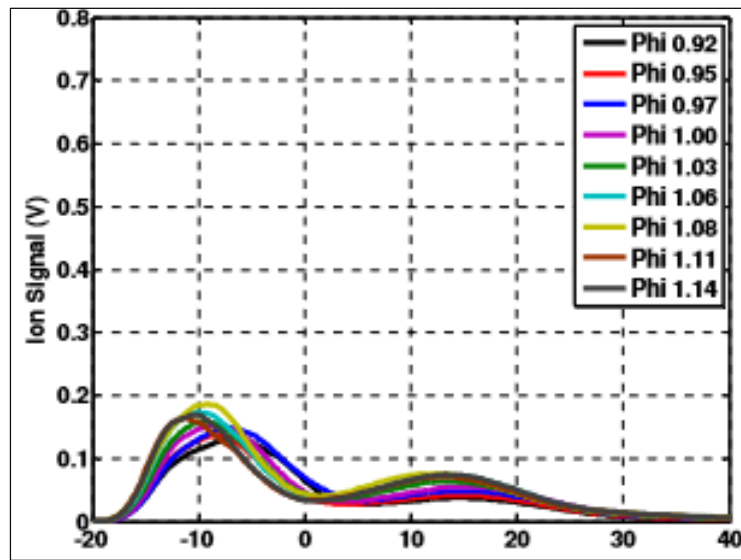


Figure 2.5, Ion signal obtained at 1000 RPM and 3000 RPM for different values of phi. [2]

### 2.1. II Ionization in Spark Ignited Gasoline Engines, Simulation:

Naoumov, et al. developed a three zone simulation model for the ion current measured by the spark plug in a spark ignition engine [5]. The model includes six reactions, shown in Figure 2.6, which were considered to occur in the small volume of the flame inside the gap between spark plug electrodes. The following “physical” scheme of the processes in the cylinder was proposed. The cylinder was considered to be divided to two sections separated by the flame front. The first section was a zone of the burned mixture with a variable volume. The second section was a zone of the fresh air-fuel mixture that

compressed because of the raising of the temperature and pressure. During the flame front propagation the fresh air-fuel mixture diffuses into the flame front where it was consumed. This model used chemical non-equilibrium approach and the complete mechanism of chemical reactions for simulating the ionization in a spark ignition engine. The results of tests showed that the second peak of the ion current signal was caused mainly by the thermal ionization of NO forming  $\text{NO}^+$  ions. Figure 2. 7, shows a comparison between the measured ion signals and simulated results.

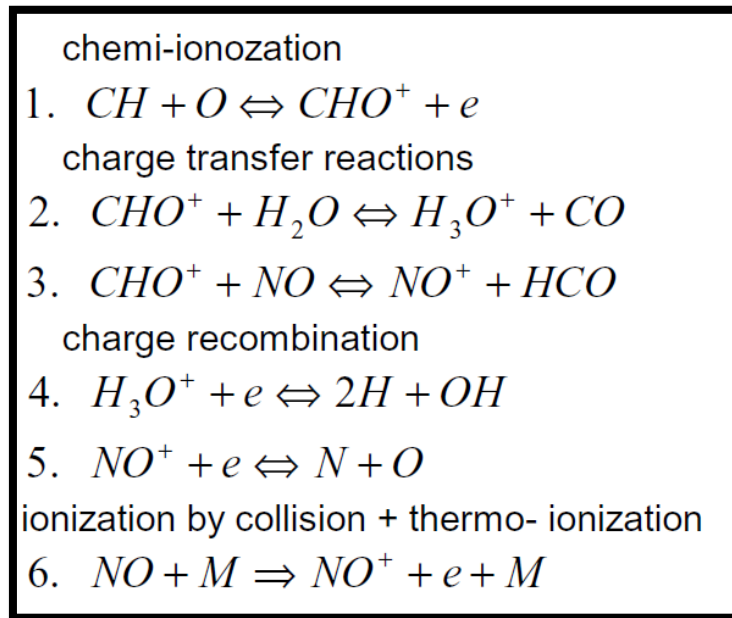


Figure 2.6, The 6 reactions used in the three zone ionization model [5]

The current challenge for spark ignition engines is to reduce fuel consumption and meet the current tailpipe emissions standards while maintaining drivability. Several solutions are being pursued by automotive manufacturers and a downsized (smaller displacement and/or fewer cylinders), boosted (high specific power) engine in combination with direct fuel injection (GDI) is regarded as one. However, a phenomena that has not been previously observed in gasoline engines, known as sporadic pre-ignition, is limiting the increase in the specific power of the direct injection gasoline engine.

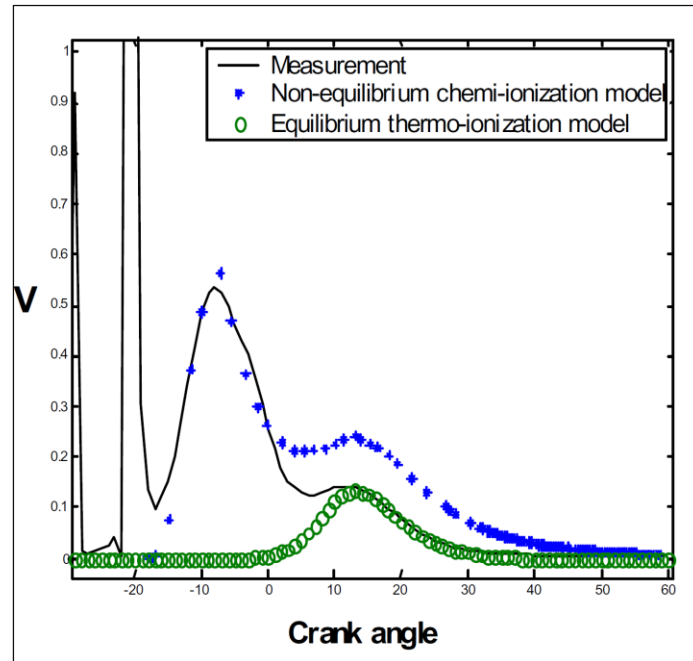


Figure 2.7, Ion current measured and simulated results considering non-chemi-ionization and equilibrium thermo-ionization [5].

## Pre-Ignition in a spark Pre-ignition in a gasoline engine engines

### 2.2. Sporadic Pre-Ignition in Spark Ignition Gasoline Engines:

#### 2.2. 1. Introduction

A highly boosted, small displacement engine can produce the same power as 8 cylinders engine incase if we are using turbocharger. Efficiency increases due to the reduction in friction and pumping losses for the smaller engine and significant improvements in fuel economy can be realized. However, running the engine at high levels of specific power can be stressful on engine components such as the piston and the liner, and can lead to an increase in knock, reducing engine efficiency by forcing either a reduction in compression ratio or retarded spark timing or both which will lead to power loss. Most probable reasons that increase the tendency of occurrence of Pre-Ignition in a spark ignition engine and the research work carried out to suppress of Pre-Ignition and knocking are discussed in detail in the following sections.

### 2.2.2. Pre-Ignition induced by Hot Surfaces and by Oil Droplets:

Optical measurements using a sensitive high-speed camera system were performed to gather information about of pre-ignition origins and their progress. The numerical simulations included the analysis of the mixture auto-ignition behavior was depending on the pressure, temperature and reaction mechanisms. Furthermore, 3D CFD simulations were conducted the conditions that might lead to pre-ignition. The results from combining the results of the experimental and numerical investigations help extracting the important parameters that increase the tendency of pre-ignition, Christoph Dahnz, et. al [67]. Oil dilution because of the spray impingement due to lateral positioning of injector was found to be a probable reason for oil release from cylinder liner which auto-ignites and casus pre-ignition was because of the lateral position of the fuel injector.

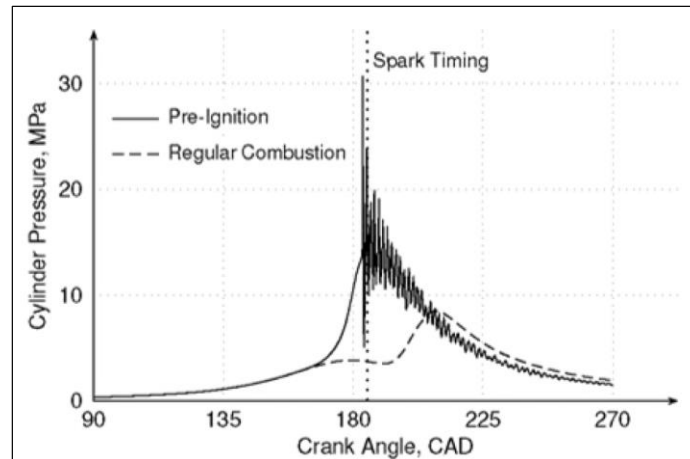


Figure 2.8: Pressure traces for regular combustion and pre-ignition [67]

Engine Specification	
Displacement	1983cc
Bore	82.5 mm
Stroke	92.8 mm
Compression Ratio	10.5:1
Equivalence Ratio	0.95
Engine Speed	1750 rpm
Brake Torque	360 Nm

Table 2.1: Engine specification and test conditions [67]

### 2.2.3. Pre-Ignition due to Deposits Peeling from Combustion Chamber Walls and Oil Dilution:

Another way to produce pre-ignition is by adding oil and other combustible particulates to intake air, which will go through the intake manifold to reach the combustion chamber [67]. These particles require at least two combustion cycles to reach the state that might lead to ignition source. As a result, deposits from the oil of combustible particles peeling from combustion chamber walls through piston crevices were identified as a new source of sporadic pre-ignition. Combustible particles can also be generated from oil droplets leaving the engine crank case going to the combustion chamber.

According to the ignition mechanism proposed by Yoshihiro Okada et al [66], oil droplets are brought into the combustion chamber by crankcase ventilation and auto-ignite during the compression stroke. Furthermore, deposits that comes from another places such as the cylinder head and piston reach the same temperature as the combustion gas during combustion and causes pre-ignitions. They form a pre-ignition, Figure 2.9, combustion source early in the next combustion cycle. The amount and evaporation characteristics of fuel impinging the liner and the temperature of the liner itself was correlated to frequency of pre-ignition. The characteristics of the oil such as the auto-ignition temperature and viscosity are very important parameters affecting the tendency of pre-ignition.

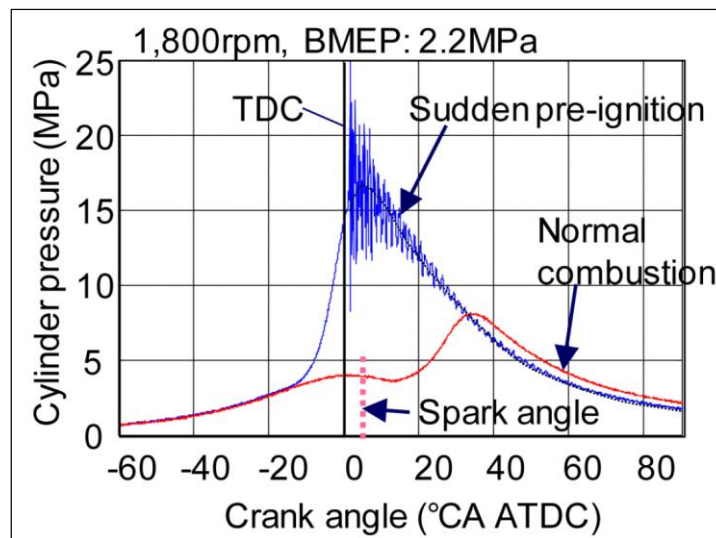


Figure 2.9: Cylinder pressure of LSPI [66]

Test Conditions	
Engine Speed	1800 rpm
Load (BMEP)	22 bar
Brake Torque	350.31 Nm
MAP	0.3 bar
Air/Fuel ratio	14.6
Displacement	1997 cc
No of cylinders	4
Compression	10:1

Table 2.2: Engine specifications and Operating conditions [66]

### 2.2.3. a. Hot Surfaces:

Ignition induced by hot surfaces in the combustion chamber from the hot parts such as spark plug or exhaust valves or the combustion chamber itself are suspected to be a reason for pre-ignition. A similar phenomena has been known as “surface ignitions” as it is the ignition of the fuel mixture due to high surface temperature.

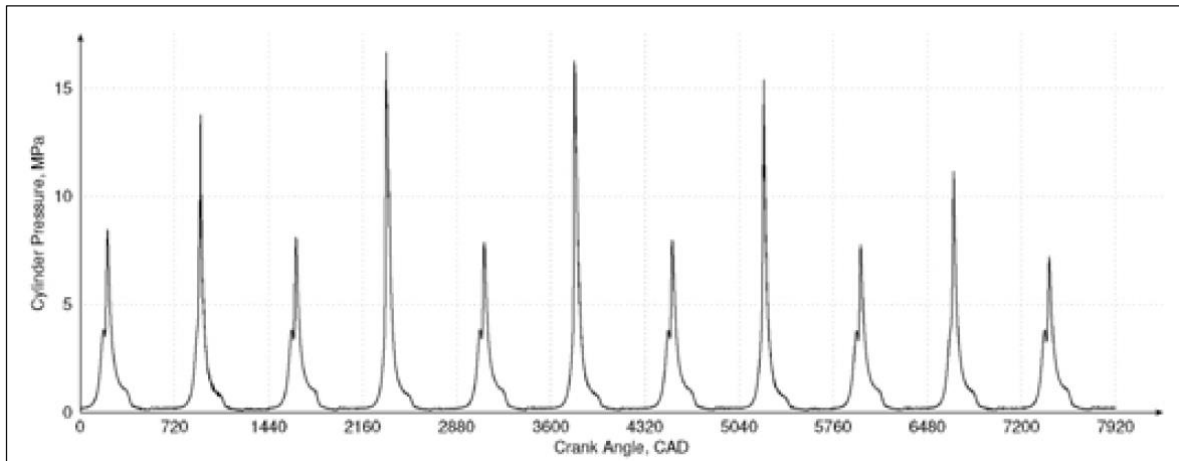


Figure 2.10: Typical occurrence of pre-ignitions in an intermittent sequence [67]

Surface ignition starts before the electric spark at hot spots in the combustion chamber. These hot spots increase the tendency for pre-ignition. These hot spots come from the carbon deposits on the wall, on the bottom of the exhaust valve and the central electrode of the spark plug. Combustion by surface ignition increases the temperature of the combustion chamber which might cause earlier auto-ignition not the same cycle but in the next cycle or two. Consecutive auto-ignition can damage the engine.

structure. Consequence pre-ignition as shown in Figure 2.10. Furthermore can cause damage to the engine parts such as the piston rings.

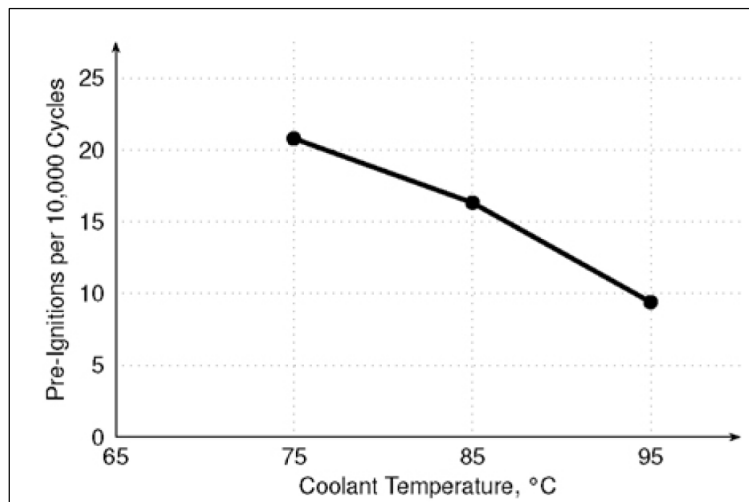


Figure 2.11: Effect of coolant temperature on pre-ignition frequency [67]

Increasing coolant temperature would help increasing surface temperature of the cylinder liner as shown in Figure 2.11, resulting in decreasing the ignition delay of the carbon particles in the fuel air mixture. In sporadic pre-ignition, a different trend was observed where the higher coolant temperatures reduce the frequency of sporadic pre-ignition frequency. In summary, the pre-ignition due to the hot spots is not the same as the sporadic pre-ignition.

### 2.2.3. b. Sporadic Ignition by Oil Droplets:

The lateral positioning of the injector helps the other side of the cylinder liner to causes dilution of oil film as shown in Figure 2.12. Dilution lowers the oil surface tension and viscosity which will increases the probability of releasing oil droplets from the crank case that potentially helps increasing the frequency of sporadic pre-ignition.

On one hand oil dilution reduces the hydrodynamic film thickness which should have no direct effect on pre-ignition as the oil cannot ignite while adhering to the wall. On the other hand, the reduced surface tension increases the probability of droplet release out of the top land due to inertia forces as the piston decelerates just before reaching the top dead center.



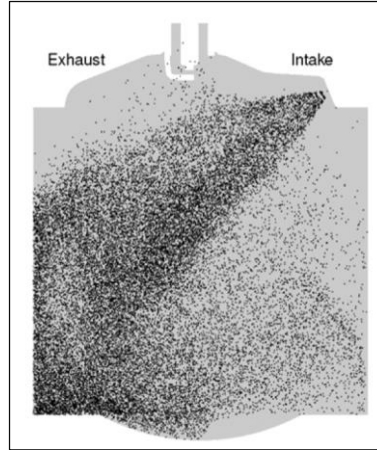


Figure 2.12: Spatial distribution of fuel droplets at the end of injection, lateral view [67]

## 2.2.4 Effect of Engine operating parameters

### 2.2.4.1 Effect of Induction Manifold Angles on Pre-Ignition:

The effect of the mixture equivalence ratio has been proposed as one of the factors increasing the probability of pre-ignition. Experimental investigation conducted by M. S. Radwan et. al [94] to study the effect of equivalence ratio on pre-ignition rate.

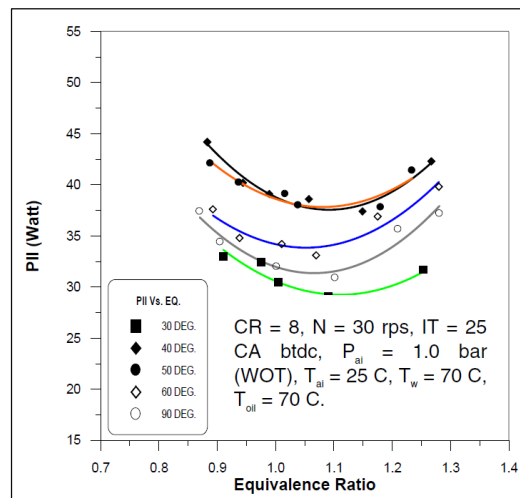


Figure 2.13: Effect of equivalence ratio on the PI resistance for various induction manifold angles [94]

Figure 2.13, it shows that 5% to 10% richer than stoichiometric has the more tendency for pre-ignition. On the other hand, the slightly rich or lean stoichiometric have lower tendency to pre-ignition because of the difficulty in burning that mixture.

### 2.2.4.2 Effect of Compression Ratio:

The pre-ignition frequency increases considerably with increases in the engine compression ratio due to increasing the gas temperature and pressure before the spark timing. Figure 2. 14 shows the effect of compression ratio on the tendency of pre-ignition. The new designs of spark-ignition engine is moving always toward higher CR for efficiency considerations and fuel economy. The results showed that the tendency for pre-igniting has changed with the design of the intake manifold and the compression ratio as a combination

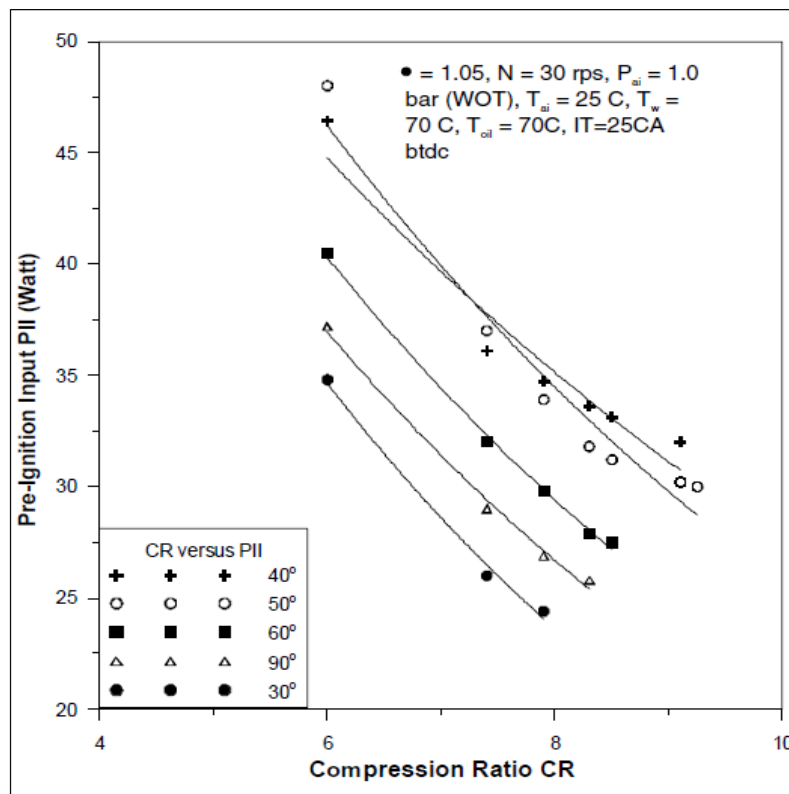


Figure 2.14: Effect of compression ratio on the PI resistance for various induction manifold angles [94]

### 2.2.4.3 Effect of injecting strategy:

Zahdeh et. al. [64], investigated the effect of the injection strategy, the single and double injection on the frequency of sporadic pre-ignition. They concluded that the combustion stability is very small for the given highly charged condition. In average over a series of tests the pre-ignition frequency can be reduced by a factor of four when using double injection strategy see Figure 2.15. This Figure shows Pre-

ignition rate, fuel specific number, the coefficient of variation of mean effective pressure and the MBF 50%. By using double injection, the wall impingement behavior can be changed significantly due to the change in the wall impingement and creating the hot spots and the fuel dilution.

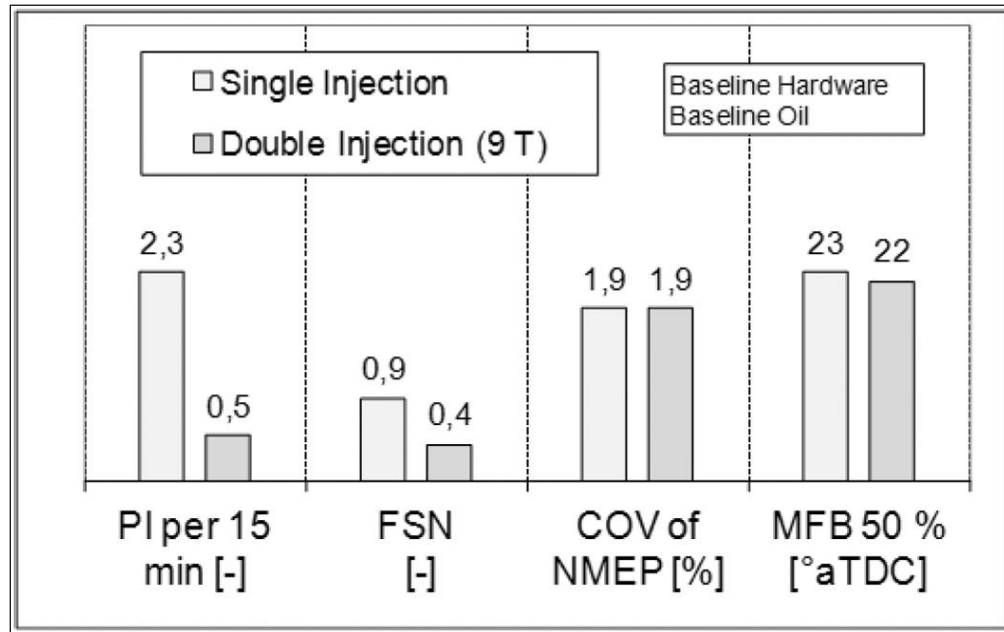


Figure 2.15: Comparison of single and double injection [64]

Another observation showed that the early and late injection timings show significant increases the tendency for pre-ignition. Figure 2.16 shows the relationship between injection timing and the low speed pre-ignition because the amount and location of fuel impingement changes dramatically with injection strategy timing. Injection system and strategy can affect the in-cylinder mixture quality and mixing index. As described by Manfred Amann et.-al. [81] as shown in figure 2.16, injection timing between 68 and 120 aTDC showed less tendency of low speed pre-ignition because between this timing, there is less fuel droplets hits the piston surface which will reduce the wall wetting.

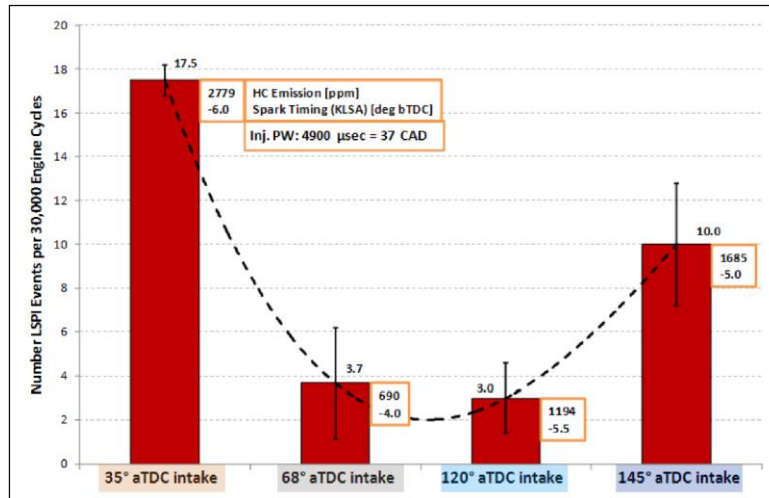


Figure 2.16: GDI Injection timing effects on LSPI [83]

#### 2.2.4.4 Effect of Inlet Air Pressure and temperature:

Zahdeh et. Al [64], conducted experimental investigations to determine the effect of manifold intake pressure and manifold intake temperature on the frequency of pre-ignition. From Figure 2.17, it appears that, the pre-ignition tendency increases with increasing the boosting pressure while the intake temperature kept constant. This occur because increasing the manifold pressure will increase the compression pressure which will help the mixture to ignite before the spark timing.

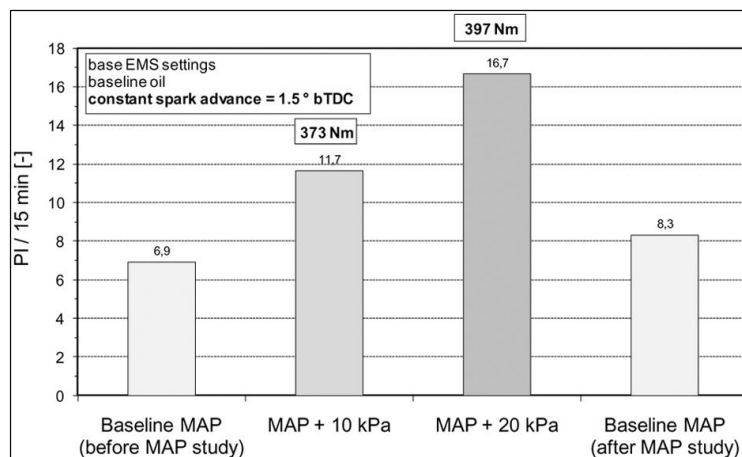


Figure 2.17: Influence of Manifold Pressure on Pre-ignition [64]

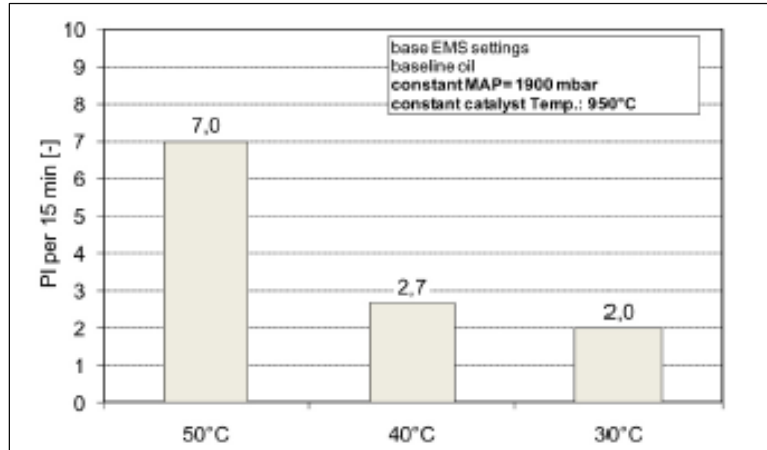


Figure 2.18: Effect of Intake Manifold Temperature on Pre-ignition [64]

In addition, Zehdah et. al [64], conducted the effect of intake air temperature on the tendency of LSPI. The experimental investigation showed that as the intake air temperature increases, the tendency to pre-ignition increased. They concluded that the mixture preparation is improved due to the faster evaporation of the fuel droplets through the intake time as shown in Figure 2.18. The improved mixture preparation will help reduce wall wetting which in consequence will help reducing the tendency of pre-ignition.

#### 2.2.4.5 Effect of EGR:

Manfred. A. et. al. [84], studied the effect of cooled EGR ratio on the frequency of pre-ignition under different engine operating conditions that may cause low speed pre-ignition. Figure 2.19 shows the frequency of LSPI events per 30,000 cycles at two EGR levels and several different loads. They repeated the tests to see the independency of the test conditions on the test results and they considered the average values of all the runs. They concluded that increasing the EGR ratio decreases the compression temperature which will reduce the tendency of Pre-ignition.

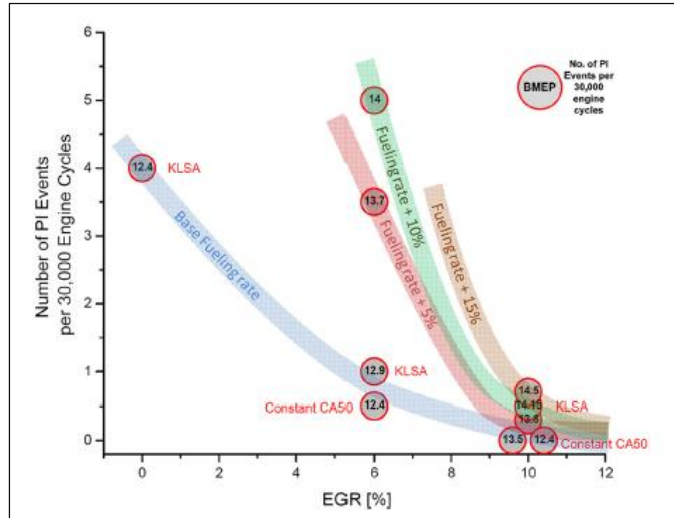


Figure 2.19: Effect of Cooled-EGR Effects on LSPI [84]

#### 2.2.4.6 Effect of Engine coolant temperature:

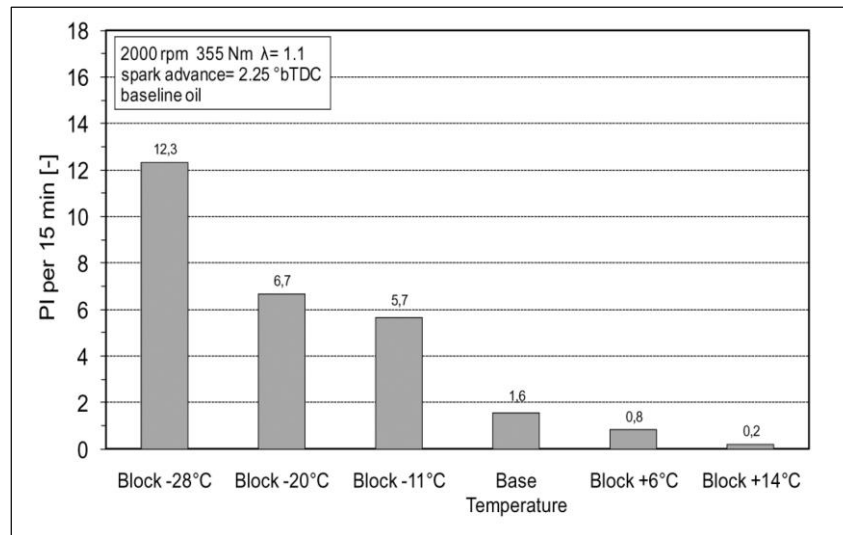


Figure 2.20: Effect of Cooling on Pre-ignition [64]

Figure 2. 20, shows results reported by Zehdah et. Al [64] that depicts an increase in the tendency of pre-ignition at lower block temperatures. They conclude that, changing the coolant temperature changes the liner temperature and cylinder liner temperatures somehow correlate with the pre-ignition ranking of cylinder 1, 4 which are inner cylinders because cylinder 1 and 4 are colder. The colder liner

walls reduce fuel evaporation of droplets hitting the oil coated surfaces and increase its dilution which enhances droplet formation and SPI.

### 2.2.5 Fuel Octane and Volatility Effects on Pre-Ignition:

Dr. Dahnz and co-workers [67] studied the effect of research octane number of the fuel on sporadic pre-igniting frequency. Figure 2. 21, shows a decrease in the rate low speed pre-ignition with an increase in the RON of the fuel. However, when the RON 100 fuel that had the lowest SPI rate was retested, it then showed the highest SPI rate. They concluded that octane number (RON) was not the correct factor or property to use to correlate to sporadic pre-ignition tendency.

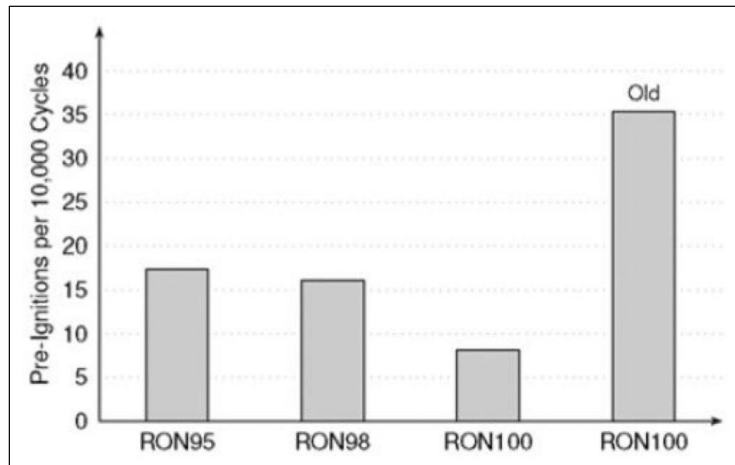


Figure 2.21: SPI frequency for different fuels from Dahnz study [67]

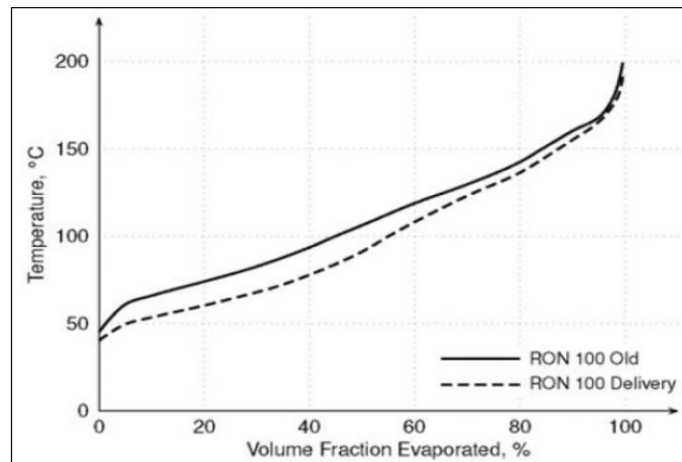


Figure 2.22: Boiling curves of fuels used during fuel variations from Dahnz study [67]

Figure 2. 21 shows the sporadic pre-ignition frequency for different fuels and Figure 2. 22 shows the boiling curves of fuels used during the sporadic pre-ignition test. The conclusion drawn was that low fuel volatility tends to have more tendency to sporadic pre-ignition than fuels with higher volatility.

In another more recent study, Zahdeh and co-workers [64] also preformed sporadic pre-ignition test with various fuels in two different turbocharged direct-injected engines. As shown in Figure 2. 23, work conducted by Zahdeh et. Al [64], they observed trends of the fuel RON number and the sporadic pre-ignition rate do not correlate which contradict with the results concluded by Dr. Dahnz et. Al. [67]. They believe that the fuel did not correlate because it appeared to be due to a change to the boost pressure in the engine test condition.

As the author notes, this is related to the method used that the engine torque was controlled by the ECU. Higher RON fuels allowed the ECU to advance the spark and boost compensated in order to maintain the engine running at the MBT. This change in boost also influenced the sporadic pre-ignition frequency. The results from Dahnz and co-workers [67] did agree with the results from Zahdeh and co-workers [64] except for the Ron 100.

The two fuels with the the lowest sporadic pre-ignition rate were the high Dry Vapor Pressure Equivalent fuel and the fuel with RON 100.

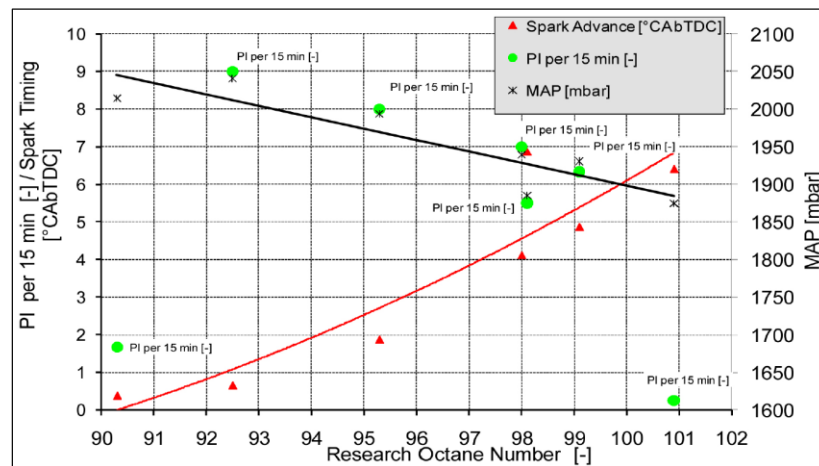


Figure 2.23: Comparison of Research Octane Number (RON) to SPI events from Zahdeh study [64]



Engine Specification	
Displacement	1998cc
Bore	86mm
Stroke	86mm
Compression Ratio	9.2:1
Fuel Injection	Direct Injection
Injector Location	Side Mounted
Injector Type	Multi-hole
Engine Speed	2000 rpm
Load (BMEP)	14.5 bar

Table 2.3: GM 2.0L turbocharged, Spark Ignition, DI engine specifications and test conditions [64]

### 2.2.6 Fuel Impact of Lubricant Composition on LSPI

Zahdeh et. Al [64] studied the sporadic pre-ignition frequency of various engine oil. Oil A is based on polyalphaolefines (PAO) and contains very little amount of additives and little sulphur ash. Additional tests with two different intermediate oil specifications B and C - one with hydrocrack base oil and the other one reduced amount of additives - the other with PAO (Poly-alpha-olefin) oil and a regular amount of different additives have indicated that both parameters contribute to the excellent performance of the oil as shown in Figure 2. 24.

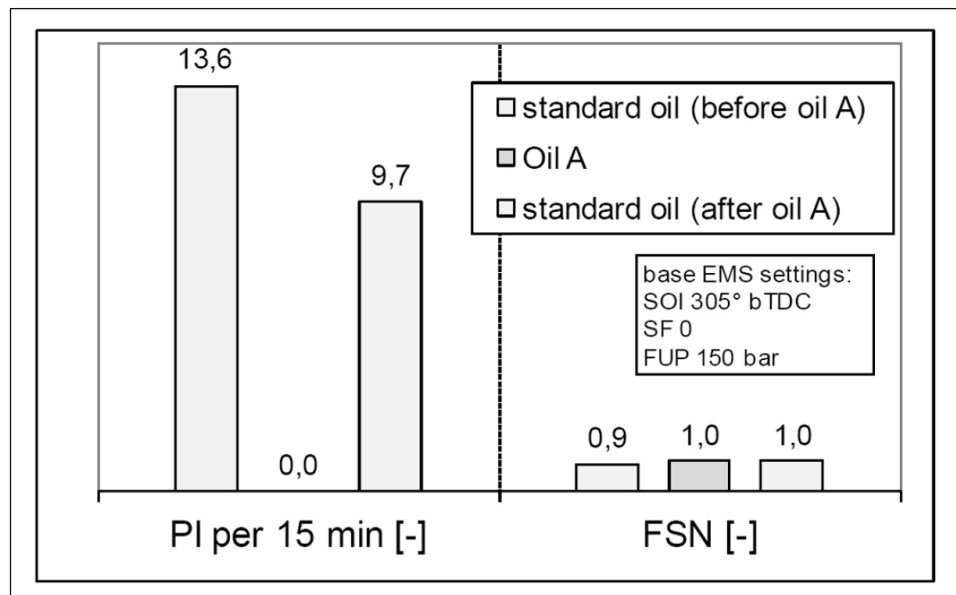


Figure 2.24: Influence of Oil on Pre-ignition [64]

### 2.2.7 Effect of intake valve diameter on pre-ignition

Analysis and development efforts are described for the 0.43 liter test engine by William P. Attard et. al. [65], which was fitted with a port fuel injection fuel delivery system. The inline four cylinder engine used to develop to enable 25 bar BMEP to be able to produce sporadic pre-ignition. They studied the effect of the piston geometry and the number of the compression rings on the tendency of sporadic pre-ignition [65]. They found that piston/piston ring design have the most effective in extending the engine power to 25 bar BMEP. In addition, they found that keeping the intake valve size as the same size of the exhaust valve size, reduced the frequency of pre-ignition. The intake side was shown to be the region of highest knock intensities because it was the last place where the flame arrives lately, with the cooler surfaces indicating that gas knock of the end gas as shown in Figure 2. 25. Figure 2. 26 shows the results of the test after using the new valve design and the two compression rings.

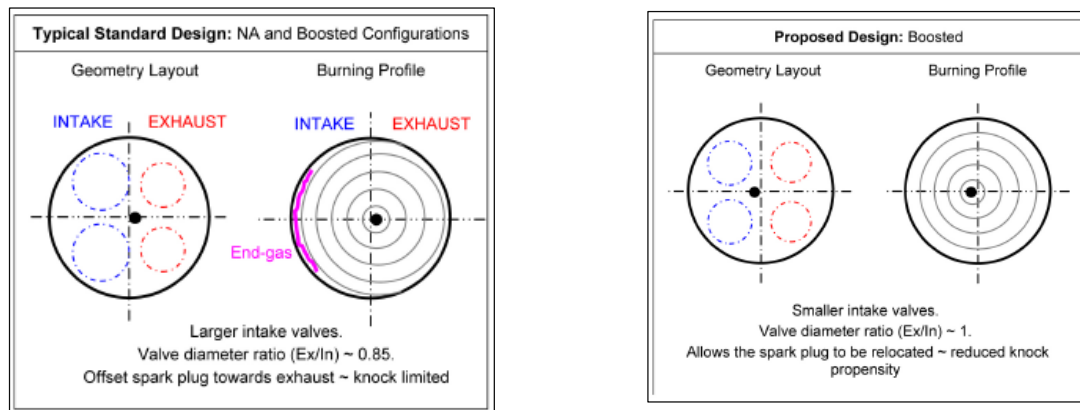


Figure 2.25, Proposed pent roof design to reduce the intake side knock propensity found from experiments, Offset spark plug towards the intake side. [65].

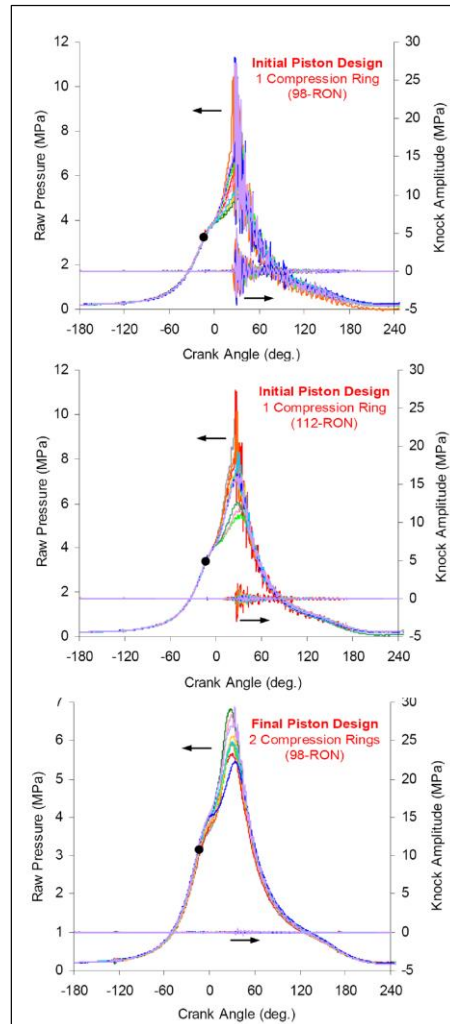


Figure 2.26, Turbocharged PFI combustion effects of various piston including varying the number of compression rings and fuel quality. 7000 rev/ min, 200 kPa MAP, CR = 10, 12° BTDC spark timing. [65].

### 2.2.8 Summary of Sporadic Pre-Ignition in Spark Ignited Gasoline Engines:

Sporadic pre-ignition have been identified as the main factors limits increasing the power density of the spark ignition gasoline engine. After deep investigation, the research results claimed that there is an oil droplet evaporate and ignite at the end of the compression stroke before the spark event. In addition, they proved that pre-ignition is likely started around the spark plug. Some of the research done injected some of the oil droplets in the combustion chamber at the beginning of the intake stroke and the results showed a good agreement that the oil droplets is the main cause of pre-ignition. There are still some doubts about that oil droplet contribution in SLPI. It is clear that more research is needed to gain a

better understanding of the causes of this phenomena and for the development of strategies for their control.

### **2.3. Cycle to Cycle Variation in Spark Ignited Gasoline Engines:**

Under steady state operating conditions all types of internal combustion engines experience variation in the cylinder gas pressure from one cycle to the next. The reasons behind c-t-c variation have been under investigation for many years and found to depend on many design and operating parameters. Since this phenomena occurs in GDI engines, a review of the research conducted on gasoline PFI (port fuel injection) engines will be made and the results compared with the findings in this investigation.

#### **2.3.1. Effect of access air on cycle to cycle variation.**

Jinhua Wang et. al [98], studied the effect of the access air on the cyclic variability. The investigation has been done on a spark ignition engine running with natural gas–hydrogen blends He found the COVimep% maintains at a low level under the stoichiometric and the relatively rich mixture operation while it decreases smoothly with the increase of hydrogen fraction in the fuel under lean mixture operation. In addition, he proved that the excessive air ratio at COVimep % 10% extended to the lean mixture side with the increase of hydrogen fraction. Hydrogen addition into the natural gas can decrease engine cycle-by-cycle variations as shown in Figure 2. 27.

Bengt Johansson [97] investigated the cycle to cycle variation in a spark ignition engine. They mainly investigated the flow behavior of the mixture around the spark plug at the ignition time. The investigation conducted on spark ignition optical engine to visualize the flow. They supported their experimental investigation by computer simulation. The authors concluded that If the fuel and air are well mixed and the engine load is high, the main cause of variations in the early combustion is the flow in the spark plug vicinity.

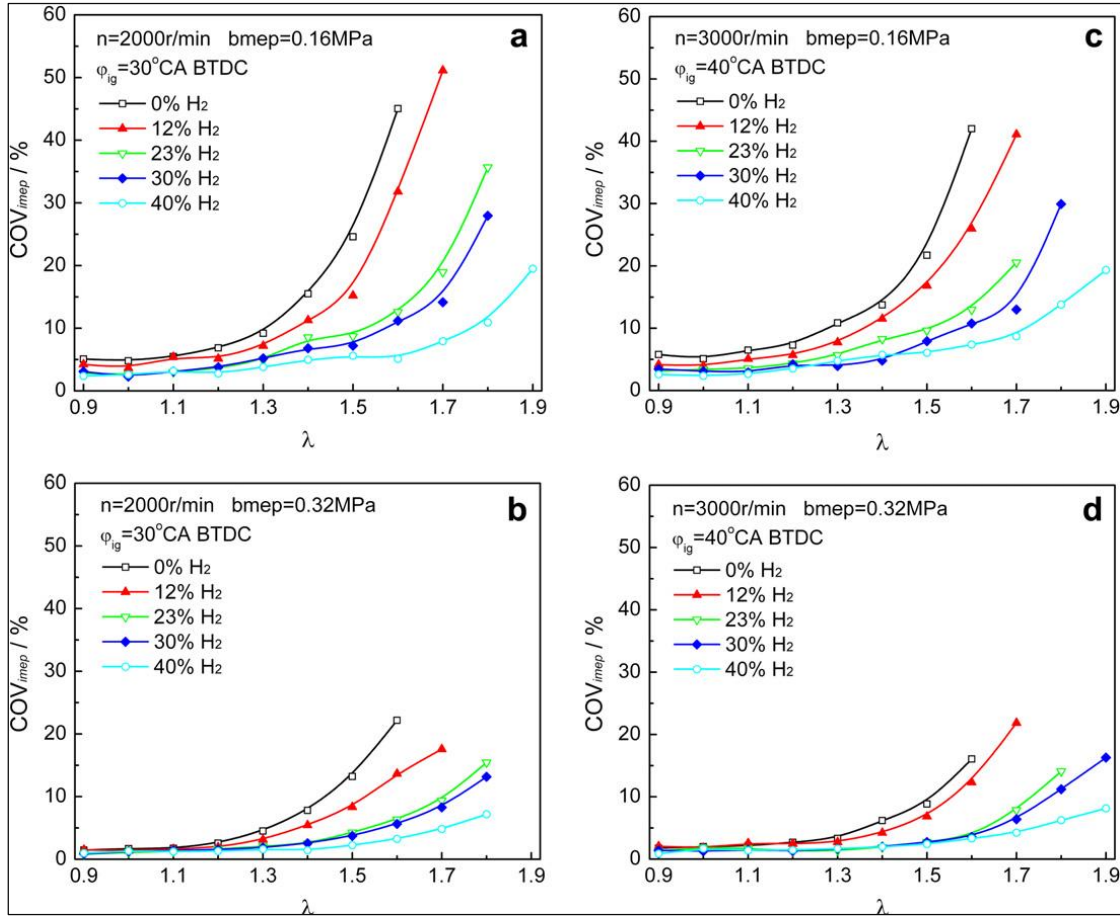


Figure 2.27. COVimep versus excessive air ratios [98].

### 2.3.2 Effect of EGR on cycle to cycle variation.

Bin Huang et. al. [101] investigated the Cycle-by-cycle variations in a spark ignition engine operated with natural gas–hydrogen blends combined with EGR. The research done on HH368Q gasoline engine with three cylinders and compression ratio 9.4. The authors found that Cylinder peak pressure and maximum rate of pressure rise are decreased remarkably with the increase of EGR ratio, and the cyclic variability increased as much as the EGR percent increases. Figure 2.28 shows the variation of IMEP with respect to the EGR %. They concluded that the cycle-by cycle variations of indicated mean effective pressure are increased with the increase of EGR ratio.

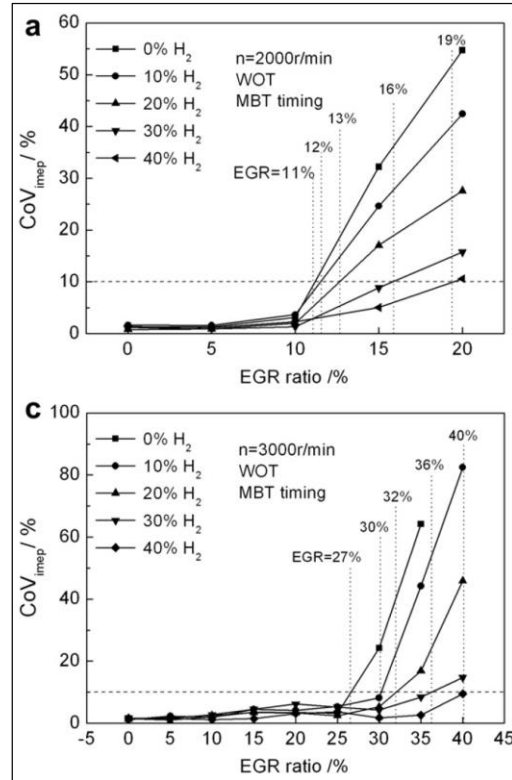


Figure 2.28.  $\text{CoV}_{\text{imep}}$  versus EGR ratio and hydrogen fraction [101]

### 2.3.3 Effect of Load cycle to cycle variation.

Stephen Samuel et. al. [42] investigated the combustion characteristics and cycle-by-cycle variations gasoline direct injected spark ignition engine with cooled turbocharger. The investigation conducted at a wide range of operating conditions. They characterized cycle-by-cycle variations by the coefficient of variance of in-cylinder gas pressure against crank angle, the indicated mean effective pressure (IMEP) and MBF 50 %. The combustion characteristics and cyclic variability of the DISI engine are compared with data from throttle body injected engines throughout the analysis to draw conclusions as shown in Figure 2.29. His identified that the COV of pressure reaches a minimum value at the end of the compression stroke and this minimum value is independent of engine type and the loading conditions investigated. It also identified that the maximum COV value of the pressure against crank angle during combustion does not change significantly with load for the throttle body injected engine. However, the changes are significant for DISI engine.

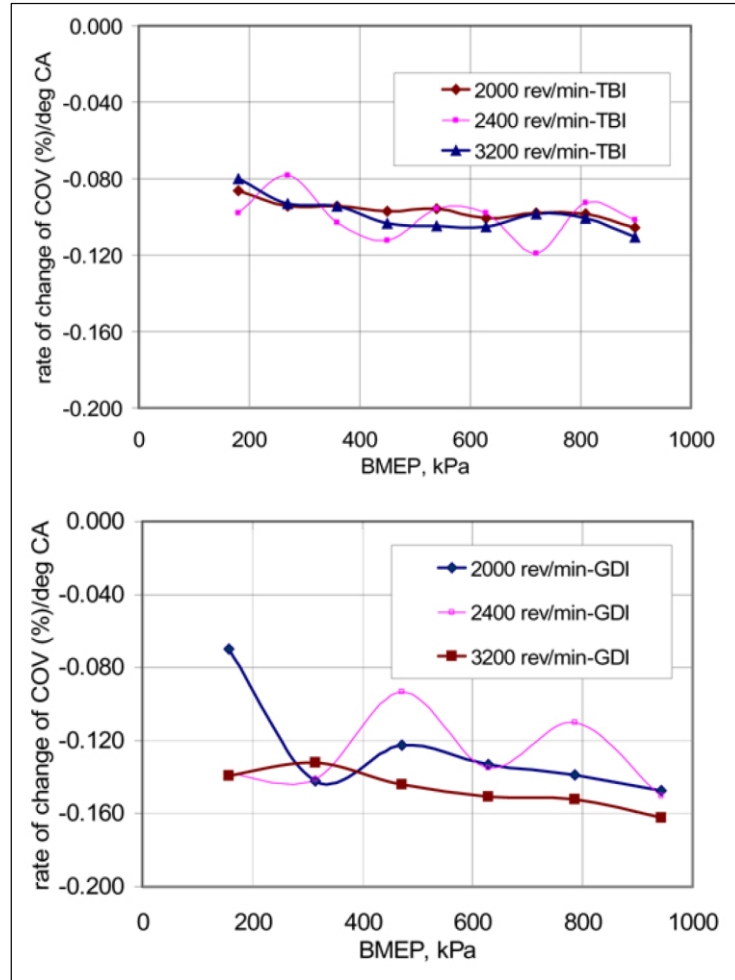


Figure 2.29. Rate of change of COV of cylinder pressure during compression for GDI

They concluded that, the COV analysis using COV of pressure against crank angle provided more insight into the cyclic variations that happen during different sections of the cycle which could be detected using the analysis type of measuring the variability of the IMEP. It also showed that the minimum value for COV of pressure at the end of compression stroke does not depend on the engine load and speed and also engine type as shown in Figure 2.29.

#### 2.3.4 Effect of ignition and injection timing on cycle variation.

Changming Gong et al. [99] studied Cycle-by-cycle combustion variation in a direct injection spark ignition engine running with methanol. In this study, the authors have discussed the effect of some of the calibration and performance parameters on cycle to cycle variation in terms of combustion stability in a

four stroke gasoline direct injection engine. The operating condition is 1200 rpm and at wide open throttle conditions. They observed that cycle to cycle variation increases with changing the injection timing and ignition timing but there is a point where there is a minimum COV shown in Figure 2. 30.

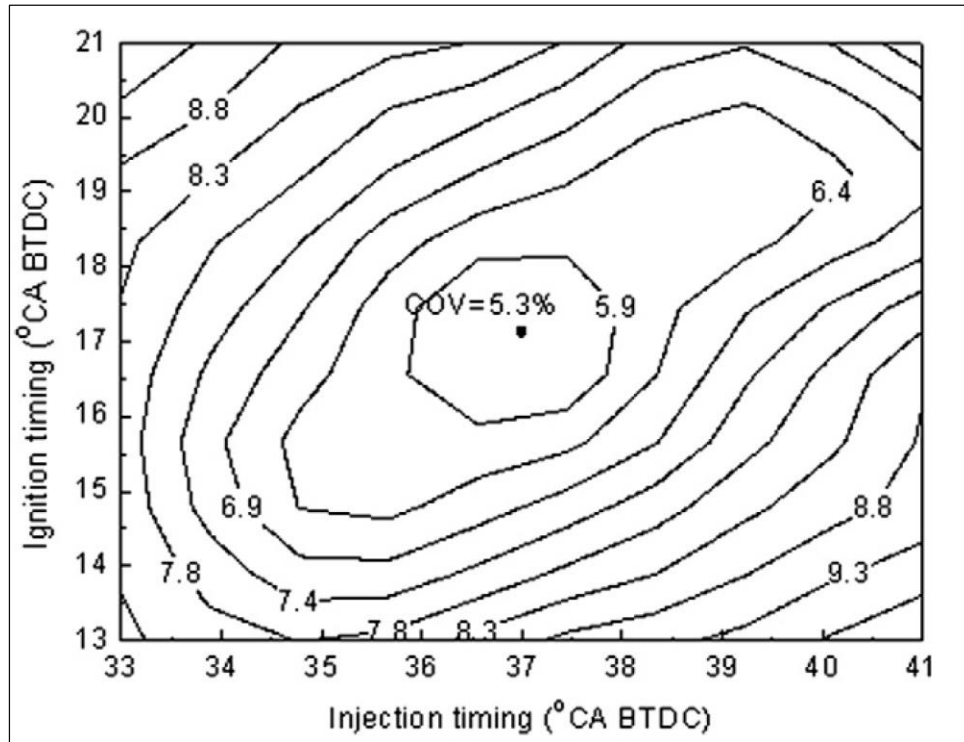


Figure 2.30. COV map in an engine using an injector of type A at an engine speed of 1200 rpm, 100% load, and a compression ratio of 14:1 [99].

Additional investigation conducted by Changming Gong et al. [99] showed in Figure 2. 31, shows that the COV at a compression ratio of 14:1 is less than that at a compression ratio of 16:1 at light load, and vice versa at high load. This may be due to that the methanol engine may form a mixture concentration distribution to promote the flame propagation with the increase of BMEP. In addition, The COV decreases with the increase of engine speed in spark ignition engine. This may be due to the increase of swirl intensity to form a more uniform mixture concentration distribution with the increase of engine speed which seems not desirous.



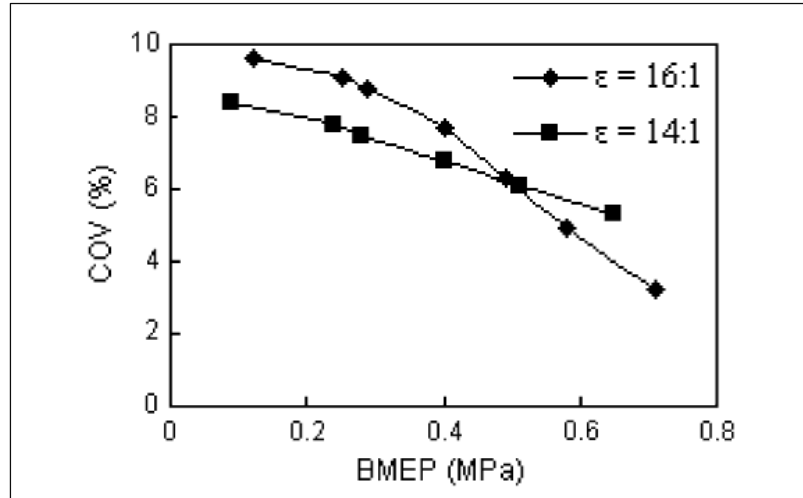


Figure 2.31. Effect of BMEP on COV in an engine using an injector of type A at a compression ratio of 16:1 or 14:1, an engine speed of 1200 rpm and an optimal injection and ignition timings. [99]

### 2.2.5 Effect of engine speed on cycle variation.

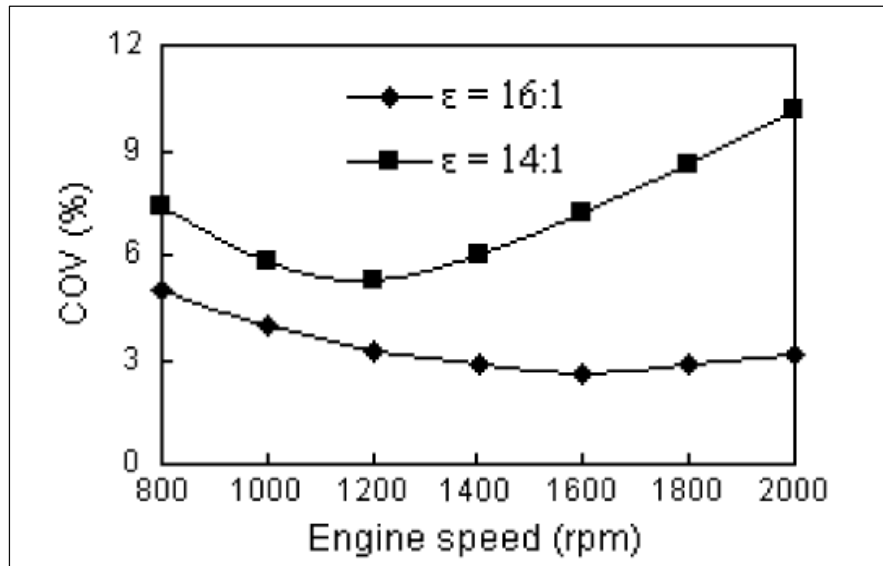


Figure 2.32 Effect of engine speed on COV in an engine at a compression ratio of 16:1 or 14:1, 100% load, and an optimal injection and ignition timings. [99]

Another research conducted by David L.S. Hung and Jie Zhong [55] and carrying out experiments on spark ignition direct injection engine for understanding the cyclic variability of fuel injection. Optical investigation conducted to visualize the presence of liquid at the local area of injector tip as shown in Figure 2. 33. They used two fuel injectors with solenoid actuated. A remarkable difference in the fuel

injection which analyzes the start of fuel cycle to cycle variation. The results demonstrate that there is a difference of the start of fuel injector from one cycle to another one which causes the variation in IMEP.

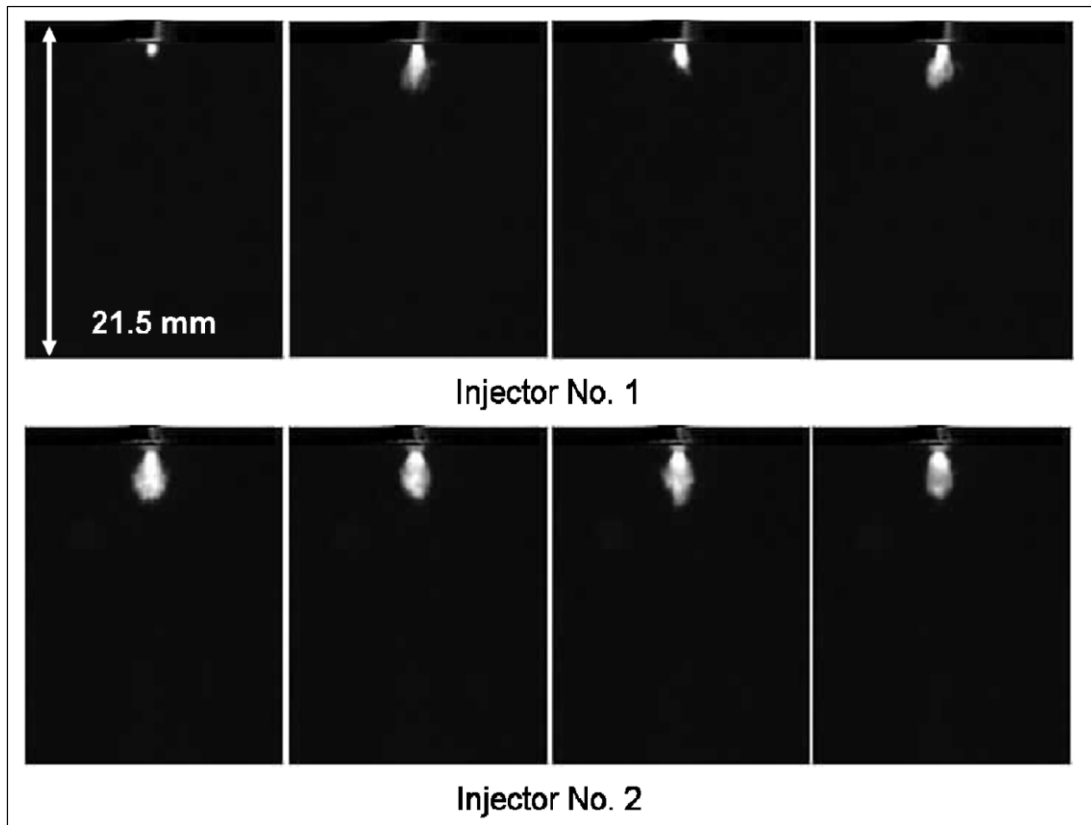


Figure 2.33. Illustrations of start of fuel variations at 0.4 ms after SOI from two different fuel injectors (Four different injection cycles). [55]

Francis Morey and Patrice Seers [90] have compared the variability of the exhaust gas temperature with the variability of IMEP cycle by cycle. Experimental investigation conducted on 4 cylinder PFI spark ignited engine. It is observed that cyclic variability increases with an increase in excess air as shown in Figure 2.34.

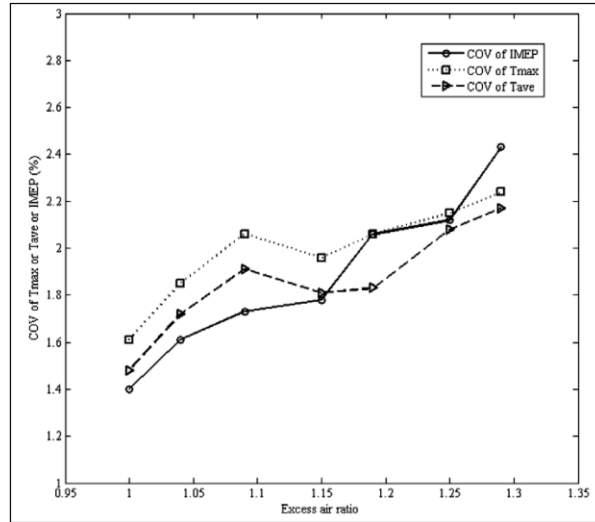


Figure 2.34. Coefficient of variation as a function of excess ratio at 1500 rpm, BMEP of 262 kPa, and MBT spark timing. [90]

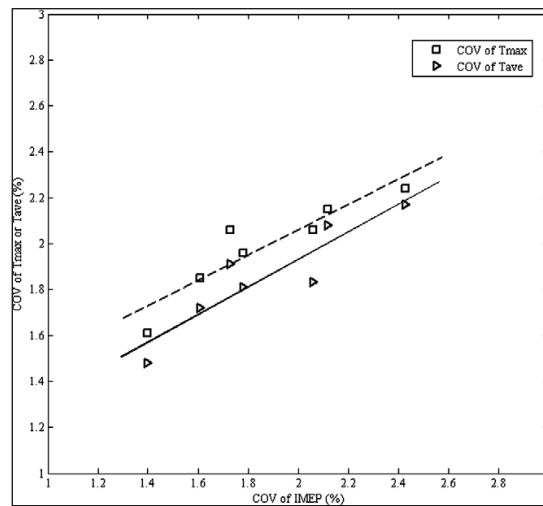


Figure 2.35. COV of  $T_{max}$  and  $T_{av}$  as a function of COV of IMEP at 1500 rpm, BMEP of 262 kPa, and MBT spark timing. [90]

The COV value of maximum and average temperatures, determined from a group of cycles, can be linked to the COV of IMEP. COV of  $T_{max}$  is strongly correlated to COV of IMEP when the cause of the variation is associated to spark timing and/or excess ratio of the mixture as shown in Figures 2.34, 2.35 and 2.36 moving window calculation of COV on a small number of cycles has shown that combustion deterioration can be monitored by using the COV of maximum exhaust-gas temperature.

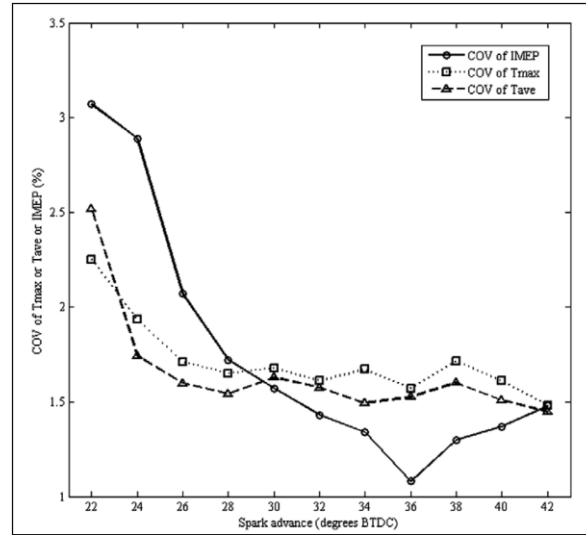


Figure 2.36. COV of IMEP as a function of COV of  $T_{max}$  and COV of  $T_{ave}$  for different spark timing values at 1500 rpm, BMEP = 262 kPa, and  $k = 1.00$ . [90]

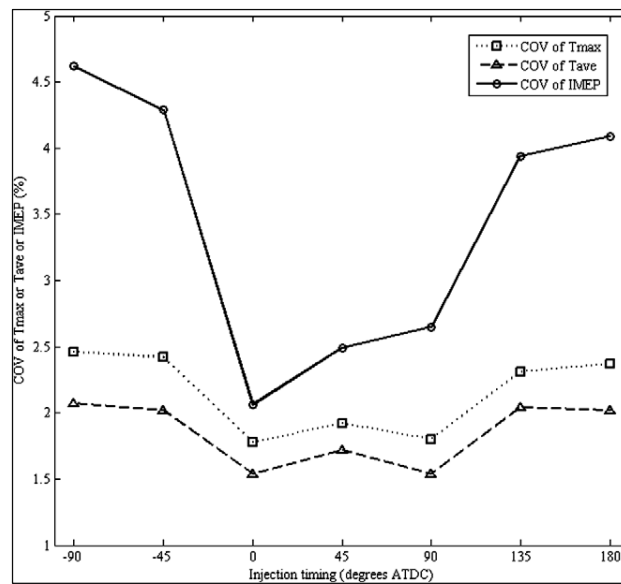


Figure 2.37. COV of IMEP as a function of COV of  $T_{max}$  and COV of  $T_{av}$  for different injection timing at 1500 rpm, BMEP of 393 kPa,  $k = 1.10$  and MBT spark timing. [90]

Figure 2.36 and Figure 2.37 showing that COV of exhaust temp shows a cordial relationship with COV of in cylinder pressure which becomes more sensitive at maximum temperature. Figure 2.38 shows almost similar variation of cyclic variability of max gas temperature at exhaust with the cycle to cycle variation of IMEP. However, average maximum temperature shows no variation with injection timing.

Rakesh Kumar et. al [75], experimentally analyzed the cyclic instability of combustion and performance parameters in a homogeneous charge compression igniting engine running with two types of fuel, methanol and gasoline. It is observed that as the air fuel mixture is increased the cyclic variation increases. From the Figure 2.38 it can be observed that mean in cylinder gas pressure reduces as the air fuel ratio is increased for the two types of fuels. It can also be observed from Figure 2.38 that cyclic variability decreases as we go on a leaner side. In addition, maximum rate of pressure rise decreases as we move towards leaner side.

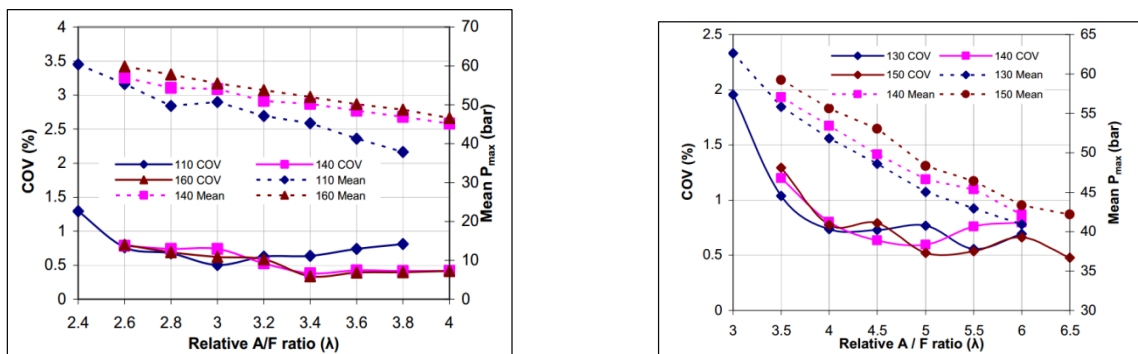


Figure 2.38. Cycle-to cycle variation of P<sub>max</sub> for gasoline and methanol at different intake air temperatures [75]

Fanhua Ma et. al [52], conducted experimental study on a six cylinder spark ignition engine to analyze the effect of addition of hydrogen on cyclic instability. It is observed from Figure 2.38 that adding the as much as adding hydrogen to natural gas fuel, it increases the burning velocity in addition to decreasing the peak pressure variation in different cycles. Thus will increase the overall cycle to cycle variation in the engine IMEP. Also, on adding the hydrogen in an engine running with a very lean mixture will help reducing the variability as well as NO<sub>x</sub> emission due to the high increase in the flame speed and lowering the in-cylinder temperature.

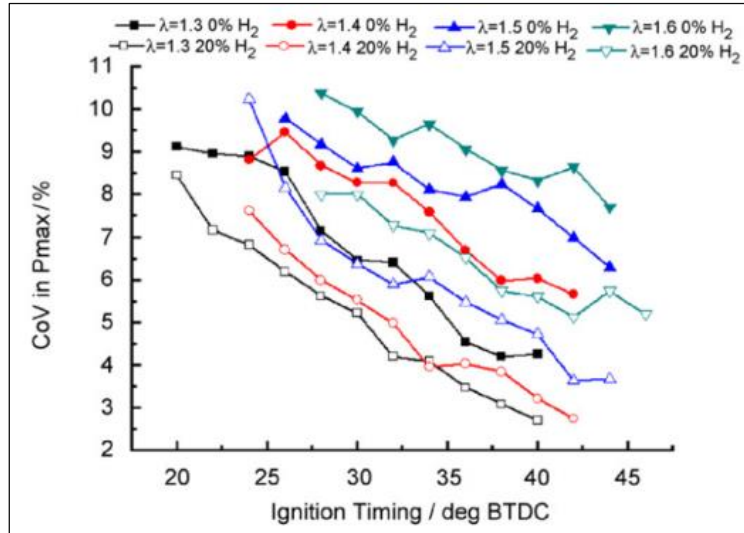


Figure 2.39 CoV in maximum pressure at various excess air ratios at 0.55 MPa BMEP [52].

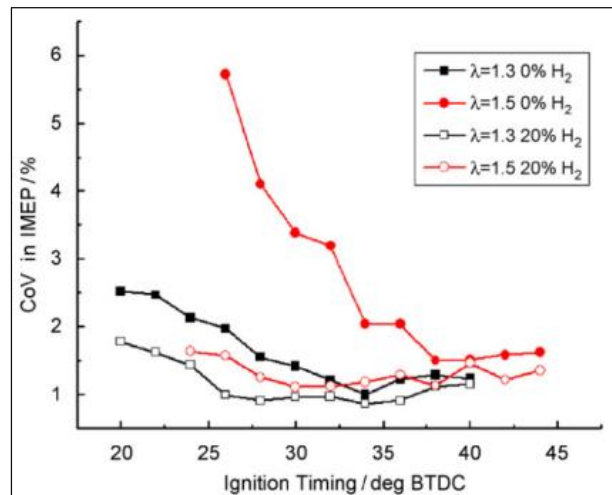


Figure 2.40. CoV in IMEP at various excess air ratios at 0.55 MPa BMEP. (A) Lambda = 1.3,1.5 (B) lambda = 1.4, 1.6 [52]

M.A. Ceviz et. al [37], conducted cyclic dispersion on a spark ignition engine operated under lean operating conditions when running with Liquefied Petroleum gas and gasoline . They observed that during the combustion process, cyclic instability becomes acute in case of both LPG and gasoline and increases with increase in the air to fuel ratio. In both, gasoline and LPG as fuel, the engine losses will increase remarkably due to the increase in wall temperature. In addition reduction in burning velocity observed due to the high increase in the cyclic variability. Figure 2.41, it can be concluded that rate of increase of

cyclic instability of the indicated mean effective pressure decreases with higher air to fuel ratio while rate of increase of cycle to cycle variation of IMEP increases due to more volatile nature of LPG which results in better mixing of fuel with air.

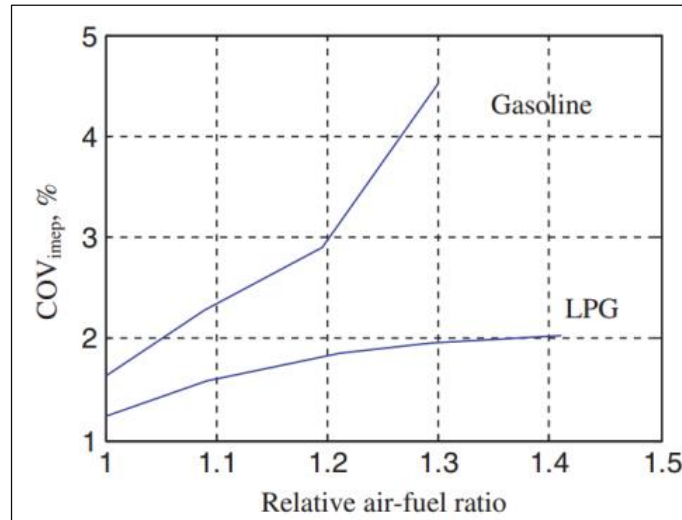


Figure 2.41. Variation of coefficient of variation in indicated mean effective pressure with relative air-fuel ratio.

### 2.3.6 Summary of Cycle to Cycle Variation in Spark Ignited Gasoline Engines

There is an agreement that the irreproducibility of turbulence is the main cause of cycle to cycle variation in GDI as well as in PFI gasoline engines. Most of the researcher investigated extensively the cyclic variation experimentally on actual production engine and considered COV in IMEP as a measure of cycle-to-cycle variation. In this investigation, the cycle to cycle variation in a GDI engine will investigated by using two ion current sensors in addition to a pressure transducer to investigate the effect of different parameters on cycle to cycle variation.

## CHAPTER 3 EXPERIMENTAL SETUP AND INSTRUMENTATION

### 3.1 Introduction

The focus of this chapter is to discuss the experimental setup used in this research. It aims to thoroughly describe the engine setup, the coupling with the dynamometer, the instrumentation, as well as the control equipment and ionization techniques that were utilized to measure the ion signals from the combustion chamber. It also includes an explanation of the custom electronic circuits that were used in many measurements.

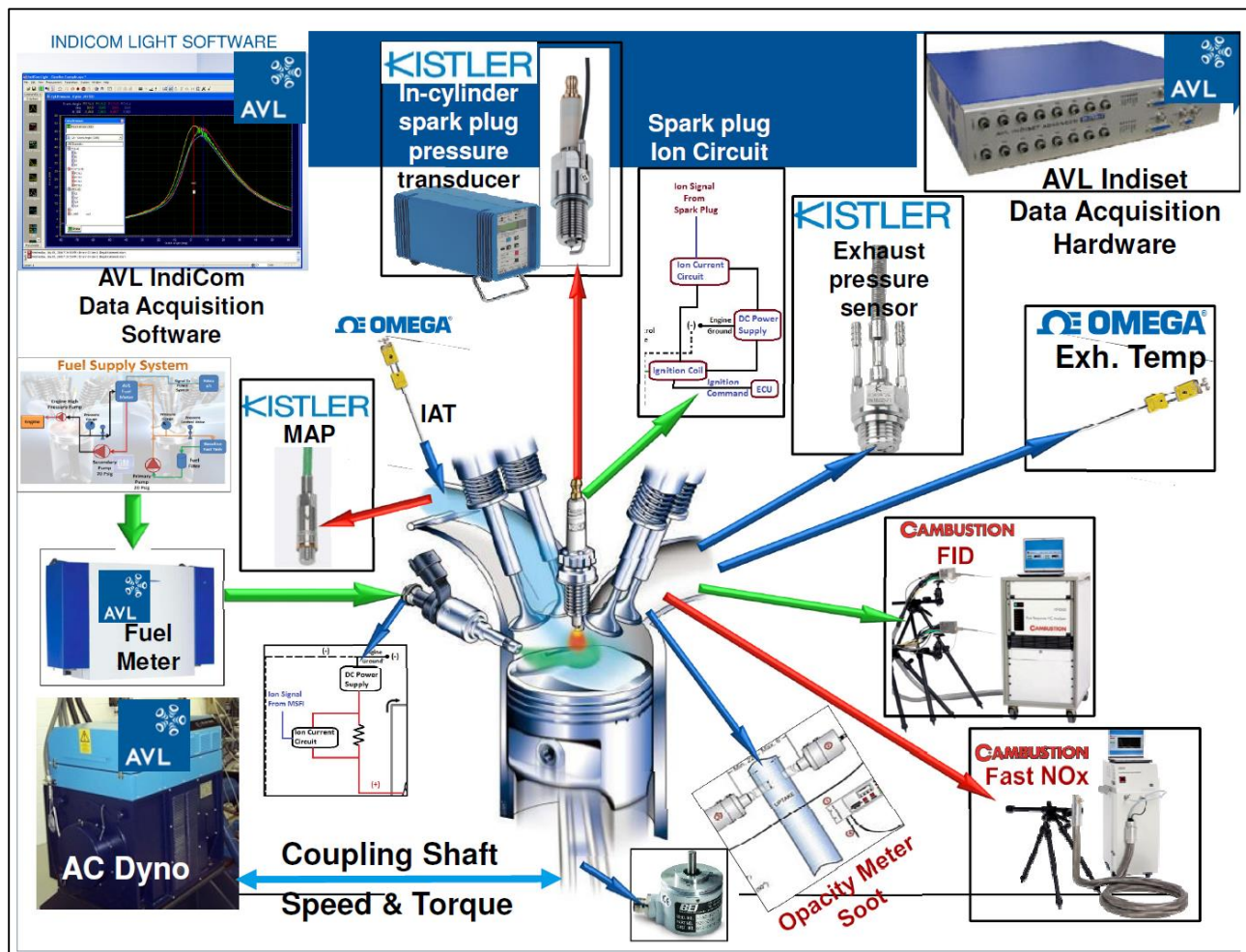


Figure 3.1, the schematic diagram for the test cell



### **3.2 Test Facility Description**

The test cell is one of the Center of Automotive Research laboratories in the Mechanical Engineering department, located in the Engineering Building at Wayne State University. It is equipped with fresh air and exhaust systems and has the necessary foundation required to support and balance the engine, as well as absorb its vibration. In addition, the test cell is equipped with all the safety precautions that may be needed in case of any emergency. Figure 3.1 illustrates the schematic diagram for the entire test cell.

### **3.3 Torque and speed measurement and control**

An AVL PUMA system is used to measure and control the engine's torque and speed. This system consists of an AC dynamometer- an ELIN AVL model with a maximum speed of 5000 rpm and maximum operating torque of 500 N.m. The software is an AVL PUMA 1.2 user interface system, licensed to Wayne State University. This system is capable of running the engine at steady and transient operating conditions.

Regarding the physical connection, the AC dynamometer was connected via a flexible coupling which was used to absorb any vibrations and misalignments of the engine with respect to the dynamometer.

### **3.4 Engine Specifications**

Experiments were conducted on a GM dual scroll turbocharged gasoline direct injection 2.0L engine with dual continuously variable cam phaser (D-CVCP). The engine is a 4-cylinder Ecotec engine with 86 mm bore, 86 mm stroke, and 145 mm connecting rod length. It has a compression ratio of 9.2. A six-hole injector is side mounted in the cylinder and is connected to a common rail fuel injection system operated by a production ECU. Table 3.1; shows engine specifications.

Engine Type	Unit	2.0 L ECOTEC SIDI Turbo
Fuel Injection System		High Pressure SIDI
Displacement	Cm <sup>3</sup>	1998
Bore Distance	mm	96
Bore / Stroke	mm	86/86
Conn. Rod	mm	145.5
MOP-Angle Ex / In	°CA after gas exchange TDC	-120 / 126
Compression Ratio	-	9.2
Max. Torque @ engine speed	Nm @ rpm	350 @ 2000
Max. Power @ engine speed	KW/HP @ rpm	194/260 @ 5300
Fuel Quality	RON	87 & 95

Table 3.1, T-GDI engine Specifications used in the current investigation.

### 3.5 Crankshaft Encoder and the TDC determination

An optical ACCU crankshaft encoder shown in Figure 3.2 was mounted on the engine crankshaft. This encoder generates six series of pulses phased as shown in Figure 3.3. The physical connection between the crankshaft and the encoder shaft was made via a flexible coupling which was used to absorb any vibrations and misalignment of the encoder with respect to the engine. This was done to ensure the elimination of any vibration that may cause any miscounting in the encoder marks.



Figure 3.2: The ACCU crankshaft encoder

The encoder has a resolution of 2880 marks per rotation. The resolution of this encoder is 0.125 crank angle degrees, which provides a high resolution to investigate accurately any changes in any signal.

Three signals- A, B and Z- were used to determine the engine's speed. The A- signal gives 2880 pulses per revolution, while the B-signal gives similar pulses per revolution, but they are shifted by a half mark from the A-signal. The Z-signal gives one pulse per revolution. Using the Z-signal, the system counts two revolutions as one cycle since the engine we use in this research is a four stroke engine

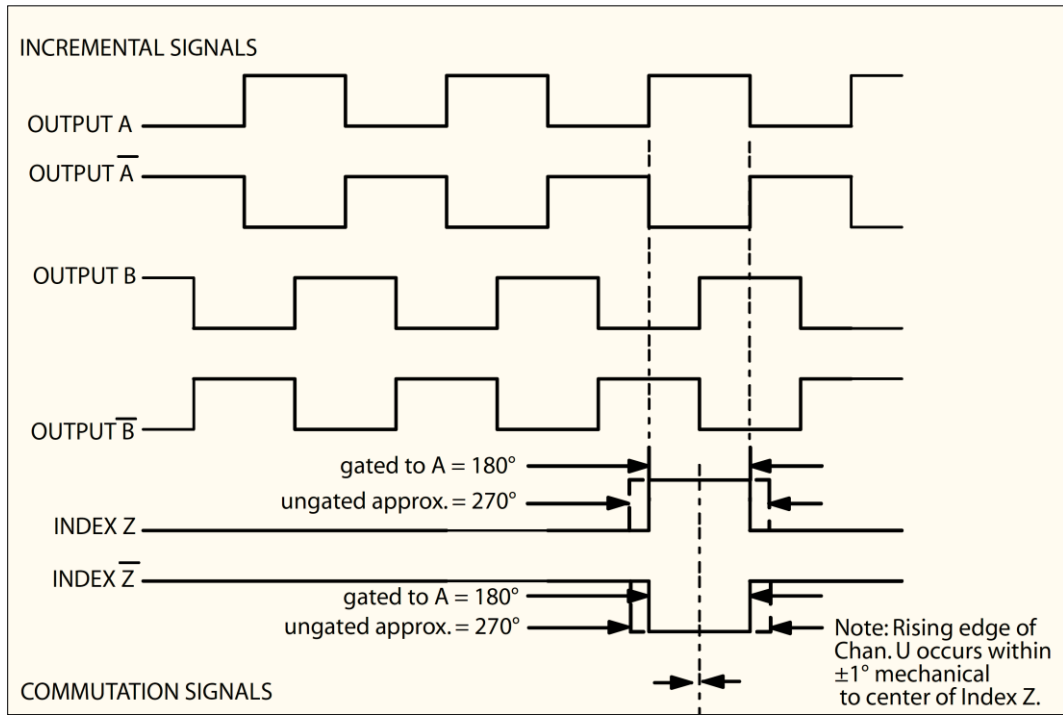


Figure 3.3: The output signals waveform diagrams from the encoder, (Image source: NI 9411 Encoder setup manual)

### TDC determination

Multiple variables must be identified to attain the correct location of the TDC as shown in Figure 3.4. In consecutive order, the variables are as follows: the motoring peak pressure, the A-signal and the Z signal. To further elaborate, the system articulates the location of the peak pressure with respect to the A-signal by matching it to one of the 2880 pulses, and then it determines how many marks this point is away from the z-signal. Once identified, the system automatically fixes this location in its memory as a reference point.

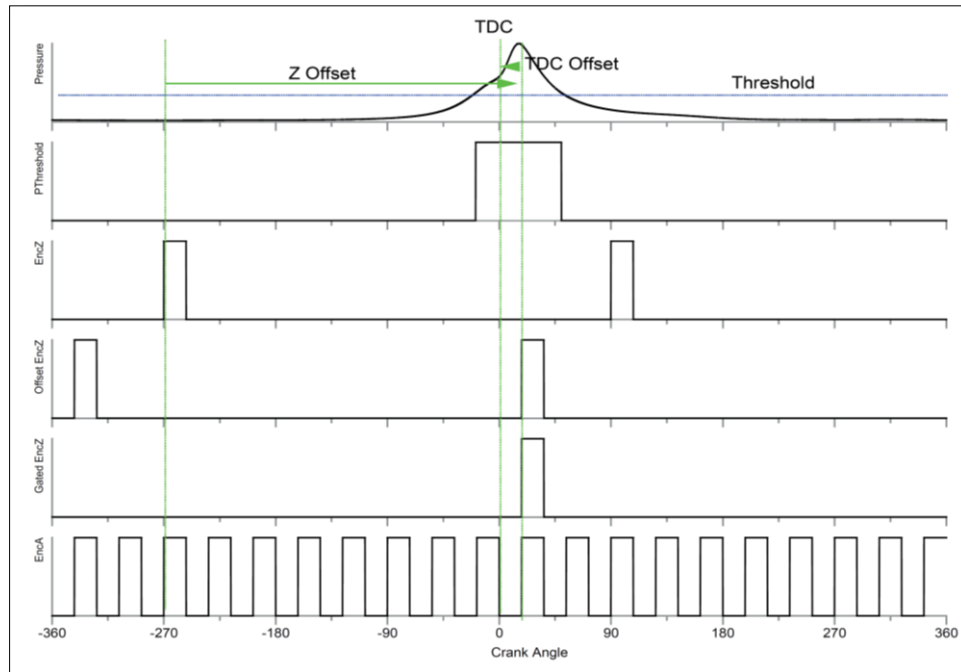


Figure 3.4: The TDC determination using the encoder waveforms and the motoring pressure (Image source: NI 9411 Encoder setup manual)

### 3.6 High-speed data acquisition

A high speed data acquisition system provided by AVL was used to acquire the signals from the sensors. The hardware is an AVL INDISET ADVANCED PLUS with 16 analog channels as shown in Figure 3.5. Such data acquisition is equipped by all of the signal conditioning processes required to give an accurate signal.



Figure 3.5: AVL high Speed data acquisition system (Image source: AVL INDISET manual)

The software used for data acquiring is an AVL IndiCom 1.6 user interface program licensed to Wayne State University. It is capable of obtaining the data from the hardware and makes all the appropriate signal conditioning processes so as to yield a good signal.

### 3.7 In-cylinder pressure measurement

To eliminate any custom work in the engine cylinder head, the engine is fitted with a Kistler spark plug pressure transducer for in-cylinder pressure measurements. The pressure transducer model number is 6118BCD25 as shown in Figure 3.6 is used in this investigation. The technical data of this pressure transducer is shown in Table 3.2.

Pressure range	<b>bar</b>	<b>0 ----- 200</b>
Overload capacity	<b>bar</b>	<b>250</b>
Sensitivity at 200 °C	<b>pC/bar</b>	<b>≈10</b>
Natural frequency (acoustic) spark plug with integral sensor	<b>kHz</b>	<b>≈65</b>
Sensitivity drift over range: 200 (+/-)50 °C	<b>%</b>	<b>&lt;±1</b>
Insulation resistance, sensor at 20 °C	<b>Ω</b>	<b>10<sup>12</sup></b>
Dielectric strength	<b>kV</b>	<b>&lt;35</b>
Capacitance of sensor with 1 m cable	<b>pF</b>	<b>110</b>

**Table 3.2: Technical data of spark plug pressure transducer**

The pressure transducer is fast enough to capture any variation in the cylinder pressure per 0.1 crank angle degree at a speed of 5000 rpm. This allows the detection of any micro changes in the signal for a better investigation of the cycle-to-cycle variation.

A Kistler charge microprocessor-controlled piezoresistive amplifier type 4603B, as shown in Figure 3.7, is connected to the transducer. This type of amplifier parallels two types of outputs: current

and voltage. The latter is scalable to 1, 2, 5, 10 V, according to a particular sensor measuring range. In addition, an output with load-independent current 0/4 ... 20 mA is also available.

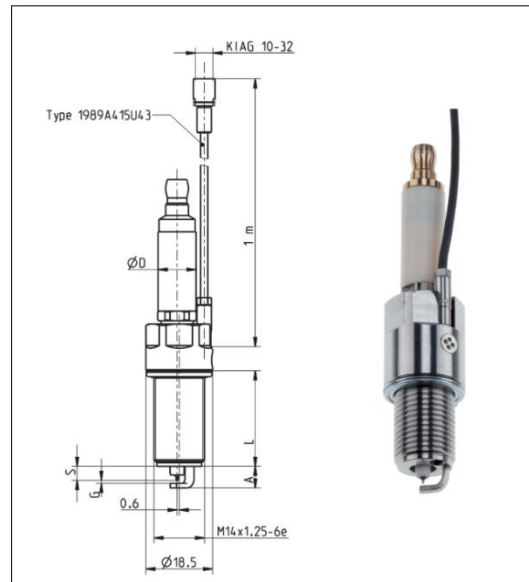


Figure 3.6: Kistler spark plug pressure transducer for in-cylinder pressure (Image source: Kistler pressure transducer manual)



Figure 3.7: Kistler charge amplifier type 4603B for the pressure transducer (Image source: Kistler pressure transducer manual)

The amplifier functions can be set in a dialog form by the means of a two-line LCD high-contrast display. It provides the opportunity to make changes in the following variables: type of supply,

calibration current (for current-fed sensors), pressure measuring range, sensor sensitivity, zero offset, zero shift, unit pressure (bar, Pa, psi), low-pass filter, output voltage and current.

### 3.8 Manifold intake air temperature and pressure measurement

#### The manifold intake air temperature, IAT:

The intake air temperature is measured at the intake manifold using a fast response k-type thermocouple. Such a response is fast enough to capture the changes in the intake temperature with respect to one crank angle degree at high speed up to 5000 rpm.

#### The manifold intake pressure:

The manifold intake pressure is measured using two sensors. The first sensor is the original engine manifold absolute pressure, MAP, which is not fast enough to capture any changes in the charge pressure during the opening and closing of the intake valves. Rather, the MAP sensor is used to determine how the engine control unit (ECU), controls the boost pressure.

The second sensor is a diaphragm type pressure transducer, supplied from Omega, as shown in Figure 3.8, with a pressure range of 0 .... 60 Psi gauge.



Figure 3.8: Omega Pressure transducer model PX209-060G5V, for MAP measurement (Image source: Omega MAP manual)



The response time for this pressure transducer is 1 msec, which is able to capture the change in the boost pressure. This pressure transducer is mainly used to measure the boost pressure after the after cooler of the turbocharger.

### 3.9 Cylinder # 1 Intake air temperature and pressure measurement.

To understand the causes of cycle to cycle variation, many studies have indicated that the fresh charge has a large weight as one of the main causes; therefore, there are two sensors installed on the intake port of cylinder #1. Those sensors are installed in a location just before the intake valves, as shown in Figure 3.9.

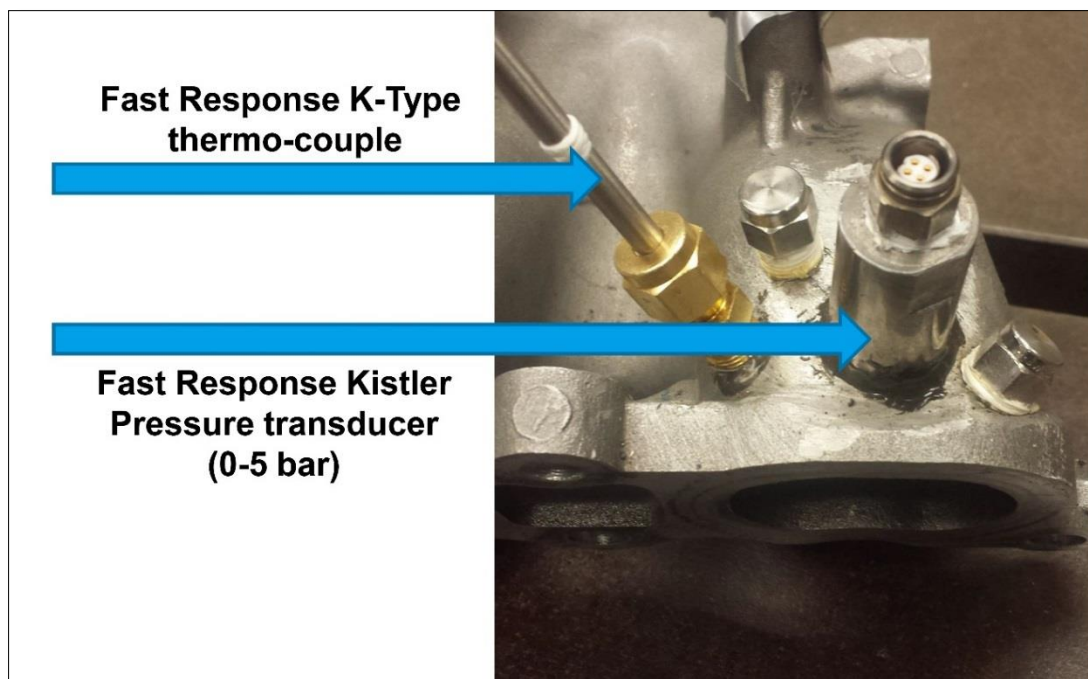


Figure 3.9: The intake manifold, with the locations of the pressure and temperature sensors.

As shown in Figure 3.9, location (1) indicates the location of the pressure transducer installed at the intake port of cylinder # 1. The pressure transducer used for this kind of investigation is fast enough to capture the very small changes in pressure that will accure since the intake valves opens (IVO) till the complete close of the intake valves (IVC) including the ramp of opening and closing. A kistler

Piezoresistive absolute Pressure Sensor for temperatures up to 120 °C, M12x, is used as shown in Figure 3.9

This sensor is installed carefully to be flashed with the internal surface of the intake manifold to prevent any change in the air flow or create any additional swirl in the way that the air flows from the manifold itself to the intake port of cylinder # 1.

The temperature sensor used at the intake port of cylinder #1 is a very fast response type-K thermocouple in order to capture the change in the fresh charge total temperature. Figure 3.9, shows the exact location of the temperature sensor.

### 3.10 Cooling system.

In the test cell the engine radiator is not used as the heat exchanger to cool the engine coolant water, but we used an external heat exchanger with a PID control to manage the mass flow rate of the cooling water to simulate the engine radiator.

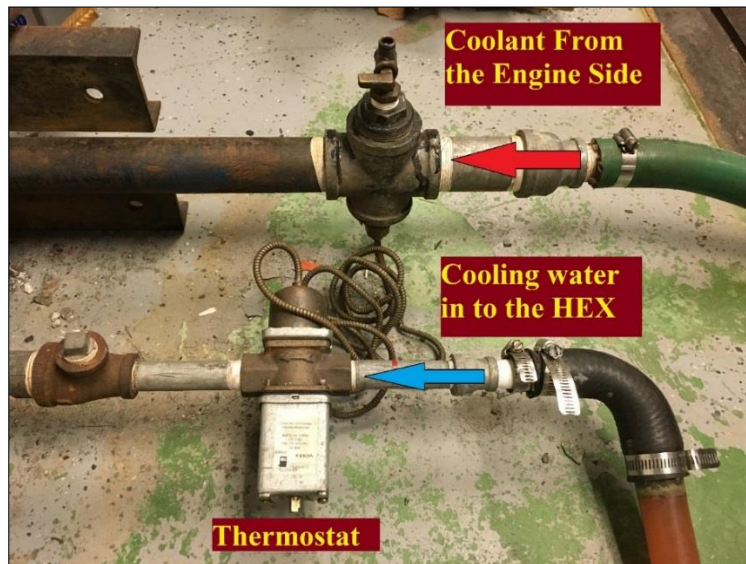


Figure 3.10: Image of the water to water HEX to control the engine coolant temperature

Figure 3.10, shows the external cooling circuit. This water circuit is initially pressurized before start running the engine, and the initial pressure of this circuit is 18 Psig as recommended by the

manufacture. A regular coolant mixture of 50% antifreeze and 50% water is used. The engine is equipped with a vapor extraction valve to prevent any vapor or air to accumulate in the circuit which much causes high thermal stress on the engine cylinder head.

### 3.11 After cooler system.

The engine used in this research is a turbocharged gasoline direct injection engine. The temperature of the air coming out of the compressor is very high and needs to be cooled down to increase the density of the air to get more air into the cylinder. A cross flow water-to-air after cooler is used to cool the air coming out of the compressor before getting in to the intake manifold and then to the combustion cylinder.

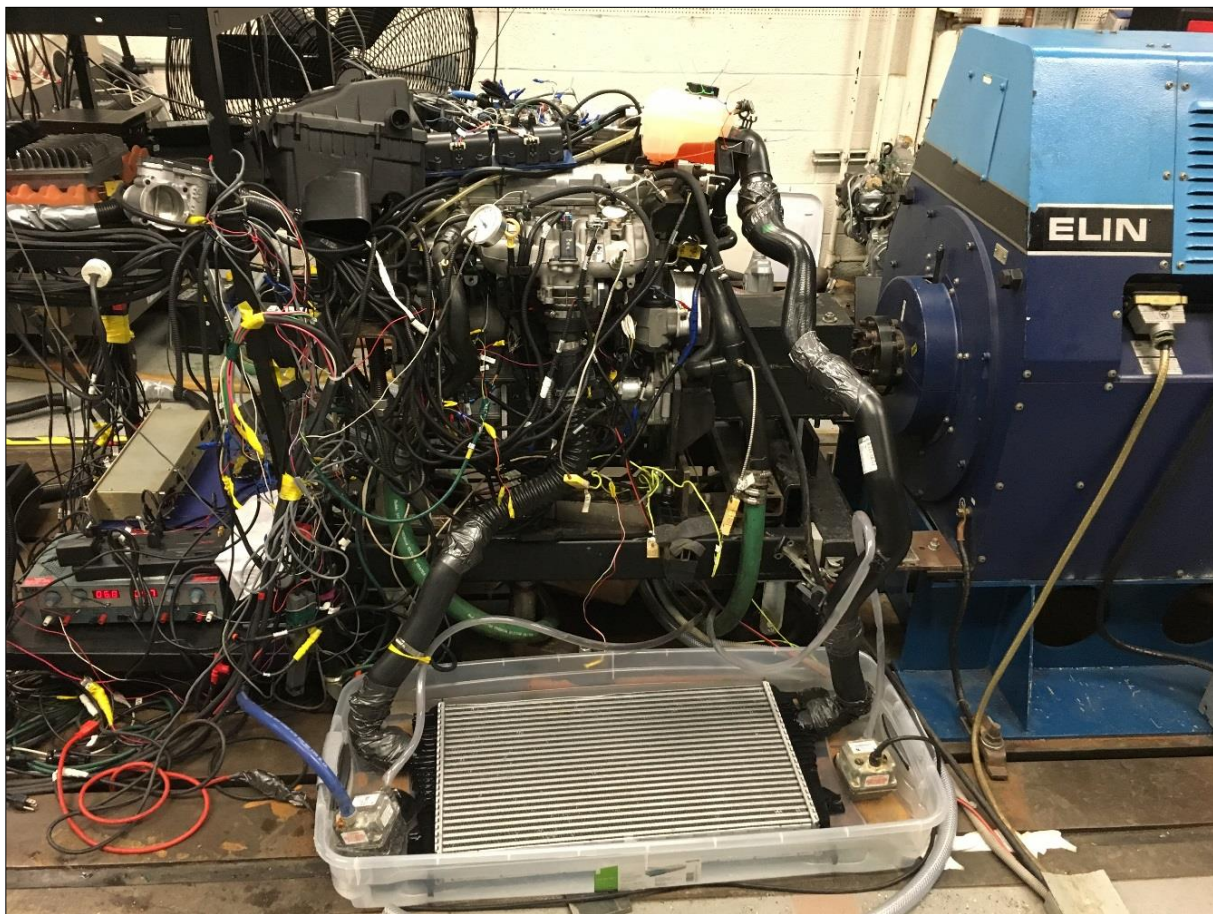


Figure 3.11: Image of the water to air cooled after-cooler

Figure 3.11 shows a schematic diagram of the after cooler system in addition to the two thermocouples used before and after the intercooler to monitor the after cooler performance. There are two external fans with flow rate of 3000 CFM to cool the after cooler. These two fans run steady without any external control.

### **3.12 Engine coolant measurement**

The engine cooling system is under the engine control unit control, the engine thermostat run at two stages. The first stage, at low load and part load, the thermostat is open partially to keeps the engine coolant temperature at 86 C°. The second stage, at high load, the thermostat opens fully and keeps the temperature at 95 C°. The thermostat is connected electronically to the water pump which runs at variable speeds to satisfy the temperature controlled by the thermostat to keep the engine at the appropriated operating conditions by maintaining the wall temperature at the optimal setting.

### **3.13 Exhaust temperature and pressure measurement**

Many studies have indicated that one of the main causes of cyclic variability in the spark ignition engine is the residuals to stays in the combustion chamber from the previous cycle and mix with the fresh charge for the new cycle. At steady state operating conditions, the pressure and the temperature of the exhaust products could give an approximate idea about the residuals stays in the combustion chamber.

A Ksitler fast response pressure transducer is installed at the exhaust port of cylinder # 1 to capture the change in the exhaust pressure from cycle to cycle. In addition, a fast response thermocouple, Omega, K-type is installed at the exhaust port of cylinder # 1 to capture the change in the exhaust temperature from one cycle to another. Figure 3.12 shows the location of the exhaust pressure transducer and the installed fast response thermocouple.



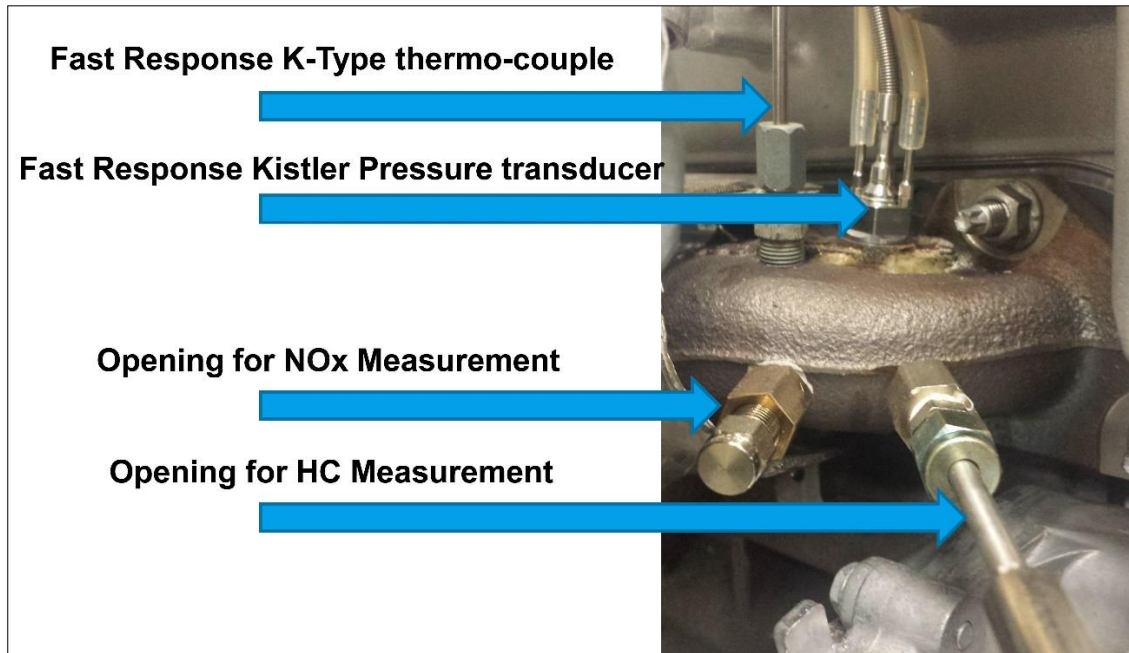


Figure 3.12: Location of the exhaust manifold equipped by the pressure transducer and the thermocouple.

### 3.14 Air mass flow rate measurement

The engine is originally equipped by a MAF sensor mass air flow sensor that is used with the lambda sensor to control the air to fuel ratio. This sensor monitors the mass air flow and is installed just after the air filter. This sensor is fast enough to detect the change in the mass air flow due to the change of the throttle position and boosting pressure.

### 3.15 Fuel mass flow rate measurement system

The AVL fuel mass flow meter shown Figure 3.13 is used to measure the fuel flow rate. This flow meter is a highly precise and continuous fuel consumption measurement system; it measures the total fuel mass flow rate for the four cylinders. The fuel measurement system is designed in two separate systems as shown in Figure 3.14. The primary circuit is designed to draw the fuel from the fuel tank to the AVL fuel measurement device. This circuit is equipped with a fuel filter and fuel pump running at 30 Psig to just overcome the friction loss in the pipes and the difference in heights between the tank and the AVL device. This primary pump is equipped with a return line and pressure control valve. In the

secondary circuit, there is a fuel pump to withdraw the fuel from the AVL device and pressurize it to a 60 Psig to supply the fuel to the engine high pressure fuel pump. The secondary circuit is equipped with a pressure control valve with a return line to keep the fuel supply pressure at 60 Psig.



Figure 3.13: The AVL fuel mass flow meter.

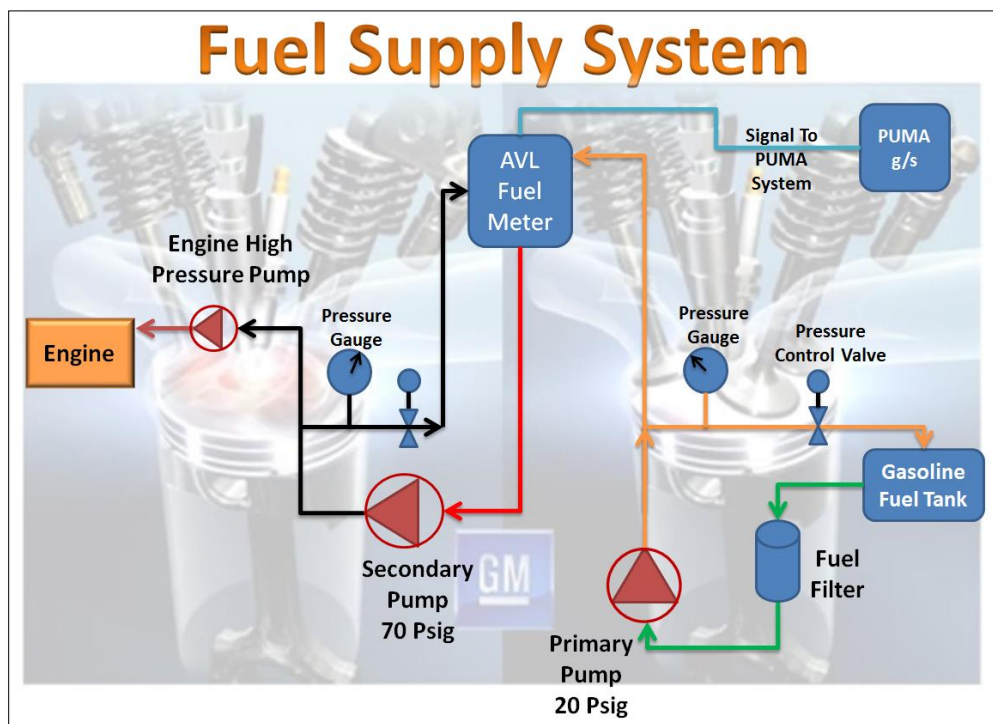


Figure 3.14: schematic diagram for the primary and secondary fuel measurement system.

### 3.16 Common rail pressure measurement

The engine used in this research is a gasoline direct injection spark ignition engine. There is a common rail to supply the fuel to the four injectors. A Kistler pressure transducer with medium response is used to measure the common rail pressure just after the high pressure fuel pump line. A Kistler pressure transducer is installed at the inlet of the common rail. In addition, the engine's original injection pressure sensor of the engine is used to measure the average value of the injection pressure, to control the solenoid valve that controls the operation of the high pressure pump. Both of those signals are monitored on the data acquisition system.

### 3.17 Cylinder # 1 injection pressure measurement

One finding of this research is that the injection pressure just before the injector inlet is not the same from cycle to cycle even if the engine is running at steady operating conditions; this will be discussed later in the Results chapter. The change in the injection pressure just before the injector inlet means that the amount of fuel injected inside the cylinder in each cycle is not the same, which will cause cyclic variability. As a result, a very fast response with a high precision Kistler pressure transducer is installed just before the injector of cylinder # 1 to measure the variability of the injection pressure from one cycle to another. Figure 3.15 shows the measuring chain of the pressure transducer.






Measure	Connect	Amplify	Output	Analyze
 Type 87XX... Low impedance	 Type 1761B... 10-32 pos BNC pos.	 Type 5114... Power supply / signal conditioner	 Type 1511 BNC pos. BNC pos.	 not supplied

Figure 3.15: Measuring chain of pressure transducer at the injector of cylinder #1.

Choosing the location where we could install the pressure transducer was a challenge because a change in the original design of the common rail or any change in the connection between the common rail and the injector itself will change the accuracy of the results. This is due to the fact that the common rail and the injector are very compact parts, and the flow inside both of them is designed according to a careful study to get the best damping of the pressure wave caused by the water hammer happening when the injector suddenly opens and closes. Figure 3.16 shows the location where the pressure transducer is installed the

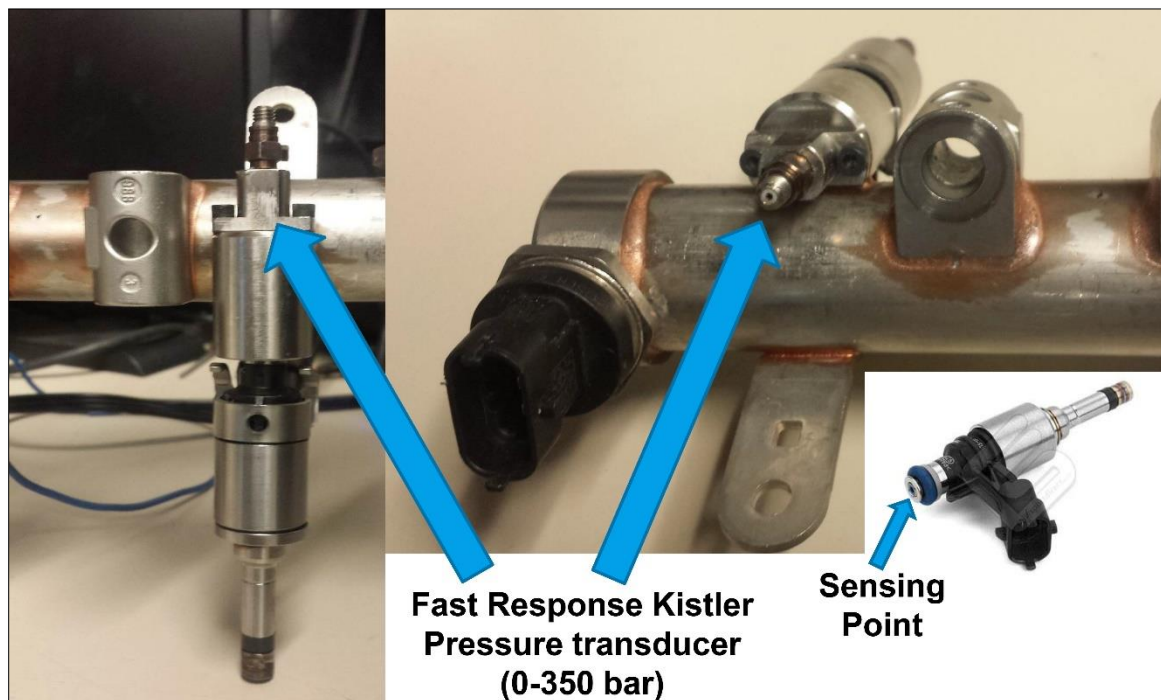


Figure 3.16: Image for the injection pressure measurement setup

### 3.18 Soot measurement.

An opacity meter is used to measure the soot from the engine. This device is installed just after the turbocharger to collect the total soot present from the engine. This opacity meter is operates based on the optical theories that scatter a light and measure the reflation of this light through the exhaust gases.



### 3.19 Nox measurement.

A very fast response Nox sensor designed by Continental is shown in Figure 3.17. It is a compact sensor based on the optical theory. The sensor is connected to the NI PXI system and there is a LabVIEW program is developed separately to control the operation of this sensor.



Figure 3.17, Continental fast response sensor for Nox measurement (Image source: NI Nox fast sensor)

### 3.20 Summary

The engine is heavily instrumented with all the necessary sensors and equipment to monitor all the conditions that might cause any variation between one cycles to another one. At the locations of the intake and exhaust ports of cylinder # 1, the temperatures and pressures are monitored using fast response sensors to capture the very small variations in 0.1 crank angle degree to study the effect of the fresh charge and the effect of the residuals. NO<sub>x</sub>, HC and soot have been measured instantaneously. The two Ion current circuits will be discuss in details in chapter 5.

## CHAPTER 4 ENGINE CONTROL UNIT DEVELOPMENT

### 4.1 Introduction

This chapter describes and outlines the open ECU developed to control the different engine parameters during tests such as injection timing, ignition timing, and turbocharger waste gate and throttle control. This in house ECU developed in one of the Center of Automotive Research laboratories in the Mechanical Engineering department, located in the Engineering Building, at Wayne State University.

The open ECU was developed using National Instrument (NI) software and DRIVVEN module hardware that is compatible with the NI software with a very fast impeded controller with a 500ks/s which allows the system to receive signals, make the appropriate and required analysis and calculations, come up with the recommended command for the ignition system and injection system, and then apply it on the engine.

The software used to develop the block diagrams is the LabVIEW 2012, which has the tools needed to develop the feedback control loop. Many block diagrams are developed separately and then merged together to work in the same calculating loop and some imported from the examples that is already provided with LabVIEW software.

Two types of hardware are used in this process. The first one used a data acquisition cards to receive the signals from the sensors mentioned in chapter 3, like the in-cylinder pressure, the ion signals from the fuel injector (MSFI) and the ion signal from the spark plug. The second type of hardware used to send the commands from the closed loop to the injection, ignition and throttle to control the engine.

### 4.2 The Developed ECU

The following section will describe in detail the open ECU and will include the following items:

1. The engine synchronizer
2. Data acquisition.

3. Ignition control
4. Injection control
5. Throttle control
6. Turbocharger waste gate controller

#### 4.2.1 The engine synchronizer

In order to control the engine and send a feedback signal at a specified time by the controller, first, we have to teach the controller how to detect the exact top dead center of the firing cylinder. In addition, start reading the signal from the sensor that is installed on the engine based on a crank angle degree, CAD, an engine synchronizer module, NI 9411, is connected to the encoder which is mounted on the engine crankshaft

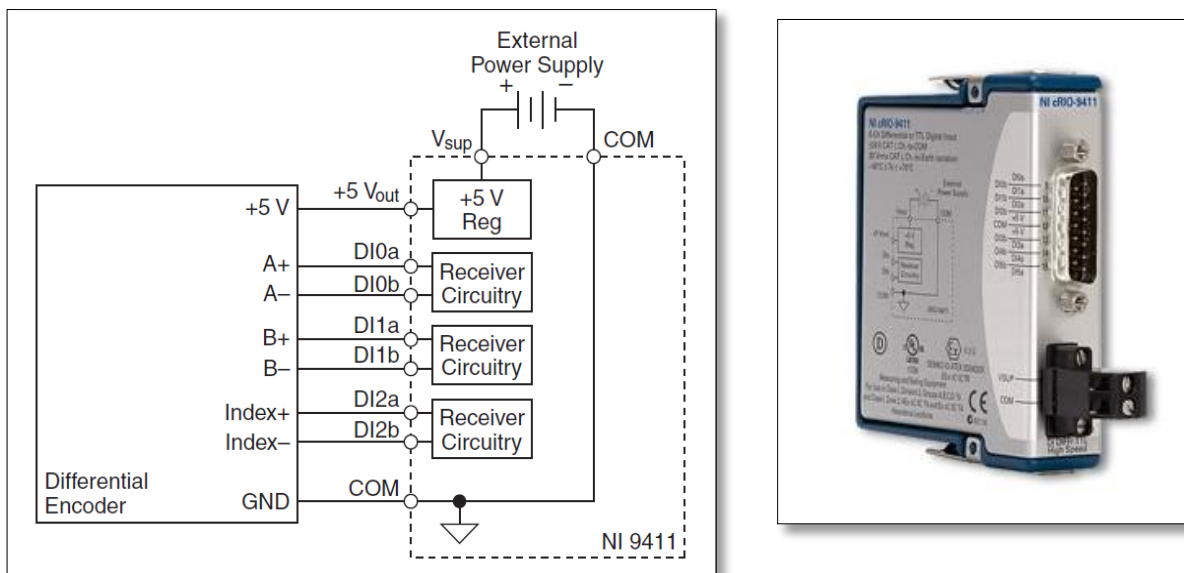


Figure 4.1: connecting a differential device to the NI 9411 (Image source: National Instrument NI 9411 Manual)

Figure 4.1 shows the schematic diagram of how the synchronizer, NI 9411, is connected to the ACCU encoder installed on the engine, connecting the A-signal, B-signal and Z- signal, to get the exact engine rpm and the reference cylinder, the fringing cylinder.

#### 4.2.2 Data Acquisition

Send a feedback signal to the engine needs to obtain some data from the engine first to make the appropriated calculation and analysis, then sending the desired command. Data acquisition card is used to acquire the data from the engine such as, in-cylinder pressure, engine rpm, intake manifold pressure and temperature, valve timing, etc.

A NI PXI 6123 high speed data acquisition card with a BNC 2110 analog/digital data acquisition board are used to acquire that data from the sensors mounted on the engine.



Figure 4.2: NI PXI 6123 high speed data acquisition card and BNC 2110 analog/digital data acquisition  
(Image source: National Instrument NI PXI 6123 Manual)

Figure 4.2 shows the data acquisition card and the 8-channel BNC board as all the sensors are connected to the data acquisition card through the BNC board using a BNC cables. This data acquisition card is fast enough to acquire the data in 500 kHz, which gives the controller the real time signal to make the right decision.

#### 4.2.3 The ignition control

Controlling the ignition is very critical because most automotive companies adjust the spark timing to run the engine on a point so they could achieve the maximum break torque, MBT, by taking into consideration the knock limit. To satisfy this criteria, we used a high accuracy ignition control

system using the DRRIVEN ignition module to send the ignition command, the square wave command (TTL output module), to the ignition coil at the desired spark timing with the desired volt.

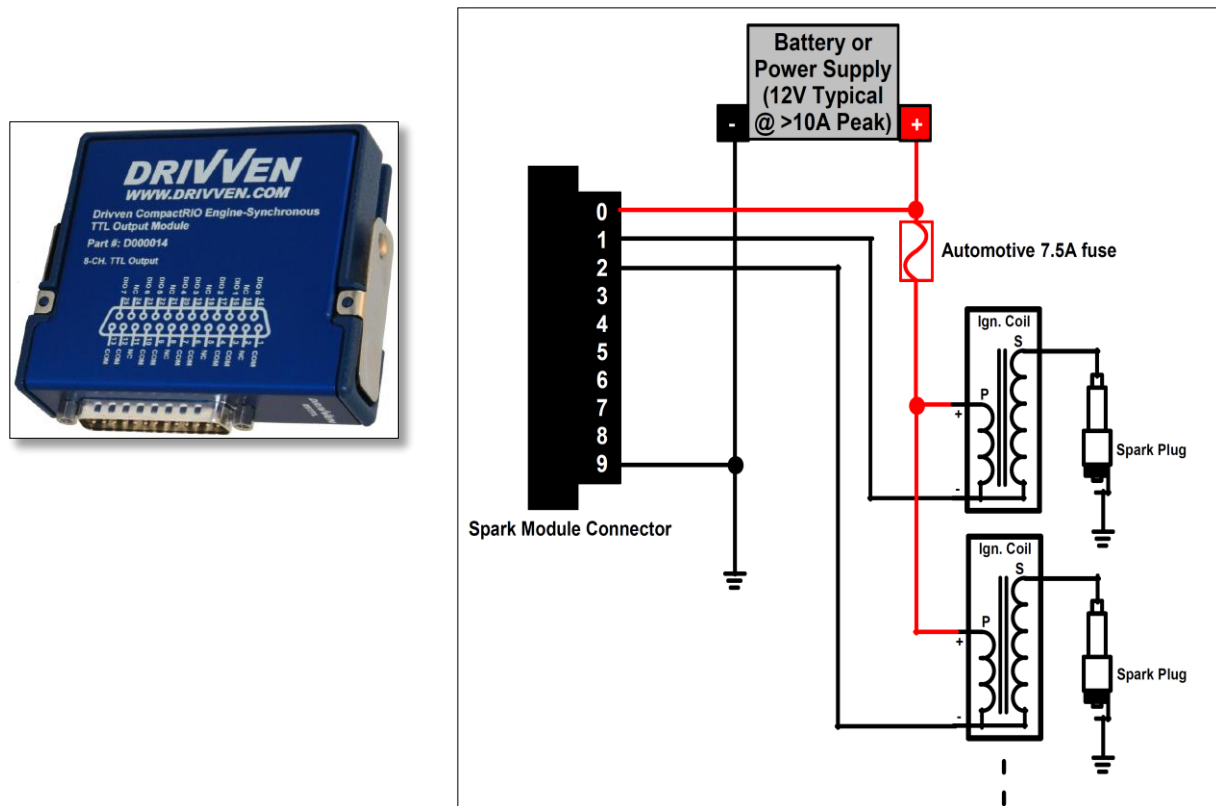


Figure 4.3. Connecting ignition coils to the driver module. (Image source: National Instrument NI PXI 6123 Manual)

Figure 4.3 shows the ESTTL module and the circuit that connect the ignition module to the engine ignition coil. This system uses a battery as the power source to simulate the power supply from the car battery. The engine synchronizer sends the accurate location of the top dead center to this loop, and this loop has a manual control to determine the start of the coil charge as well as the charging time and the discharge time based on the crank angle degree to advance or retard the spark timing regarding the test conditions. In addition, this loop is designed to control the spark timing in msec.

#### 4.2.4 The injection module

The engine used in this research is a gasoline direct injection engine, and the injector used inside the combustion chamber to inject the fuel is a solenoid injector. The fuel injector is designed by the manufacture to respond to a certain injection profile as shown in Figure 4.4

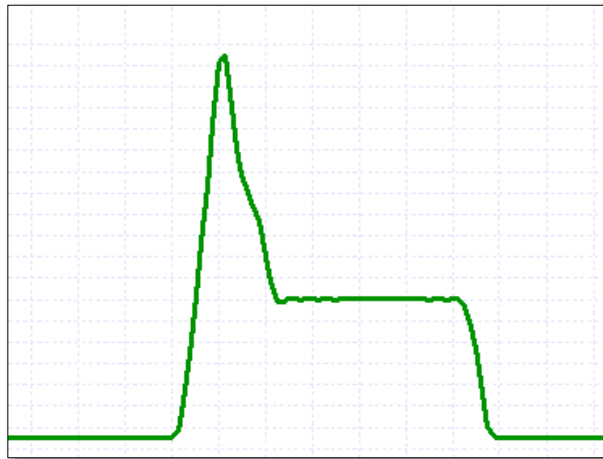


Figure 4.4: GDI injection profile.

Figure 4.5 shows the connection between the fuel injector and the direct injection module, each module designed to control three injector; therefore, two modules used to control the four injectors because the engine used in this research is a 4-cylinders engine.

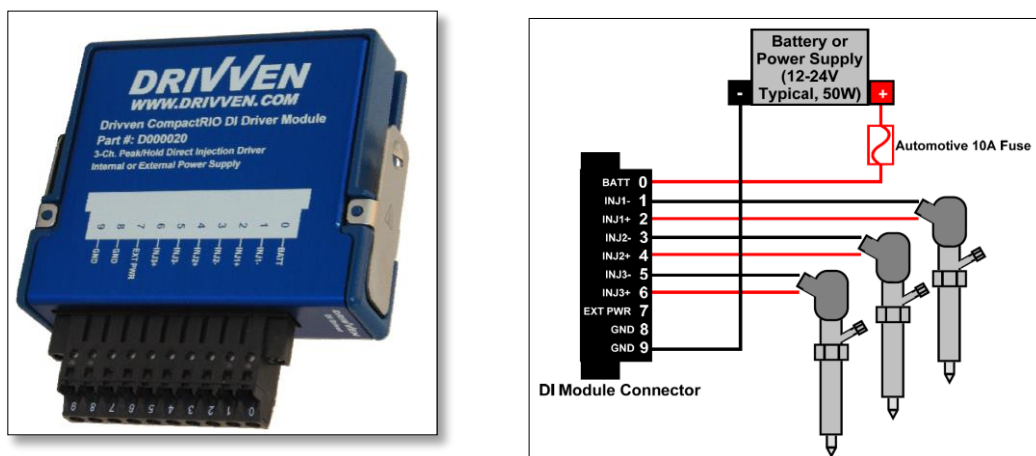


Figure 4.5. Connecting direct-injectors to the driver module (Image source: National Instrument injector driver control Manual)

#### 4.2.5 The throttle module

With the new technology, the electronic throttle control is used as the control system for the amount of charged air getting into the engine. This throttle has two sensors: one to control the idle, and the other to control the normal operating conditions.

A LabVIEW program is used to control the throttle; interface hardware is used between the throttle control block diagram, and the engine throttle body is a DRIVEN throttle driver module D000017 as shown in Figure 4.6. The schematic diagram of the connections between the throttle body and the module is shown also in Figure 4.6

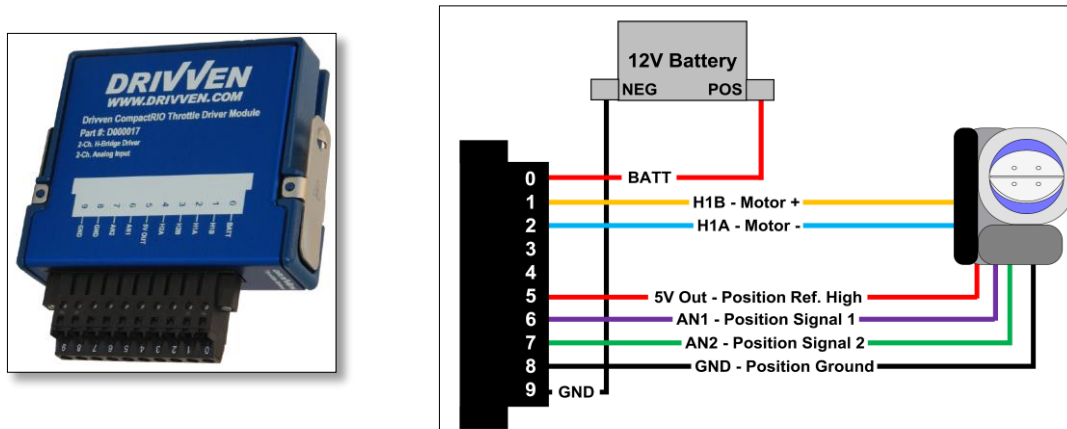


Figure 4.6. Module terminal connections to a single electronic throttle body (Image source: National Instrument throttle body control Manual).

#### 4.3. Summary

The engine control module developed for this engine has full control over the main engine operating parameters such as the spark timing (start, end, and duration), the injection characteristic (start of injection, end of injection, and the injection profile), the turbocharger waste gate and the throttle control. In addition, this feedback closed loop control was developed to gather the data from the engine and use these data to adjust the spark, injection and the throttle to reduce cyclic variability in addition to maintaining the engine running at the maximum brake torque.

## CHAPTER 5 IONIZATION CHARACTERISTICS TURBOCHARGED GASOLINE DIRECT INJECTION ENGINE

### 5.1 Introduction

The ionization in gasoline engine is of two types, chemical and thermal. The next sections explain in details the sources of ionization in spark ignition engine.

### 5.2 Sources of the Ion Current in Hydrocarbon-Air Flames

In hydrocarbons air flames, the main sources of the ion current are chemi-ionization and thermal ionization [12, 15, and 16].

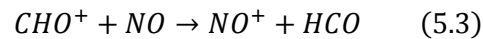
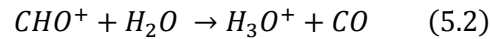
#### 5.2.1 Chemi-Ionization

Chemi-ionization in hydrocarbon-air flames is mainly caused by reactions between the CH radical and the oxygen atom and other combustion intermediates according to the following reactions: [17, 18, 19, 20, and 21]:

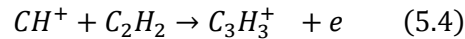


It should be noted that the initiation of ionization is by the CH radical. The ion current was not detected in a gasoline engine fueled by hydrogen [22].

Reaction (1) is slow compared to the following charge transfer reactions:



Reaction (5.2) is dominant in lean and slightly rich hydrocarbon air-flames and produces H<sub>3</sub>O<sup>+</sup> ions [23]. In rich and sooty hydrocarbons air flames, reaction (5.4) is dominant [23, 24] and produces C<sub>3</sub>H<sub>3</sub><sup>+</sup> ions.

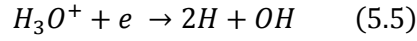


In sooty flames, charge transfer may occur between small ions such as C<sub>3</sub>H<sub>3</sub><sup>+</sup> and H<sub>3</sub>O<sup>+</sup> and large poly nuclear aromatic hydrocarbons. The ionization potential of these large molecules is small



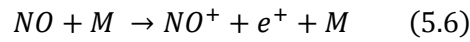
enough that the charge transfer is thermodynamically favorable [26]. In addition negative ions can be formed and contribute to the ion current.

The ionic recombination reactions are:

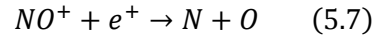


### 5.2.2 Thermal Ionization

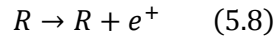
The formation of ions at high temperatures in close-to stoichiometric hydrocarbon-air flames is mainly caused by the following reaction



“M” is any species that can chemically interact with the NO molecule at high temperature to produce an ionized NO molecule. The destruction of  $NO^+$  ions is by



In fuel rich hydrocarbon-air flames, a fraction of the large hydrocarbon molecules and soot particles, both presented by R, can be ionized directly by reaction (5.8) [25].



## 5.3 Characteristics of Ion Current Signals

### 5.3.1 Ion Current signal from the Spark Plug

Figure 5.1 shows the electric circuit used in this research to measure the ion current in SI engines using the spark plug as an ion current sensor. A DC voltage, V, is applied across the spark plug gap, directly after the discharge of the main electric charge to produce the spark required to ignite the mixture and start the combustion process. In the current investigation, the central electrode is the cathode. Figure 5.2 shows sample traces of the ion current, cylinder gas pressure, rate of heat release and integrated rate of heat release.

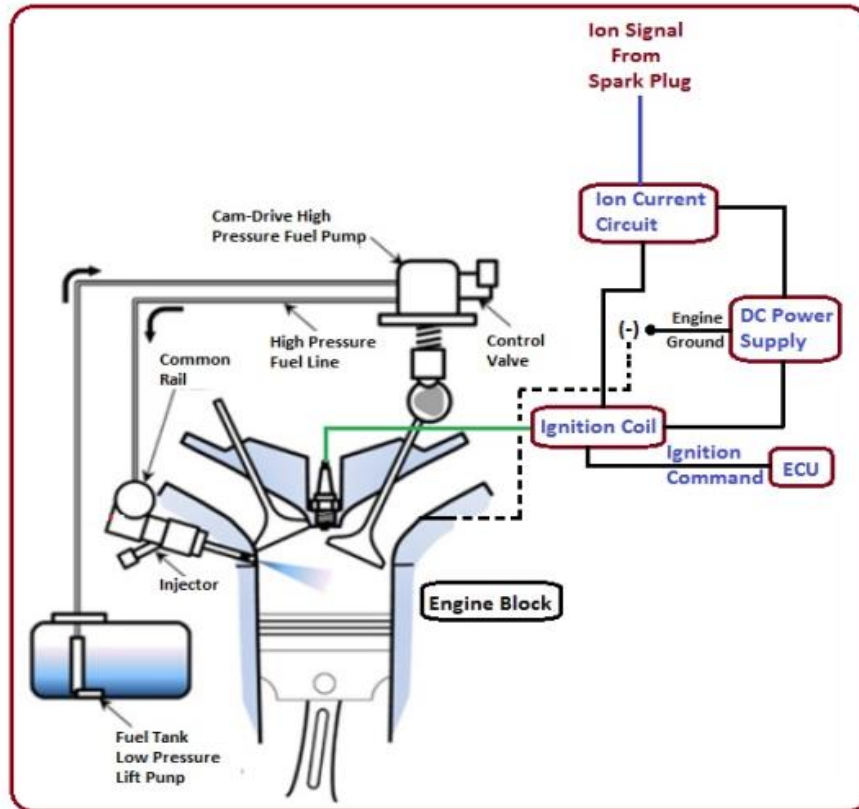


Figure 5.1: Electric circuit for ion current measurement in a spark plug

The figure shows that a spark breakdown occurred at 14 degree bTDC, and the positive rate of heat release started at 3 degree dBTC when the chemi-ionization is detected. There are two major peaks in an ion current signal. The first peak indicates the formation of a high concentration of chemi-ionized species around the spark plug gap, caused by the flame kernel in the very early stages of the combustion process. The first peak, caused by reactions 5.1, 5.2, 5.3 and 5.4, is followed by a drop in the ion current produced by the recombination reaction 5.5. The second peak is due to the thermal ionization of combustion products, such as NO, caused by the increase in the local temperature as indicated in reaction 5.6.

The increase in the local temperature is caused by the increase in the cylinder gas temperature associated with the increase in cylinder gas pressure.

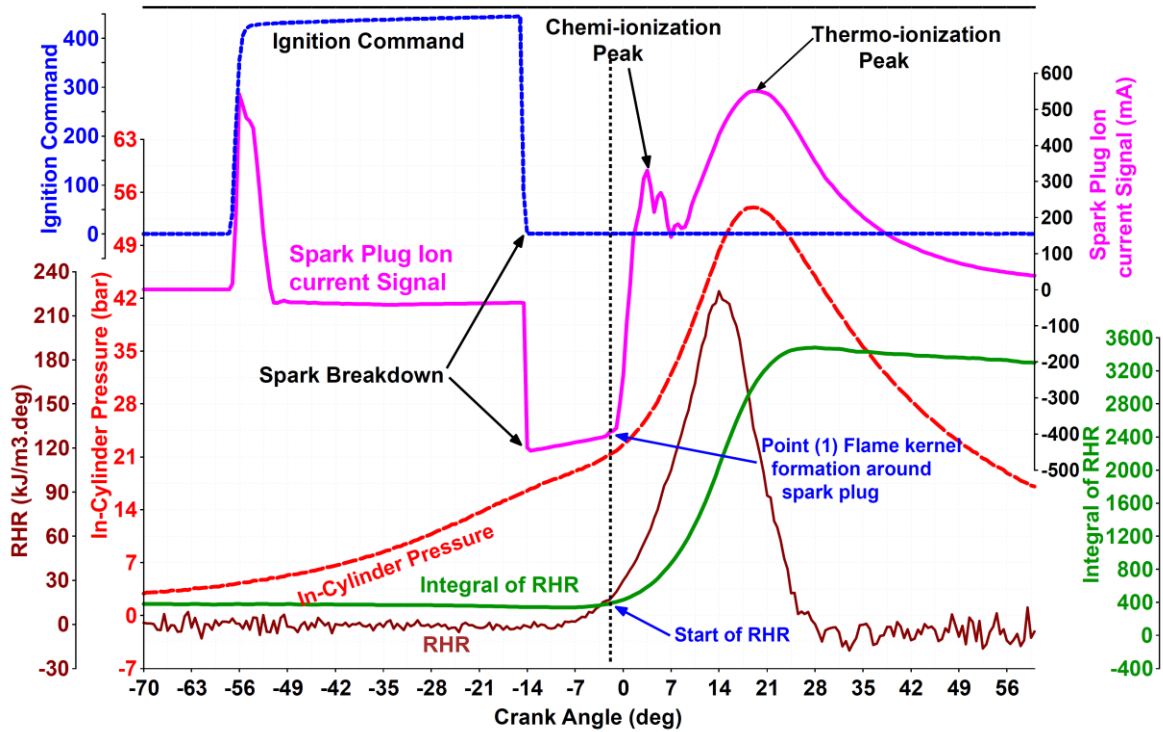


Figure 5.2 Sample of cylinder gas pressure, ignition command, and the ion current signal from the spark plug, zoomed in traces at 1500 rpm, 175 N. m (11.0 BMEP).

### 5.3.2 Ion Current signal from the fuel injector (MSFI).

Figure 5.3 shows a schematic sketch of the multi-sensing fuel injector (MSFI) system. The system consists of a pair of electrically isolated electrodes separated by a gap where the fuel injector nozzle acts as one electrode and the engine block acts as the other electrode. The fuel injector, located within the combustion chamber of the GDI engine, is electrically insulated from the rest of the engine body using non-conducting material.

The electric circuit for the injector includes a 100 V DC power supply. The negative potential terminal is connected to the engine body. The ion current signal from the MSFI is measured in terms of voltage drop across a resistor. A signal conditioning unit and an amplifier are included in the circuit. The amplifier can be integrated with low pass or high pass filters to reshape the incoming sensor output signal for control purposes.

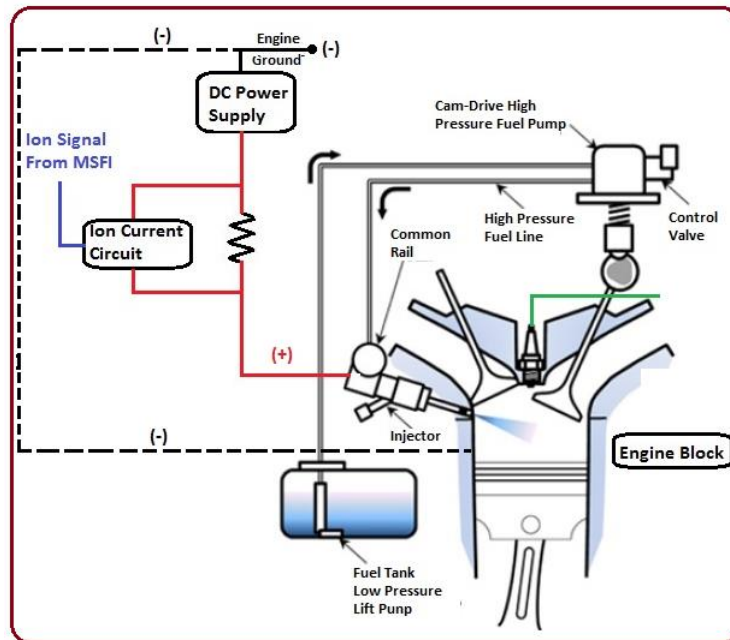


Figure 5.3 Electric circuit for use of the injector as an ion current sensor.

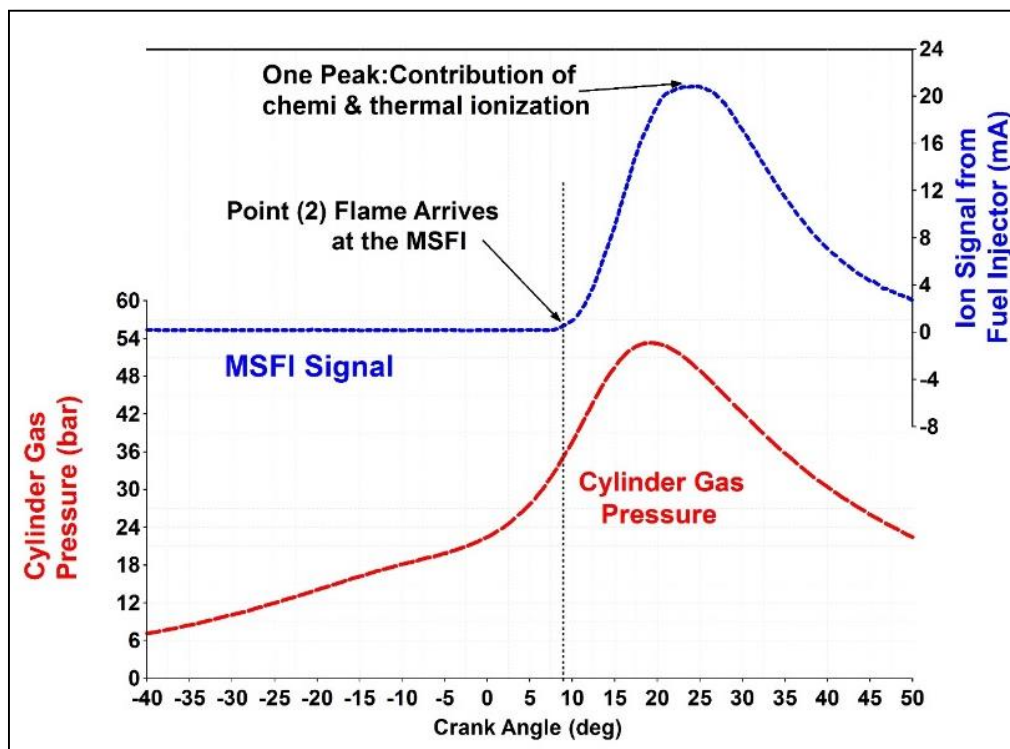


Figure 5.4 Sample of cylinder gas pressure and the ion current signal from the fuel injector. Zoomed in traces at 1500 rpm, 175 N.m (11.0 BMEP)

Figure 5.4 shows sample traces obtained from the MSFI and the cylinder gas pressure. The rise in the signal indicates the time of arrival of the flame at the tip of the injector. The phase shift between the ion current signals from the injector and the spark plug is the time taken by the flame to travel between the two locations.

#### 5.4 Sensors location in the combustion chamber

The in-cylinder pressure transducer is mounted in the middle of the combustion chamber, and the fuel injector is mounted at the peripheral of the combustion cylinder. The distance between the tips of the two sensors is 41.5 mm.

Figure 5.5 shows the configuration of the two sensors inside the combustion chamber. Point (1) is the location of the tip of the spark plug pressure transducer, and point (2) is the location of the tip of the fuel injector (MSFI); the distance between them  $\Delta x$  is equal to 41.5 mm.

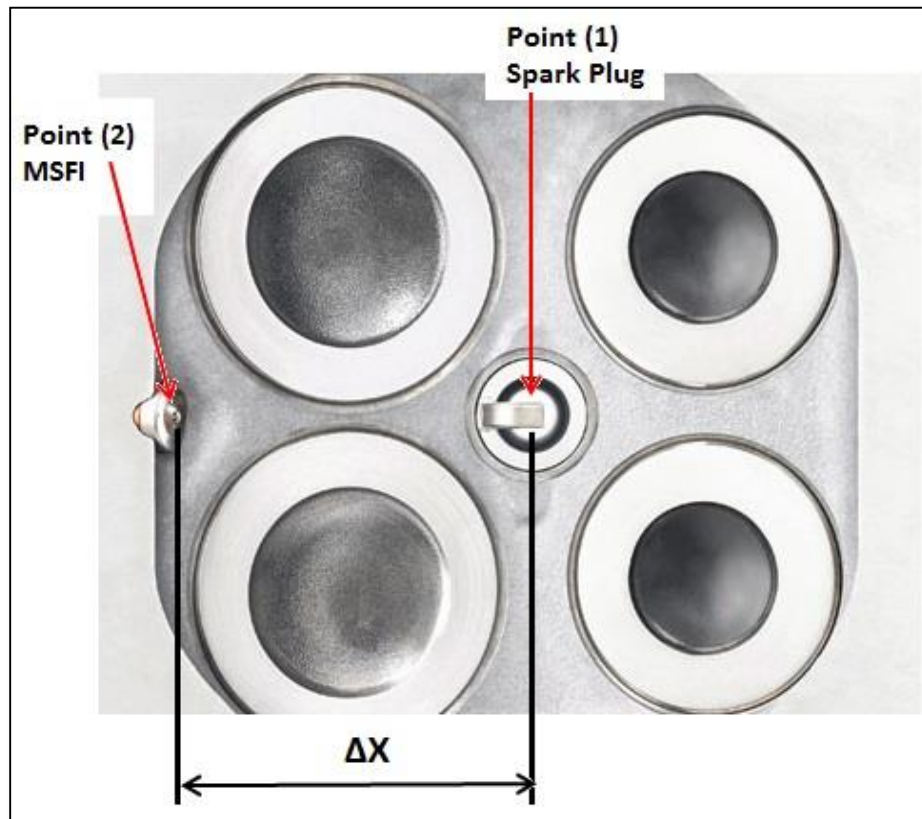


Figure 5.5 Picture of the cylinder head showing the locations of the MSFI and spark plug.

Figure 5.6; shows sample traces of the cylinder gas pressure, injection command, and ion current measured by the spark plug, as well as ion current measured by MSFI and ignition command. The traces are the average of 100 cycles. Engine speed was kept constant at 1500 rpm with the throttle valve fully opened.

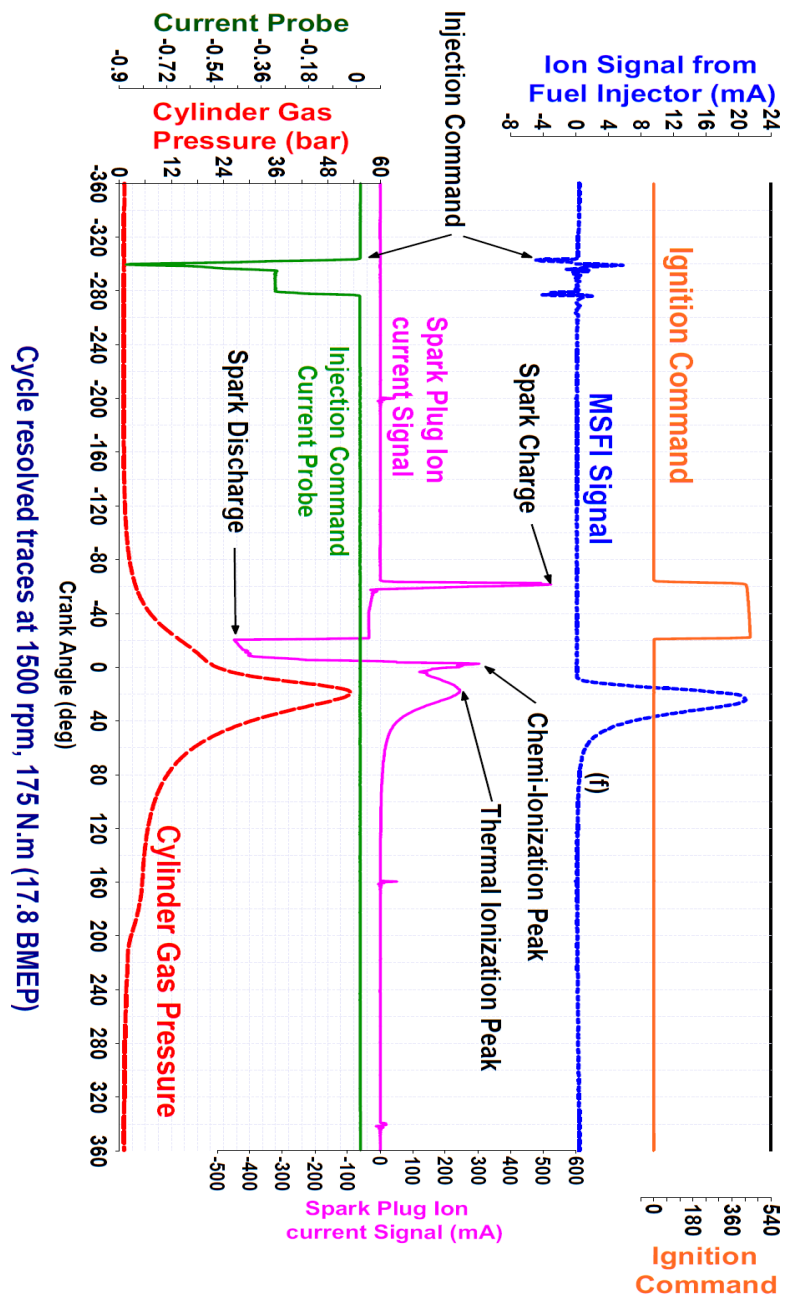


Figure 5.6 Cycle-resolved traces for the ignition command, MSFI signal, spark plug ion current, injection command and cylinder gas pressure.

### 5.5 Ionization in the combustion chamber

Figure 5.7 shows zoomed-in traces of cylinder gas pressure, the ion current from the spark plug and from the MSFI. The signal from the spark plug indicates the timing of the ignition coil charge and discharge. Point (a) represents the start of ionization at the spark plug. Point (b) is the first peak of the spark plug ion current, point (c) is the start of the ion current due to flame arrival at the injector, point (d) is the second peak of spark plug ion current, point (e) is the peak of the ion current signal from the fuel injector, and point (f) is the end of detection of ionization at the fuel injector. The location of piston at each of the above points is given in Figure 5.8.

Figure 5.8 shows the location of the piston in six positions from the flame kernel formation around the spark plug to the end of the ion current detection by the MSFI.

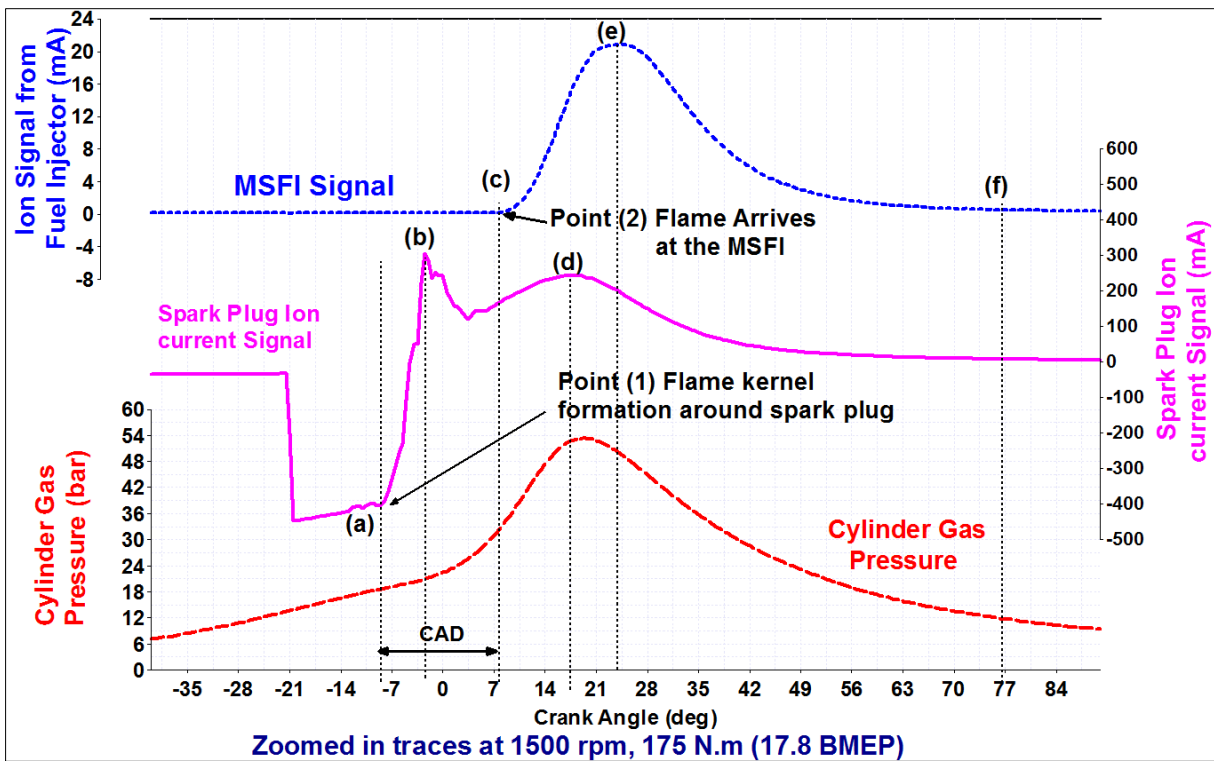


Figure 5.7 Zoomed in traces at 1500 rpm and 175 N.m (11.0 BMEP)

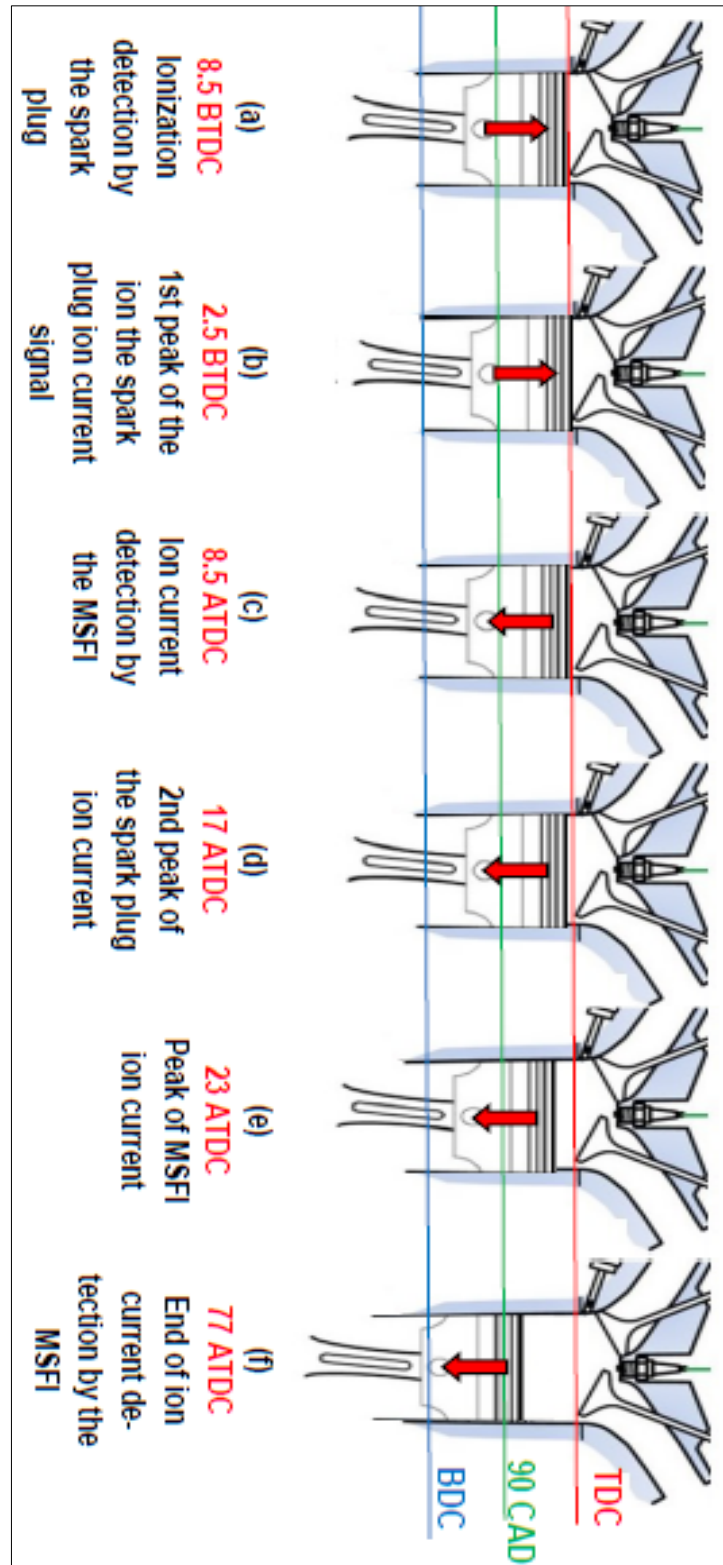


Figure 5.8 Piston locations at key points of the figure



## 5.7 Summary

The spark plug and the fuel injector have been used as ion current sensors. Signals received from the two sensors are processed and the phase shift between them is determined. The two signals were received by custom designed electronic circuit to make the necessary conditioning to feed them into the data acquisition system for and processing and phasing with crank angle degrees with a resolution of 0.5 CAD.

The ion current signals from the fuel injector and spark plug were able to detect the engine knock with 0.1 crank angle degree resolution. This detection compared to the data from the knock sensor and the knock detected by ionization showed a good agreement with the knock detected by the knock sensors. This results could allow the engine designers to replace the knock sensors and use the ionization technique to detect engine knock from each cylinder and allow cycle to cycle ignition control as well as cylinder to cylinder control.

## CHAPTER 6 BURNING VELOCITY IN GDI ENGINE

### 6.1 Introduction

Many approaches have been taken to determine the burning velocity in internal combustion engines. Experimentally, the burning velocity has been determined in optically accessible gasoline engines by tracking the propagation of the flame front from the spark plug to the end of the combustion chamber. These experiments are costly as they require special imaging techniques and major modifications to the engine structure. Another approach to determine the burning velocity is using 3D CFD simulation models. These models require basic information about the mechanisms of combustion which is not available for distillate fuels in addition to many assumptions that have to be made to determine the burning velocity. Such models take long periods of computational time to execute and have to be calibrated and validated through experimentation.

This section presents a new technique to determine the burning velocity in a production engine without making any modification to its structure or use any high speed imaging equipment. This technique is based on the combustion-produced ionization measured at two defined locations in the combustion chamber. In the engine used in this investigation, the spark plug is used as an ion current sensor which indicates the time the flame kernel is formed around the spark plug gap. In addition, the fuel injector is used as an ion current sensor, after which it is electrically insulated from the cylinder head. The time between the start of the ionization at the two locations is used to calculate the burning velocity. The use of this technique to determine the cycle to cycle variation in the burning velocity and other combustion parameters is demonstrated with the engine operation at a steady speed and load.

Demands for improved fuel economy and high power density, in addition to reduced emissions, require an improved understanding of combustion processes in direct injection gasoline engines, which are widely used in passenger cars and light duty vehicles. This requires a detailed analysis of complex fluid dynamic, thermodynamic and chemical processes which affect the combustion process. Due to

changes in these processes during the engine cycle, there is a need for computer simulations to determine the effect of different design and operating variables on combustion. Computer simulations enhance the development of strategies for the engine control unit (ECU) to optimize engine operation and achieve the production targets. Of primary importance is the validation of the simulation predictions with experimental data to ensure the validity and accuracy of the models. One of the key parameters that would indicate the quality of a simulation model is the burning rate of the fuel-air mixture.

## **6.2 Ionization in the combustion chamber**

Figure 6.1 shows zoomed in traces for cylinder gas pressure and ion current from the spark plug and from the MSFI. The signal from the spark plug indicates the timing of the ignition coil charge and discharge. Point (a) represents the start of ionization at the spark plug. Point (b) is the first peak of the spark plug ion current, point (c) is the start of the ion current due to flame arrival at the injector, point (d) is the second peak of spark plug ion current, point (e) is the peak of the ionization from the fuel injector, and point (f) is the end of detection of ionization at the injector. The location of the piston at each of the above points is given in Figure 6.2.

Figure 6.2, shows the location of the piston in six positions from the flame kernel formation around the spark plug to the end of the ion current detection by the MSFI.

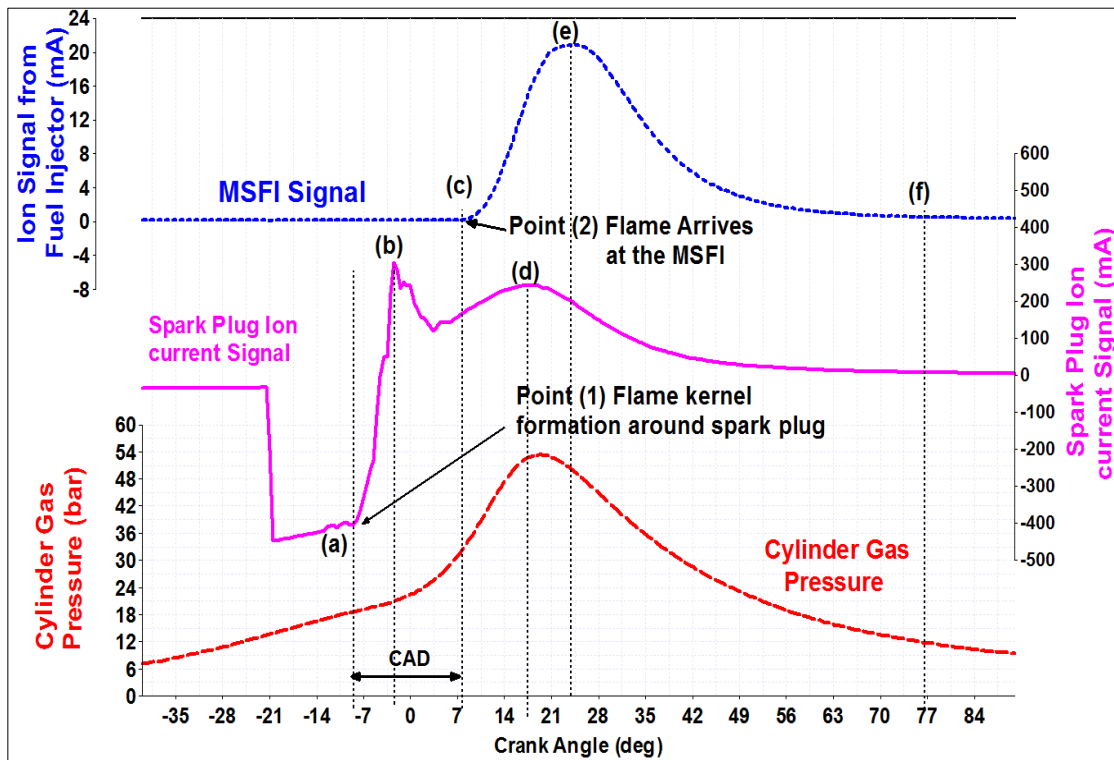


Figure 6.1 Zoomed in traces at 1500 rpm and 175 N.m (11.0 BMEP)

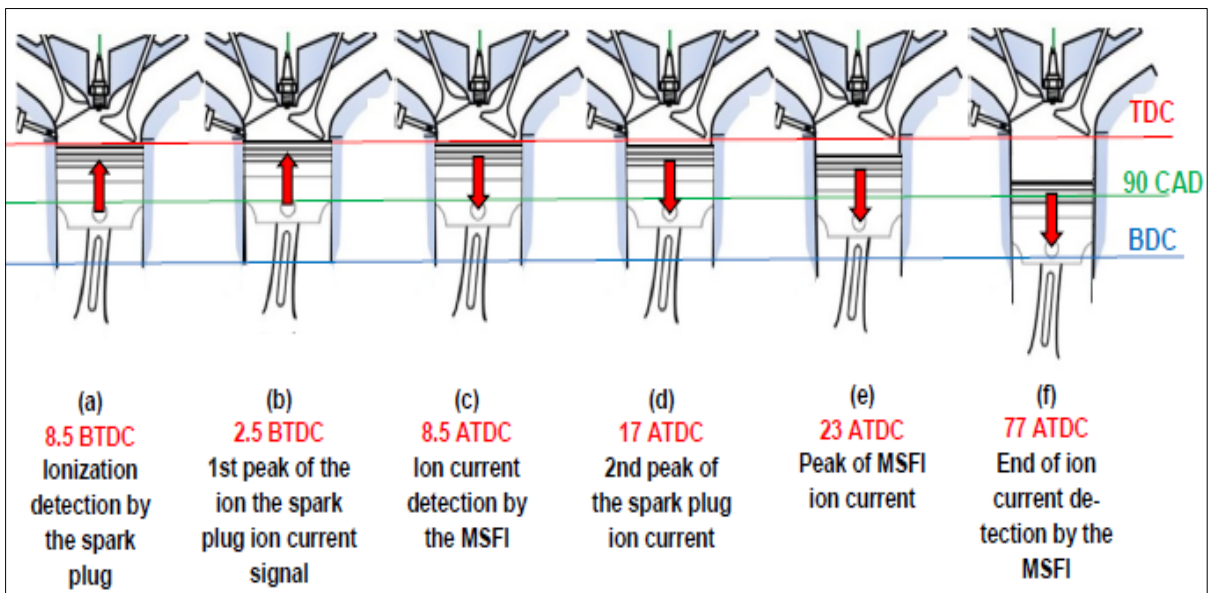


Figure 6.2 Piston location at key points of figure 6.1

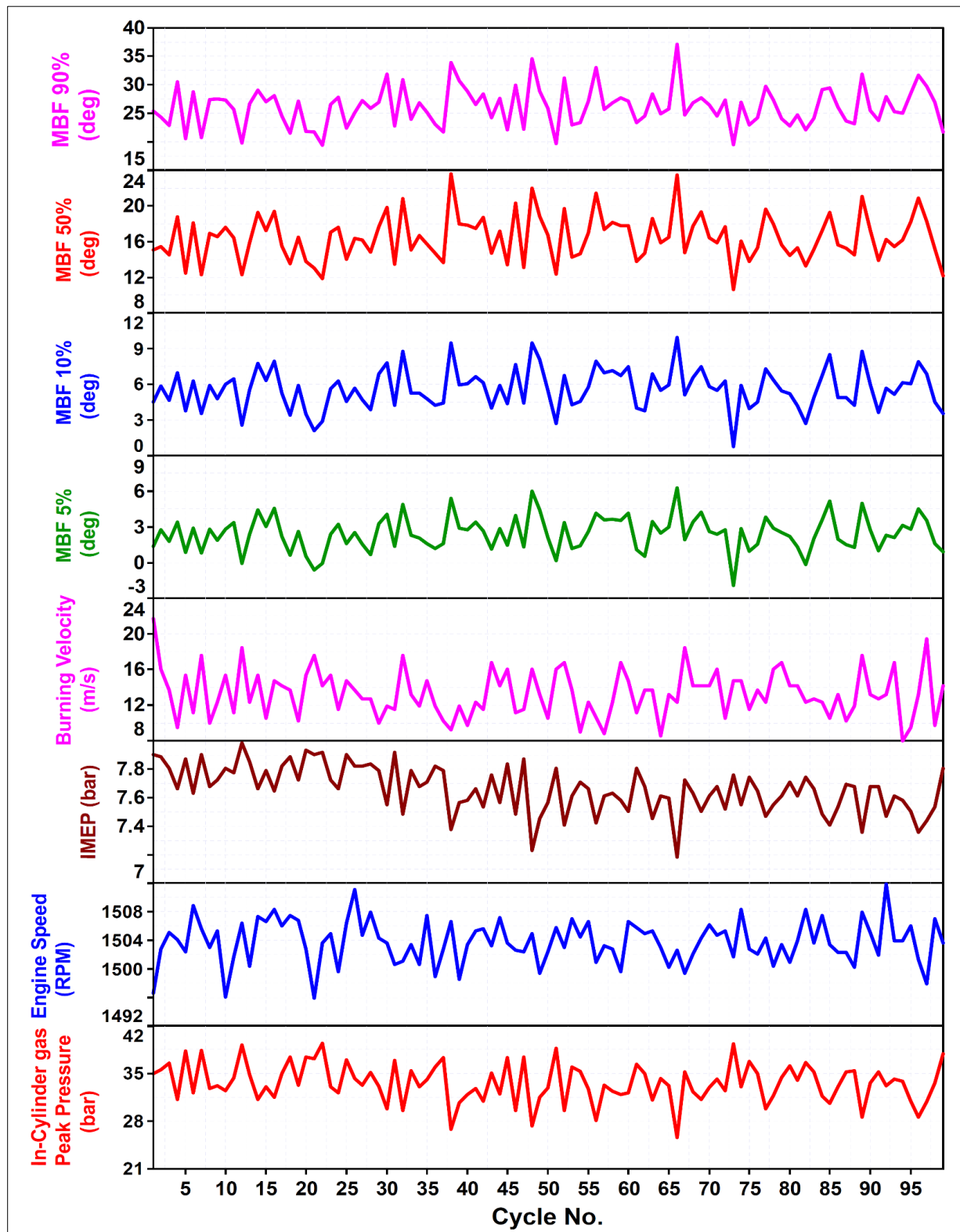


Figure 6.3 Cycle to cycle variation of 100 consecutive cycles

Figure 6.3 shows the variation of the burning velocity with the variation of the IMEP for 100 consecutive cycles. The figure shows the peak pressure, engine speed, IMEP, burning velocity, MBF 5%, MBF 10%, MBF 50% and MBF 90% for each cycle for 100 consecutive cycles. These data showed that the burning velocity for each cycle showed a variation that agreed with the variation of the IMEP of each cycle. That could lead to a conclusion that the burning velocity for each cycle represent the cyclic variability of IMEP.

### 6.3 Effect of Speed and Load on Burning Velocity

Figure 6.4 shows the effect of engine load on the average burning velocity at different engine speeds. The average burning velocity increases slightly with the increase in load up to about around 50% of a full load, followed by a sharper increase up to 75% of a full load, and it continues to increase at a lower rate until there is a full load. This sharp increase is because the turbocharger started to act to increase the boosting pressure and in consequence increasing the tumble and turbulence. This shows that the turbulence increases the burning velocity and enhancing the combustion process.

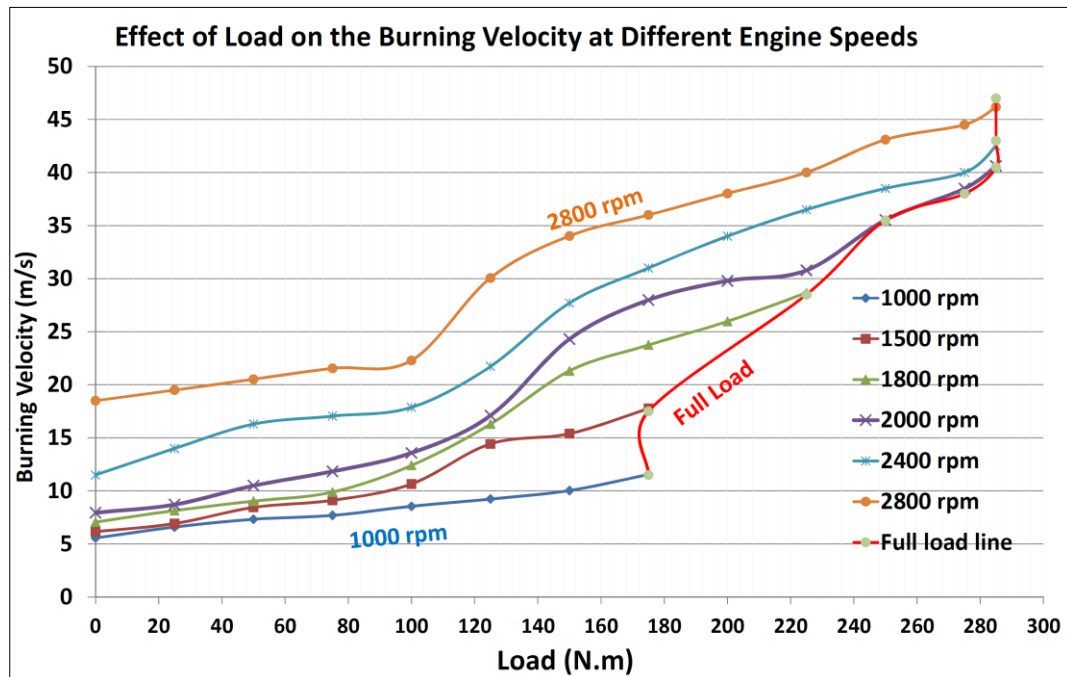


Figure 6.4. The effect of engine load on burning velocity at different engine speeds

The results shown in Figure 6.4 are plotted in Figure 6.5 to show the effect of speed on burning velocity at different engine BMEP. The burning velocity increases continually with speed but at different rates which depend on the engine load.

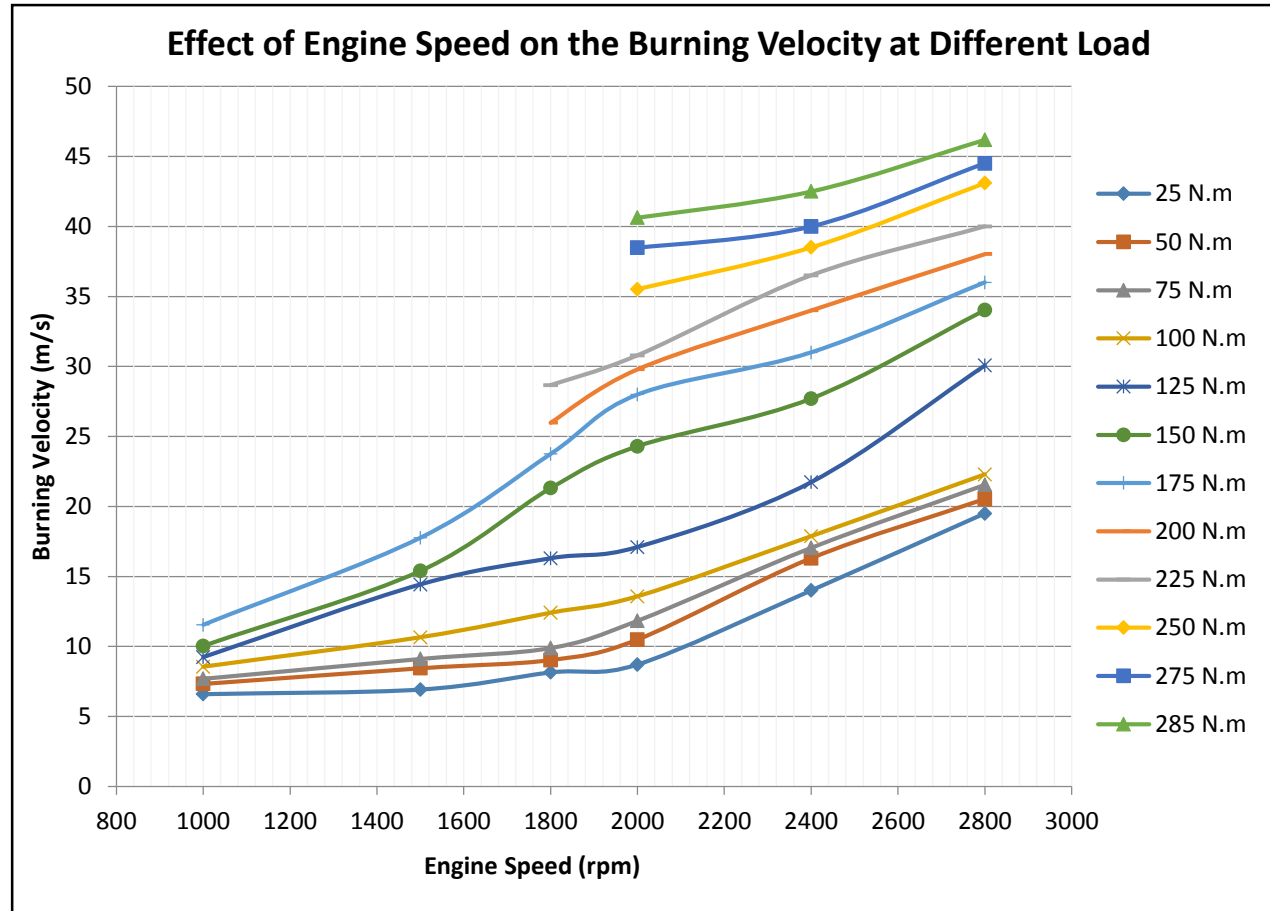


Figure 6.5. Effect of engine speed on burning velocity at different engine loads

#### 6.4 Effect of injection timing and spark timing on Burning Velocity

Figure 6.6 shows the effect of ignition timing on the burning velocity at a constant operating condition of 1750 rpm and 50 N.m. The burning velocity decrease with spark advance or retard as well the IMEP decreased too. This results showed that the point that has the highest IMEP which represent the MBT, also, is the point that has the highest burning velocity. This conclusion can be used in engine control to keep the engine running on the MBT continually.

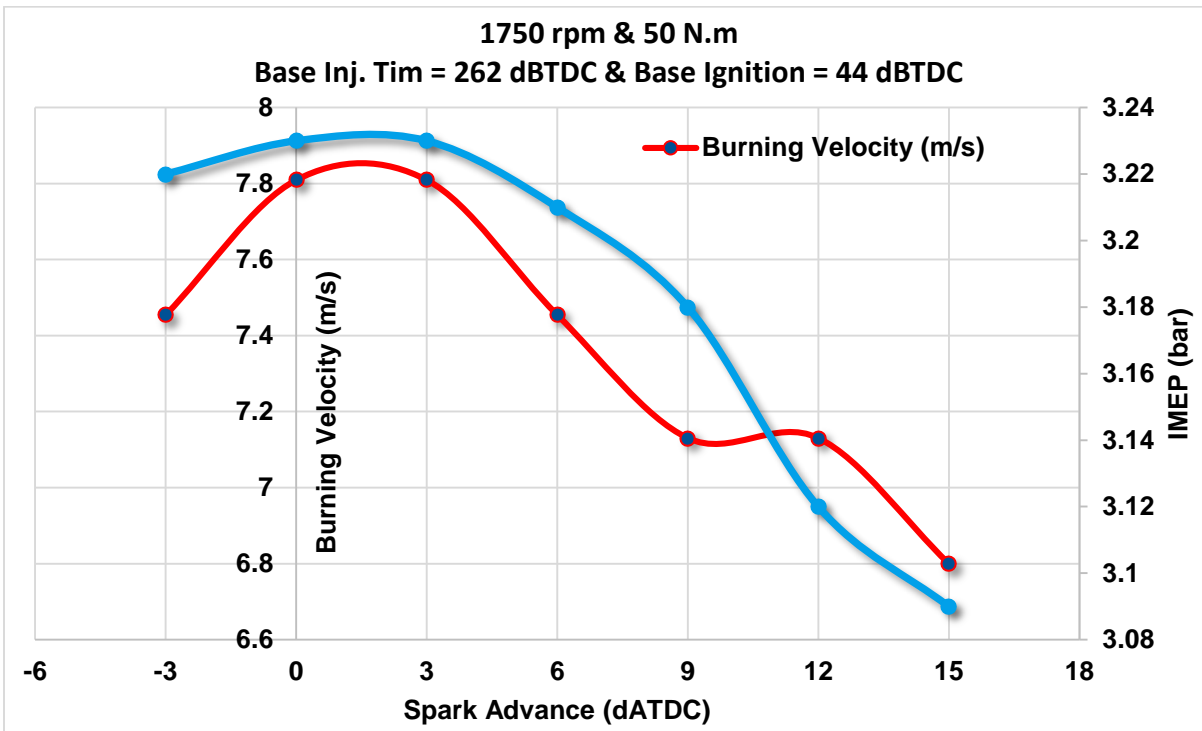


Figure 6.6. Effect of ignition timing on burning velocity at 1750 rpm and 50 N.m.

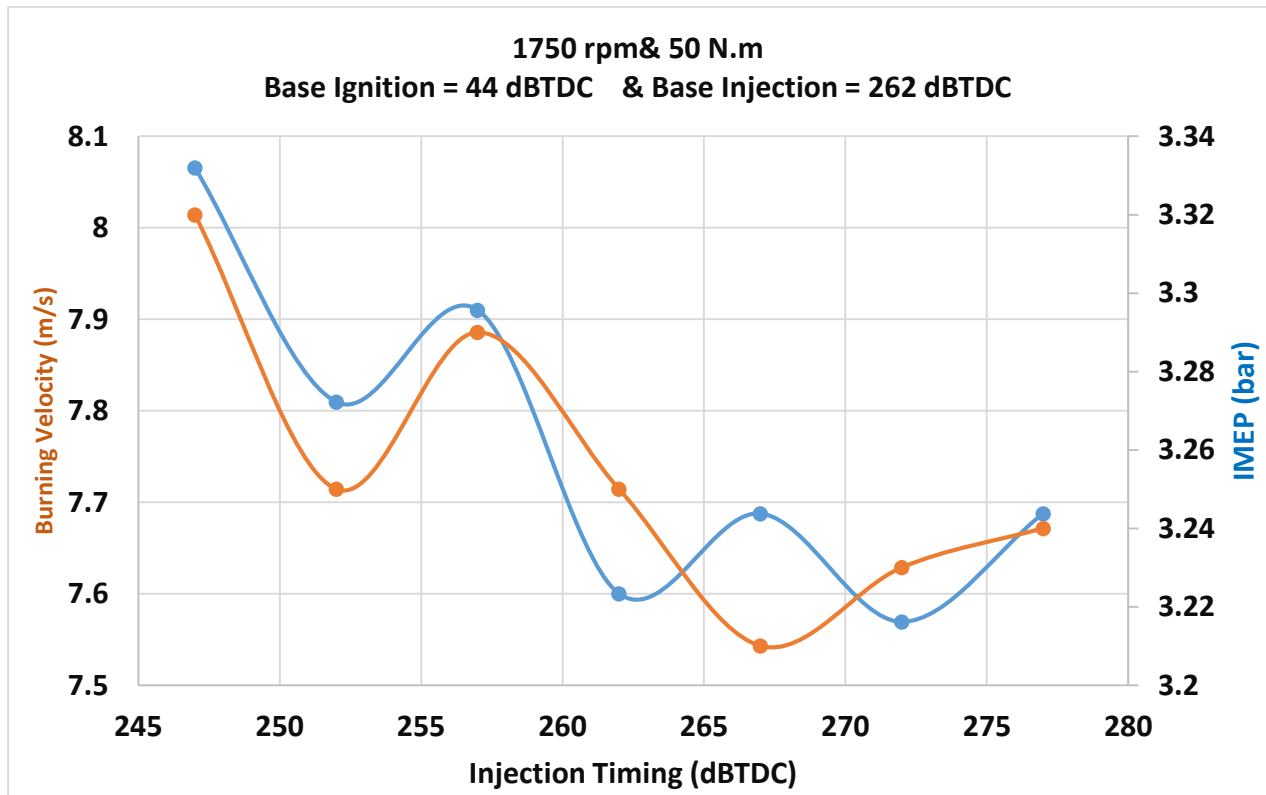


Figure 6.7. Effect of injection timing on burning velocity at 1750 rpm and 50 N.m.



The effect of injection timing on the burning velocity is shown in Figure 6.7. Injecting the fuel early into the intake stroke is increasing the chance for fuel hits the walls; then the piston surface allows some of the fuel not to mix with the air which in consequence will decrease the equivalence ratio at the spark plug and will increase the ignition delay. On the other hand, retarding the injection to a certain limit decreases the probability of the fuel hitting the wall and will enhance the overall equivalence ratio which will help decreasing the ignition delay and enhance the early flame development stage MBF 0% to MBF 10%. The results are shown in figure 6.7 proved that the burning velocity improves when retarding the injection timing to enhance the mixing process and start the combustion at the desired timing to keep the engine running at the MBT.

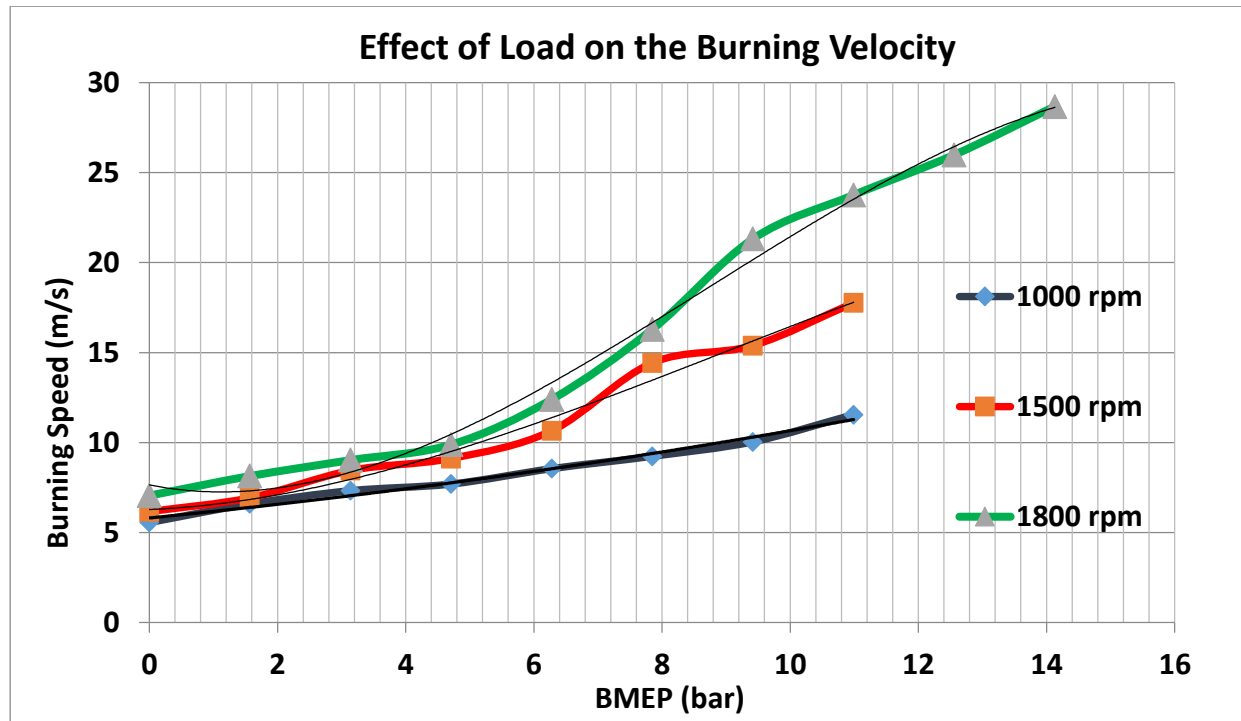


Figure 6.8. Effect of engine speed on burning velocity at different engine load.

The burning velocity is affected by the engine load as shown in Figure 6.8. The general trend is that the burning velocity increases with engine IMEP at fixed engine speed. Correlations have been developed to correlate the engine load (IMEP) to the burning velocity. The burning velocity can be calculated from the two ion current signals; therefore, the developed correlation can be used to

accurately calculate the actual IMEP generated from one cylinder without the need for pressure transducer. This information is used as a feedback signal to the closed loop ECU that developed in this research

## **6.8 Summary**

A new technique has been developed to determine the burning velocity between two key locations in the combustion chamber of a direct injection gasoline engine: the spark plug and the fuel injector. This technique is unique, since it does not add any component to the engine and does not require any modification to the engine. It utilizes the spark plug and fuel injector as ion current sensors. Results of sweep tests indicated the strong dependence and continual increase in the burning velocity at higher speeds and loads.

## CHAPTER 7 CYCLE TO CYCLE VARIATION INVESTIGATION

### 7.1 Introduction

This chapter will discuss in details all the parameters that causes cyclic variation in cylinder # 1 in a gasoline direct injection engine. We believe that the cyclic variability will manly depend on all the inputs to the current cycle including the effect of the previous cycle on the current cycle. In order to track the cyclic variability, this research will focus on cylinder # 1, to track all the inputs and outputs from this cylinder and study cycle by cycle. The schematic diagram shown in Figure 7.1 shows the cylinder as a control volume and explains all the inputs to and outputs from the cylinder as follows;

- 1- The intake air pressure and intake air temperature and valve duration which represent the amount of fresh charge get into the cylinder.
- 2- The exhaust pressure and temperature from the previous cycle and EVC which represent the amount of residuals remaining the cylinder from the previous cycle.
- 3- Instantaneous injection pressure and injection command characteristics which represent the amount of fuel injected in the
- 4- Piston speed during the intake stroke and combustion stroke which affect the turbulence during the mixing process and the combustion duration.
- 5- Effect of valve overlap.

### 7.2 Cyclic variation experimental test matrix

The experimental investigation has been conducted on a GDI engine on the common operating conditions. The selected operating conditions has been chosen deepen on the regular range of engine speed from 1000 rpm to 2000 rpm with increment 250 rpm. In addition, at each operating speed, we loaded the engine from 0% load to 60% of the rated engine torque. The test matrix is shown in the Table

							COV% of 300 consecutive cycles						
Test #	Speed (rpm)	Load (N.m)	IAT	T <sub>win</sub> C <sub>o</sub>	T <sub>wout</sub> C <sub>o</sub>	T <sub>exh</sub> C <sub>o</sub>	COV % IMEP	COV % PP	COV % SOIC	COV % MSFI Peak	COV % SOI	COV % EOI	COV % Inj_Dur
1	1000	22	31	29	78	233	2.43	9.67	36	28.4	0.133	0.2	7.51
2		52	30	30	80	290	2.12	9.07	86	30.9	0.068	0.287	9
3		76	30	29	82	340	1.68	8.09	112	27.8	0.062	0.284	7.33
4		95	31	31	83	390	3.28	11.15	67	25.5	0.549	0.685	5.79
5		120	32	31	84	452	3.18	9.67	63	26.15	0.099	0.233	4.84
6	1200	26	36	30	80	308	2.12	5.53	32	26.6	0.158	0.197	3.92
7		48	38	30	82	367	2.09	8	38	37.6	0.06	0.34	9.9
8		70	34	30	82	410	1.74	7.01	38	33.44	0.07	0.09	2.11
9		91	32	31	83	455	1.91	8.6	27	32.5	0.135	0.171	2.16
10		108	32.5	32	85	536	2.79	11.02	17	28.9	0.084	0.162	2.31
11		131	33.5	31	86	579	2.71	8.58	32	27.5	0.104	0.135	2.16
12		145	33.2	31	87	621	2.51	7.23	85	26	0.033	0.135	1.98
13	1500	26	37	31	81	362	1.55	7.17	32.8	30.11	0.141	0.277	6.27
14		51	37	31	83	414	1.45	7.14	47	30.8	0.06	1.04	23
15		76	37	31	85	465	1.25	6.95	56.6	24.7	0.06	1.42	29
16		104	36.5	32	85	520	2.09	10.07	86	26.42	0.08	1.14	17
17		129	36.7	32	86	562	2.22	8.7	52	25	0.1	0.88	10.8
18		152	34	30	87	620	2.48	7.63	46.8	20.8	0.07	2.21	24
20	1800	25	32	30	80	360	2.7	9.6	135	38.5	0.1	0.139	1.89
21		51	30.5	31	82	406	2	9.8	44	34.6	0.11	0.227	3.7
22		75	29	31	83	447	1.48	8.31	51.5	26.5	0.12	0.55	9
23		105	29	29	83	530	1.97	9.12	86	26.5	0.1	1	11.5
24		128	29	30	84	578	1.61	7.8	111	25	0.107	1.15	12
25		149	28	31	85	625	2.18	7.84	57	26	0.072	1.6	14.5
26		175	29.5	31	86	643	1.52	6	89	22.3	0.063	2.04	15.7
27	2000	27	35	33	82	418	2.65	11	101	30.8	0.07	0.114	1.7

28		52	35.5	32	83	465	1.64	9.25	53.7	30.6	0.07	0.85	14.5
29		77	35	32	84	507	1.44	8.1	62	23.12	0.107	1.73	28.7
30		101	34	32	85	540	1.73	8.68	92	25.7	0.129	2.14	26.9
31		127	33	33	85	594	1.5	7.81	108	22.13	0.08	2.63	27.8
32		150	31	29	86	644	2.26	8.07	46	23.33	0.081	3.2	28.7

Table 7.1 Cyclic variability test matrix

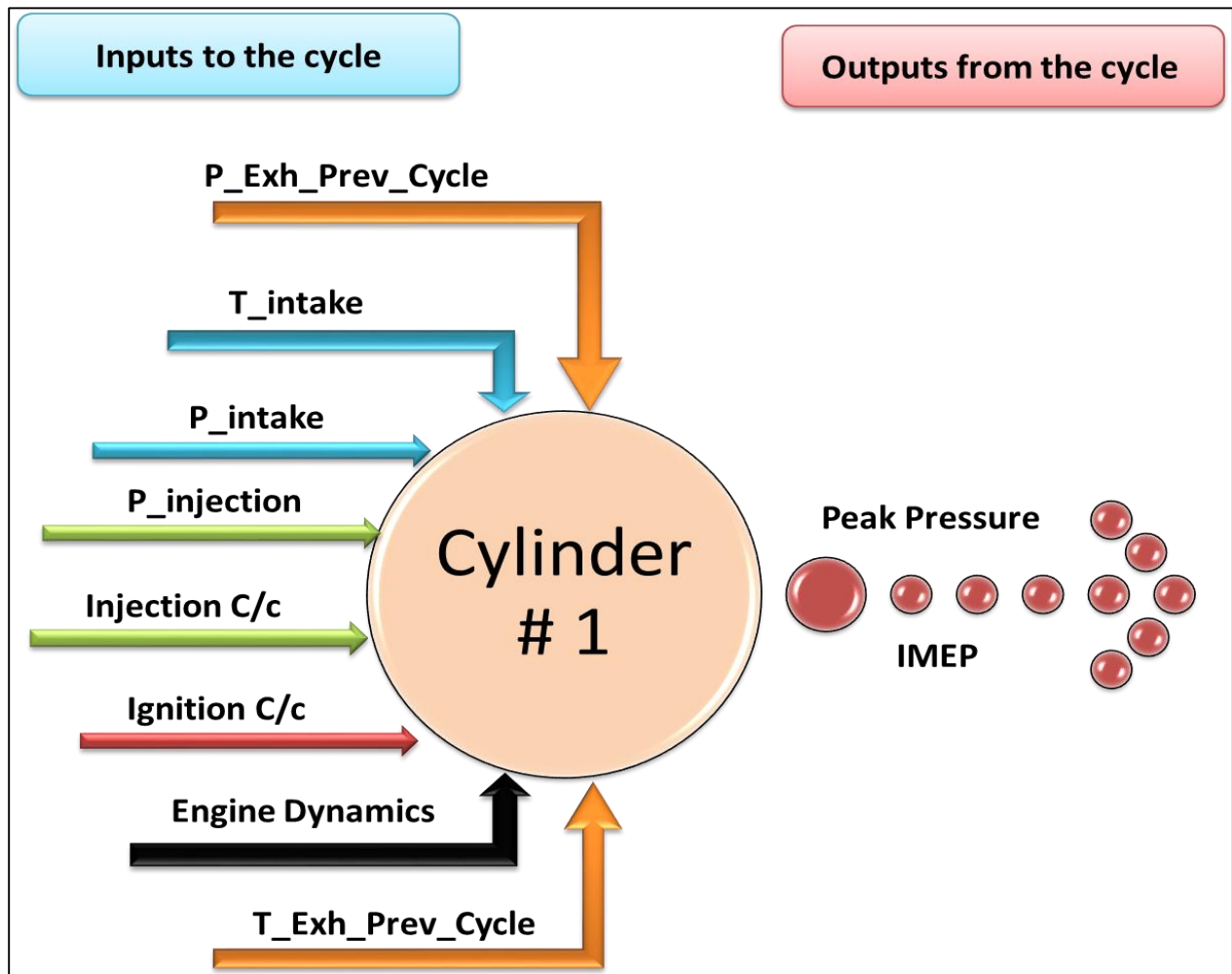


Figure 7.1. Input and output parameters of cylinder # 1

For each operating conditions, all the inputs have been measured in real time. All the sensors used in this investigation are fast response sensors that could capture the variation in 0.1 CAD at the speed of 5000 rpm. 500 consecutive cycles have been recorded for each operating condition as follows:

- Intake pressure at the intake port of cylinder # 1

- b) Intake Temperature at the intake port of cylinder # 1
- c) Injection pressure at the injector inlet of cylinder # 1.
- d) The injection command current.
- e) The ignition command, voltage and current goes to the ignition coil.
- f) Instantaneous engine speed using high resolution encoder.
- g) Exhaust pressure at the exhaust port of c cylinder # 1
- h) Exhaust temperature at the exhaust port of c cylinder # 1.

#### **Parameters represent the cyclic variability**

This section will discuss the parameters that affect the combustion stability in cylinder No.1 and determining if it is a major or minor factor that causes cyclic variation. Studying these parameters will allow for a better understanding of the combustion stability in a gasoline direct injection engine.

#### **7.4 Effect of early flame development (CA0% - CA10%) on cycle to cycle variation.**

The early stage development, CA 0% - CA 05%, of the flame has the highest impact of developing the flame to burn the rest of the fuel faster. Figure 7.2 shows a set of data of 100 consecutive cycles of the in-cylinder pressure trace at 1000 rpm and IMEP 5.79 bar. Figure 7.3 shows zoomed traces of the same data set.

The pressure trace marked in blue has the highest peak pressure and highest IMEP, cycle no. 72, and the pressure trace marked in red has the lowest peak pressure and lowest IMEP, cycle no. 52.

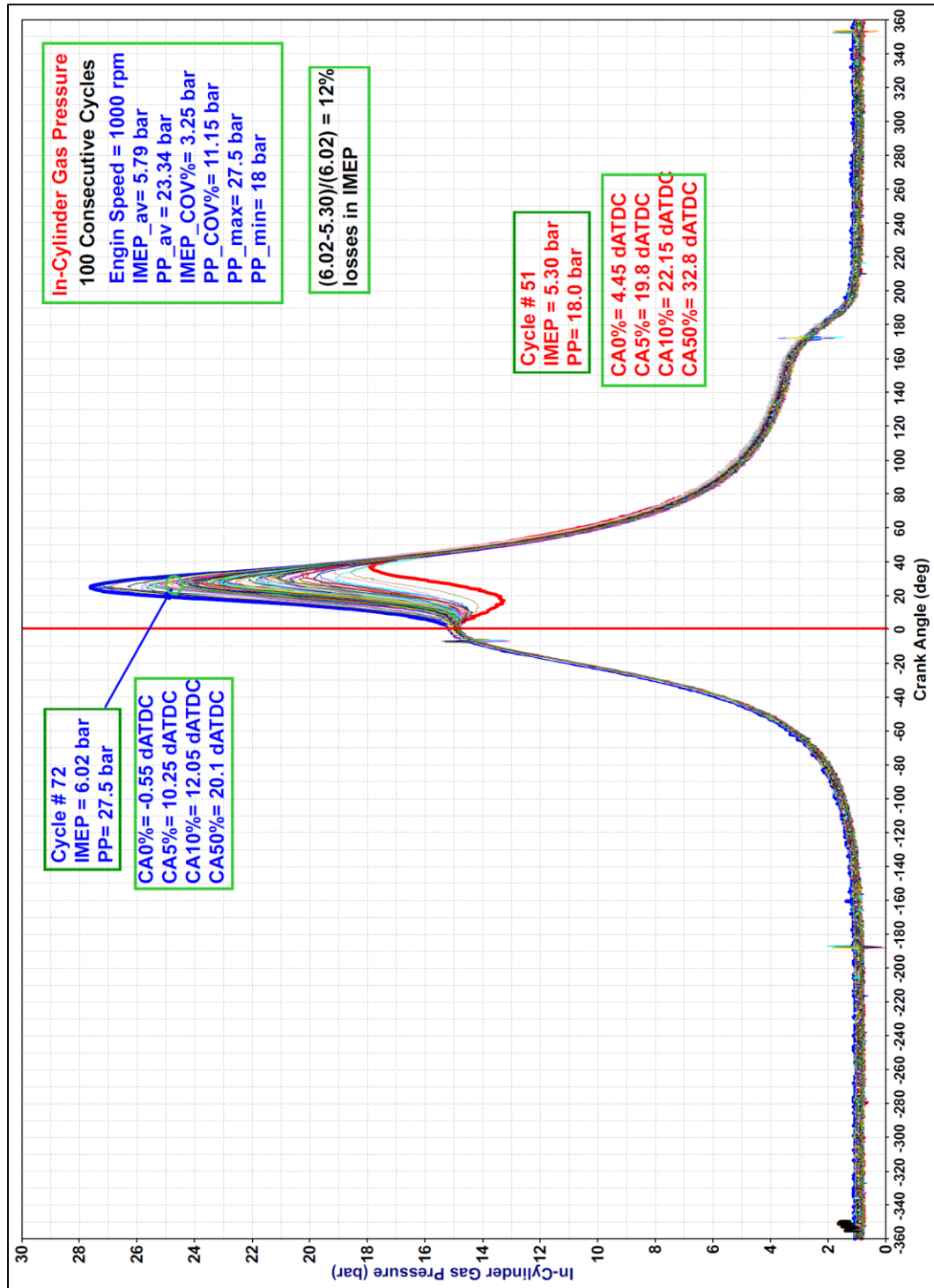


Figure 7.2. In-Cylinder gas pressure of 100 consecutive cycles at 1000 rpm and 5.79 IMEP.

The spark timing is at 5 deg BTDC and the two pressure traces showed a big difference in the early stage of the flame development. The combustion of cycle 72 started at 0.5 deg BTDC while the SOC of cycle 52 started at 4.45 dATDC, there is a difference of around 4.95 CAD angels in the early stage of the flame development.

In addition, the CA 05% of cycle No. 72 is at 10.25 dATDC, while the CA 05% of cycle No. 52 is at 19.8 dATDC. From these values, for cycle No. 72 the combustion started early and the period of CA 0% - CA 5% was equal to 10.75 degrees while for cycle No. 52, the combustion started late and the period of CA 0% - CA 5% is equal 15.35 degrees. This difference in the early stage of the flame development is due to the difference in the equivalence ratio around the spark plug at the time of the spark.



### 7.5 Effect of valve overlap period and trapped mass in the cylinder.

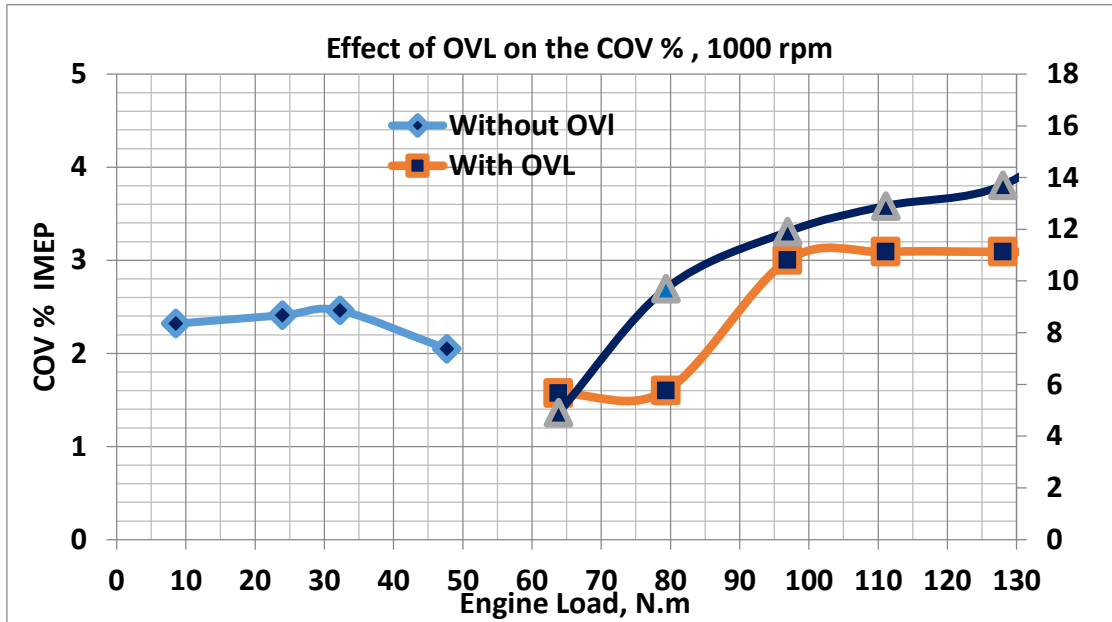


Figure 7.4. Effect of valve overlap period on the COV % at 1000 rpm and different loads

The new technology uses the trapped mass fraction in the combustion chamber and involves the exhaust products with the fresh charge to reduce the combustion temperature in order to achieve the desired emission level. In the case of using internal EGR, the valve overlap is the key parameter here to determine the amount of EGR % needed.

On the other hand, the combustion stability decreases proportionally with the amount of EGR. Figures 7.4-8 show the effect of the overlap period on the COV % of the IMEP of cylinder # 1 at different speeds and loads. For the range where there is no overlap, the COV % is lower compared to the OVL % of the period where there is overlap. Additionally, in the period where there is overlap, the COV % increases dramatically with the overlap period. In addition, the residuals from cycle to cycle is different and this indicates that the equivalence ratio at the spark plug gap is not the same from cycle to cycle due to the higher percentage of exhaust product.

From the data shown in Figures 7 4-8, in all the operating conditions there is a period of overlap where it has the lowest COV % and the best combustion stability. This study showed using the EGR to enhance the emission level plays a big role in combustion stability.

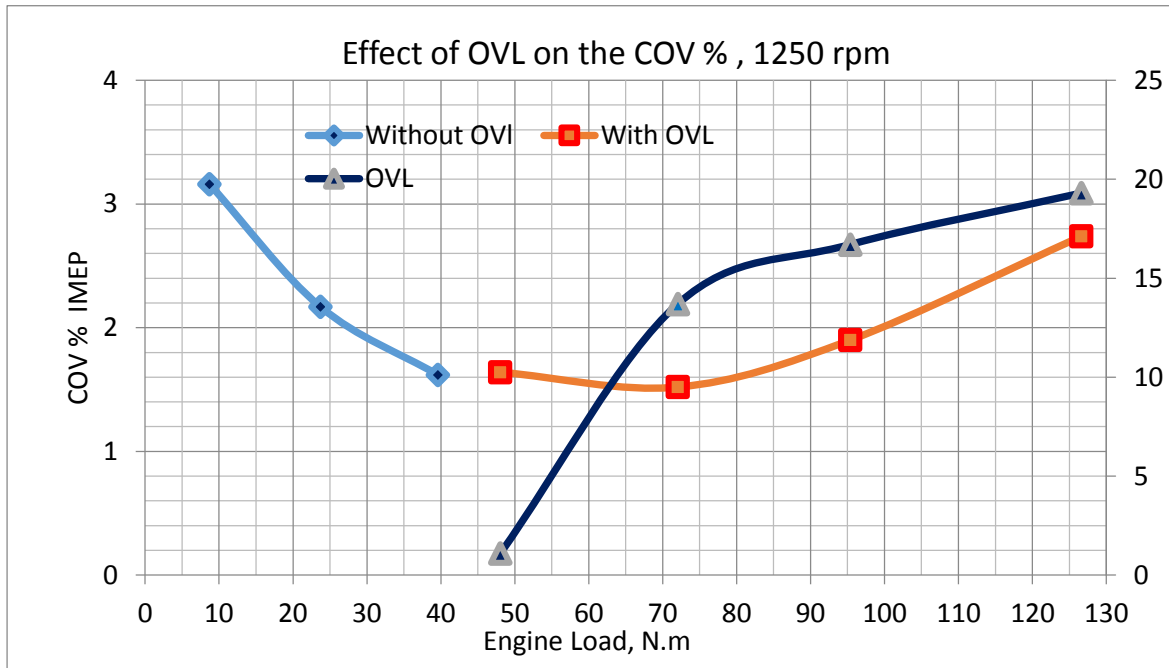


Figure 7.5 Effect of valve overlap period on the COV % at 1250 rpm and different loads

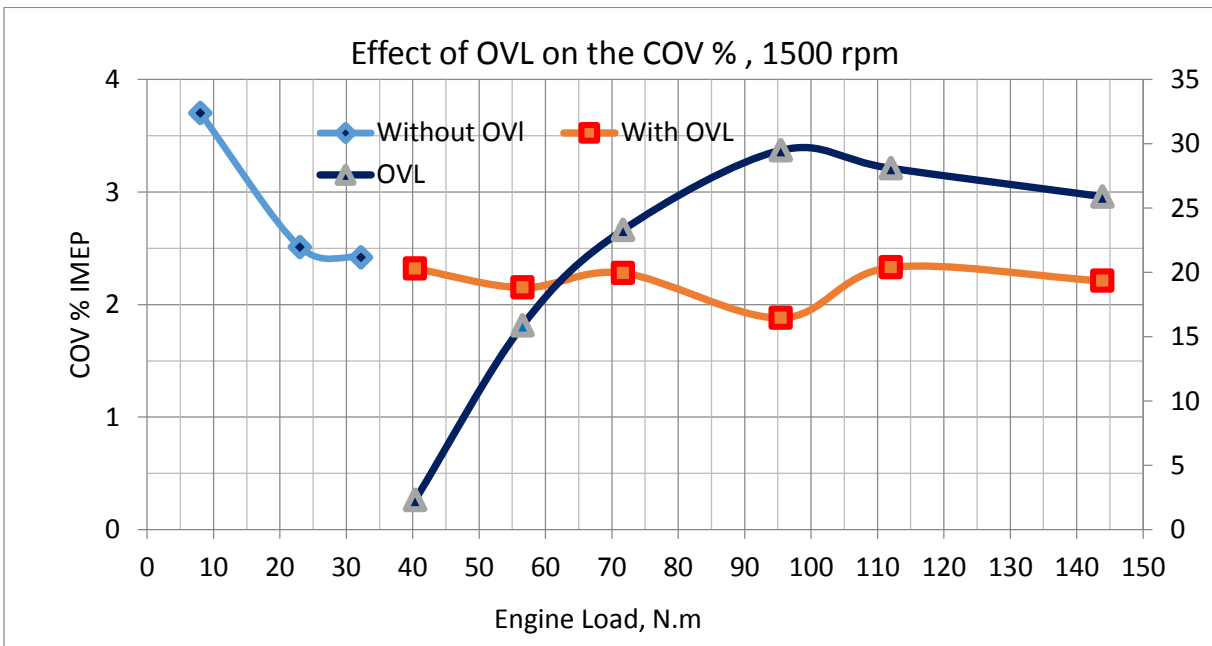


Figure 7.6. Effect of valve overlap period on the COV % at 1500 rpm and different loads

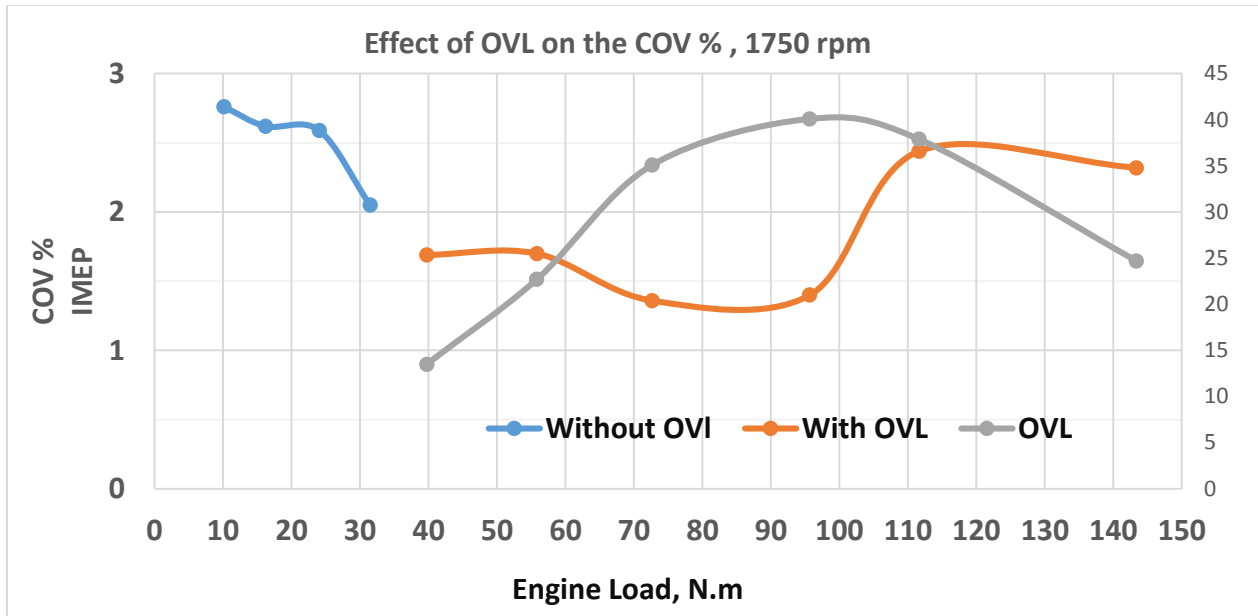


Figure 7.7. Effect of valve overlap period on the COV % at 1750 rpm and different loads

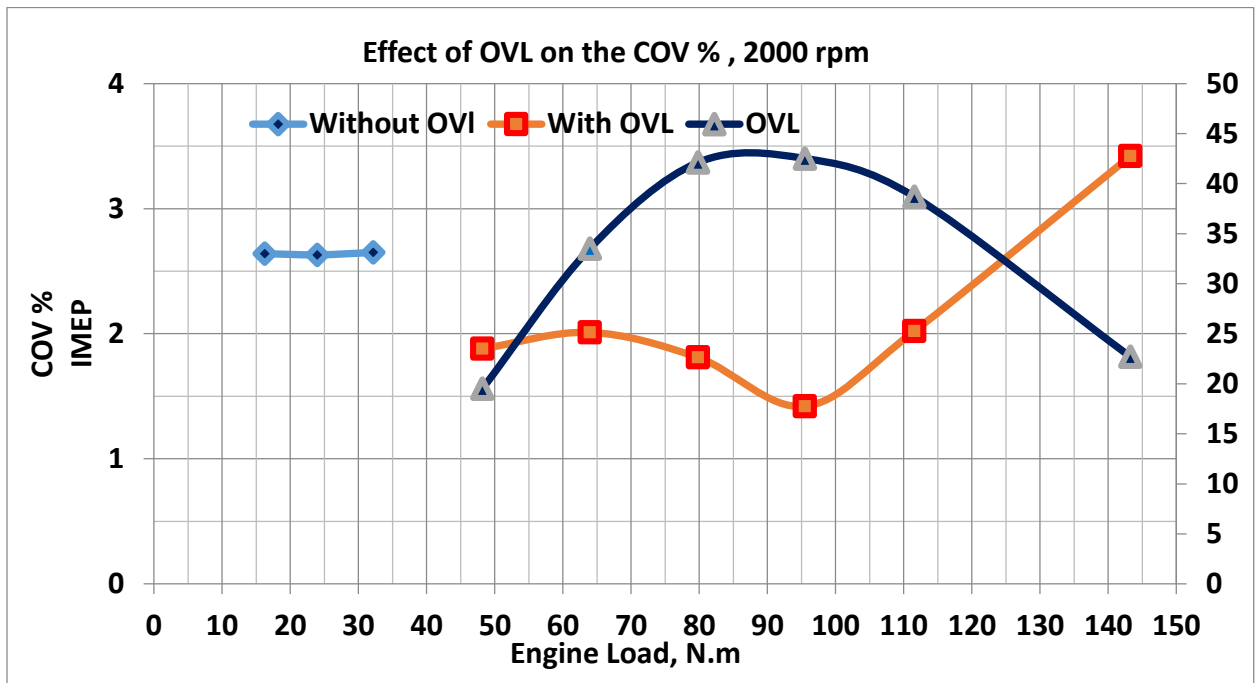


Figure 7.8. Effect of valve overlap period on the COV % at 2000 rpm and different loads

## 7.6 Effect of Spark timing on combustion stability.

The spark advance is a major factor in keeping the engine running to the point where we can achieve the MBT (Maximum Break Torque). Advancing the spark timing will lead to engine knock

because the calibrated spark time is adjusted at the point just before the incipient knock. On the other hand, retarding the spark timing will decrease the emission by decreasing the combustion temperature but will lead to power loss and the engine will run at a point where we cannot achieve the MBT. In addition, the combustion stability is so sensitive to the spark timing.

### 7.7 Effect of injection timing on combustion stability.

The injection timing in turbocharged gasoline direct injection engine is very important for the mixing process. The injecting timing usually being after the intake valve opens in the intake stroke for better mixing with air. Injecting early will allow the fuel to hit the walls and the piston bowl and will decrease the combustion stability. Figure 7.9 shows the effect of the injection retard on the combustion stability. It shows that retarding the injection to a certain limit decreases the COV % and enhances the combustion stability. Combining of the injection timing and ignition timing that have the lowest COV% will lead to overall reduction in COV% and enhance the combustion stability.

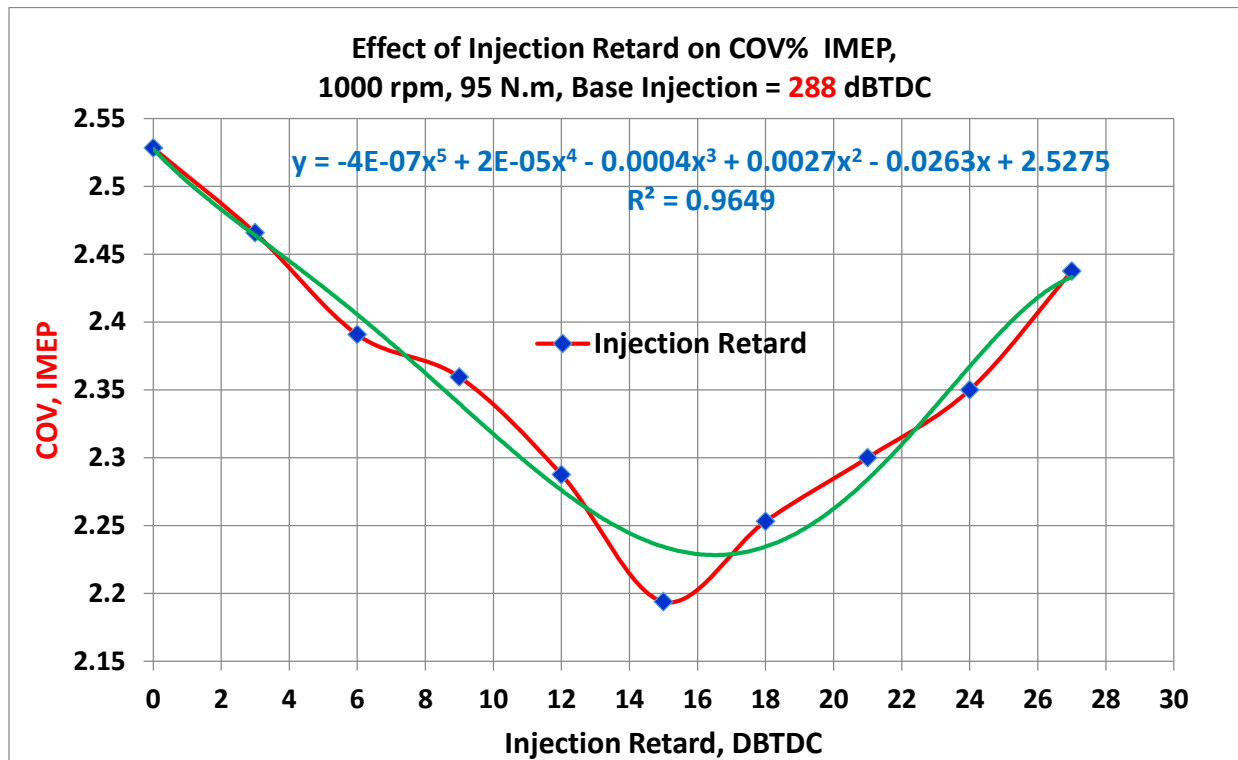


Figure 7.9 Effect of injection timing on the COV % at 1000 rpm and 95 N.m

### **7.8 Effect of intake port pressure and temperature on combustion stability.**

A very fast response Omega thermocouple of the size 0.005" is installed at the middle of the intake port of cylinder # 1. In all cases at low load or high load, the in-cylinder gas pressure is higher than the intake manifold pressure, so the pressure comes out from the cylinder and goes to the intake manifold till the pressure equalize.

During this process the piston is moving down and the in-cylinder gas pressure starts to decrease due to the increasing in the combustion chamber volume. After the in-cylinder gas pressure is being slightly lower than the pressure in the intake manifold, the fresh charge starts to enter the combustion chamber.

This thermocouple shows the time where the IVO and the combustion gases comes out from the combustion chamber; at this point, the temperature increases suddenly due to the high difference between the combustion gases temperature and intake manifold temperature.

Furthermore, the thermodynamics control this part by the ideal gas equations around the combustion chamber, and we expected when the intake manifold temperature increases, this means that the charge density will decrease, which leads to lower amount of fresh charge get into the combustion chamber. On the other hand, if the temperature decreases, this will lead to an increase in the air density of the fresh charge get into the combustion chamber.

The corresponding pressure distributions of the 100 consecutive cycles are shown in figure 7.11. Figure 7.11 shows that the pressure doesn't vary that much as to cause that huge amount of variation in the peak pressure or the IMEP. The change in pressure during the intake stroke is about 10 Pa. This variation is very small compared to the variation in the IMEP.

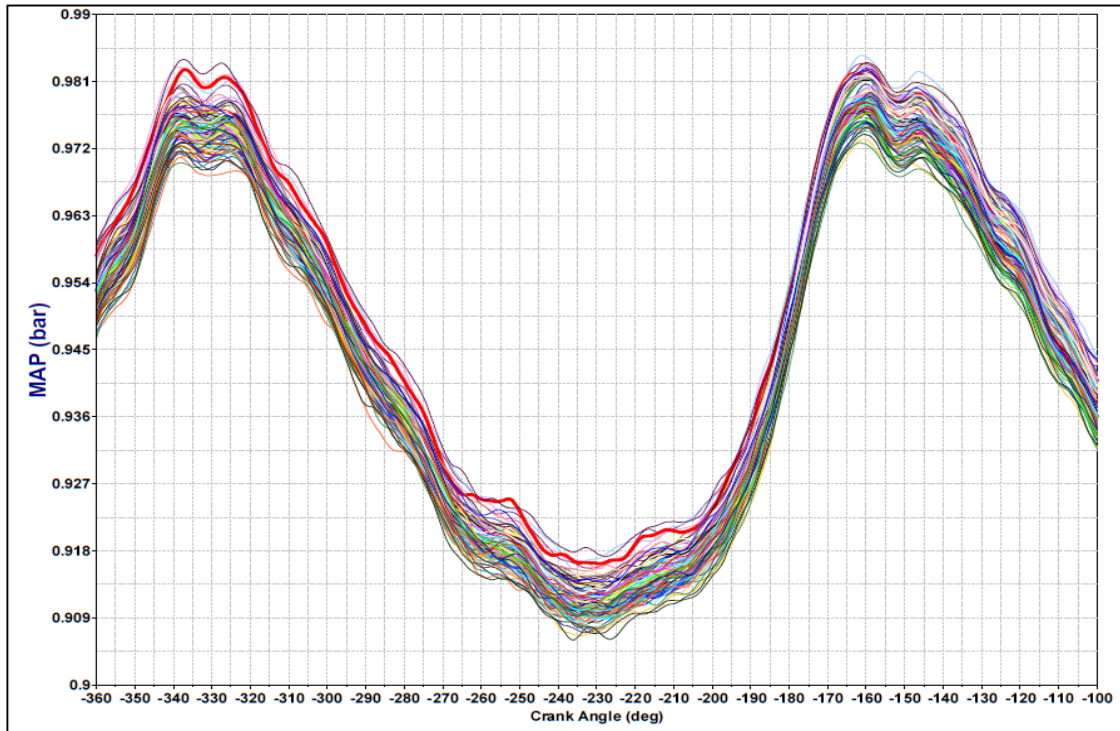


Figure 7.11. MAP of 100 consecutive cycles at 1000 rpm and 5.79 IMEP

The combustion stability mainly depends on the equivalence ratio around the spark plug gap at the ignition timing. In addition, the turbulence depends on the flow velocity inside the combustion chamber. The instantaneous piston speed has a big impact on the turbulence level at the early stage development of the flame. The instantaneous piston speed depends on the instantaneous engine speed. Figure 7.12 shows the instantaneous engine speed of 100 consecutive cycle at 1000 rpm and 5.79 bar IMEP. Cycle no. 72, which has the highest IMEP, and cycle no. 52, which has the lowest IMEP, both appear to have almost the same instantaneous engine speeds which correspond to the same instantaneous piston speed. This finding shows that the instantaneous engine speed doesn't have that much of an effect on the combustion stability.

### 7.9 Effect of instantaneous piston speed on combustion stability.

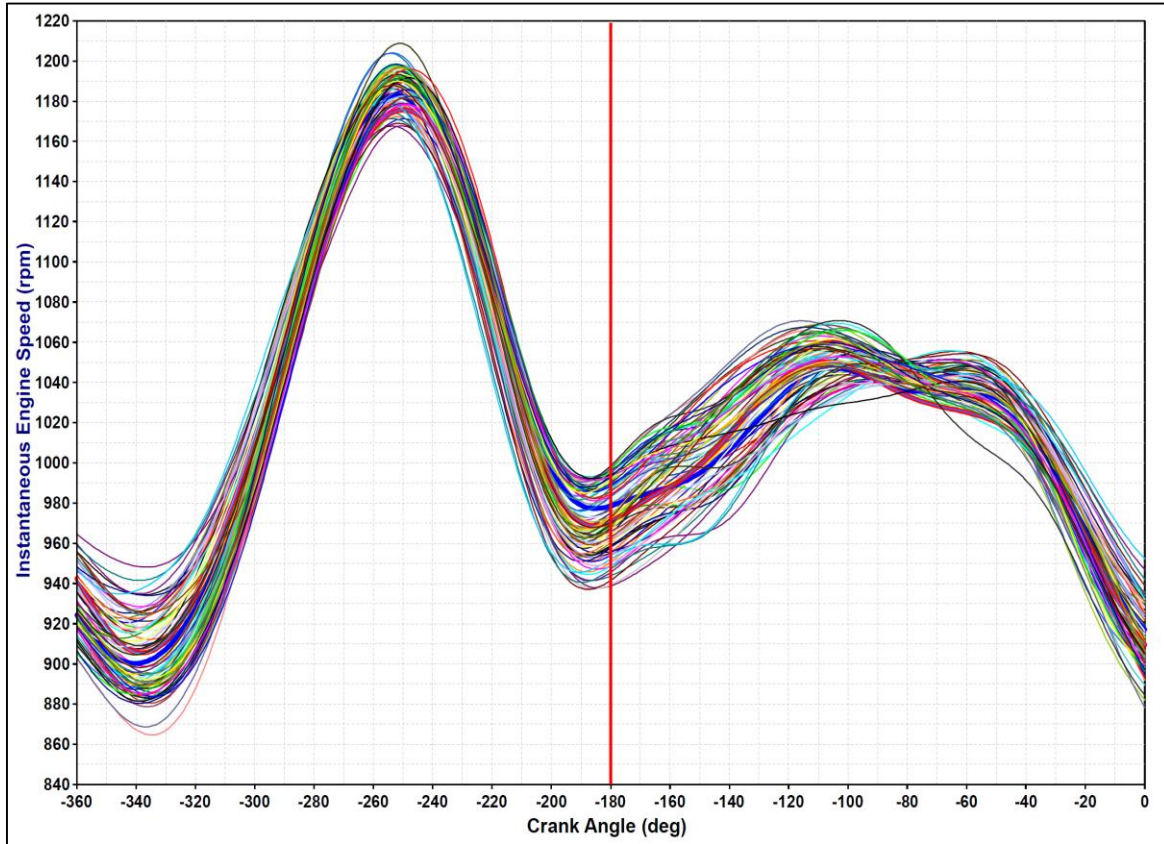


Figure 7.12. Instantaneous engine speed distribution of 100 consecutive cycles at 1000 rpm and 5.79 IMEP

### 7.10 Effect of exhaust pressure and temperature on combustion stability.

One of the most important parameters is the amount of residuals that remain in the combustion chamber from the previous cycle to the current cycle which is controlled by the exhaust pressure and temperature. Since we have higher exhaust pressure and lower exhaust temperature, the amount of residuals will be higher and will affect the equivalence ratio around the spark plug gap at the moment of sparking. Figures 7. 13 and 7.14 represent the instantaneous exhaust and pressure distribution at the exhaust port outlet of cylinder No.1. The temperature and pressure distributions of cycle No. 72 have the highest IMEP and cycle No. 52 which has the lowest IMEP are the same which means in this case the effect of exhaust pressure and temperature does not represent any factor here.



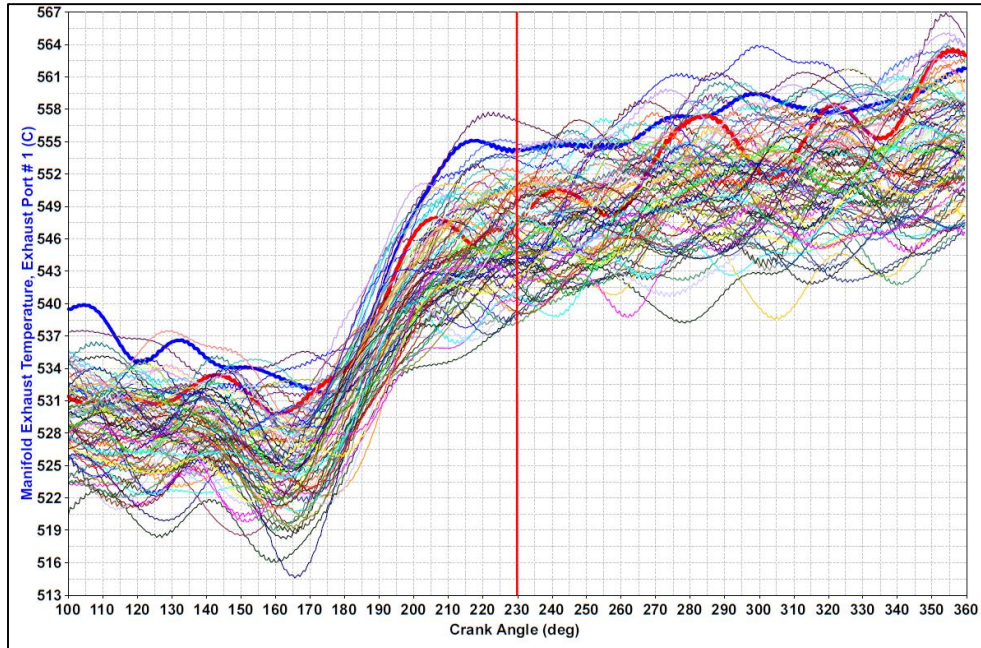


Figure 7.13. Instantaneous temperature pressure distribution of 100 consecutive cycles at 1000 rpm and 5.79 IMEP

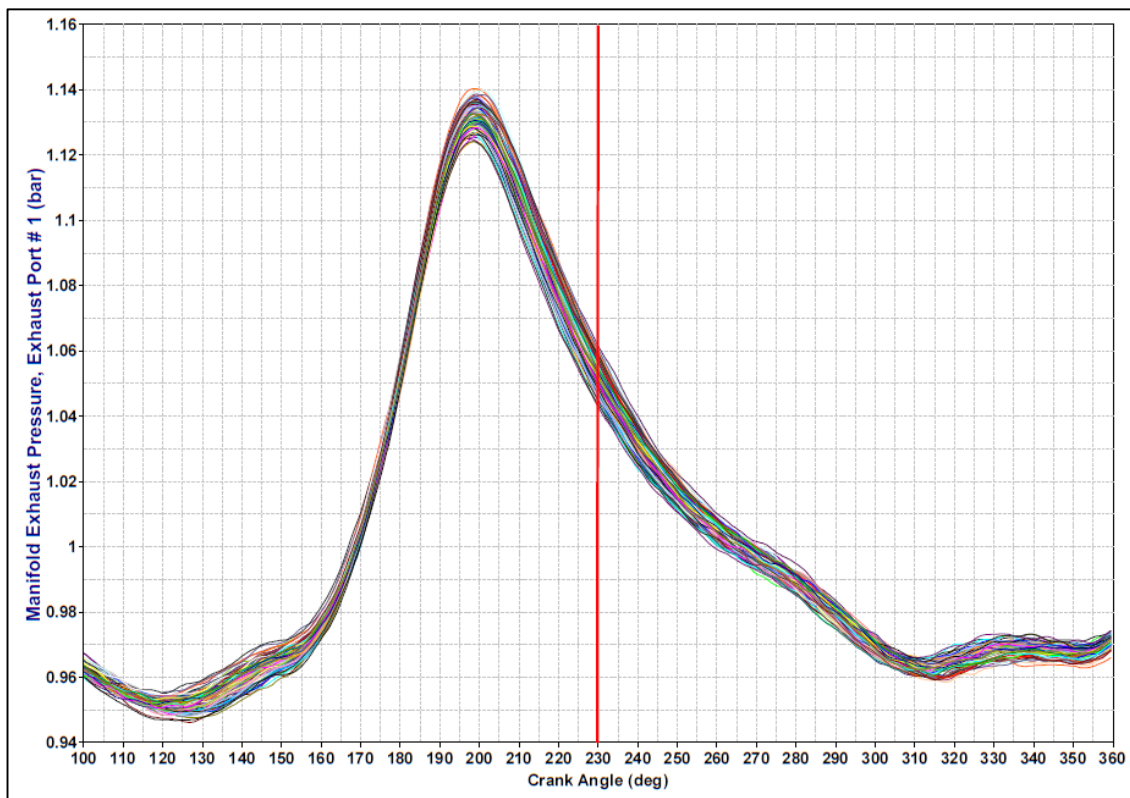


Figure 7.14. Instantaneous Exhaust pressure distribution of 100 consecutive cycles at 1000 rpm and 5.79 IMEP



### 7.11 Effect of injection command characteristics on combustion stability.

One of the most important parameters that affect the combustion stability is the amount of fuel injected in the combustion chamber. The injection command is a major factor of controlling the injector solenoid behavior which in consequence will control the needle opening and closing. Variation in the injection command will lead to variation in the amount of fuel injected in the combustion chamber. Figure 7.15 shows a 100 consecutive cycle at 1000 rpm and 5.79 bar IMEP. The signal in red represent the injection command of cycle no. 52 that has the lowest IMEP, and the signal in blue represent the injection command of the cycle that has the highest IMEP. It appears that the injection period of cycle no. 72 is larger than the injection period of cycle no. 52 by around 1.5 degrees. This means the amount of fuel injected in cycle 72 is more than the fuel injected in cycle no. 52, which explains why cycle no. 72 has a higher IMEP.

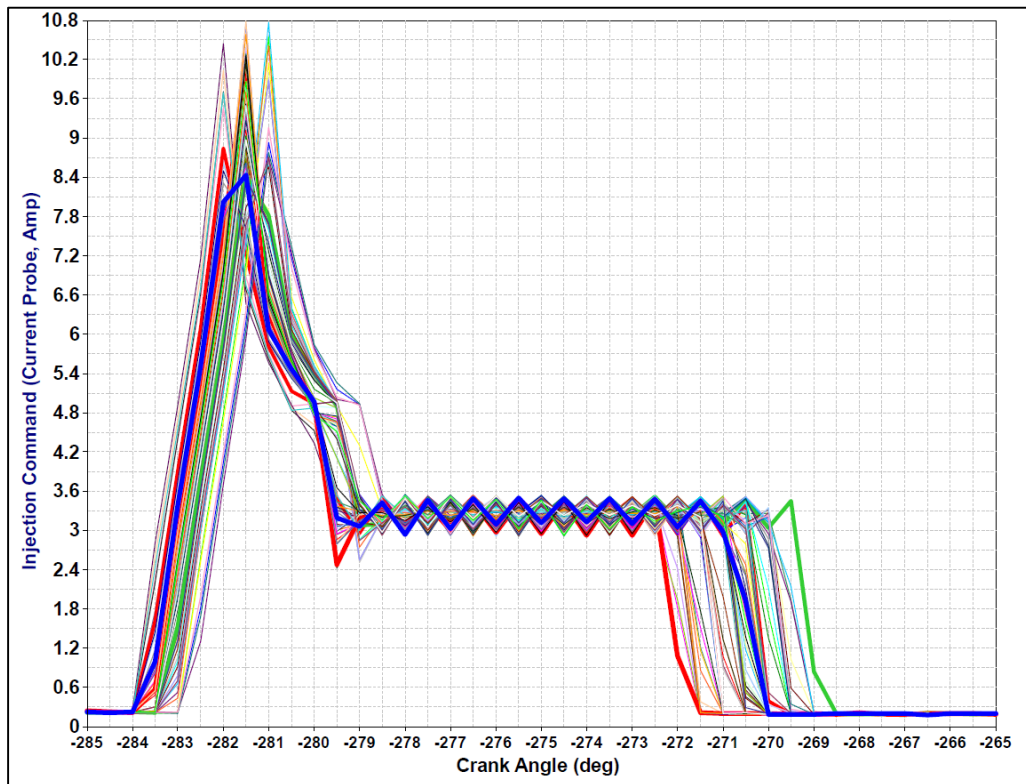


Figure 7.15. Injection command of 100 consecutive cycles at 1000 rpm and 5.79 IMEP

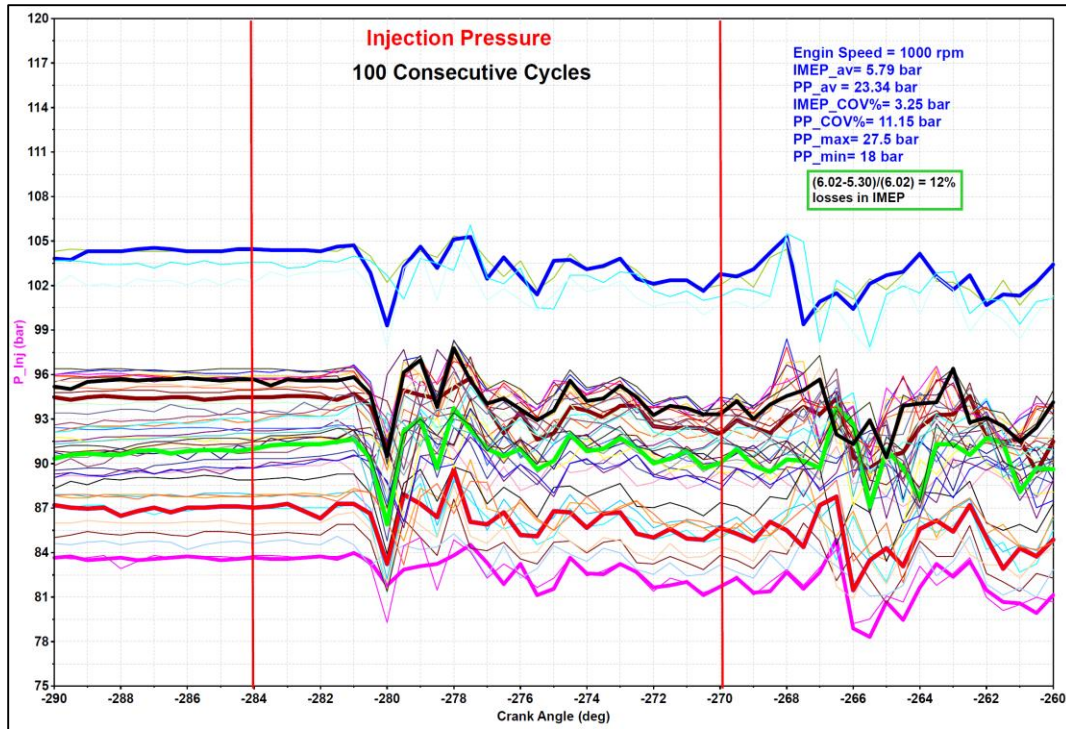


Figure 7.16. Instantaneous Injection Pressure wave of 100 consecutive cycles at 1000 rpm and 5.79 IMEP at the inlet of the injector of cylinder # 1

In addition, the injection pressure wave measured instantaneously at the inlet tip of the injector of cylinder No. 1, showed a large variation in the pressure distribution as shown in figure 7.16. High injection pressure represent higher fuel mass flow rate, higher fuel atomization and long penetration length. Lower injection pressure represent lower fuel flow rate and lower fuel atomization. The higher IMEP delivered by cycle no. 72 has the longest injection command period and higher injection pressure. The lowest IMPE delivered by cycle no. 52 has the lower injection pressure and smaller injection period. However, the cycle No. 52 that delivered the lowest IMEP have lower injection pressure, but doesn't have the lowest injection pressure, which means there are other factors that affect the cycle to cycle variation than the injection pressure. It is the combination of the injection pressure and the injection period is the major factor of controlling the cyclic variability.

These results will be used in the controller to control the injection command and injection pressure in such a way we could get the same exact injection command characteristics and injection pressure.

Additional 754 tests have been conducted to investigate a wide range of operating speeds and loads. In the next section, sample results of selected four tests have been presented. Figure 7.17 to Figure 7.44 shows the in-cylinder gas pressure, injection command, injection pressure, intake manifold absolute pressure, exhaust temperature, exhaust manifold absolute pressure and engine speed for the selected tests from the test matrix in Table 7.1. The next figures, Figure 7.17 to Figure 7.44 show the same trend of the fluctuation of the injection pressure and injection command. In addition, it shows the small variation of the intake pressure and temperature, exhaust pressure and temperature, engine speed and ignition command. This will draw a conclusion that all the tests agreed on the fact that the injection pressure fluctuation and injection command fluctuation are a major factor of cycle to cycle variation.

### 7.12 Results of 100 consecutive cycles at 1000 rpm and 1.5 IMEP

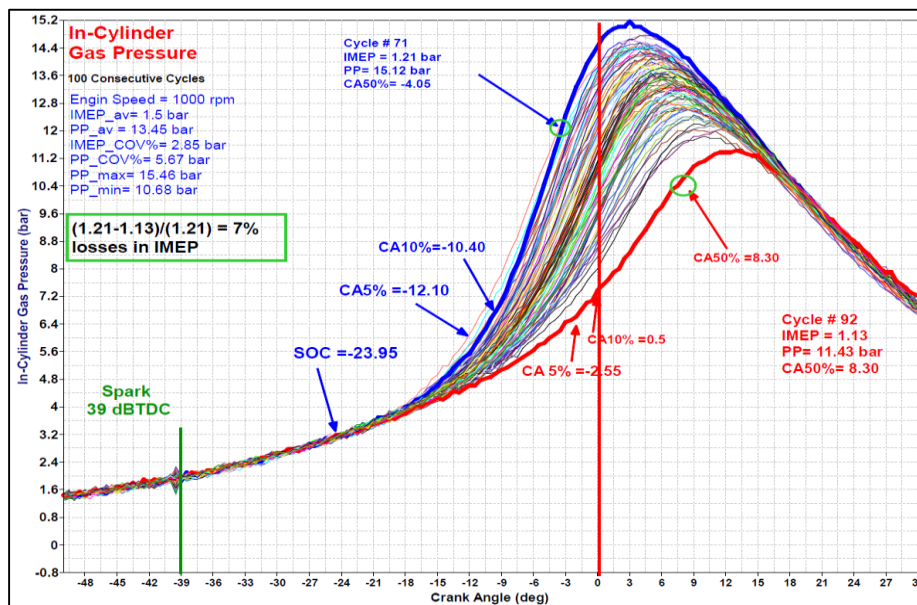


Figure 7.17. Zoomed traces of In-Cylinder gas pressure of 100 consecutive cycles at 1000 rpm and 1.5 IMEP, test # 1.



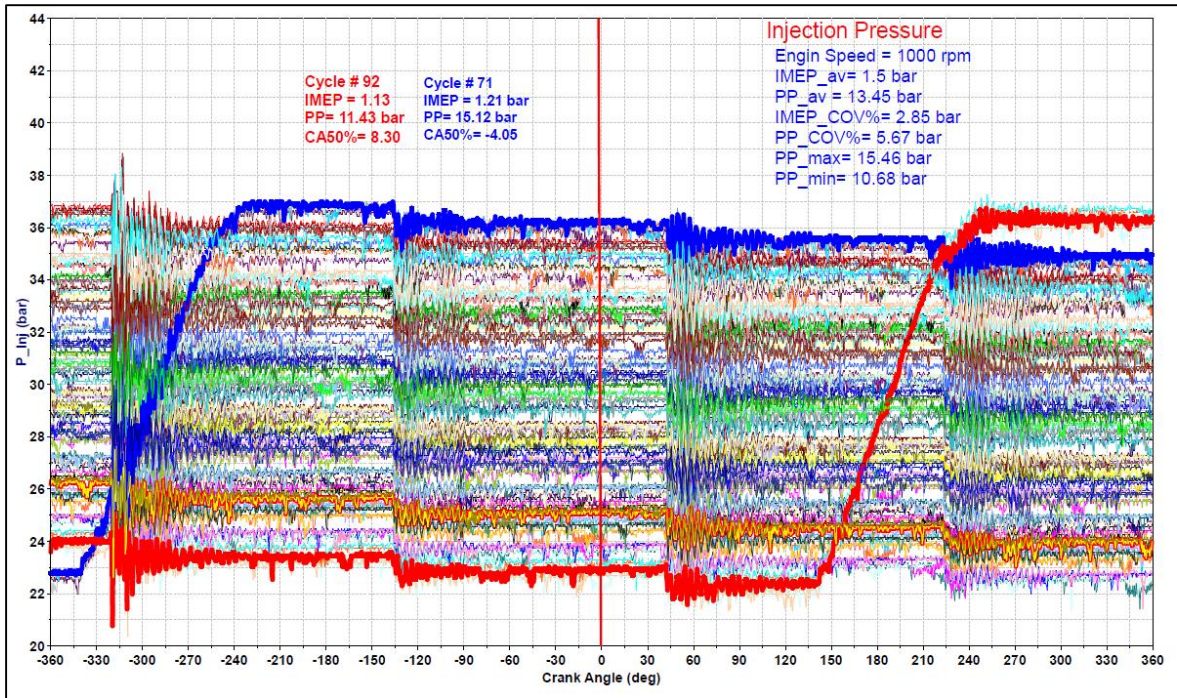


Figure 7.18. Instantaneous Injection Pressure distribution of 100 consecutive cycles at 1000 rpm and 1.5 IMEP at the inlet of the injector of cylinder # 1

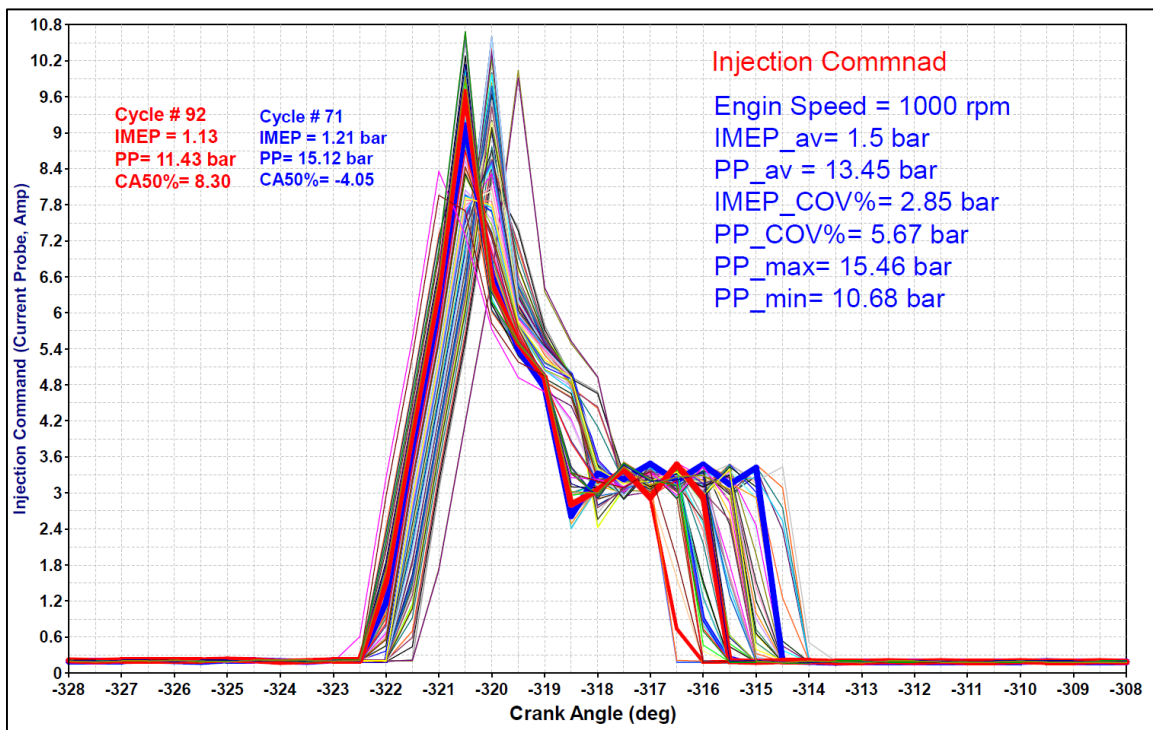


Figure 7.19. Injection command of 100 consecutive cycles at 1000 rpm and 1.5 IMEP of cylinder # 1

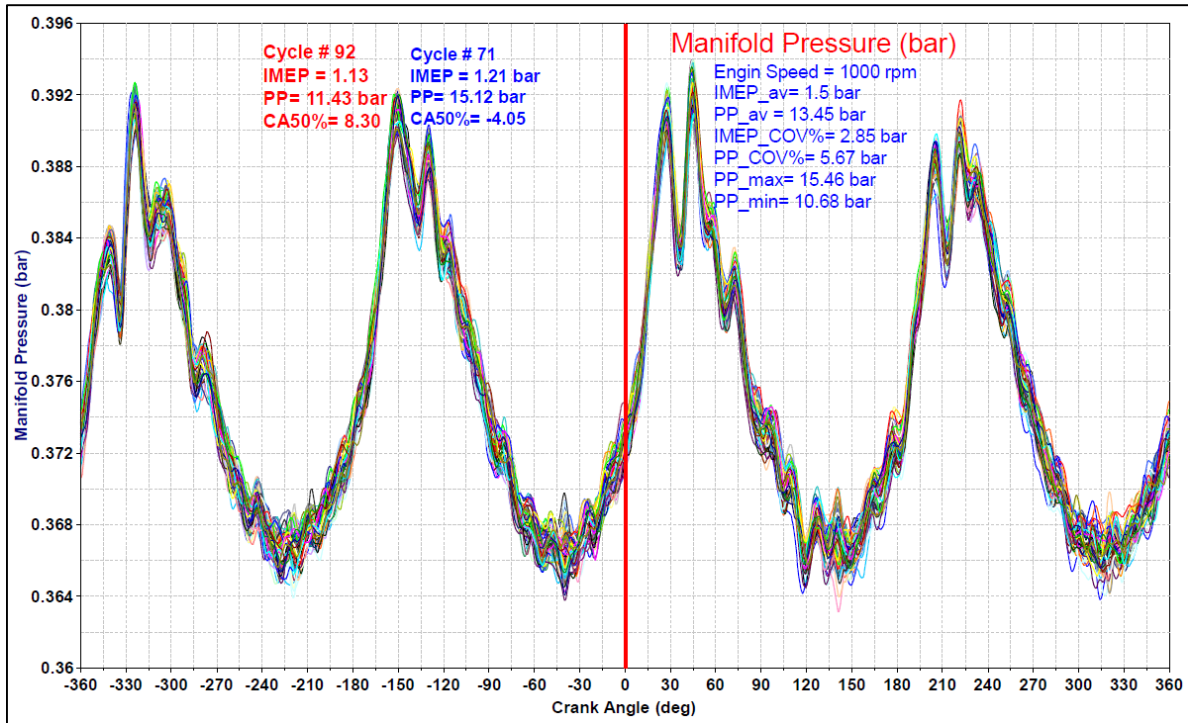


Figure 7.20 Intake manifold absolute pressure of 100 consecutive cycles at 1000 rpm, 1.5 IMEP of cylinder # 1

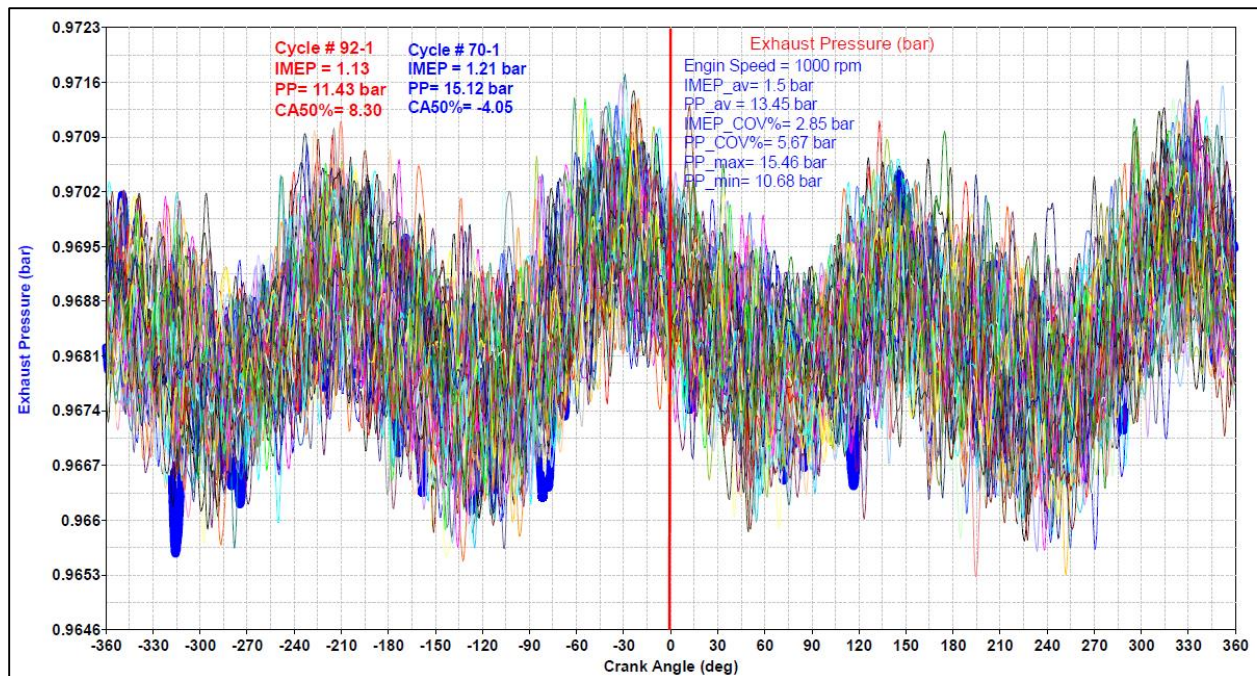


Figure 7.21 Exhaust manifold absolute pressure of 100 consecutive cycles at 1000 rpm, 1.5 IMEP of cylinder # 1



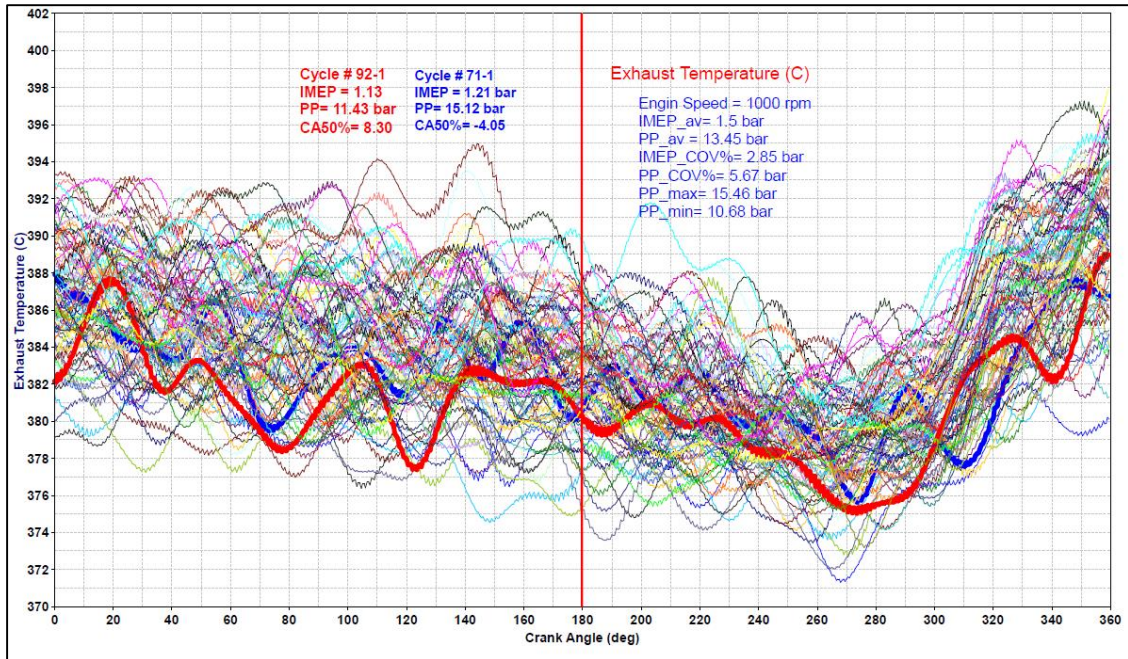


Figure 7.22. Exhaust manifold absolute temperature of 100 consecutive cycles at 1000 rpm, 1.5 IMEP of cylinder # 1

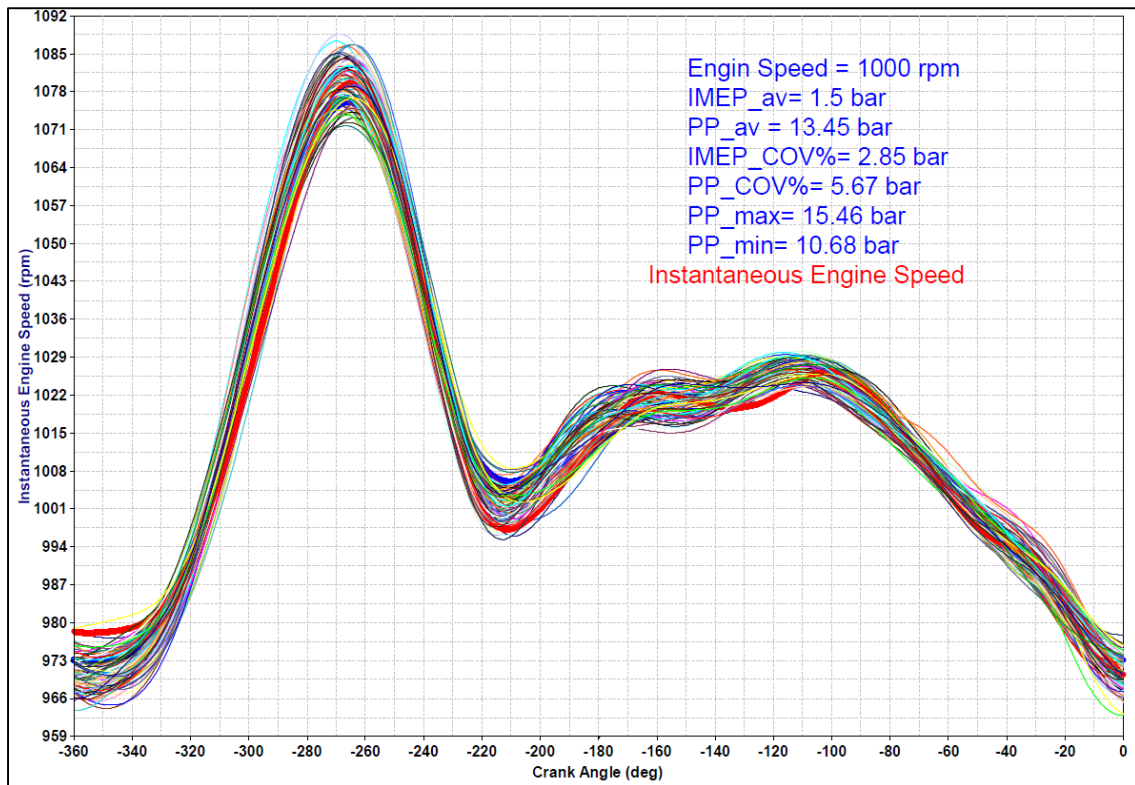


Figure 7.23. Instantaneous engine speed of 100 consecutive cycles at 1000 rpm, 1.5 IMEP of cylinder # 1

### 7.13 Results of 100 consecutive cycles at 1000 rpm and 3.9 IMEP

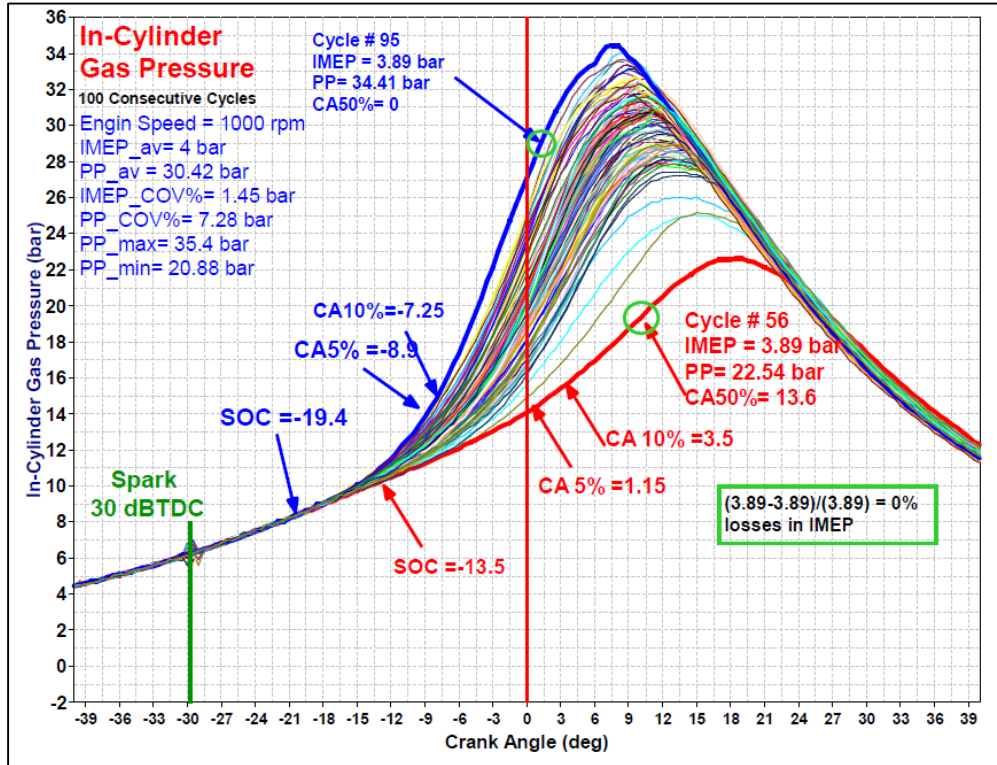


Figure 7.24. In-cylinder gas pressure of 100 consecutive cycles at 1000 rpm, 3.9 IMEP of cylinder # 1

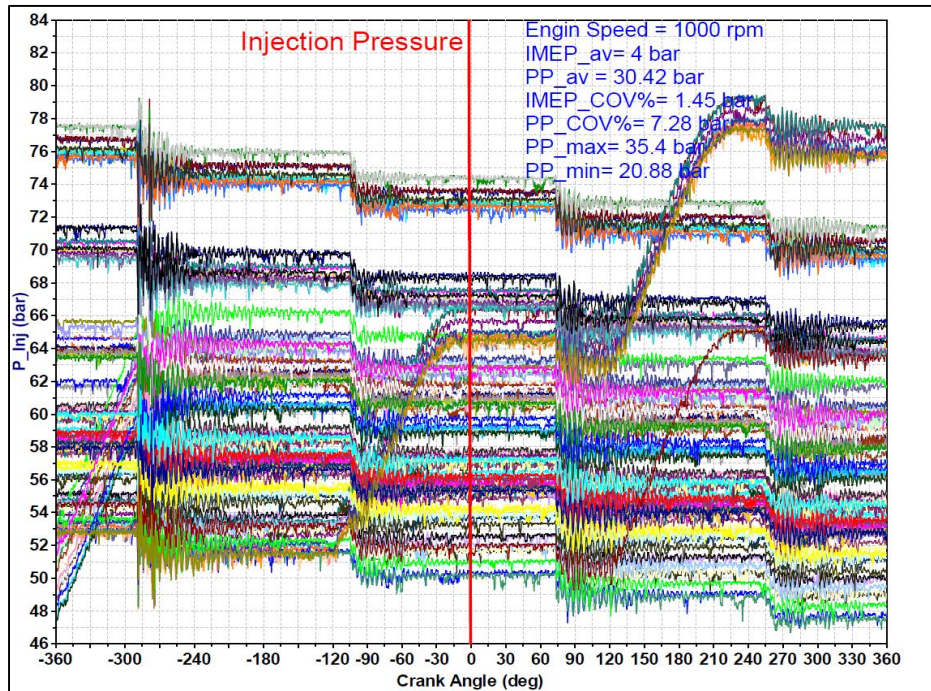


Figure 7.25. Injection pressure of 100 consecutive cycles at 1000 rpm, 3.9 IMEP of cylinder # 1



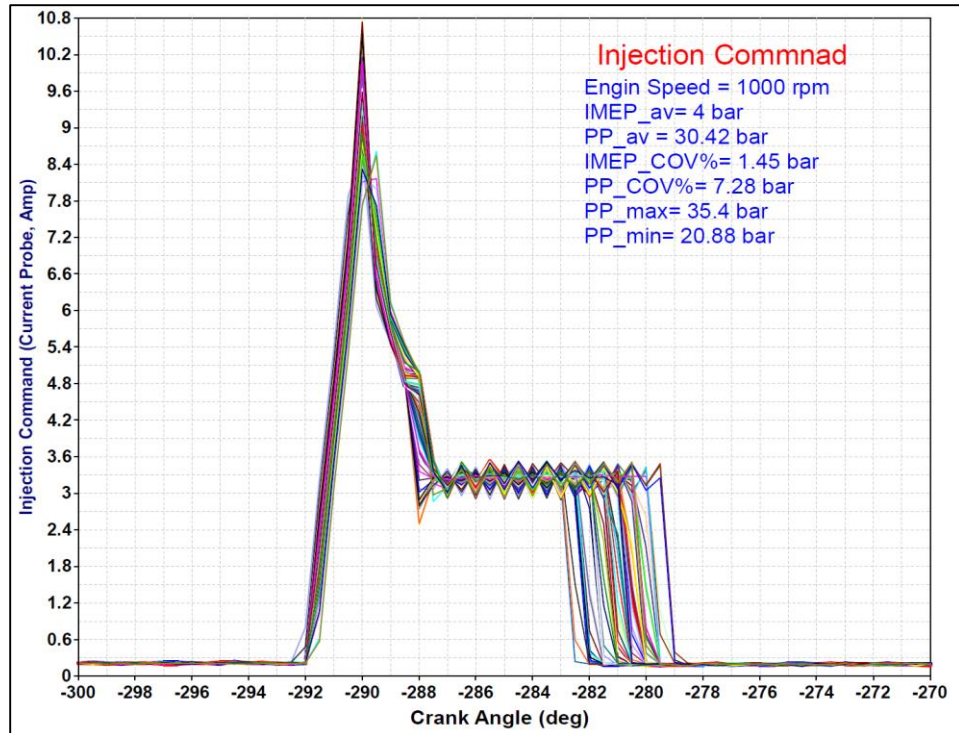


Figure 7.26. Injection command of 100 consecutive cycles at 1000 rpm, 3.9 IMEP of cylinder # 1

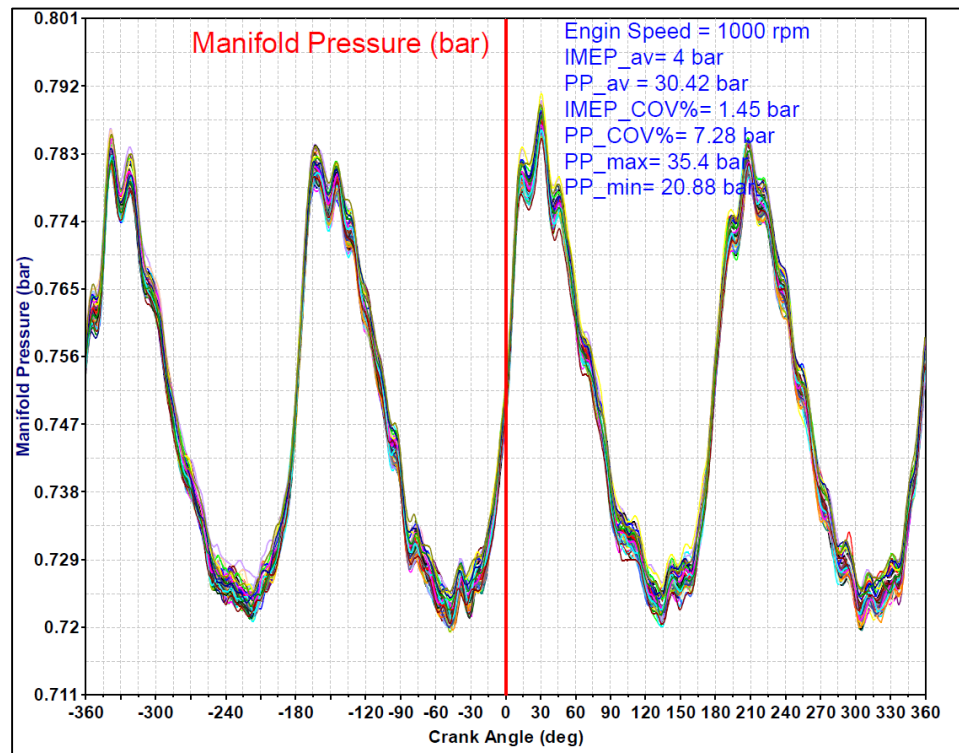


Figure 7.27. Intake Manifold absolute pressure of 100 consecutive cycles at 1000 rpm, 3.9 IMEP of cylinder # 1



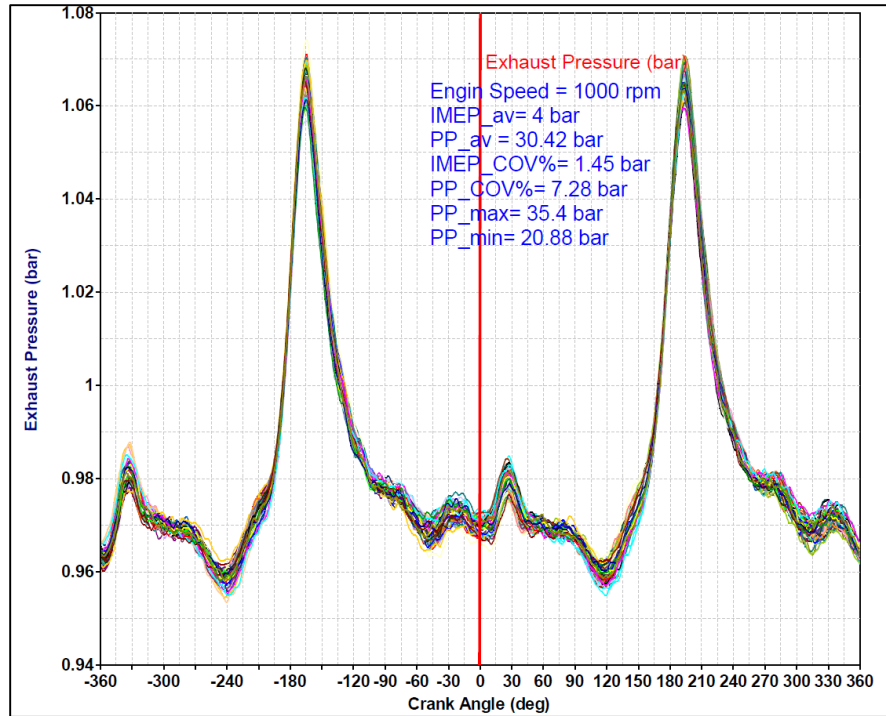


Figure 7.28. Exhaust manifold absolute pressure of 100 consecutive cycles at 1000 rpm, 3.9 IMEP of cylinder # 1

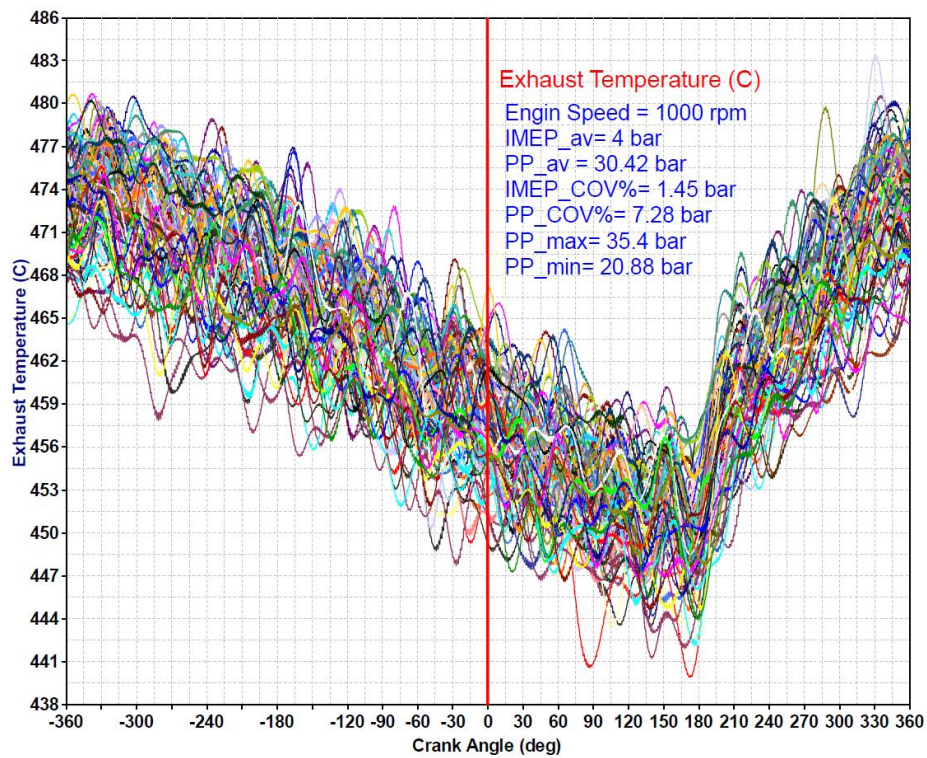


Figure 7.29. Exhaust manifold absolute temperature of 100 consecutive cycles at 1000 rpm, 3.9 IMEP of cylinder # 1

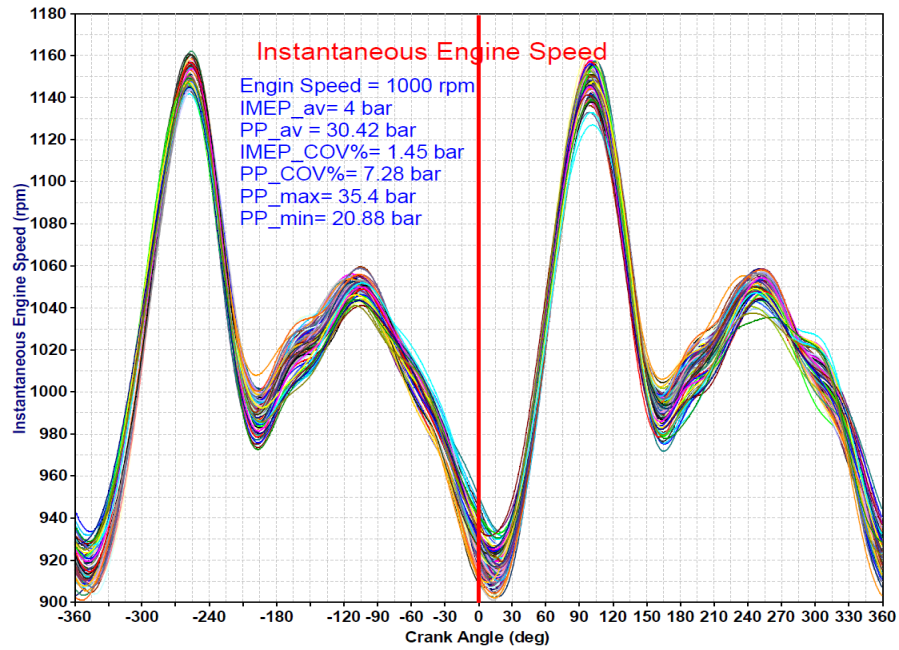


Figure 7.30. Instantaneous engine speed of 100 consecutive cycles at 1000 rpm, 3.9 IMEP of cylinder # 1

#### 7.14 Results of 100 consecutive cycles at 1000 rpm and 5.2 IMEP

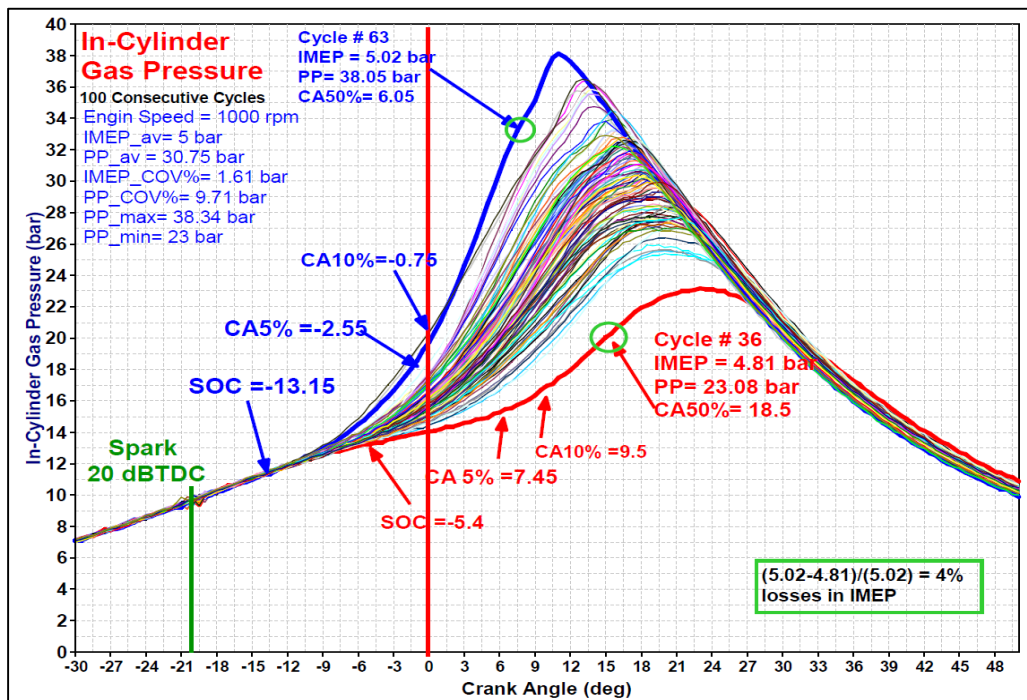


Figure 7.31. Zoomed traces of In-Cylinder gas pressure of 100 consecutive cycles at 1000 rpm and 5.2 IMEP, test # 1.

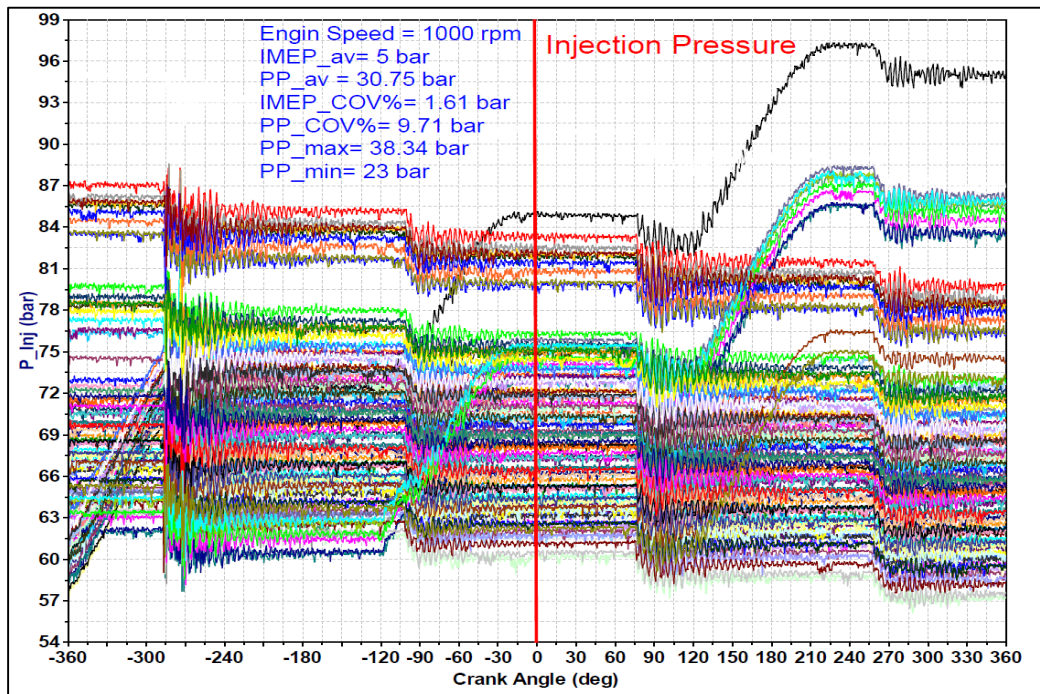


Figure 7.32. Instantaneous Injection Pressure distribution of 100 consecutive cycles at 1000 rpm and 5.2 IMEP at the inlet of the injector of cylinder # 1

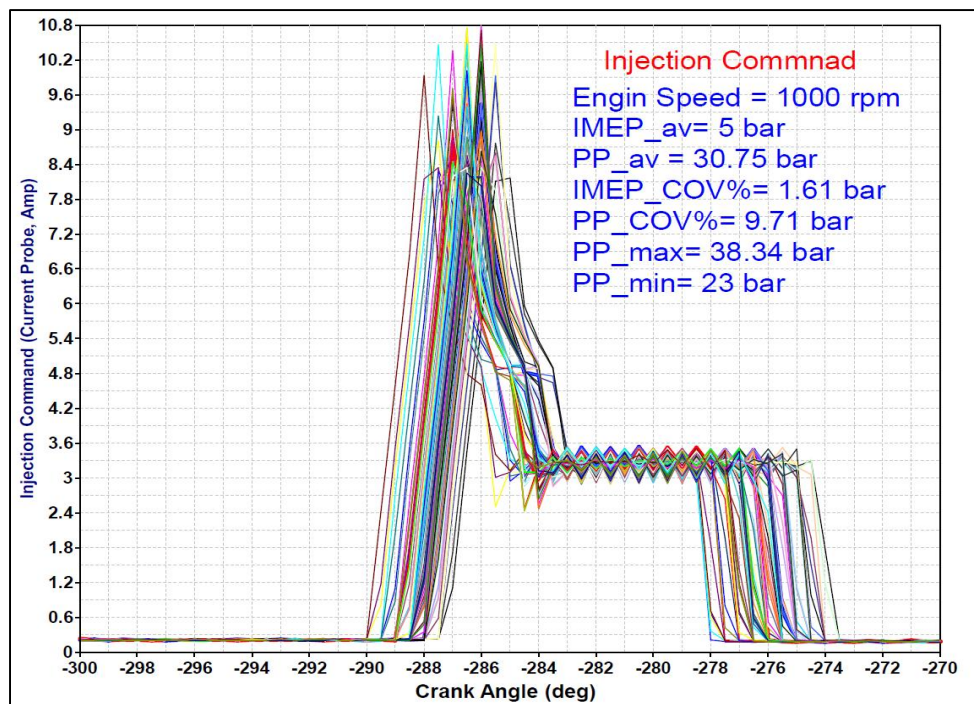


Figure 7.33. Injection command of 100 consecutive cycles at 1000 rpm and 5.2 IMEP of cylinder # 1



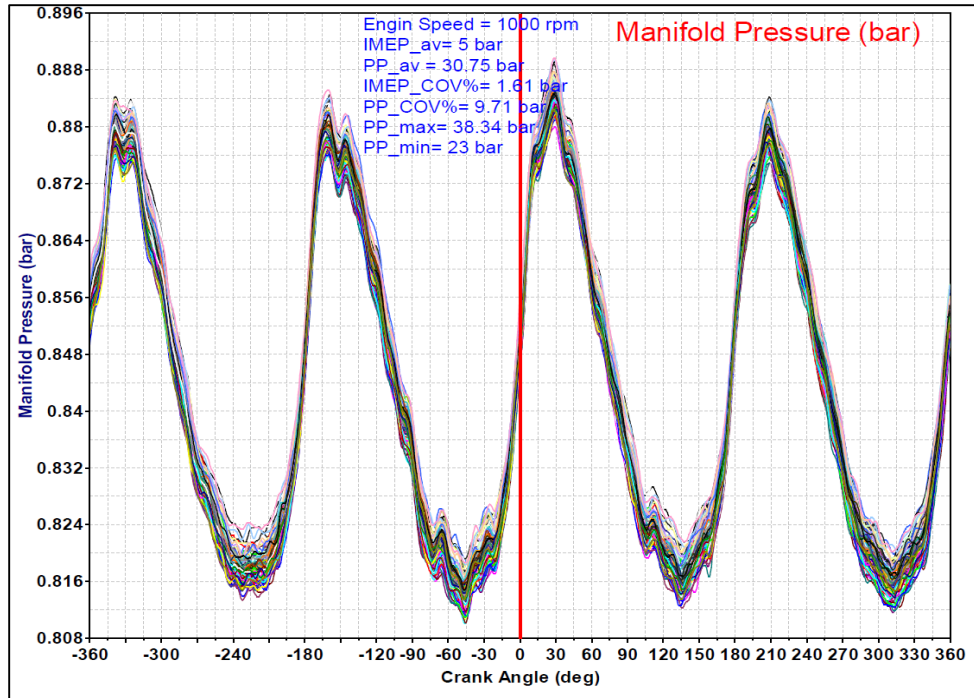


Figure 7.34 Intake manifold absolute pressure of 100 consecutive cycles at 1000 rpm, 5.2 IMEP of cylinder # 1

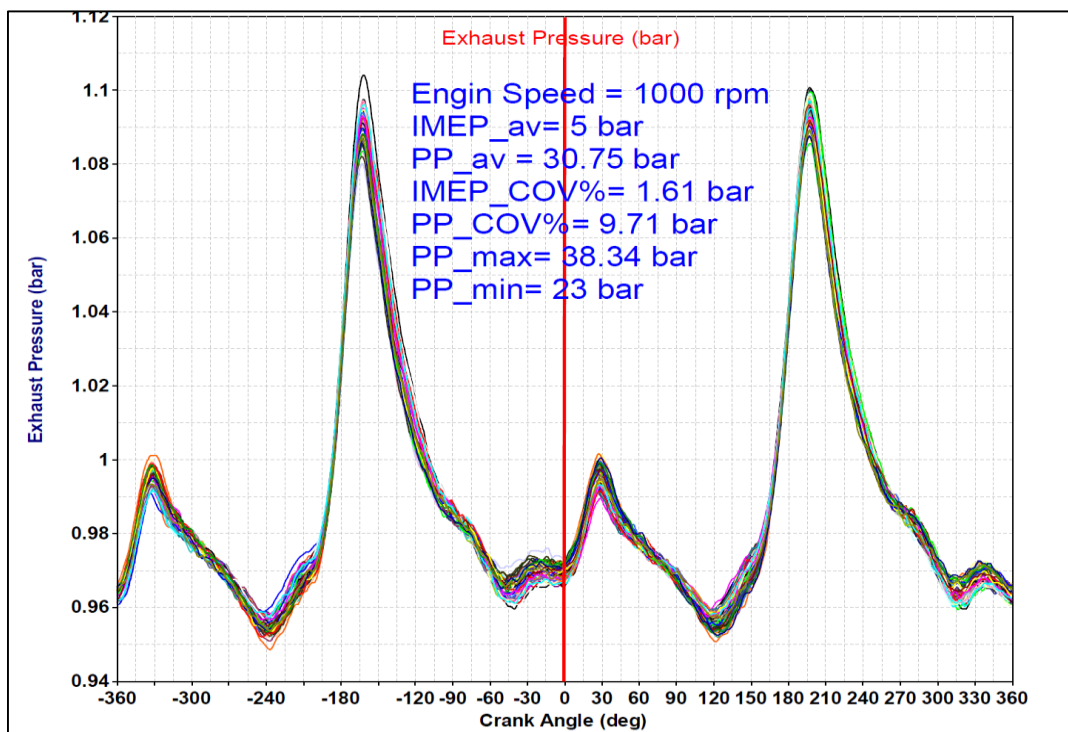


Figure 7.35 Exhaust manifold absolute pressure of 100 consecutive cycles at 1000 rpm, 5.2 IMEP of cylinder # 1

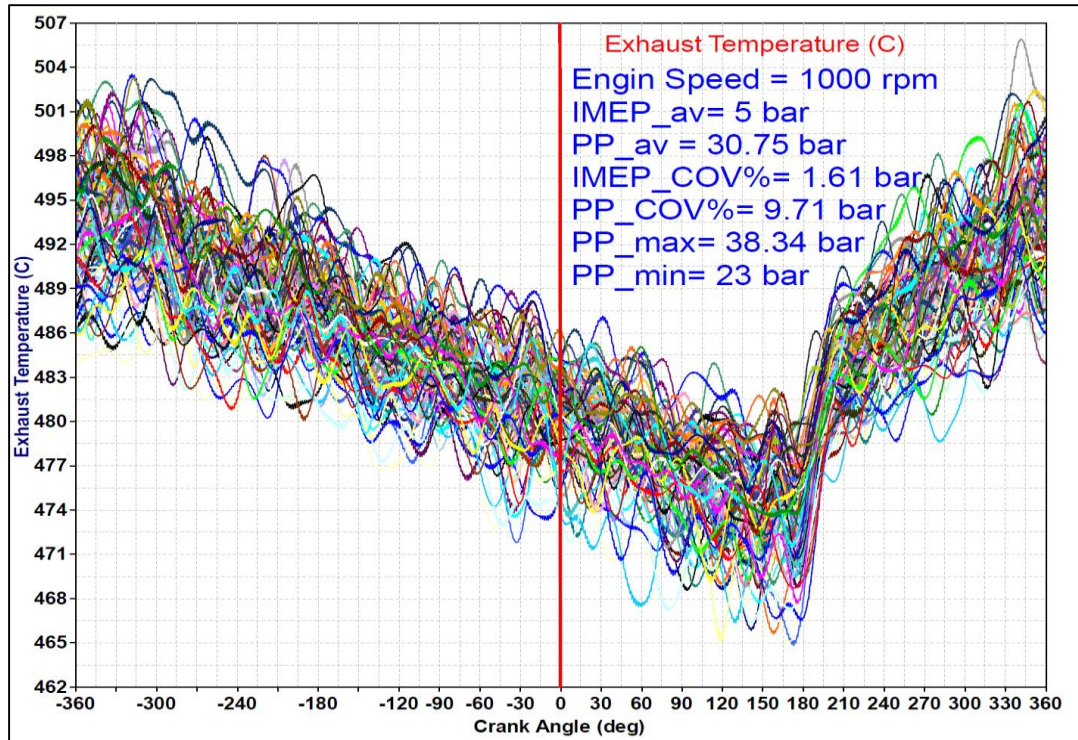


Figure 7.36. Exhaust manifold absolute temperature of 100 consecutive cycles at 1000 rpm, 5.2 IMEP of cylinder # 1

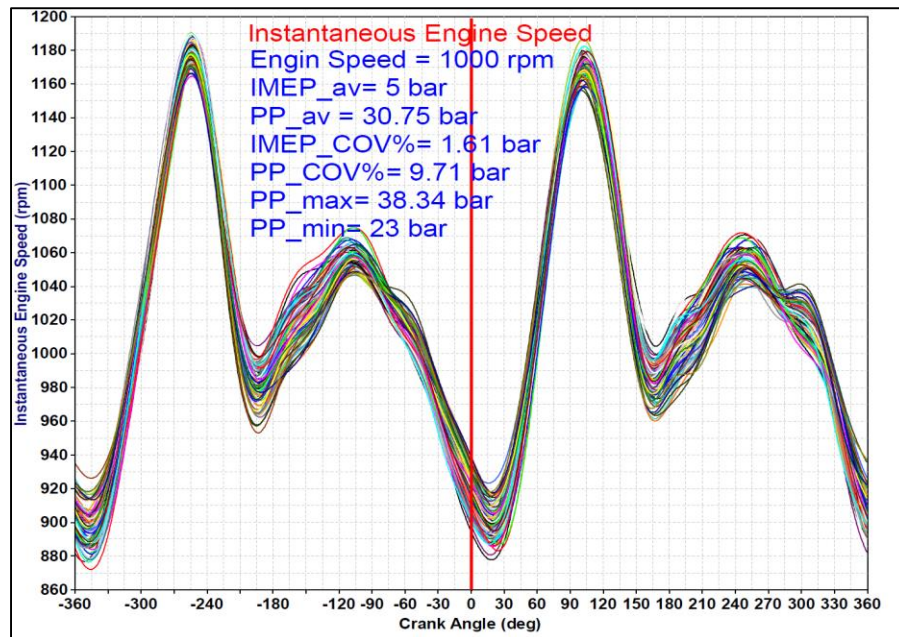


Figure 7.37. Instantaneous engine speed of 100 consecutive cycles at 1000 rpm, 5.2 IMEP of cylinder # 1

### 7.15 Results of 100 consecutive cycles at 1250 rpm and 1.5 IMEP

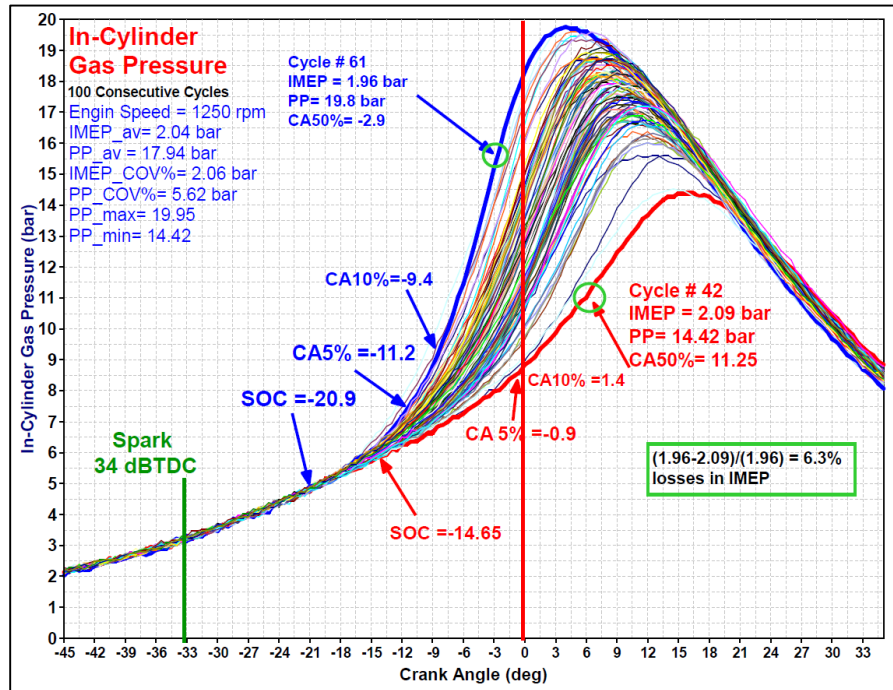


Figure 7.38. Zoomed traces of In-Cylinder gas pressure of 100 consecutive cycles at 1250 rpm and 1.5 IMEP, test # 1.

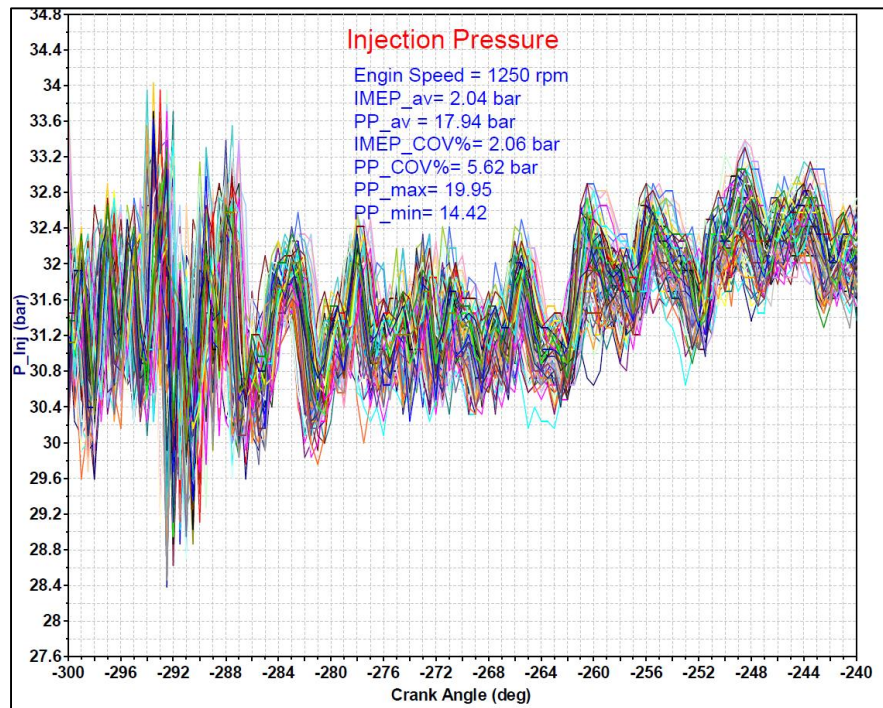


Figure 7.39. Instantaneous Injection Pressure distribution of 100 consecutive cycles at 1250 rpm and 1.5 IMEP at the inlet of the injector of cylinder # 1



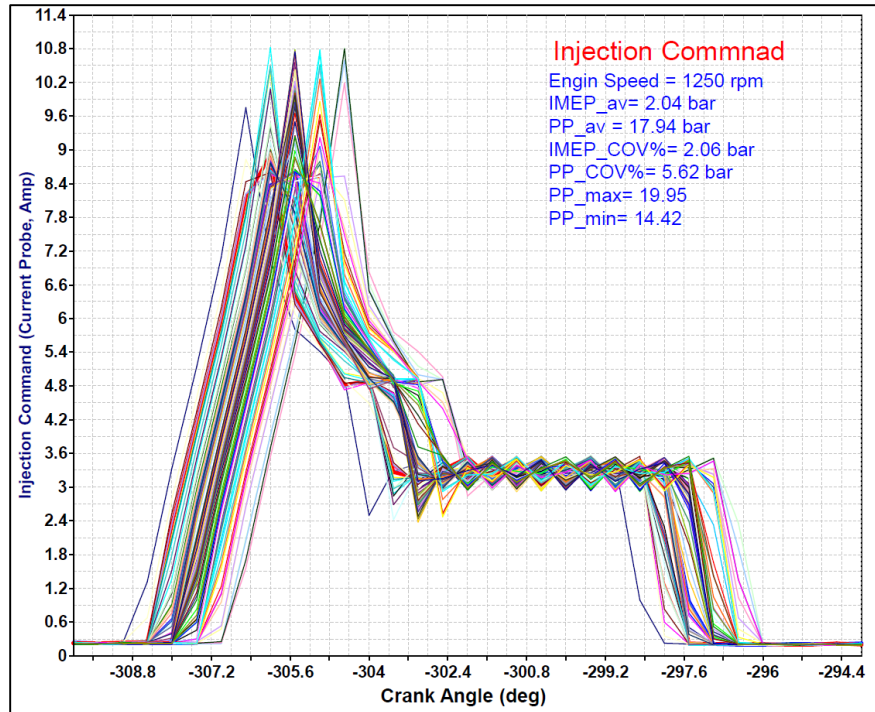


Figure 7.40. Injection command of 100 consecutive cycles at 1250 rpm and 1.5 IMEP of cylinder # 1

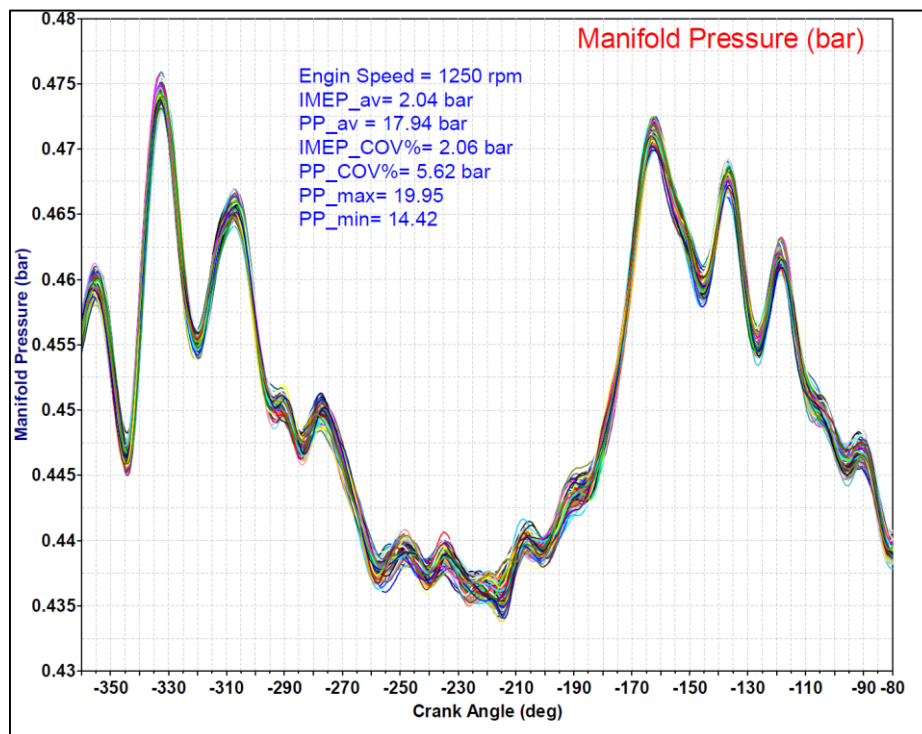


Figure 7.41 Intake manifold absolute pressure of 100 consecutive cycles at 1250 rpm, 1.5 IMEP of cylinder # 1

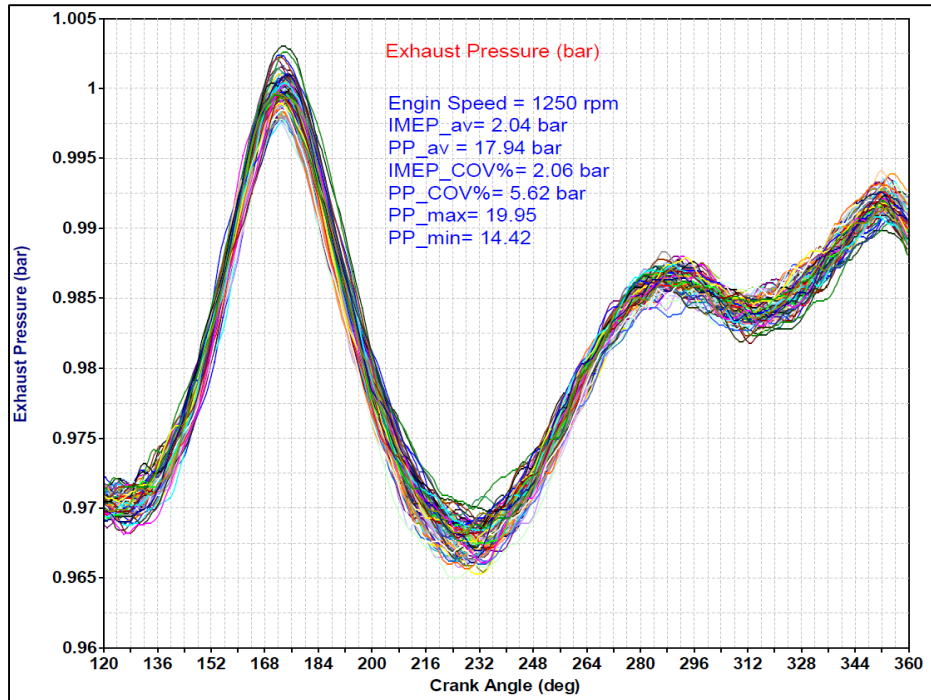


Figure 7.42 Exhaust manifold absolute pressure of 100 consecutive cycles at 1250 rpm, 1.5 IMEP of cylinder # 1

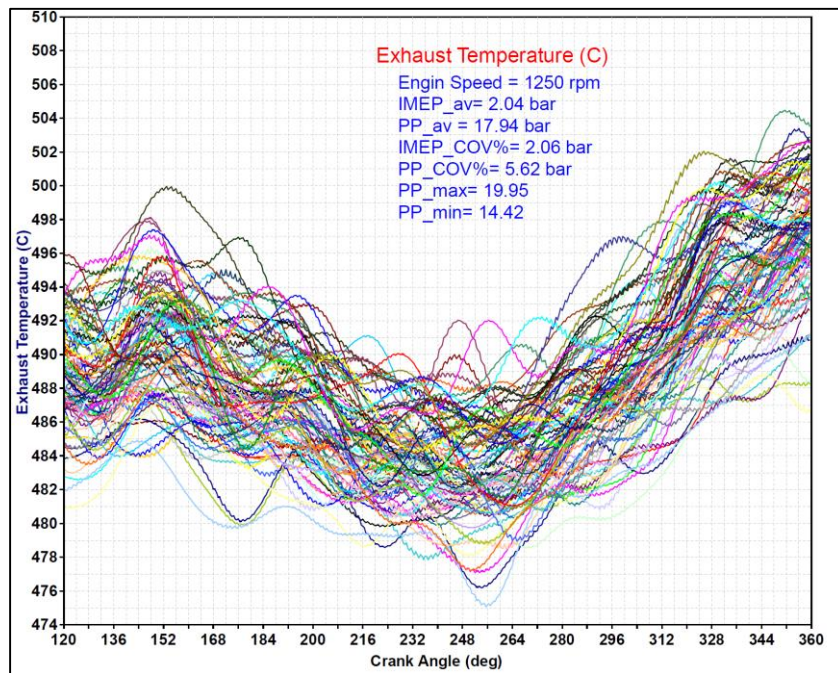


Figure 7.43. Exhaust manifold absolute temperature of 100 consecutive cycles at 1250 rpm, 1.5 IMEP of cylinder # 1



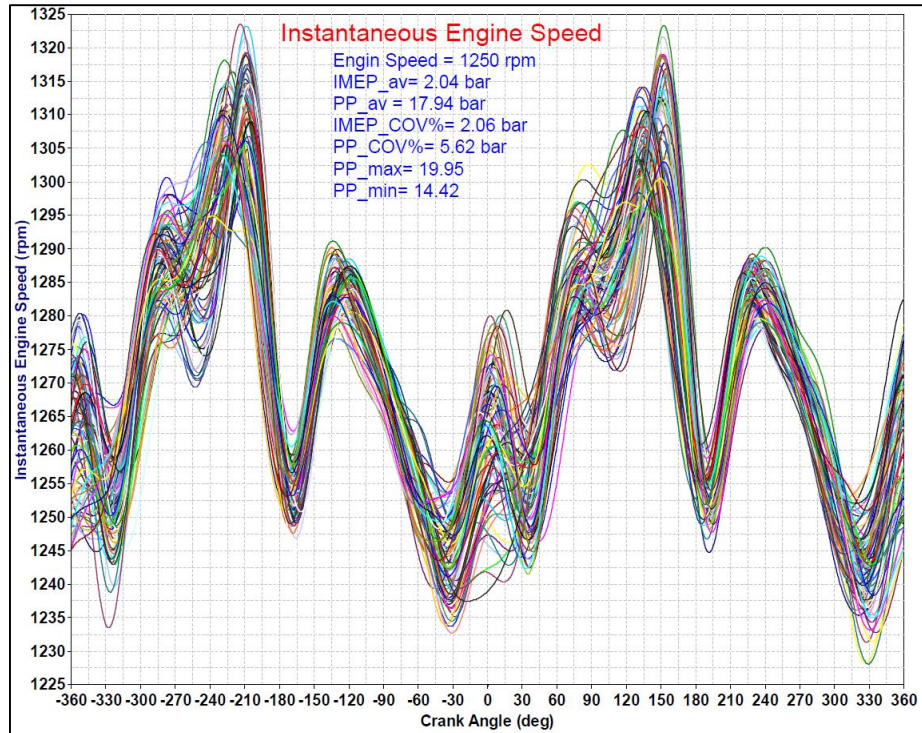


Figure 7.44 Instantaneous engine speed of 100 consecutive cycles at 1250 rpm, 1.5 IMEP of cylinder # 1

## 7.12 Summary

The fluctuation in injection pressure and injection command have been proved as a two major factors affecting the cycle to cycle variation in a gasoline direct injection engine. In addition, the results from this research showed that the cycle to cycle variation is less dependent on the intake pressure and temperature, exhaust pressure and temperature, engine speed and ignition command.

## CHAPTER 8 PRE-IGNITION INVESTIGATION

### 8.1 Introduction:

Today, increasingly more vehicles are being fitted with downsized boosted gasoline engines to help improve fuel economy. However, in these engines, improvements in torque at low engine speeds are restricted by a sudden pre-ignition phenomenon called low-speed pre-ignition (LSPI), which occurs at low engine speed high-load engine operation regions. Despite much research, the source of LSPI and the ignition mechanism have yet to be fully identified. The LSPI phenomenon targeted in this study generates very high cylinder pressure suddenly and without any preceding phenomena. As far as can be observed from in-cylinder gas pressure, combustion due to this pre-ignition phenomenon is caused by an ignition source somewhere in the combustion chamber, begins before the spark ignition timing, and is not a self-ignition phenomenon of the whole mixture. The main advantages of GTDI engine are:

1. Higher thermal efficiency due to its higher compression ratios and higher specific power density due to its higher volumetric efficiency.
2. Higher volumetric efficiency due to the effect of fuel spray evaporative cooling of the compressed air charge.

### 8.2 Major Problem in GTDI engine

Sporadic pre-ignition produces fairly high peak cylinder gas pressures and rates of pressure rise that can damage the piston and other moving parts.

### 8.3 Main Objective

Prediction of pre-ignition by combustion ionization in order to avoid it.

### 8.4 Test cell preparation for pre-ignition test.

To study the low speed pre-ignition, as recorded by many researchers, pre-ignition requires a special setup for the test cell, such as:

- 1- Engine cooling circuit, to control the coolant temperature between 60C to 95C.

- 2- Turbocharger Intercooler cooling circuit to keep the charge air temperature between 15 C° and 45 C°
- 3- Full authority over the spark characteristics to advance or retard the spark timing, or to produce double strike ignition.
- 4- Precise control over the injection timing characteristics regarding the timing, duration and injection pressure.

#### 8.4.1 Engine cooling circuit;

The engine is equipped by a special cooling circuit to bypass the engine thermostat and keep the engine block metal temperature at the desired level and vary it according to the needs. A water to water heat exchanger cooling system has been used and equipped by all the necessary fast response thermocouples to measure the temperatures at the engine inlet and outlet. A mechanical thermostat is installed at the heat exchanger engine coolant outlet to control the flow according to the desired temperature as shown Figure 8.1.

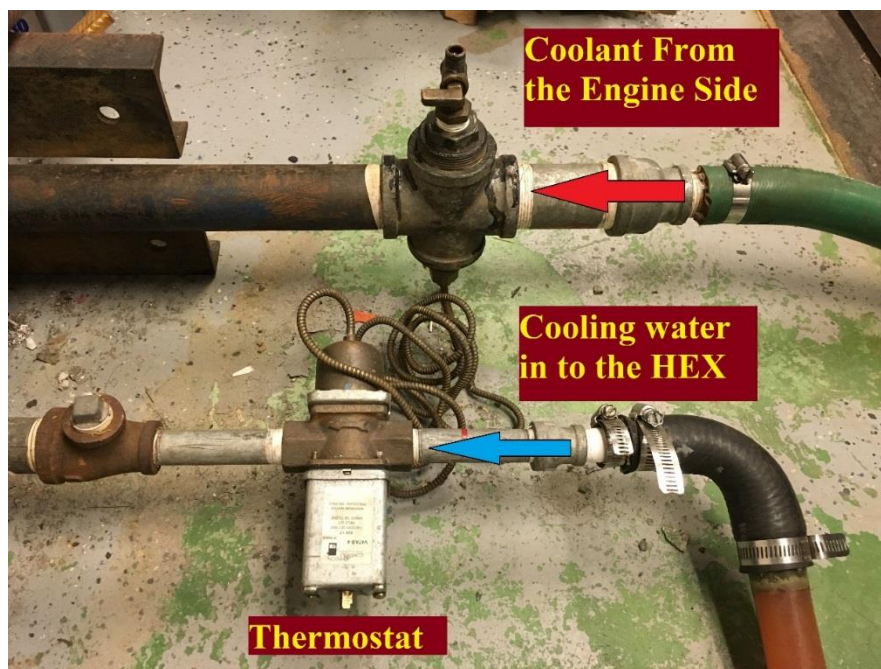


Figure 8.1. Image for the water to water HEX to control the engine coolant temperature.

#### 8.4.2 Turbocharger intercooler cooling circuit;

Pre-ignition testing requires the manifold absolute air temperature to be around 15 degrees Celsius to be able to increase charge air flow. According to the designed system, the cooling system was able to keep the manifold absolute air temperature around 20 degrees Celsius. The Water to Air heat exchanger used in this setup is shown in Figure 8.2.

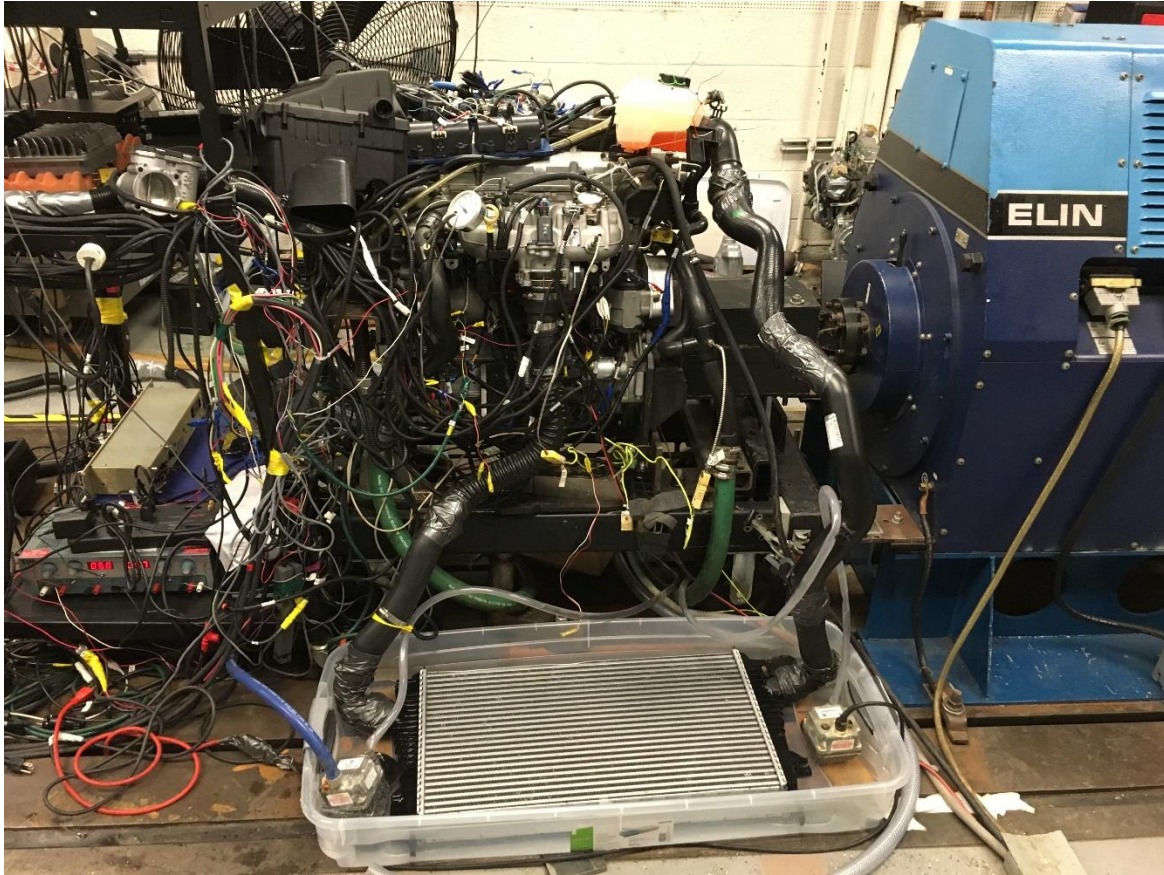


Figure 8.2. Image of the water to air cooled after-cooler

#### 8.4.3 Spark control

Advancing and retarding the spark timing is very important to achieve pre-ignition. A LabVIEW system has been developed to control the ignition timing and duration precisely. The system was able to advance the spark timing to be at the incipient knock to achieve the pre-ignition due to knock. Also, retarding the spark timing leads to late combustion and increases the residuals temperatures.



#### 8.4.4. Injection control to achieve pre-ignition.

Injection timing and targeting are highly important in hydrocarbons in exhaust products. As many researchers believed that one of the factors that could lead to pre-ignition is the hot spots [69 & 70] in the combustion chamber that could help ignite the mixture before the spark timing. A LabVIEW system has been developed to control the injection timing and duration.

#### 8.5 Characteristics of the ion signal from spark plug with the ignition command

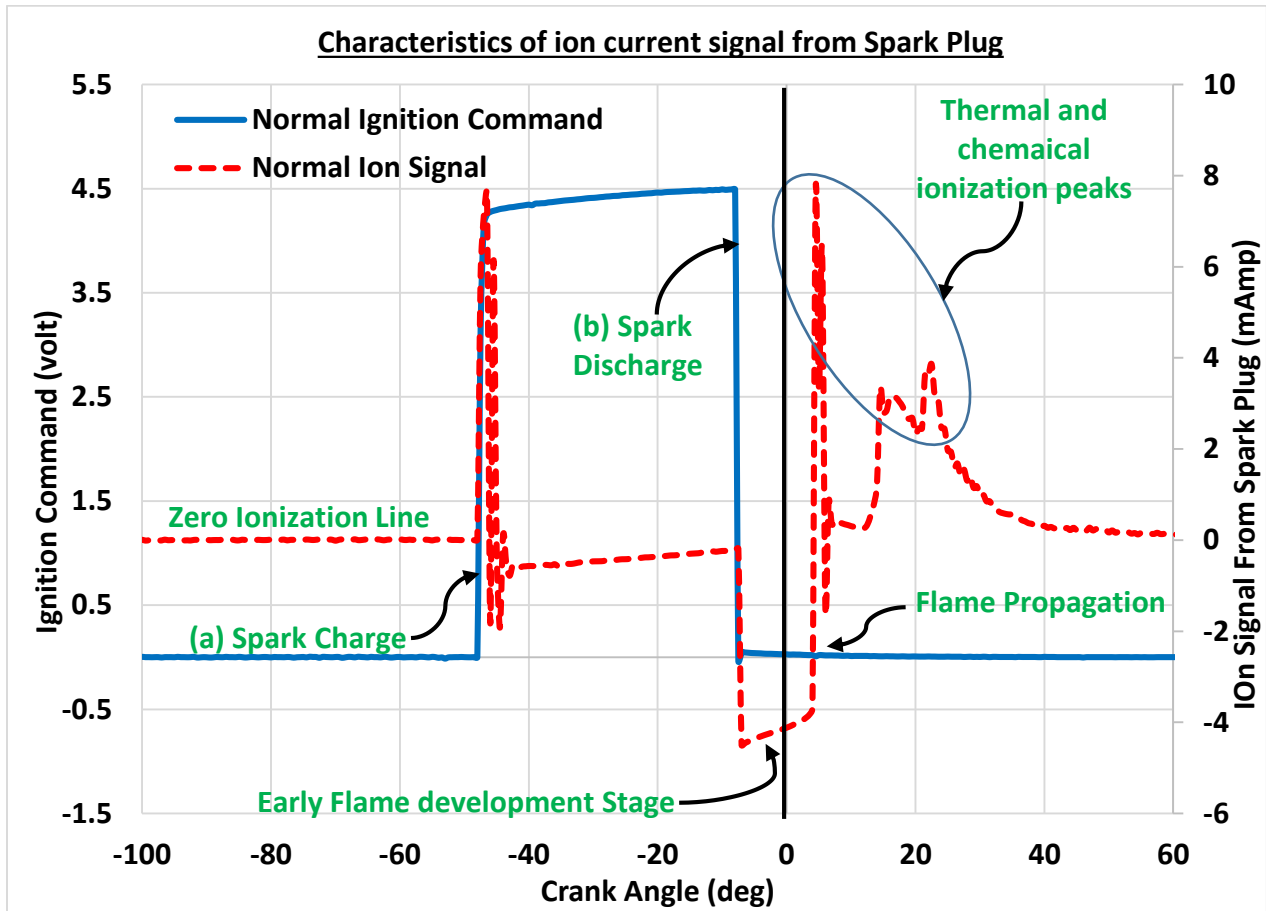


Figure 8.3. The features of the ion current signal with the ignition command

The in current signal from the spark plug ion sensor has many features including the spark charge and spark discharge. Figure 8.3 shows the characteristics of the ion current signal from the spark plug ion sensor compared to the ignition command. The characteristics of the ignition command, spark charge, charging time and the spark discharge are detected by the signal from the ion circuit. Before the spark

charge, the ion signal reading has zero amplitude as there is no ionization in the combustion chamber since no combustion has taken place yet. When the spark discharges, there is ignition delay which appears on the ion signal as the period of the early flame stage development. Then, the first ion current peak is due to chemi-ionization that occurs is due to high chemical reaction in the flame kernel around the spark plug gap. The second peak is mainly due to thermal ionization which occurs later due to the high rise in gas temperature around the spark plug electrodes. A party of the second peak can be due to chemical ionization. As the combustion ends, the ion current signal from the spark plug drops and remains at zero until the next cycle.

### **8.6 Pre-Ignition prediction.**

During a complete cycle for a four stroke spark ignition engine, the first time that the ionization should occur is when the flame starts at the spark plug gap after the spark discharge. Then, the ionization ends by the end of chemical reaction at the spark plug gap. Furthermore, in the period from the end of combustion till the flame start of the next cycle, there should not be any ionization in the combustion chamber since there is no chemical reaction at the spark plug gap during this period.

Before the spark discharge, no ionization should appear on the ion signal from the spark plug. Any pre-ignition that occurs before the spark discharge will be detected by the spark plug and appears on ion current signal. Thus, if there is any ionization detected by the spark plug ion sensor before the spark discharge, this will be an indication of pre-ignition.

In addition, one of the most important expectations is to see any change in the ion signal from the cycle before the pre-ignition cycle. Very late combustion may cause the fresh charge of the next cycle to ignite before the spark timing.

### **8.7. Pre-Ignition Test with single and double injection and synthetic oil.**

#### **8.7.1 First Pre-Ignition attempt using the engine ECU and pump gasoline.**

**Double injection and using recommended oil (5W-30 with reduced additives)**

Pre-ignition test were performed under many operating conditions as shown in Table 8.1. Most of the operating conditions were at low speed, high load to produce Low Speed Pre-Ignition (LSPI). Tests have been performed on the GDI engine using regular gasoline octane number 87, 93 and 95. The test were performed for one hour at each one of the operating conditions mentioned in Table 8.1. In addition, the tests were conducted on the engine using the production ECU with the base ignition and injection timing.

Test #	Engine Speed (rpm)	Engine Load	Control type	Fuel Octane No.	No. of PI
1	1000	75 %	Production ECU	87, 93 and 95	None
2	1050	80%	Production ECU	87, 93 and 95	None
3	1100	WOT	Production ECU	87, 93 and 95	None
4	1150	93%	Production ECU	87, 93 and 95	None
5	1200	Full Load	Production ECU	87, 93 and 95	None
6	1250	Full Load	Production ECU	87, 93 and 95	None
7	1400	98%	Production ECU	87, 93 and 95	None
8	1500	95%	Production ECU	87, 93 and 95	None
9	1600	Full Load	Production ECU	87, 93 and 95	None
10	1650	Full Load	Production ECU	87, 93 and 95	None
11	1800	95%	Production ECU	87, 93 and 95	None
12	2000	Full Load	Production ECU	87, 93 and 95	None
13	2200	Full Load	Production ECU	87, 93 and 95	None
14	2400	Full Load	Production ECU	87, 93 and 95	None

Table 8.1. Pre-Ignition test matrix using the production ECU and pump fuel

Table 8.1 shows the test matrix of the experimental tests that were conducted to investigate pre-ignition using the production ECU and the regular gasoline with octane numbers 87, 93 and 95. However, none of the above 42 tests produced pre-ignitions. The main reason behind this is the engine was running on a production engine control unit which was designed to protect the engine from getting PI.

#### 8.7.2 Second Pre-Ignition attempt using the engine ECU and special gasoline fuel.

After unsuccessful trials to produce pre-ignition using the gasoline fuel from the pump, GM provided us with a special fuel designed especially to produce pre-ignition. A test matrix has been applied on the new gasoline as shown in table 8.2.

Test #	Engine Speed (rpm)	Engine Load	Control type	Fuel Octane No.	Running time (mints)	No. of PI
1	1000	80 %	Production ECU	Special Fuel	5	None
2	1100	Full Load	Production ECU	Special Fuel	30	None
3	1205	Full Load	Production ECU	Special Fuel	3	1
4	1230	85%	Production ECU	Special Fuel	25	1
5	1500	Full Load	Production ECU	Special Fuel	30	None
6	1800	Full Load	Production ECU	Special Fuel	30	None
7	2000	70%	Production ECU	Special Fuel	60	None
8	2000	Full Load	Production ECU	Special Fuel	2	1

Table 8.2. Pre-Ignition test matrix using the production ECU and pump fuel.

#### 8.7.3 Pre-ignition results.

One of the common operating conditions that leads to pre-ignition is 1230 rpm and 148 N.m. The engine was running smoothly at this operating condition, but after 8 minutes, the engine experienced the first pre-ignition cycle in cylinder # 1. Figure 8.4 shows the pre-ignition cycle (red color) and a normal cycle



which is the cycle just before the pre-ignition cycle (blue) and cycle after pre-ignition cycle (black color). Figure 8.4 shows that the cycle before the pre-ignition cycle is a normal cycle, the spark timing is 2.0 dBTDC, the combustion started after TDC with SOC 6.5 dATDC, and the location of the peak pressure is after the TDC with PPL = 36 dATDC and MBF 50% = 30 dATDC. The ion signal from the spark plug for this cycle looks normal, and there is no change in the ionization pattern in this cycle. The cycle after the normal one experienced Pre-Ignition with start of combustion way before the TDC with SOC = 24 dBTDC and the location of the peak pressure is after TDC with PPL = 3 dATDC and MBF 50% = 0.5 dBTDC. The ionization signal from this cycle showed that the combustion started before the spark discharge. The ion signal from the spark plug was able to predict the pre-ignition before it took place.

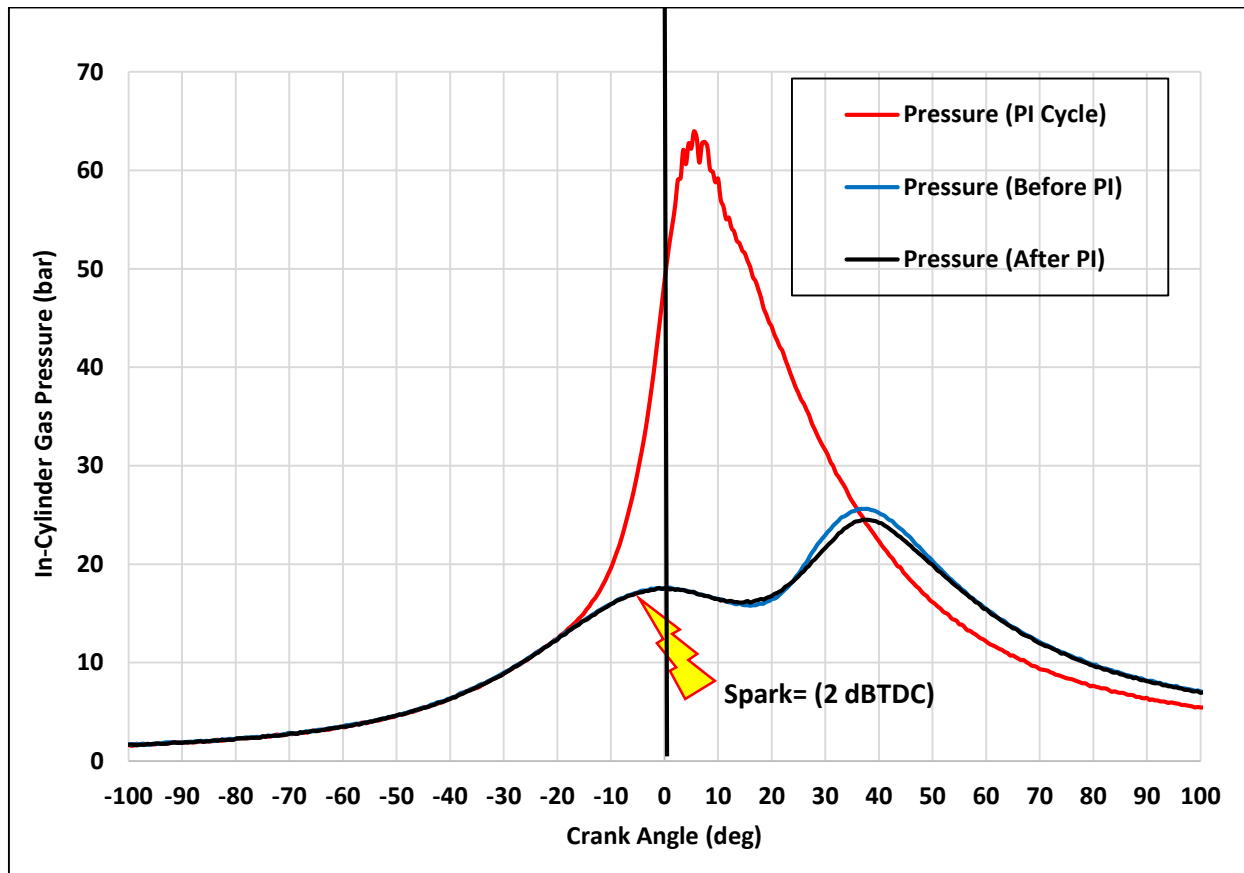


Figure 8.4. In-cylinder gas pressure for pre-ignition cycle (red), cycle before PI (blue) and cycle after PI (black) at 1230 rpm and 148 N.m, cylinder # 1.

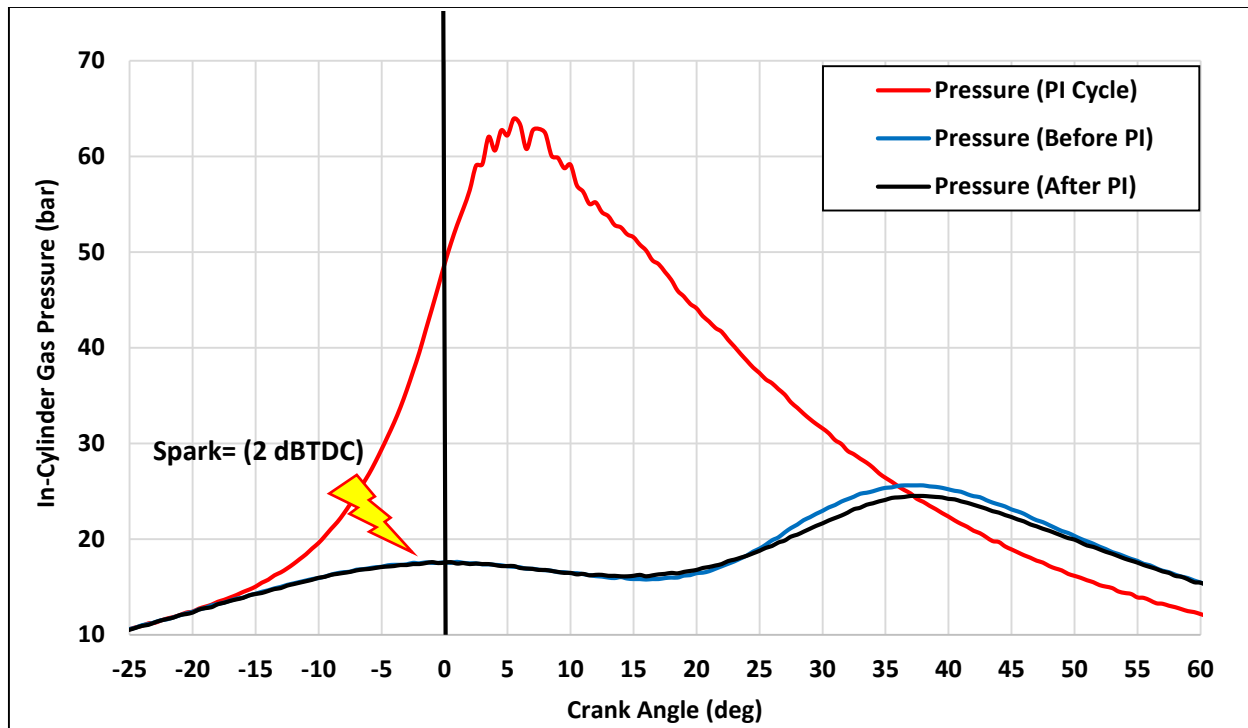


Figure 8.5. Zoomed traces for In-cylinder gas pressure for pre-ignition cycle (red), cycle before PI (blue) and cycle after PI (black) at 1230 rpm and 148 N.m, cylinder # 1

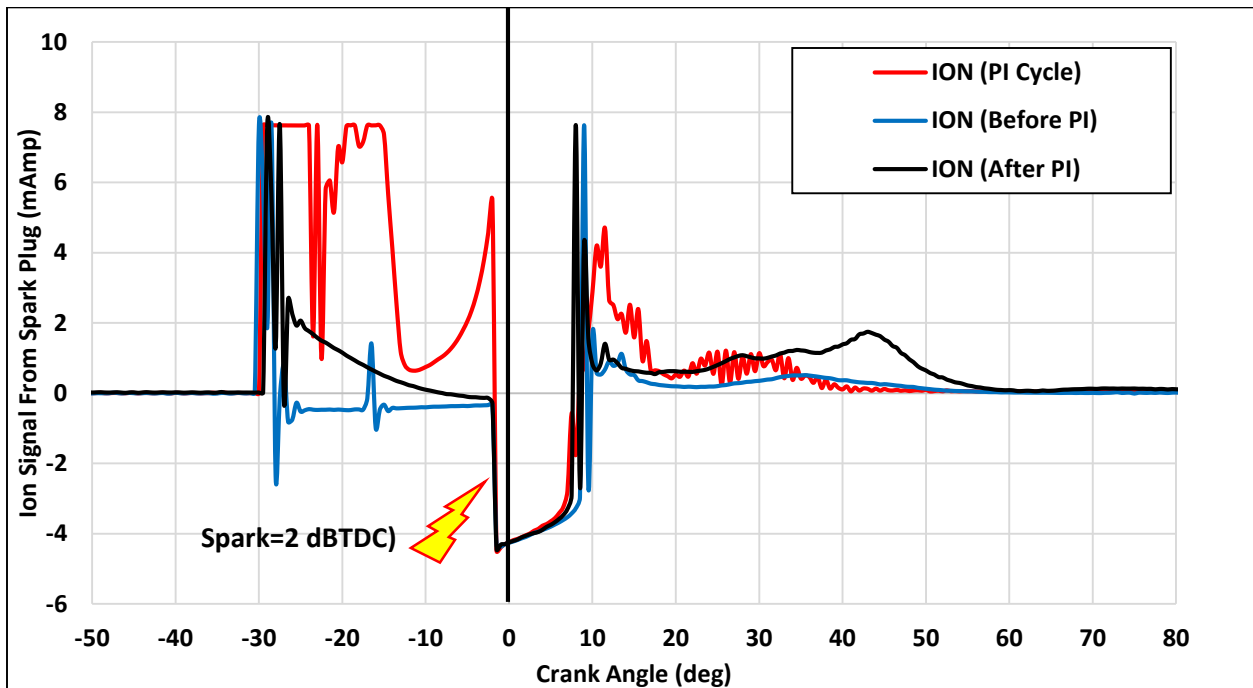


Figure 8.6. Ion signal from spark plug for pre-ignition cycle (red), cycle before PI (blue) and cycle after PI (black) at 1230 rpm and 148 N.m, cylinder # 1

Figures 8.4, 8.5 and 8.6 show the data for the Pre-ignition test at 1250 rpm and 9 bar IMEP. In this test, the pre-ignition took place in cylinder # 1 after 8 minutes after which the engine continued running at the same speed and load for while operating temperatures were steady.

Figure 8.4 shows the details of the three consecutive cycles for the in-cylinder gas pressure traces: the cycle just before the pre-ignition (blue), the pre-ignition cycle (red) and the cycle just after the pre-ignition (black). Figure 8.5 shows zoomed traces for the in-cylinder gas pressure for 1230 rpm and 148 N.m. The spark timing for this operating condition was 2 degrees bTDC, and it shows that the cycle before the PI cycle ignited normally and the SOC for this cycle is around 1 degree before TDC. In the pre igniting cycle, the combustion started around 24 degrees BTDC even though the spark timing was 2 degrees BTDC.

The peak pressure for this cycle was around three times the peak pressure for the cycle before the pre-ignition one. Figure 8.6 shows the ion current signals for the three consecutive cycles: the cycle just before the pre-ignition (blue), the pre-ignition cycle (red) and the cycle just after the pre-ignition (black). The cycle before the PI cycle has a normal trend for the ion current signal with no change that could indicate that the pre-ignition will take place in next cycle.

As explained in Figure 8.3, we were looking some changes on the ion current signal from the cycle before the PI cycle. However, the cycle before the PI didn't show any signs. The cycle after the PI cycle (black) showed something on the part that during the spark charging time. We recorded 100 consecutive cycles before and after the PI cycle, but none of them had pre-ignition. A 100 consecutive cycles before and after the pre-ignition one have been investigated. However, this change didn't show any relation with the pre-ignition since the cycles after that one showed normal combustion. On the other hand, this change in the signal might have been caused by the pre-ignition that took place on the cycle before that one.

The cycle that has pre-ignition (red) showed remarkable change on the ion current signal from the spark plug. Figure 8.7 shows the ion current signal from the spark plug and the equivalent RHR for the two consecutive cycles, the cycle before the PI and the PI cycle. The ion current signal of the PI cycle

showed saturation of ionization at the beginning of the spark charge, which means there was combustion at the spark plug gap at this time.

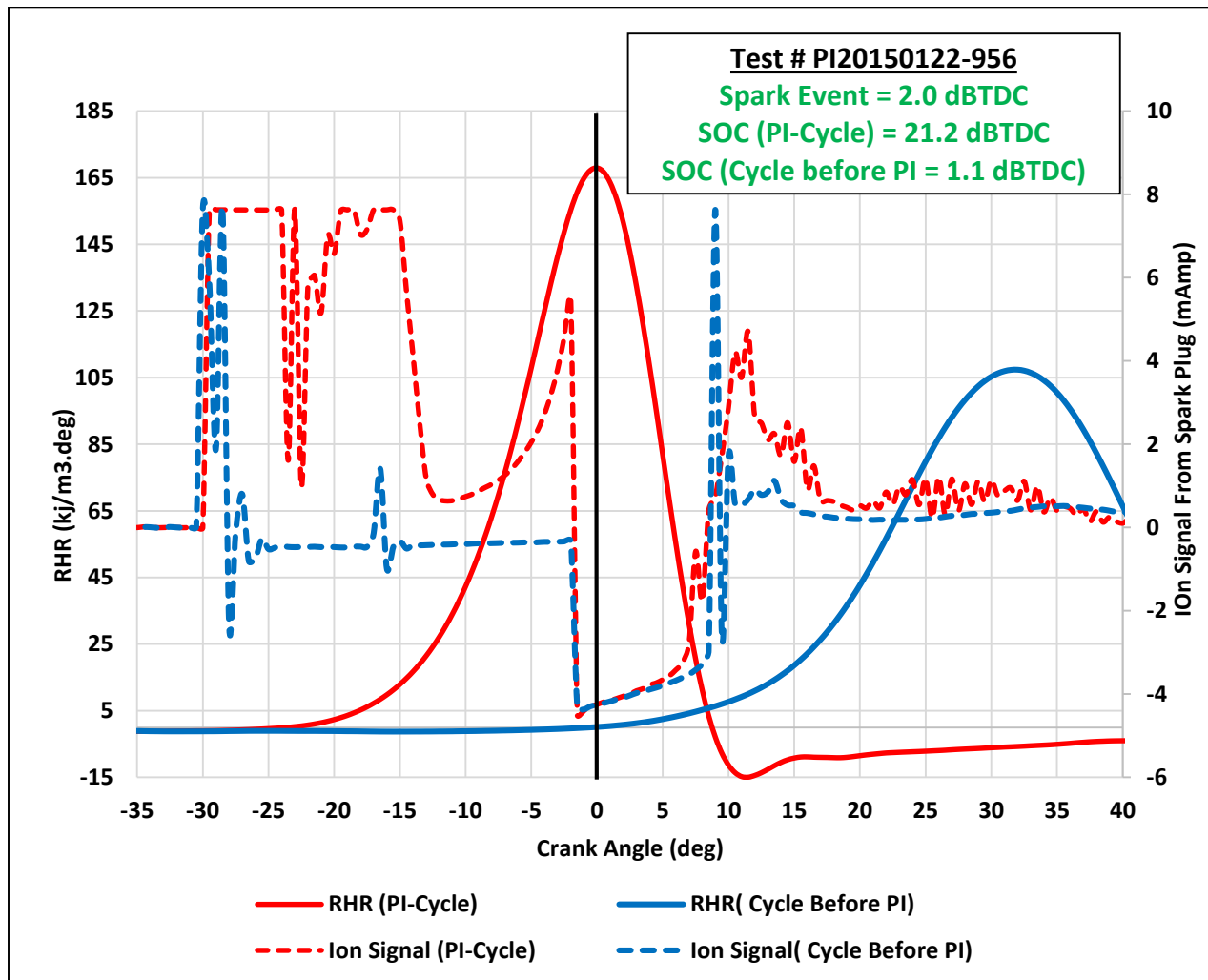


Figure 8.7. Ion signal from spark plug and RHR for pre-ignition cycle (red) and cycle before PI (blue) at 1230 rpm and 148 N.m, cylinder # 1

The SOC of normal combustion is 1.1 dBTDC, but for the PI cycle, the SOC is 21.1 dBTDC and the spark discharge time was 2 dBTDC. This explains that the combustion started at the spark plug gap before the spark discharge. However, the ion signal from the spark plug has zero amplitude in the period before the spark charge, and the ion signal was able to detect pre-ignition but wasn't able to predict pre-ignition or give any sign that the pre-ignition will take place.

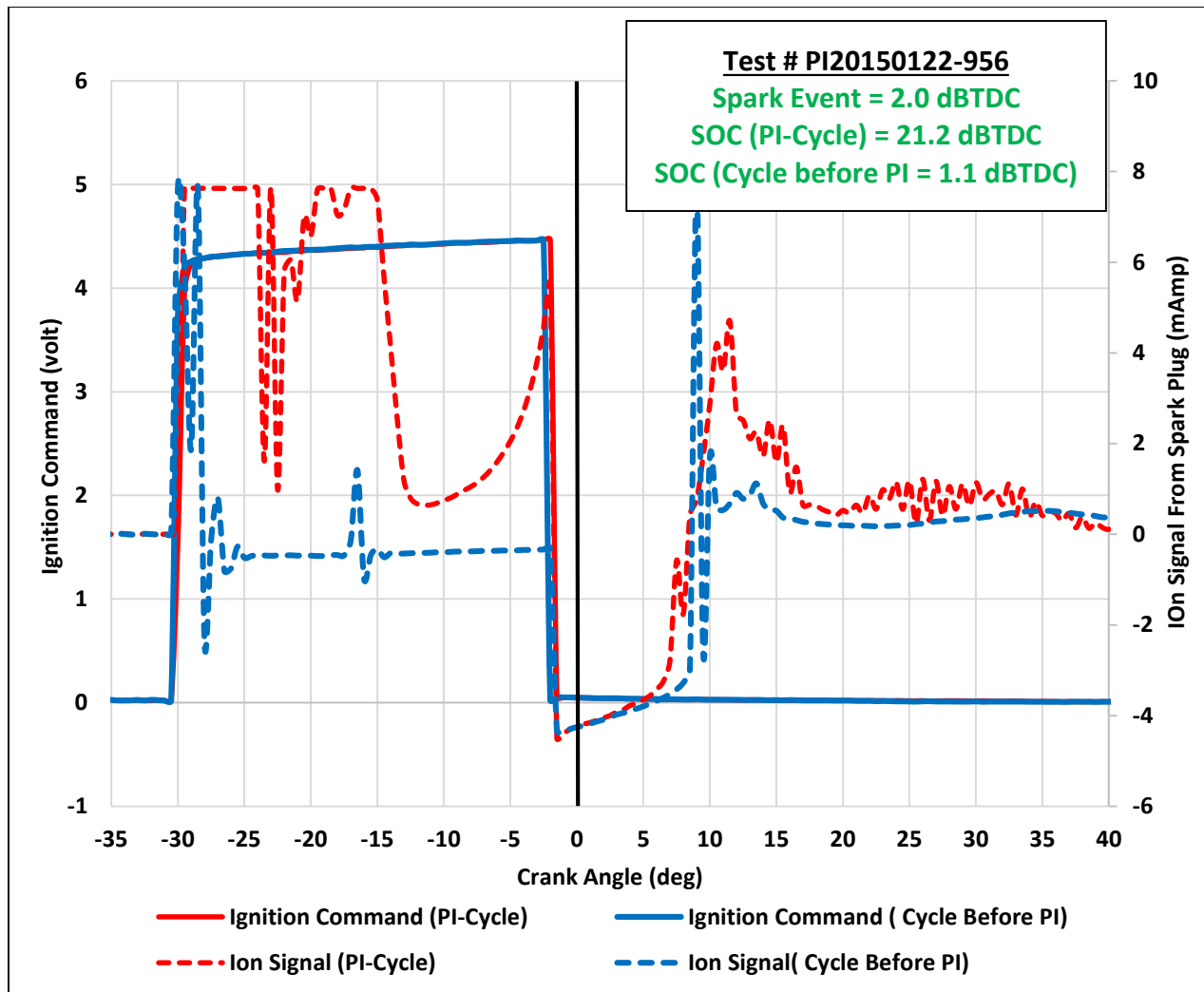


Figure 8.8. Zoomed traces for Ion signal from spark plug and ignition command for pre-ignition cycle (red) cycle after PI (black) at 1230 rpm and 148 N.m, cylinder # 1

Figure 8.8 shows the ignition command and ion signal from the spark plugs of two consecutive cycles. The blue one is the cycle before the PI and the red one is the PI cycle itself. The spark command showed that the discharge started around 2 degrees BTDC. The ion signal is from the spark plug, and it shows the characteristics of the ignition command as well. The ion signal from spark plug shows the charge time, the breakdown time and the ignition delay. Figure 8.8 shows the details of the two consecutive cycles for the ion signal traces from the spark plug of cylinder one: the cycle just before the pre-ignition (blue), the pre-ignition cycle (red) and the cycle just after the pre-ignition (black). The cycle before the PI cycle (blue) shows a normal ion signal from spark plug with normal spark charging and breakdown. In

addition, the first and second peak of this cycle had a normal combustion with no difference that can be used as a predictor for PI.

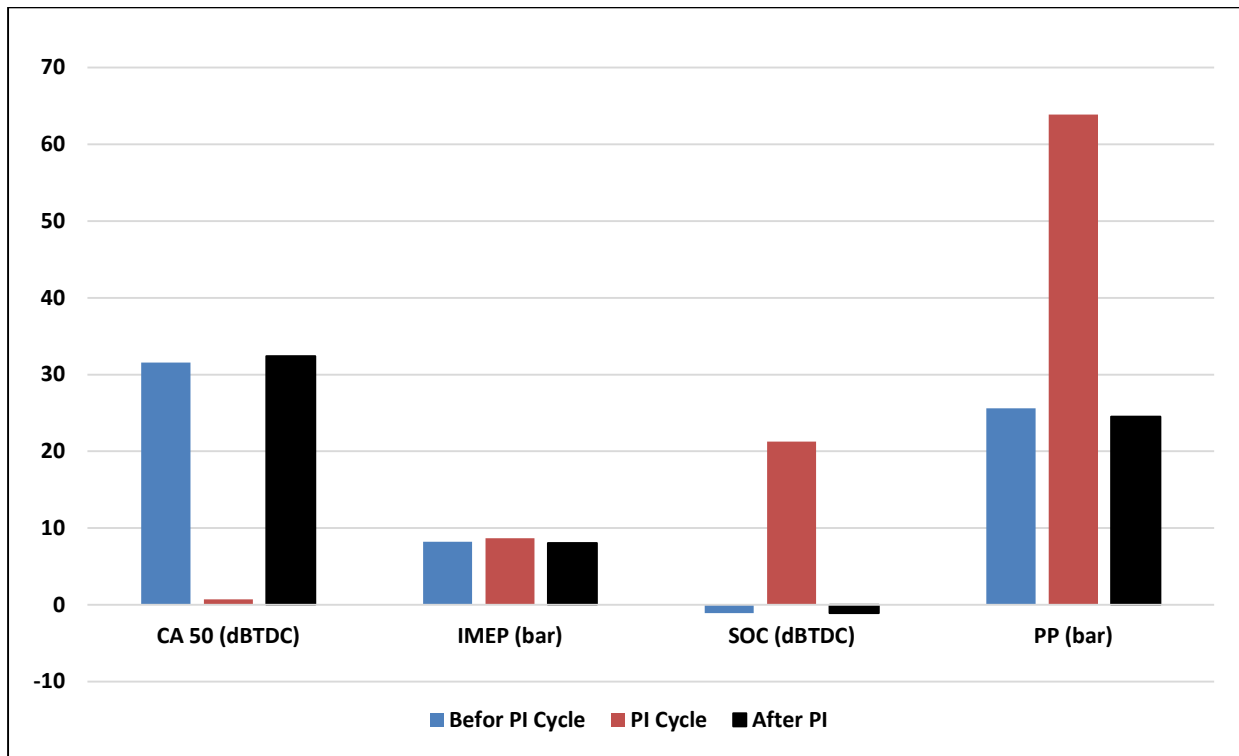


Figure 8.9. Engine performance parameters (CA50, IMEP, SOC and PP) for pre-ignition cycle (red), cycle before PI (blue) and cycle after PI (black) at 1230 rpm and 148 N.m, cylinder # 1

In addition, the first peak from the spark plug (the chemi-ionization peak) and the second peak of the ion signal (combined chemical and thermal ionization) are normal with no difference that can be used as an indicator of pre-ignition. The end of combustion appears normal on the ion signal from the spark plug. It ended normally around 60 degrees after firing TDC. Furthermore, downstream from the ion signal at 60 dATDC, nothing appeared abnormal on the ion signal that can shows any flying particles or any combusting species still combusting in the combustion chamber. The ion signal has zero amplitude after the end of combustion of the cycle before the TDC.

Figure 8.9 shows the engine performance parameters such as CA50, IMEP, SOC and PP for pre-ignition cycle (red), cycle before PI (blue) and cycle after PI (black) at 1230 rpm and 148 N.m, cylinder # 1. This figure shows that the cycles before and after the pre-ignition have normal combustion compared to

PI, which indicates that the cycle before the PI cycle didn't provide any signs to predict any information about the coming PI cycle.

Another test was done on the engine at 2000 rpm and full load (388 N.m) with coolant temperature kept at 85 degree Celsius and intake air temperature at 15 degree Celsius. After the first 2 minutes of normal running, the engine produced pre-ignition. Figure 8.10 and 8.11 shows the in-cylinder gas pressure and the ion current signals from spark plug. At this operating condition, the spark event is at 5 dBTDC and the two cycles before and after the PI cycle ignited normally with normal combustion with SOC= 0.5 dBTDC. However, the pre-ignition cycle has SOC = 6.5 dBTDC.

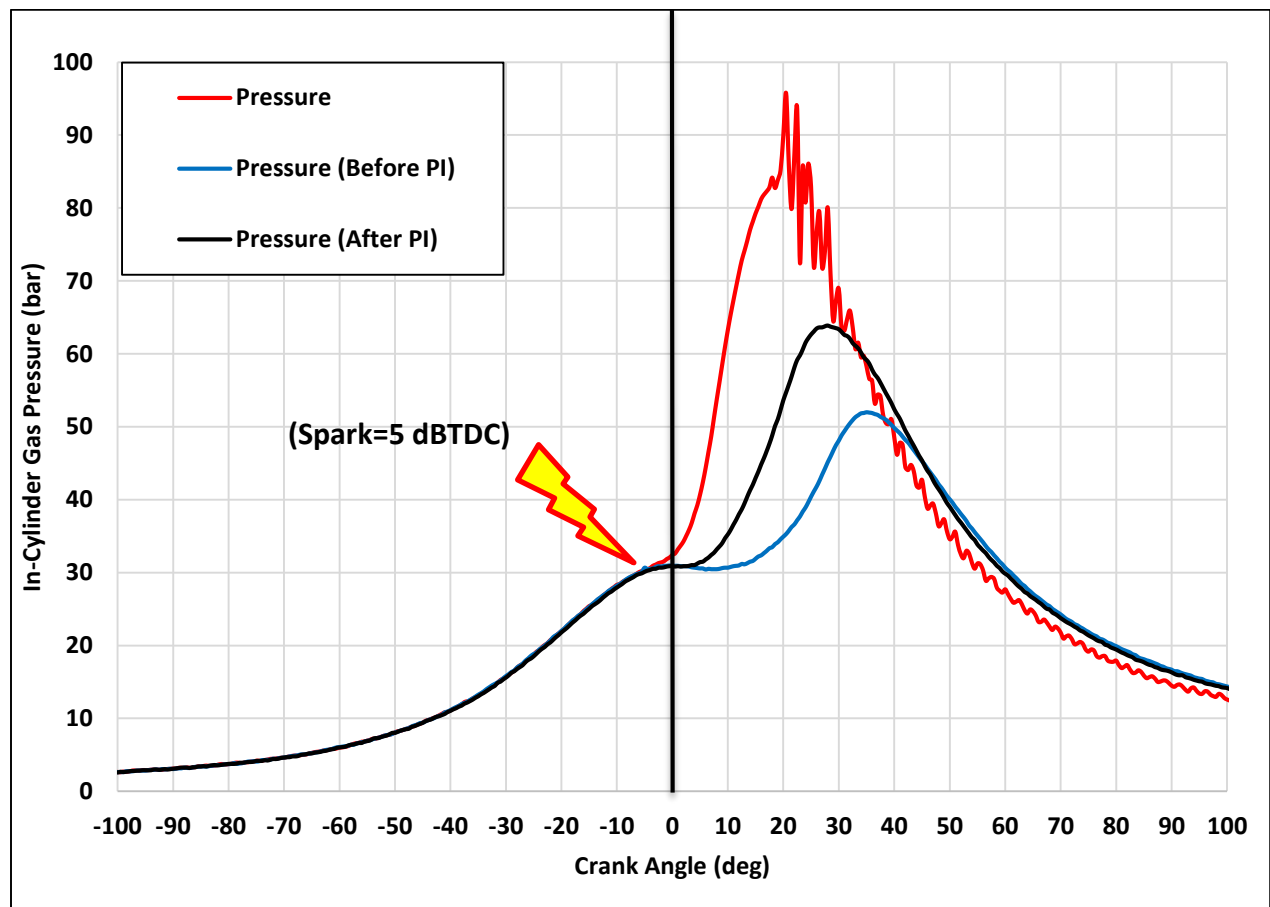


Figure 8.10. In-cylinder gas pressure for pre-ignition cycle (red), cycle before PI (blue) and cycle after PI (black) at 1205 rpm an 12 bar IMEP, cylinder # 1

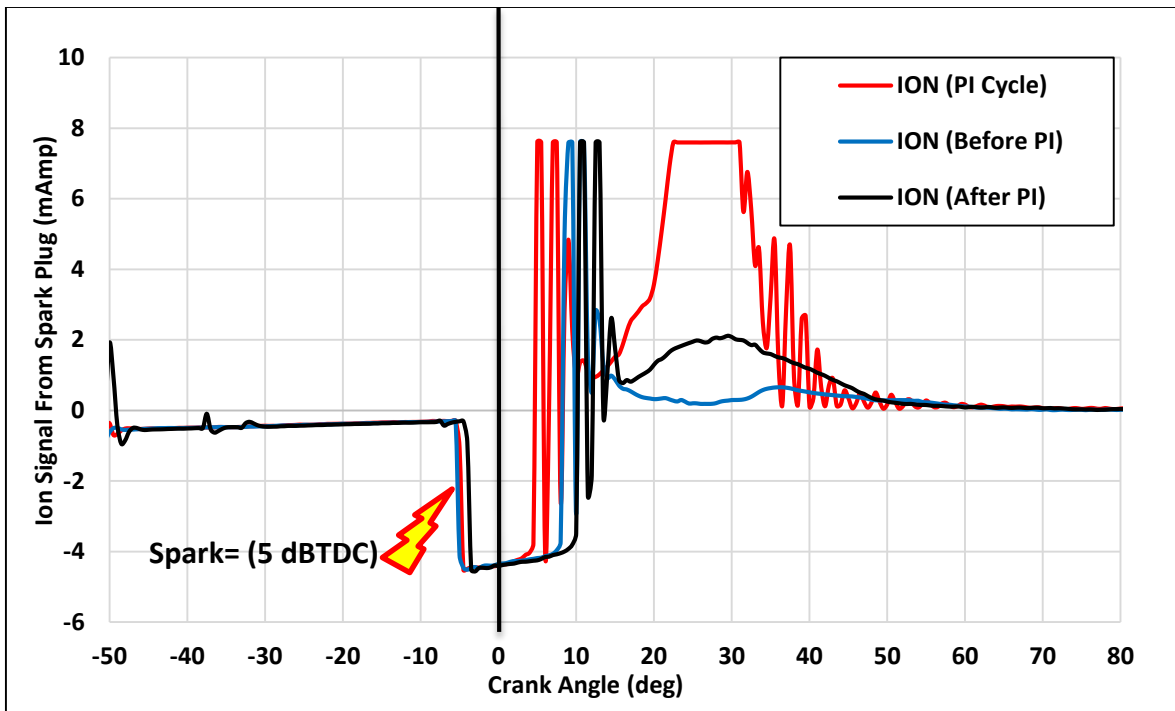


Figure 8.11. Ion signal from spark plug for pre-ignition cycle (red), cycle before PI (blue) and cycle after PI (black) at 1205 rpm an 12 bar IMEP, cylinder # 1

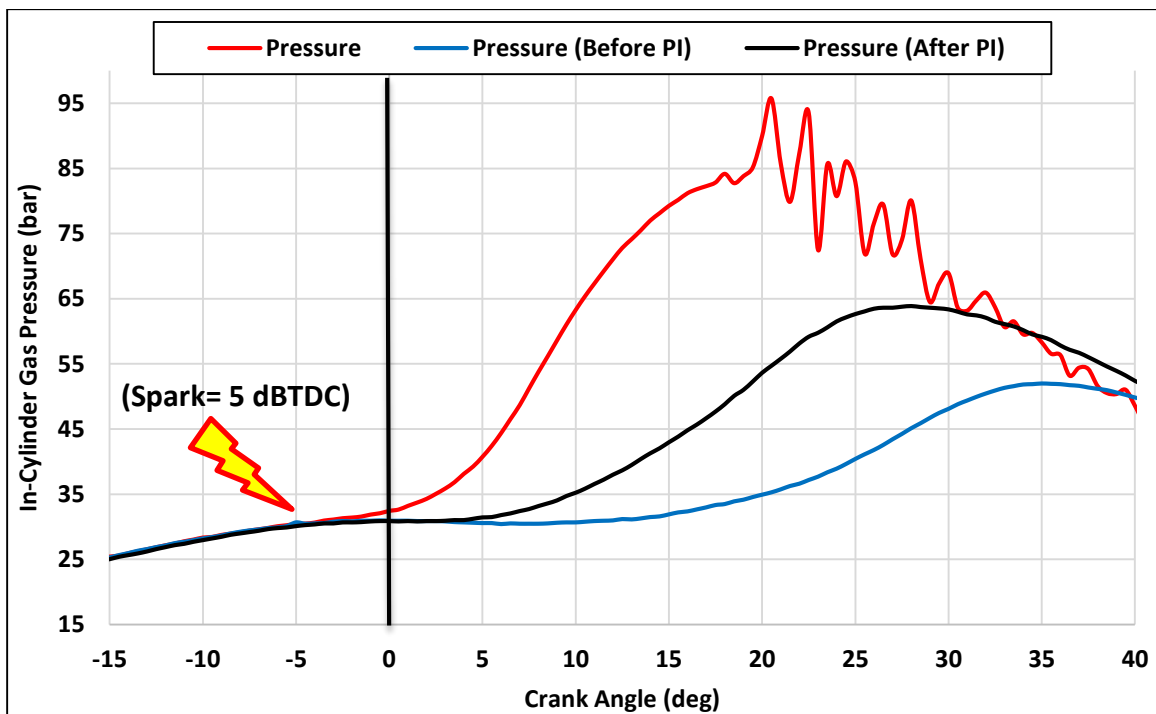


Figure 8.12 Zoomed traces for In-cylinder gas pressure for pre-ignition cycle (red), cycle before PI (blue) and cycle after PI (black) at 1205 rpm an 12 bar IMEP, cylinder # 1



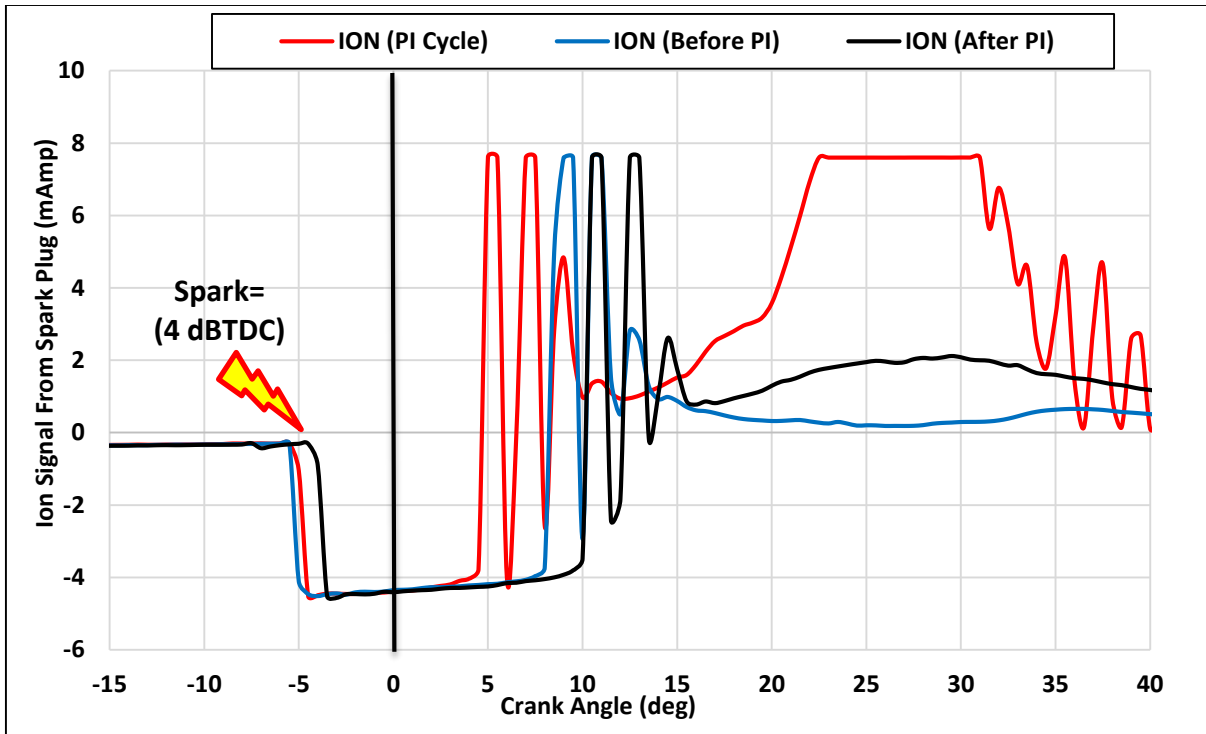


Figure 8.13. Zoomed traces for the Ion signal from spark plug for pre-ignition cycle (red), cycle before PI (blue) and cycle after PI (black) at 1205 rpm and 12 bar IMEP, cylinder # 1

Zoomed traces for the in-cylinder gas pressure for the three consecutive cycles and the ion current signal from the spark plug are shown in figure 8.12 and 8.13.

Figure 8.13 shows that in the pre-ignition cycles, the ionization started earlier than in the two cycles with normal combustion. However, that ionization started to show up on the ion current signal after the spark discharged by around 10 CAD angles. Figure 8.14 shows zoomed traces for two consecutive cycles for the ion signal from the spark plug and the RHR for the cycle before the PI cycle and the PI cycle. It shows that the ionization detected by the ion current sensor after the pre-ignition took place.

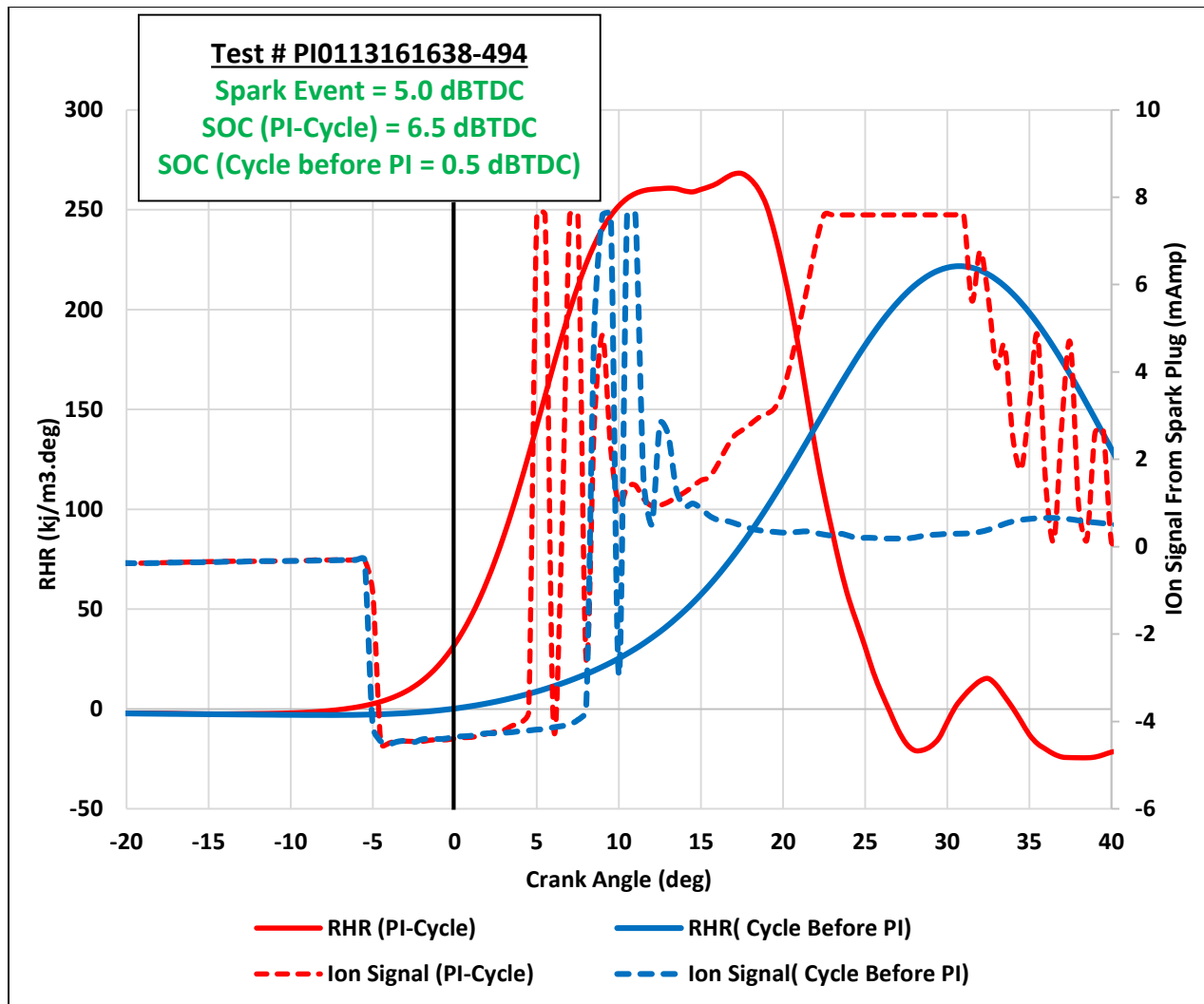


Figure 8.14 Zoomed traces for the Ion signal from spark plug and RHR for pre-ignition cycle (red), cycle before PI (blue) at 1205 rpm and 12 bar IMEP, cylinder # 1

Figure 8.15 shows the ignition command and the spark plug ion signal for the pre-ignition cycle and the cycle before the PI cycle. It's obvious that the two ignition commands are on top of each other, which means the pre-ignition took place not because of an ignition fault but because of another source of ignition. Figure 8.16 presents the engine performance parameters of the three consecutive cycles around the pre-ignition cycle. The data from this figure shows that the cycle before and after the PI have normal combustion.

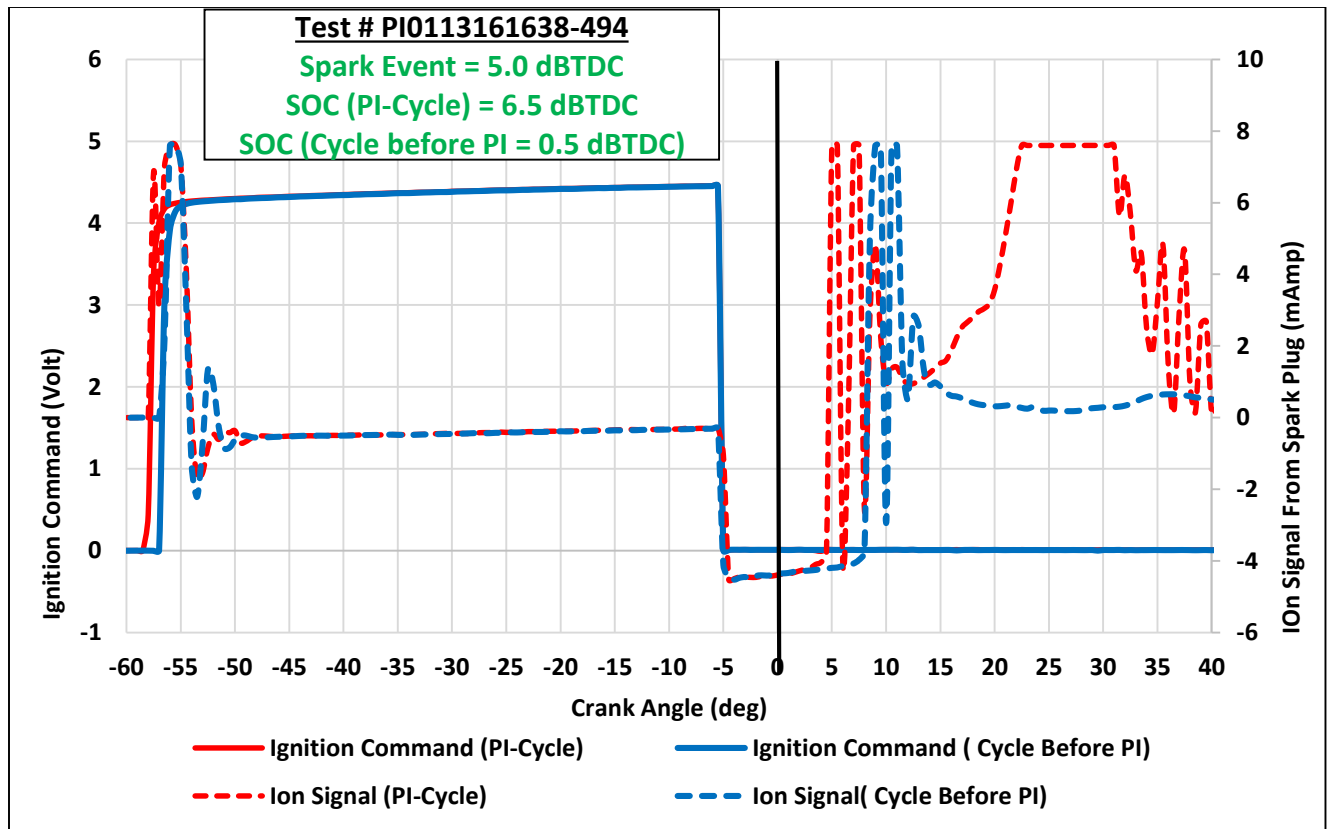


Figure 8.15. Zoomed traces for Ion signal from spark plug and ignition command for pre-ignition cycle (red) and cycle before PI (blue) at 1205 rpm an 12 bar IMEP, cylinder # 1

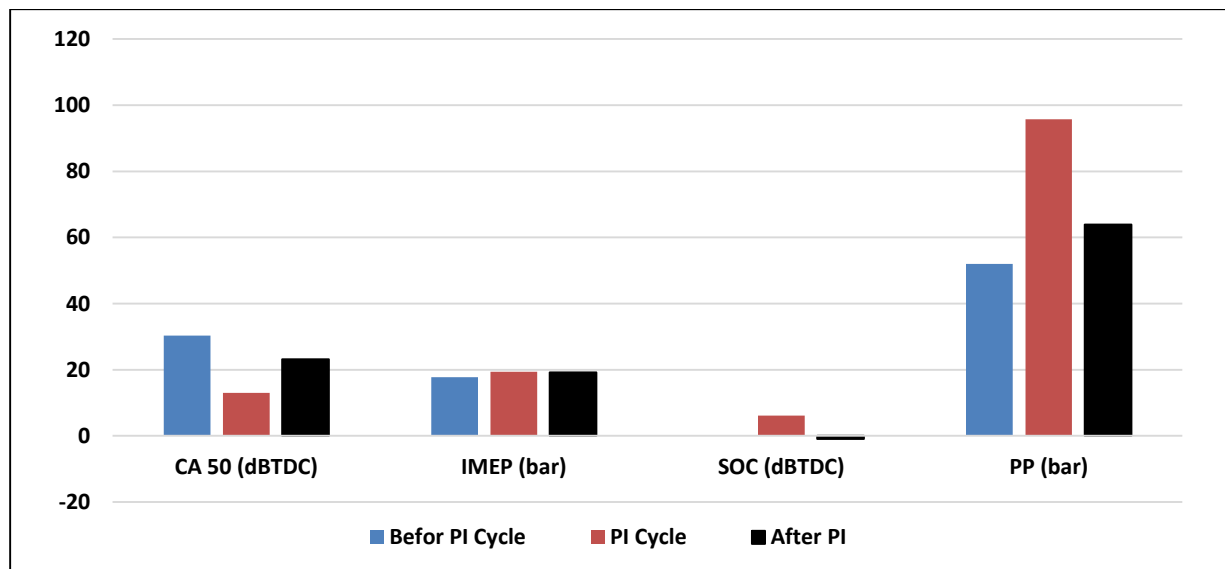


Figure 8.16. Engine performance parameters (CA50, IMEP, SOC and PP) for pre-ignition cycle (red), cycle before PI (blue) and cycle after PI (black) at 1205 rpm an 12 bar IMEP, cylinder # 1

A third test was conducted on the engine at 1205 rpm and 12 bar IMEP and the engine produced pre-ignition. As shown in Figures 8.17, 8.18 and 8.19, the spark timing was 8 dBTDC and the two cycles before and after the PI have SOC= 2.6 dBTDC, but the PI cycle has SOC= 13.6 dBTDC. There was a sudden rise and sharp decrease in the in-cylinder gas pressure around 10 dBTDC, and the peak pressure of the PI cycle was around 1.3 times the peak pressure of a normal cycle, which indicates that this pre-ignition was light but didn't knock.

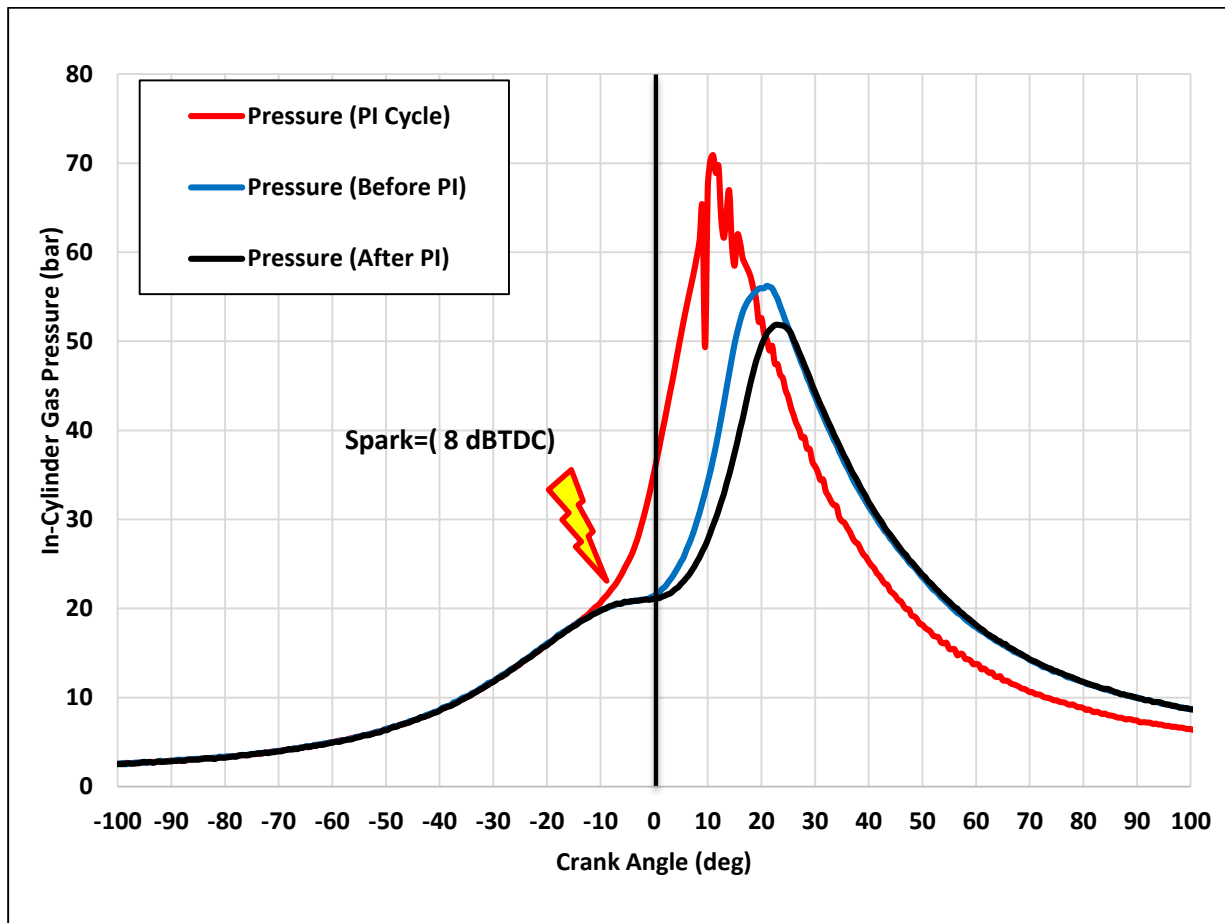


Figure 8.17. In-cylinder gas pressure for pre-ignition cycle (red), cycle before PI (blue) and cycle after PI (black) at 2000 rpm and 388 N.m, cylinder # 1

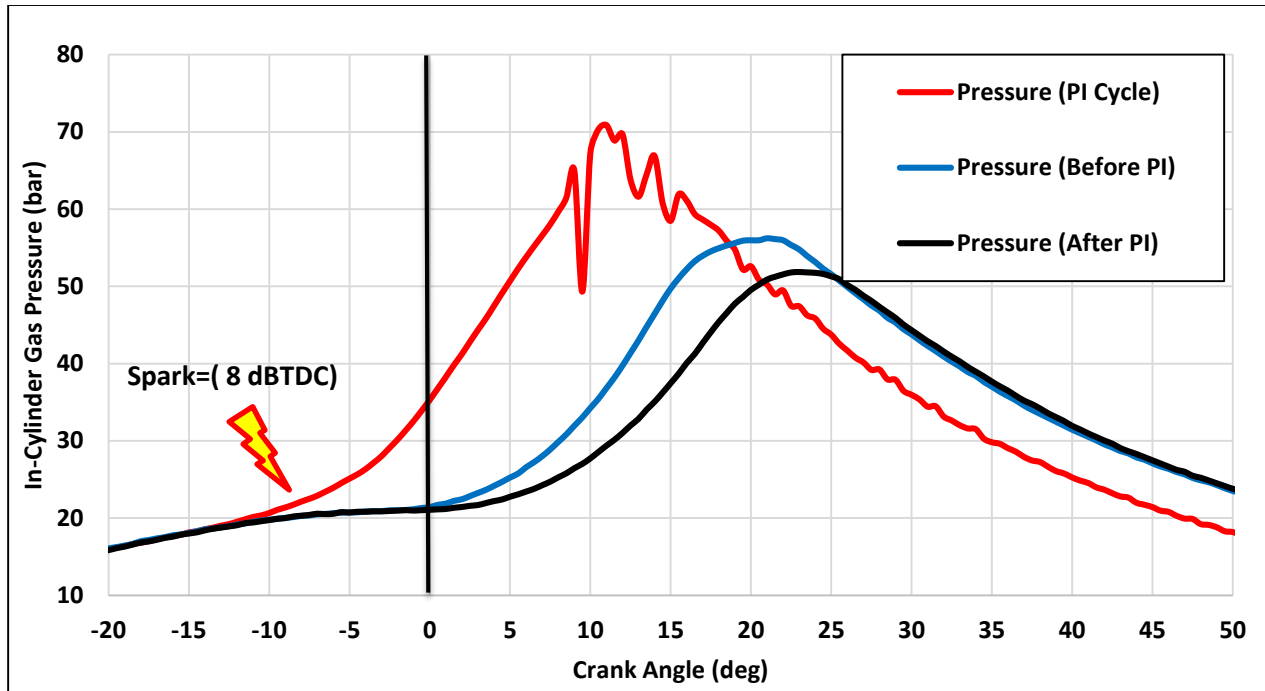


Figure 8.18 Zoomed traces for In-cylinder gas pressure for pre-ignition cycle (red), cycle before PI (blue) and cycle after PI (black) at 2000 rpm and 388 N.m, cylinder # 1

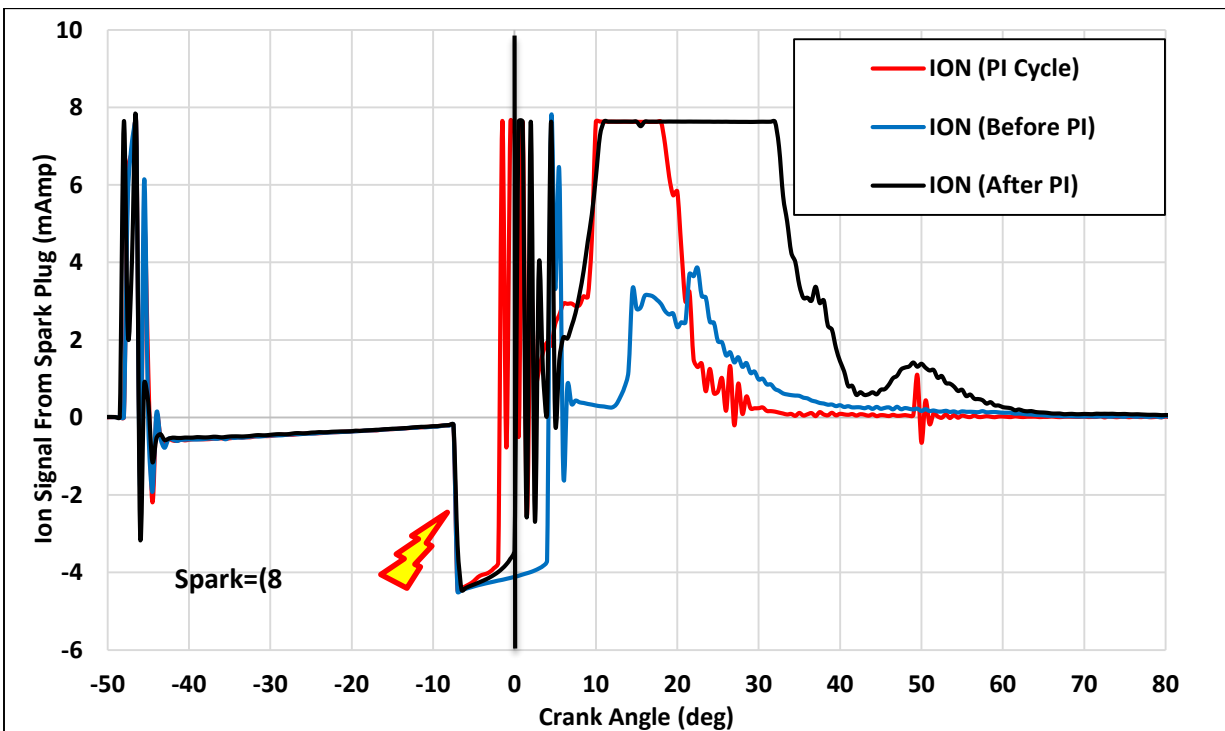


Figure 8.19. Zoomed traces for the Ion signal from spark plug for pre-ignition cycle (red), cycle before PI (blue) and cycle after PI (black) at 2000 rpm and 388 N.m, cylinder # 1

Figure 8.19 shows a zoomed traces for the Ion signal from spark plug for pre-ignition cycle (red), cycle before PI (blue) and cycle after PI (black) at 2000 rpm and 388 N.m, cylinder # 1. The spark discharges for all three cycles were at the same time including the PI cycle. The cycle before PI has normal combustion with a normal start of combustion. In addition, the ionization from the three consecutive cycles before the PI cycle didn't show any variation from the basic ion signal that could lead to any prediction for pre-ignition. The combustion of the cycles before the PI ended normally with no change in the ion current signal. However, the ionization of the cycle that had pre-ignition started earlier than the other two cycles, the one before and one after.

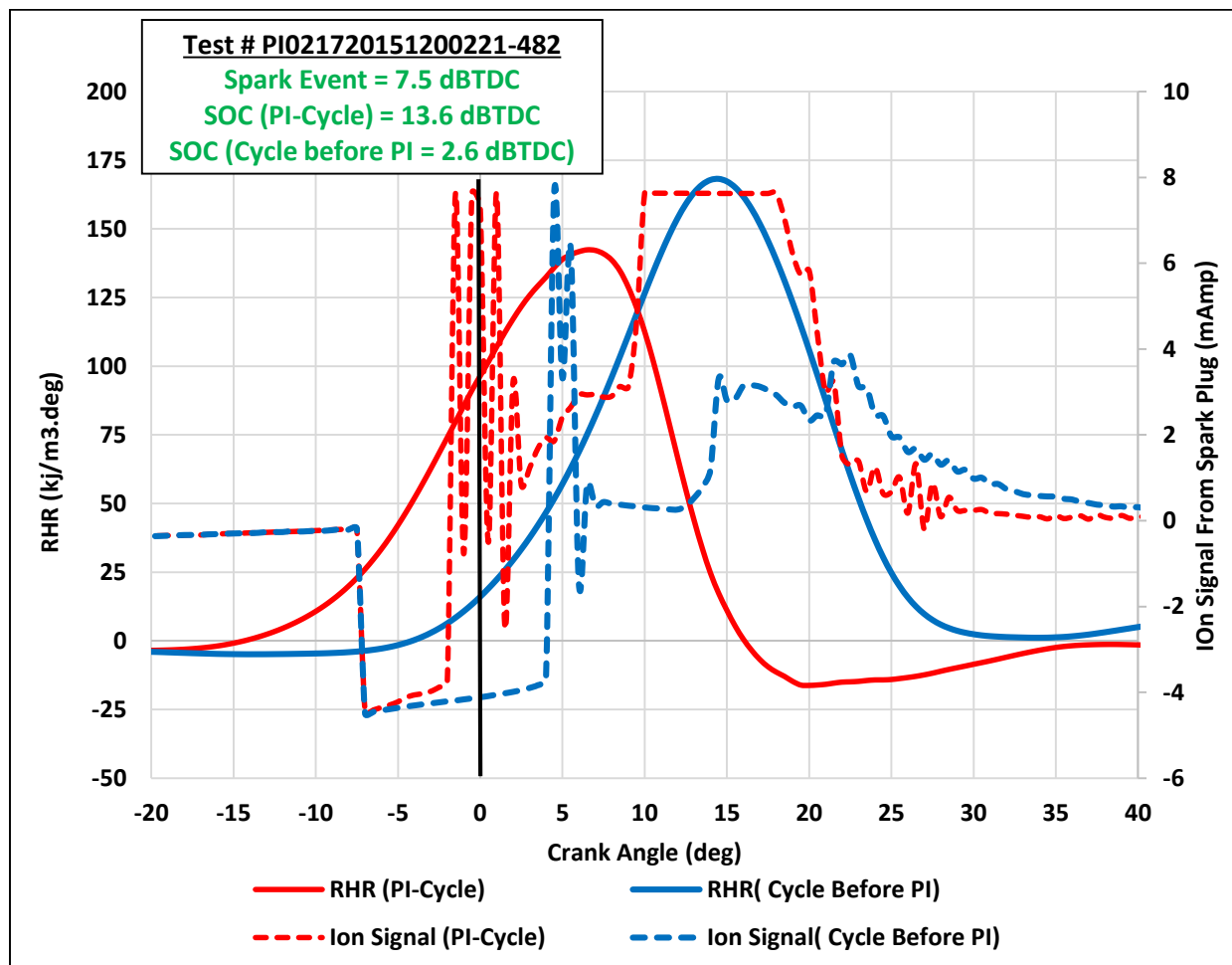


Figure 8.20. Zoomed traces for Ion signal from spark plug and RHR for pre-ignition cycle (red) and cycle before PI (blue) at 2000 rpm and 388 N.m, cylinder # 1.

Figure 8.20 shows zoomed traces for Ion signal from the spark plug and RHR for pre-ignition cycle (red) and cycle before PI (blue) at 1205 rpm an 12 bar IMEP, cylinder # 1. The spark discharges for all three cycles were at the same time including the PI cycle. The cycle before PI has normal combustion with normal start of combustion. In addition, the RHR of the cycle that has pre-ignition started earlier around 13.6 dBTC; however, this combustion didn't show up on the ion current signal.

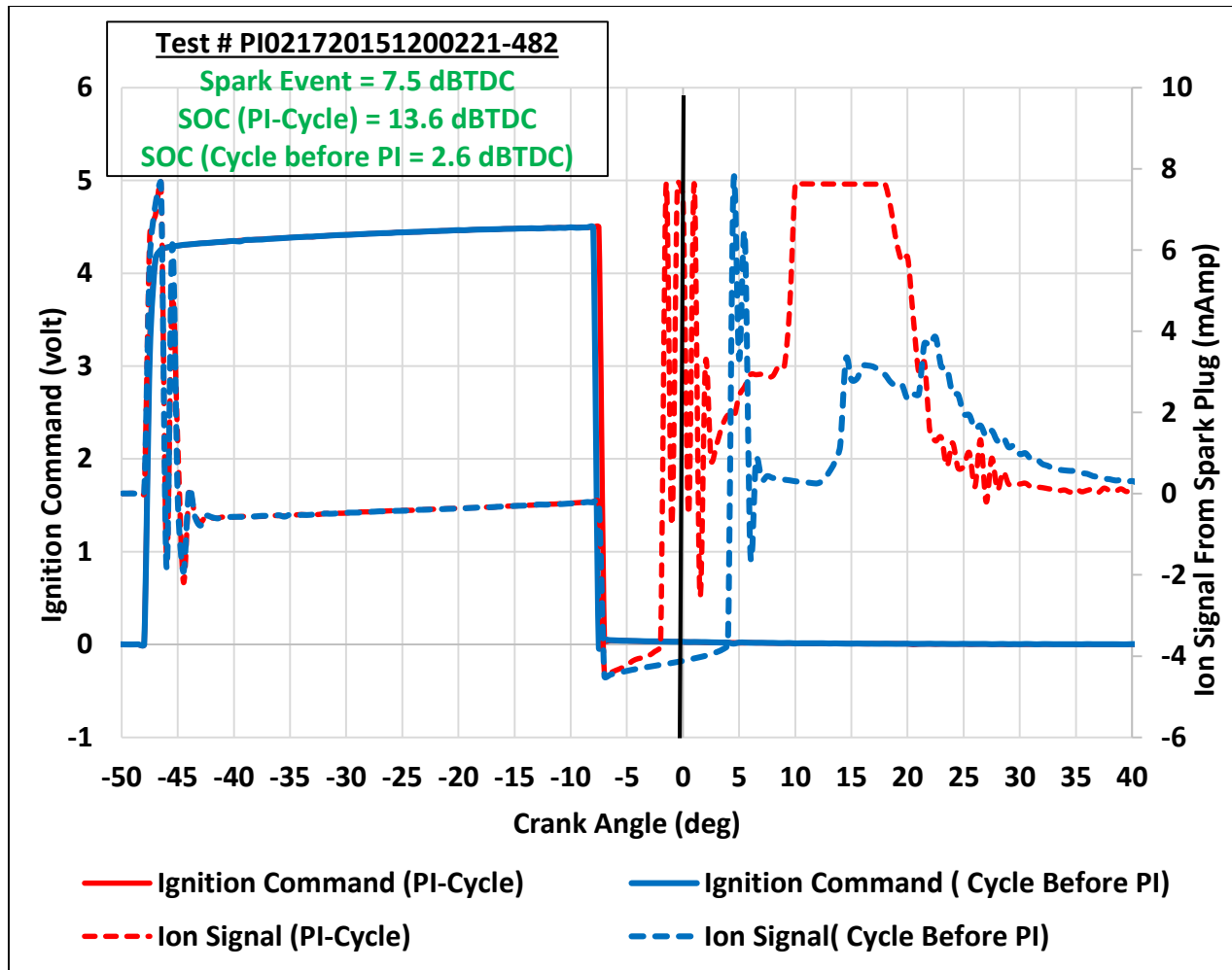


Figure 8.21. Zoomed traces for Ion signal from spark plug and ignition command for pre-ignition cycle (red) and cycle before PI (blue) at 1205 rpm an 12 bar IMEP, cylinder # 1

Figure 8.21 shows zoomed traces for the Ion signal from the spark plug and ignition command for pre-ignition cycle (red) and cycle before PI (blue) at 1205 rpm an 12 bar IMEP, cylinder # 1. The two ignition

commands started and ended at the same time without any fault in the ignition command that might cause any early ignition for this cycle.

### 8.8. Pre-ignition test with single injection and standard oil with normal additives (5W-30)

Additional test was conducted on the engine using the standard oil 5W-30 with normal additives [64]. The oil used in the investigation conducted in section 8.7 in this research was oil-A 5W-30 with reduced additives. The chemical properties of the two oils are shown in Table 8.4. From the table shown, the standard oil 5W-30 has base oil with Hydrocracked with normal amount of additives compared to oil-A which has base oil with Polyalphaolefine with reduced amount of additives.

			Standard Oil	Oil A
Viscosity class (SAE)			5W-30	5W-30
Base oil			Hydrocrack	Polyalphaolefine
Amount of Additives			"normal"	reduced
<b>PHYSICAL AND CHEMICAL DATA</b>				
<b>Parameter</b>	<b>Test method</b>	<b>Unit</b>		
Evaporative Loss (Noack)	CEC L-40-A-93, A	wt.-%	10,8	5,7 (B)
Kin. Viscosity +100°C,	EN ISO 3104	mm <sup>2</sup> /s	9,8	11,8
Viscosity-Index	DIN ISO 2909	-	155	164
Density +15°C	DIN 51 757	kg/m <sup>3</sup>	857	851
Total Base Number	LBCH02-14	mg KOH/g	11,7	6,1
Flashpoint	DIN ISO 2592	°C	240	244
Sulphated Ash	DIN 51 575	wt.-%	1,3	0,6
Sulphur	<i>suitable method</i>	ppm	2975	2000
Phosphorus	<i>suitable method</i>	ppm	885	800
Zinc	<i>suitable method</i>	ppm	997	900
Barium	<i>suitable method</i>	ppm	0	-
Boron	<i>suitable method</i>	ppm	< 10	200
Calcium	<i>suitable method</i>	ppm	3466	1100
Chlorine	<i>suitable method</i>	ppm	0	13
Copper	<i>suitable method</i>	ppm	0	0
Lead	<i>suitable method</i>	ppm	0	0
Magnesium	<i>suitable method</i>	ppm	15	0
Molybdenum	<i>suitable method</i>	ppm	0	85
Nitrogen	<i>suitable method</i>	ppm	572	1400
Sodium	<i>suitable method</i>	ppm	2,5	0
Silicon	<i>suitable method</i>	ppm	4,7	4

Table 8.3. The chemical properties p of the standard oil with reduced additive and the synthetic oil



Cycle #	SOI	Spark	SOC	MBF 5%	MBF 10%	MBF 50%	MBF 90%	PP	PPL	Status
No.	dBTD C	dBTD C	dBTD C	dATD C	dATD C	dATDC	dATDC	bar	dATD C	
191	282	2.0	-2	13.25	15.6	25.25	32.9	69.0	30.5	Normal
192	282	2.0	40.5	-29	-27.5	-22	-18	140.2	-2	PI
193	282	7.5	3.35	5.8	7.55	15.35	19.8	103.0	20	Knock
194	282	7	2.45	6.75	8.6	16.1	12.5	104.1	21.5	Knock
195	282	7.633	9.75	0.55	2.55	9.6	13.4	152.0	13.5	PI
196	282	7.03	3.75	5.95	7.8	15.4	19.85	102.2	20	Knock
197	282	7.58	12.5	2.85	1.35	3.1	5.75	221.6	6	PI
198	282	7	2.85	6.9	8.8	16.6	21.75	93.2	22.5	Knock
199	282	7.6	11.05	1.15	2.8	8.2	11.8	200.8	12	PI
200	282	7.05	3.35	6.55	8.68	16.4	21.6	96.4	22	Knock
201	282	7.58	9.1	3	4.75	11	14.8	176.6	15.5	PI
202	282	7.05	2.45	7.25	9.4	17.55	23.2	90.7	23	Knock
203	282	7.05	11.45	2.95	1.55	3.95	7.25	196.2	8	PI
204	282	7.05	3.3	7.4	9.5	18.55	23.95	91.3	24.5	Knock
205	282	7.05	3.75	6.35	8.6	17.05	22.65	97.7	23	Knock
206	282	-7	1	13.4	15.3	22.45	3.65	73.6	27.5	Normal
207	282	-7	-5.7	18.8	21.15	32.6	42.7	53.3	38	Normal
208	282	-7	-4	15.45	18.75	29.95	39.35	57.9	35	Normal
209	282	-7	-10.4	28.15	31.35	42.6	52	42.0	49	Normal
210	282	-7	8.25	2.7	4.9	12.95	16.75	121.9	17	PI
211	282	-7	-11.7	29.6	33	45.55	55.15	38.3	52	Normal
212	282	-7	-11.5	29.3	32.25	43.85	54.75	38.9	50.5	Normal

Table 8.5. Pre-ignition test results of 2000 rpm and WOT condition using the standard oil with normal additives 5W-30 and single injection with based ECU ignition timing.

A test was conducted at 2000 rpm and WOT condition using the oil type 5W-30 with normal additives. The test results are summarized in Table 8.5 and show the injection timing, igniting timing, start of combustion (SOC), MBF 5%, MBF 10%, MBF 50%, MBF 90%, peak pressure, peak pressure location (PPL) and the status of the cycle of 22 consecutive cycles. The peak pressure and peak pressure location are shown in Figure 8.22 and show that cycle 192 has a very early pre-ignition with PPL 2 degrees before TDC and peak pressure of 140 bar.

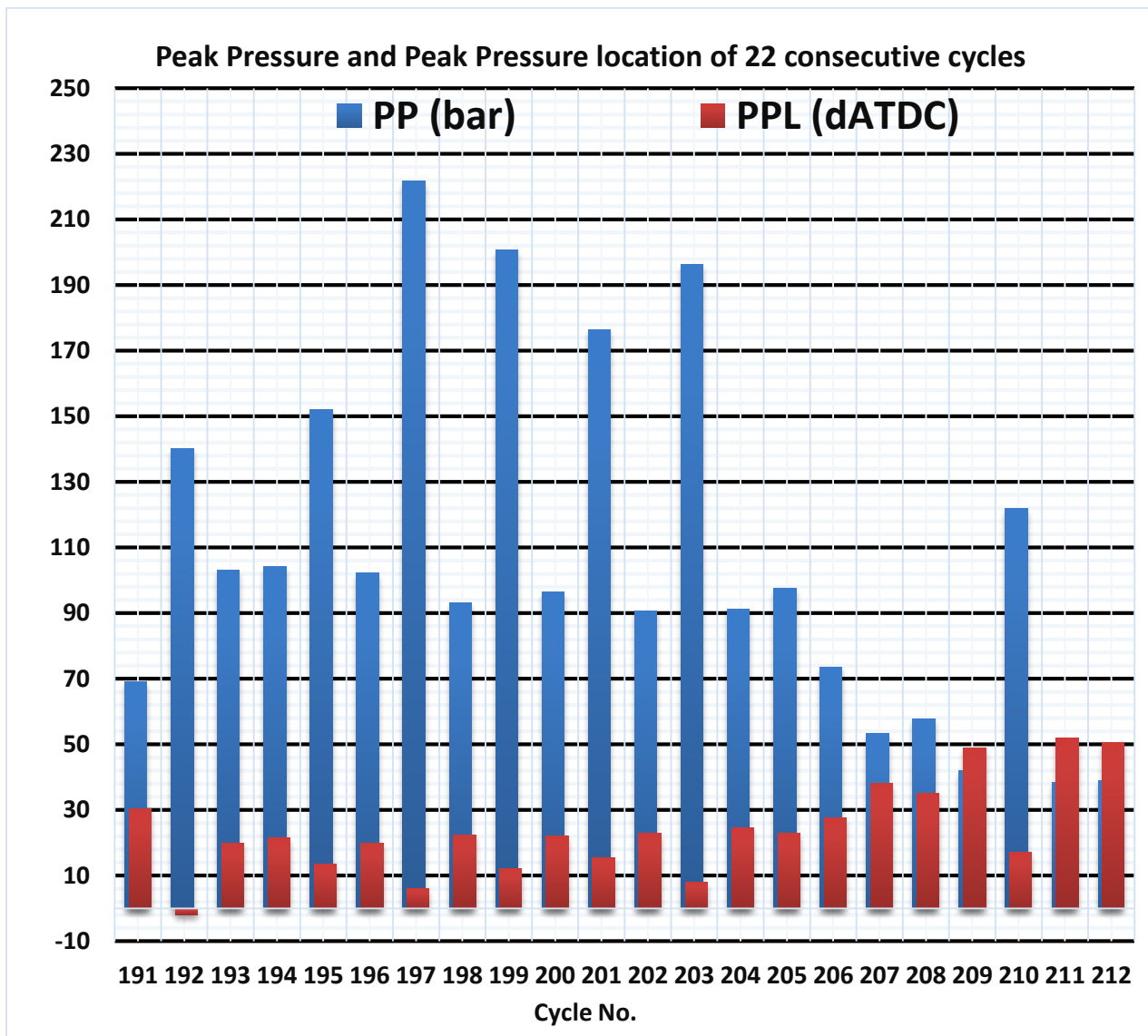


Figure 8.22. In-cylinder gas peak pressure and peak pressure location of 2000 rpm and WOT condition using the standard oil with normal additives 5W-30 and single injection with based ECU ignition timing.

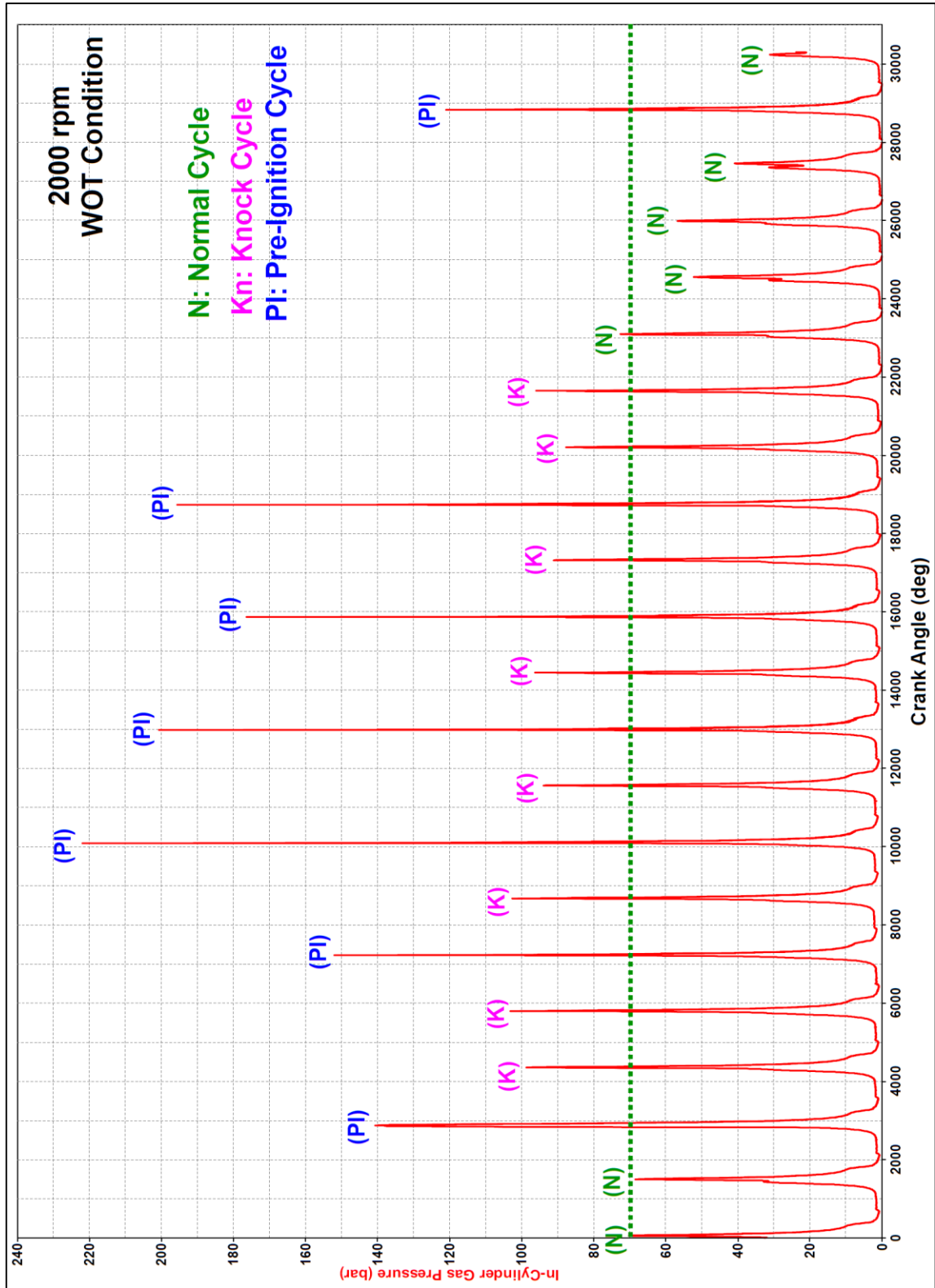


Figure 8.23. In-cylinder gas peak pressure and peak pressure location of 2000 rpm and WOT condition using the standard oil with normal additives 5W-30 and single injection with based ECU ignition timing.

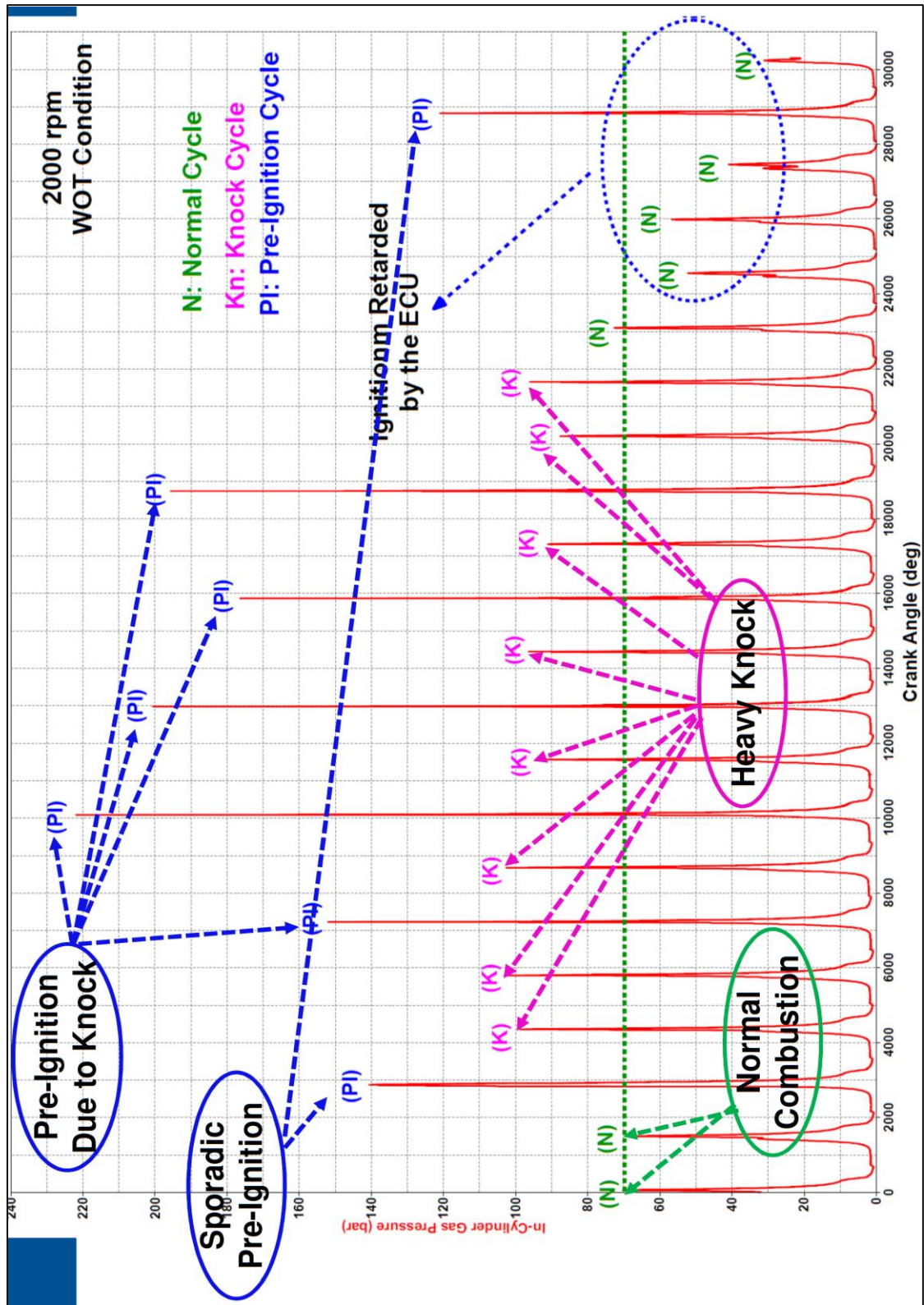


Figure 8.23-a. In-cylinder gas peak pressure and peak pressure location of 2000 rpm and WOT condition. Shows the normal combustion cycle, Nock cycle, sporadic PI and the PI due to knock,

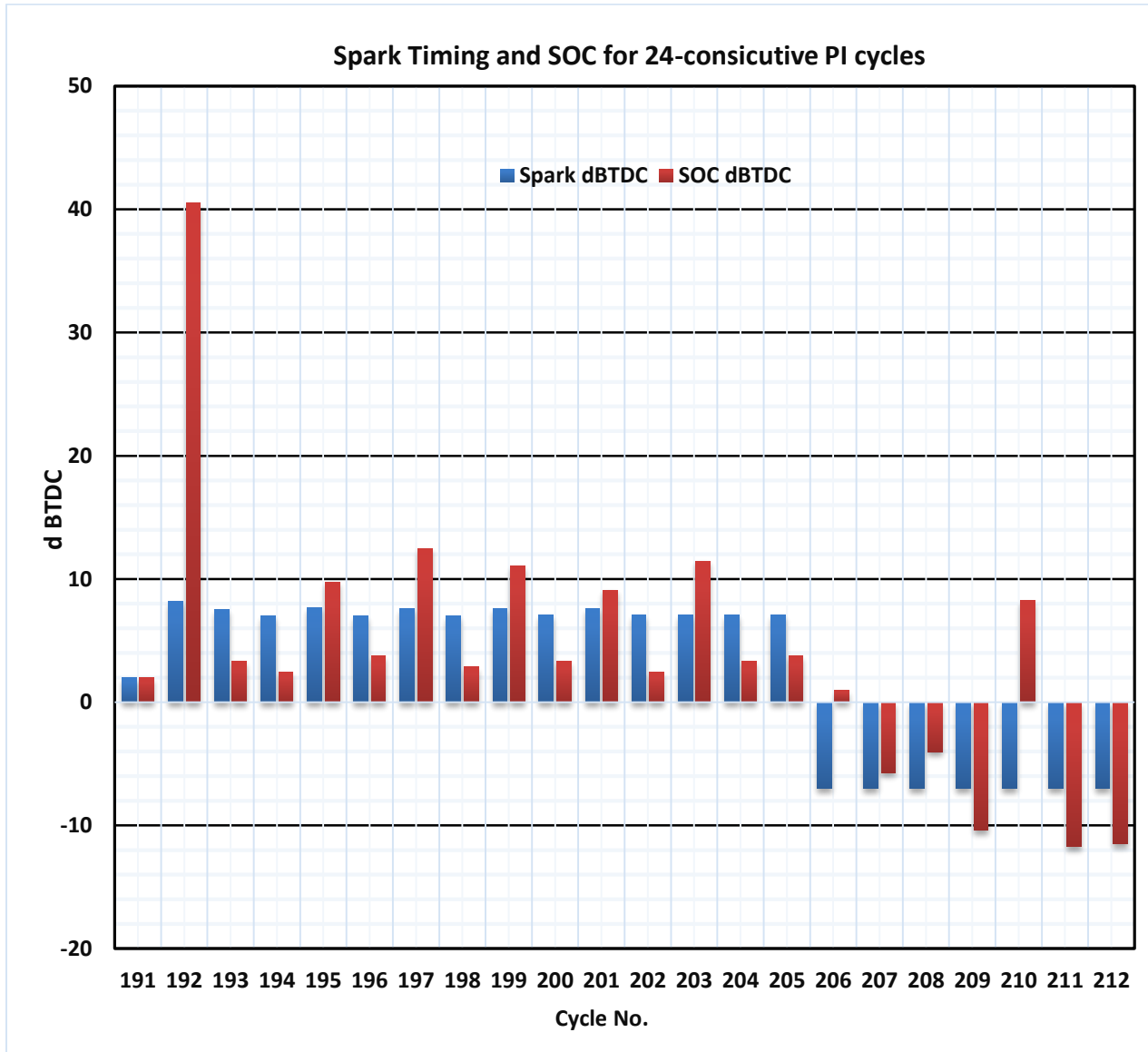


Figure 8.24. In-cylinder gas pressure an ion signal from spark plug for 2-consecutive cycles (Cycle 191 & Cycle 192) at 2000 rpm and WOT condition using the standard oil with normal additives 5W-30 and single injection with based ECU ignition timing.

Figure 8.23 and 8.23-a show the series traces of the in-cylinder gas pressure for the 22 consecutive cycles. The test started with cycles 1 at 2000 rpm and WOT conditions (398 N.m), and the first 191 cycles were running with normal combustion and there were no any indications of knocking. Cycle 191, is a cycle with a normal combustion and the pressure trace and knock sensor didn't showed any sign about

knocking. Suddenly, pre-ignition occurred in cycle 192 which shows that this type of pre-ignition is a sporadic pre-ignition. For the cycle before the PI cycle (cycle # 191), the ECU ignition timing was 2 deg bTDC with injection timing 282 deg bTDC, PP= 69 bar, PPL=30.5 deg aTDC and SOC = 2 deg aTDC as shown in figure 8.24. The PPL of this cycle was 30.5 deg aTDC which shows a normal PPL at such speed and load (2000 rpm and WOT). In addition, this cycle didn't show any signs of engine knocking. Cycle 192, the PI cycle (the cycle after the cycle with normal combustion), the ECU ignition timing was 2 deg bTDC with injection timing 282 deg bTDC, however pre-ignition occurred with PP= 140.2 bar, PPL=-2.0 deg aTDC and SOC = -40.5 deg aTDC. After this pre-ignition, the engine started to knock producing pre-ignitions. From the trend of the pressure trace, the rest of the pre-ignition cycles, cycle 195, 197, 199, 201 and 203, pre-ignition occurred because of engine knocking. This type of pre-ignition is not a sporadic pre-ignition but pre-ignition forced by knock. Then, the ECU retarded the ignition timing and the engine started to go back to normal combustion from cycle 206 to cycle 209 with Injection timing 282 deg bTDC and ignition timing 7 deg aTDC. Even though, there were 4 consecutive cycles with normal combustion and the ignition timing didn't change, pre-ignition occurred at the cycle after those four normal combustion cycles at cycle 210. Then, the engine went back to normal combustion. AT this point, we stopped the test because of the high peak pressure occurred which was around 220 bars.

The results showed that, the peak pressure value of the sporadic pre-ignition is fairly lower than the peak pressure value of the peak pressure of pre-ignition forced by engine knocking. The peak pressure of the two sporadic pre-ignition cycles were 140 bar and 122 bar, but the peak pressure for the pre-igniting due to engine knock, were in order of 221 bar which could damage the engine components like the piston rings.

Figure 8.25 show the superimposed traces of the in-cylinder gas pressure for the 22 consecutive cycles. The test started with cycles 1 at 2000 rpm and WOT conditions (360 N.m). Figure 8.26 show

zoomed traces of the in-cylinder gas pressure for the 22 consecutive cycles. In addition, figure 8.27 shows the integrated RHR of the 22 consecutive cycles of the same operating condition.

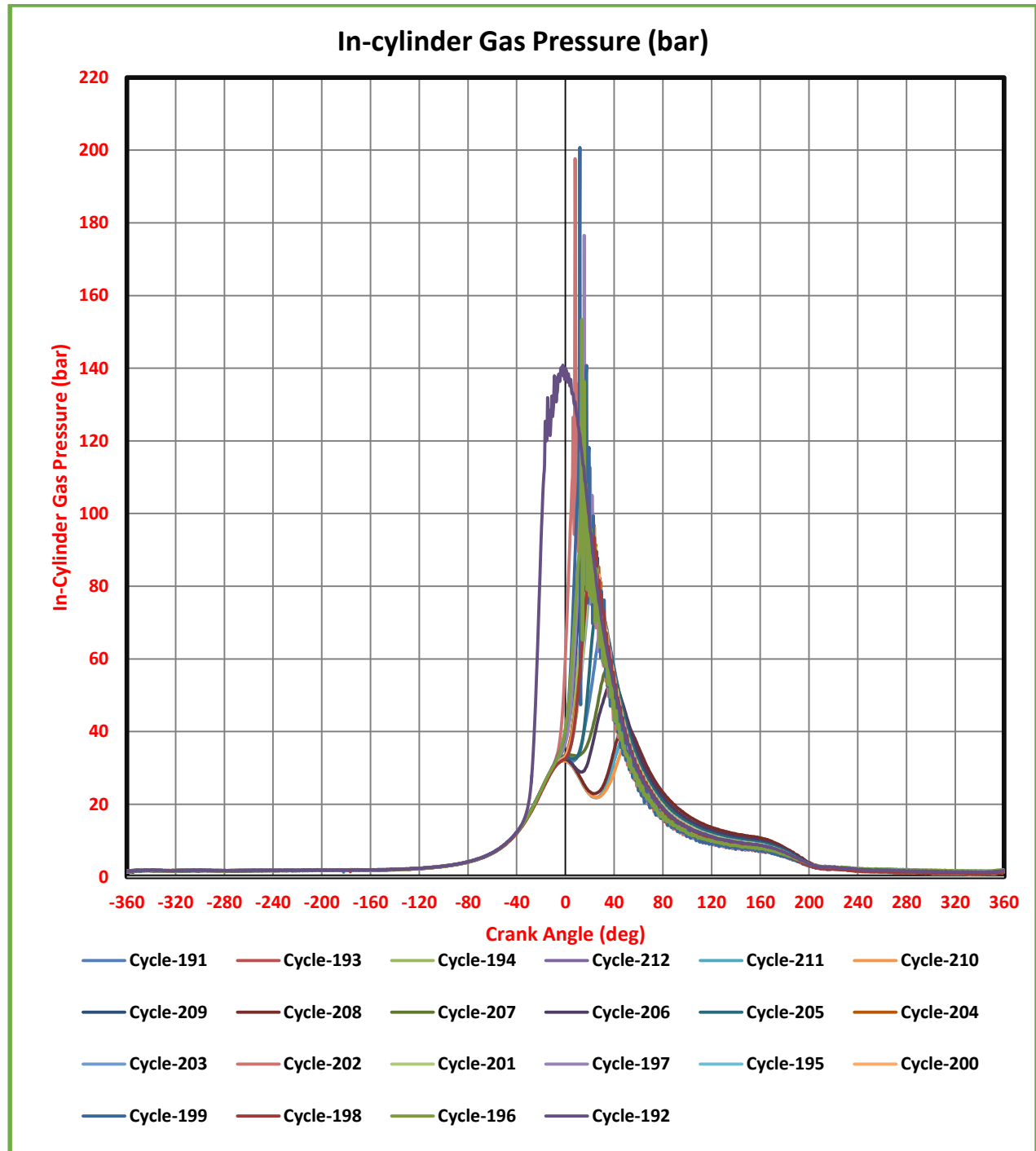


Figure 8.25. In-cylinder gas pressure of 24 consecutive cycles at 2000 rpm and WOT condition using the standard oil with normal additives 5W-30 and single injection with based ECU ignition timing, cylinder 1.

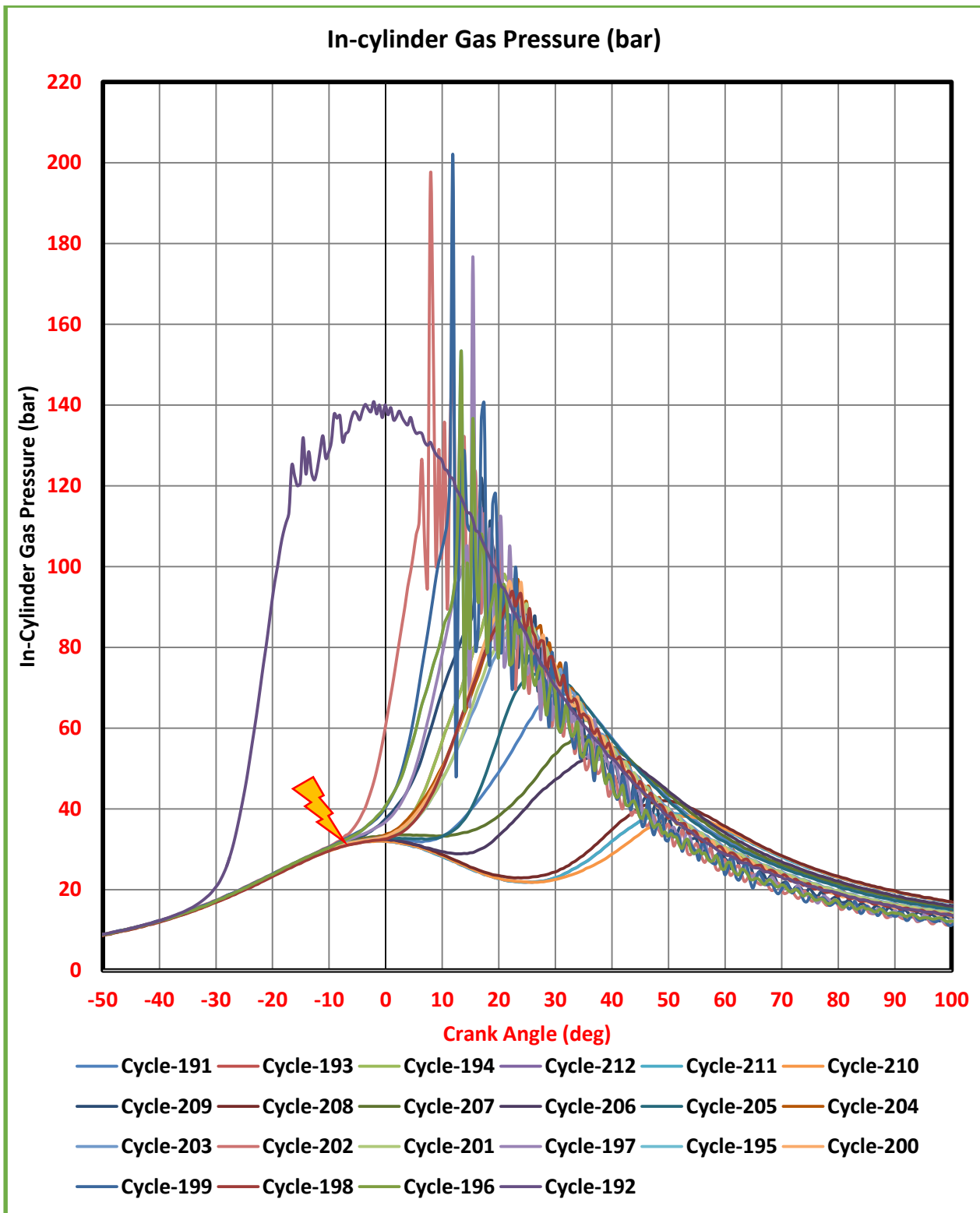


Figure 8.26. Zoomed traces of In-cylinder gas pressure of 24 consecutive cycles at 2000 rpm and WOT condition using the standard oil with normal additives 5W-30 and single injection with based ECU ignition timing.



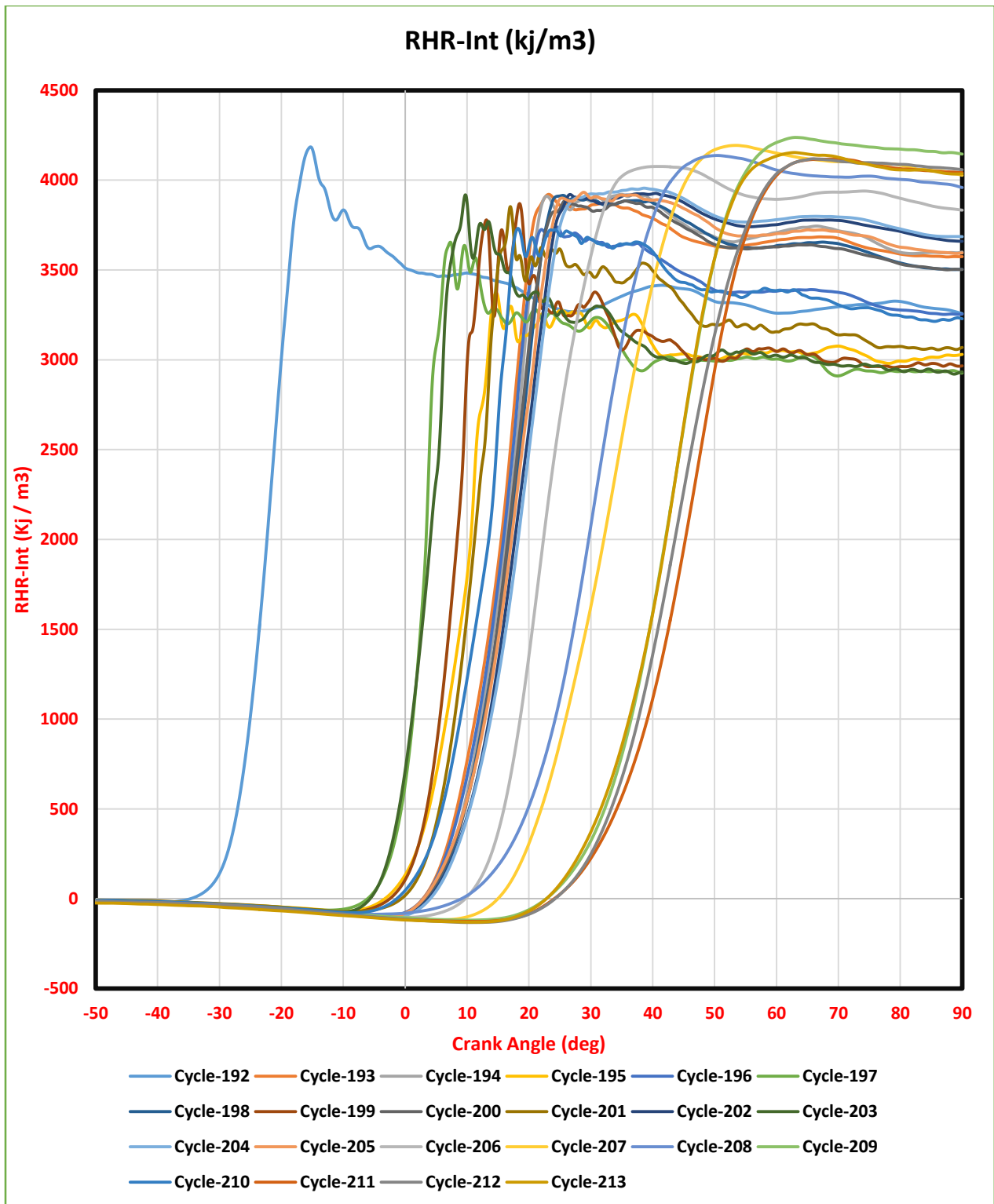


Figure 8.27. Integrated RHR of 24 consecutive cycles at 2000 rpm and WOT condition using the standard oil with normal additives 5W-30 and single injection with based ECU ignition timing.

The ion signal from spark plug is used in this investigation to study the pre-ignition. Figure 2.28 shows the integrated RHR and the ion signal from spark plug for the two consecutive cycles, cycle 191 and cycle 192. Cycle 191 is the cycle with normal combustion and cycle 192 is the cycle with sporadic pre-ignition. The blue solid curve shows the ion signal from spark plug of cycle 191, the blue dashed curve shows the RHR integral of cycle 191, the red solid line shows the ion signal from spark plug of cycle 192 and the red dotted line shows the RHR of cycle 192.

Normal combustion produces normal ionization with normal integrated RHR as shown in figure 8.28. The ion signal of cycle 191 (the blue solid line) showed the start of ignition coil charge around 53 deg bTDC and a straight horizontal line up-till the coil discharge around 2 deg bTDC, which represent a zero ionization line, then the ignition delay period, then the flame propagation which agrees with the integrated RHR of that cycle. But, for the sporadic pre-ignition cycle, cycle 192 (cycle with solid red line), the coil charge time is normal, but is followed by ionization starting from 40 deg bTDC. Notice the similarity between the rates of increase of the ion signal and the integrated RHR. This close similarity is an indication of start of sporadic pre-ignition at the spark plug. Again, this sporadic could not be predicted from the cycle before the PI cycle where the ionization is normal without any change in its decay rate after combustion which could have resulted in hot particles or spots that result in next cycle sporadic pre-ignition.

Figure 8.29 shows the in-cylinder gas pressure and ion signal from spark plug for two consecutive cycles, cycle 191 (the cycle before the PI cycle) and cycle 192 (the PI cycle). Notice, the similarity between the rates of rise of the ion current signal the cylinder gas pressure. In this cycle, ionization due to pre-ignition is so high that reached saturation at the spark plug gap.

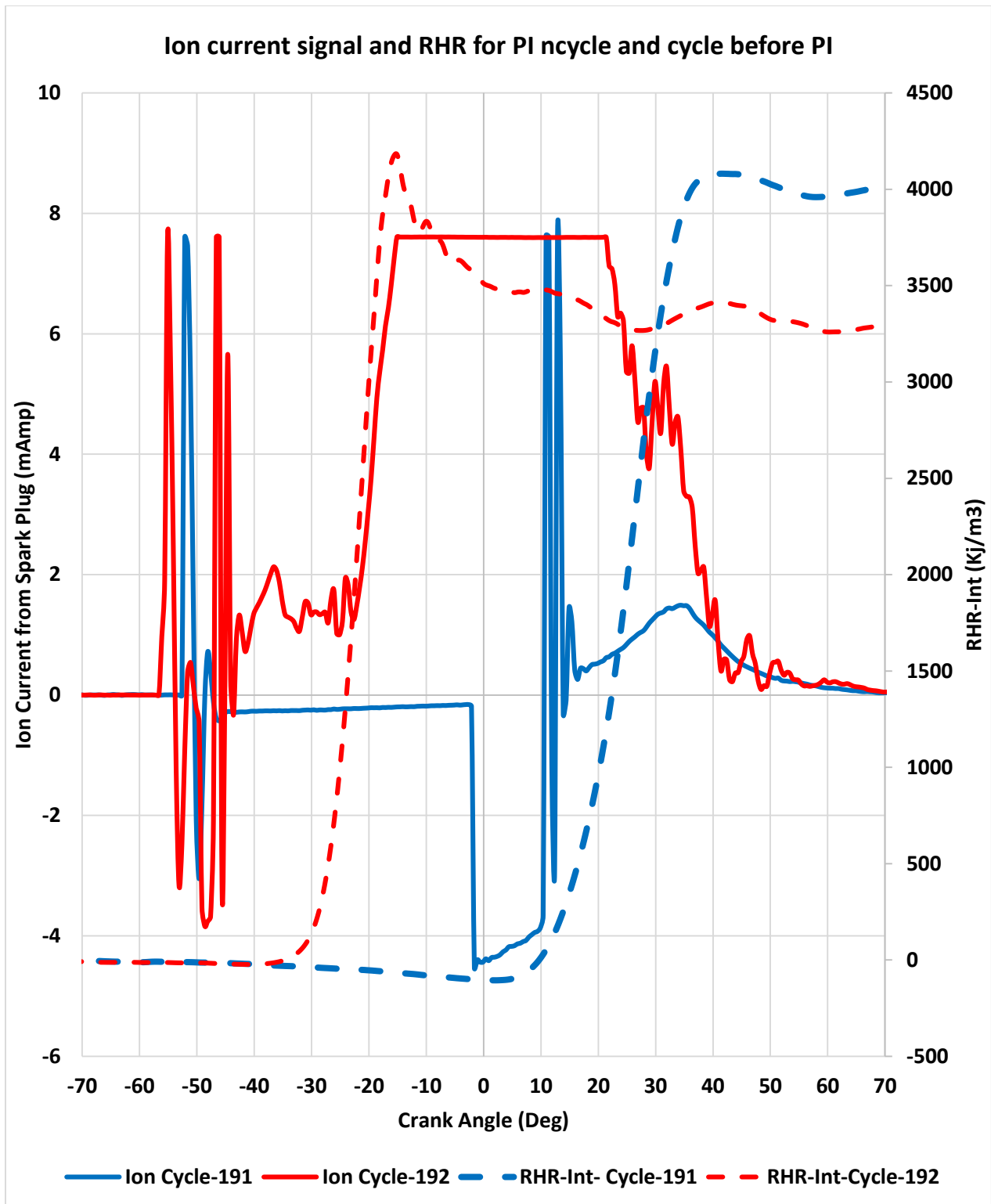


Figure 8.28. Integrated RHR and the ion signal from spark plug for 2-consecutive cycles (Cycle 191 & Cycle 192) at 2000 rpm and WOT condition using the standard oil with normal additives 5W-30 and single injection with based ECU ignition timing.

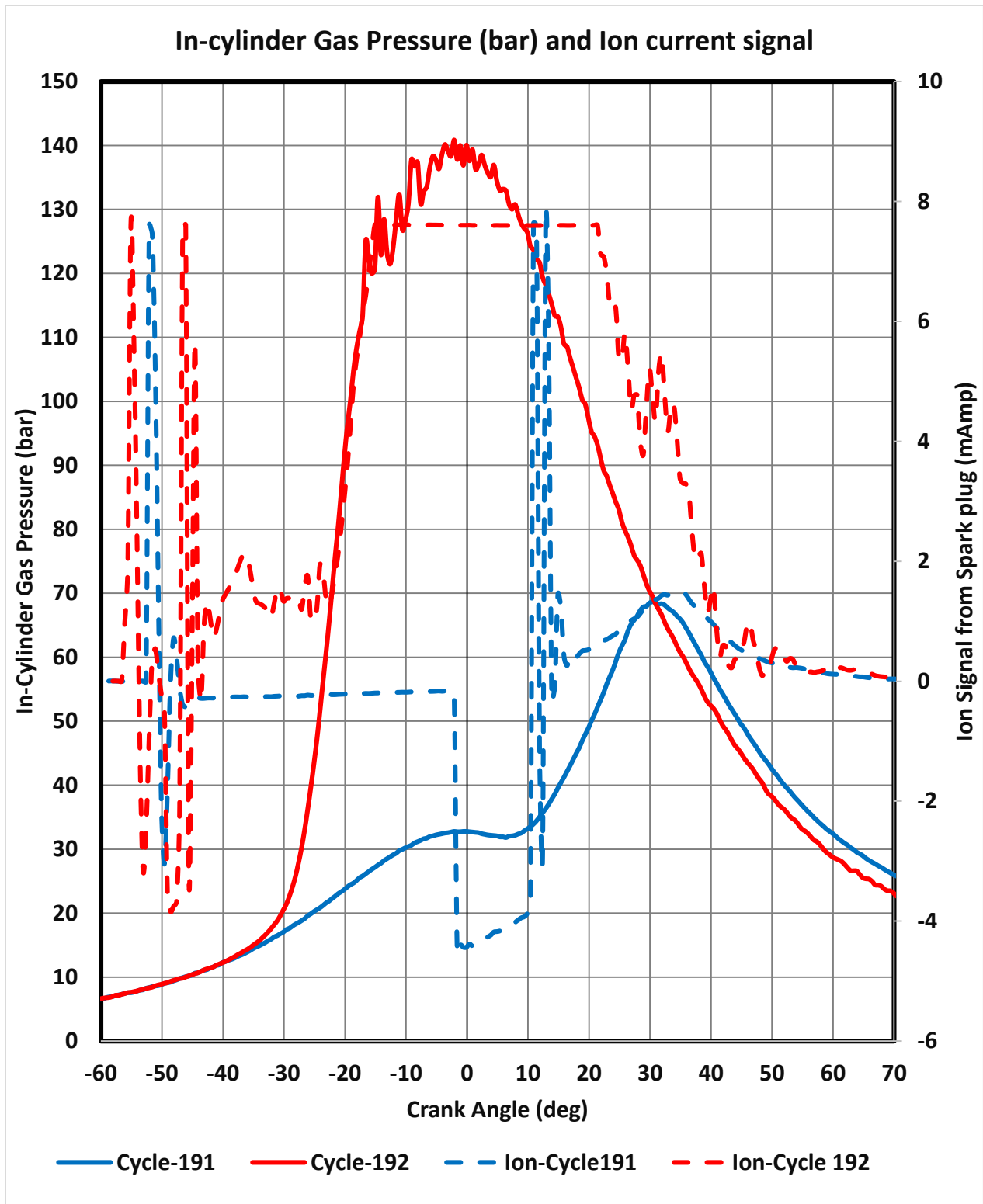


Figure 8.29. In-cylinder gas pressure and ion signal from spark plug for 2-consecutive cycles (Cycle 191 & Cycle 192) at 2000 rpm and WOT condition using the standard oil with normal additives 5W-30 and single injection with based ECU ignition timing.

## 8.9. Summary

Many attempts were made to produce sporadic pre-ignition and find out if can be predicted from the ion current signals of previous cycles. These included engine tests under a variety of operating conditions such as speeds, loads, cooling water temperatures, spark timings and different fuel injection parameters. In addition tests were conducted using different pump fuel such as gasoline 87, 93 and 95. In all these tests sporadic pre-ignition was not achieved because the production ECU protected the engine by controlling the turbocharger waste gate to prevent the engine from being overheated and exceed the desired ECT. Furthermore, tests were conducted using a special fuel provided by GM to Wayne State University (WSU), Center of Automotive Research (CAR). Pre-ignition was achieved once and could not be repeated, because the engine was under the control of the production ECU. In all these tests synthetic lubricating oil was used.

Finally, the synthetic lubricating oil was replaced with hydrocracked lubricating oil and sporadic pre-ignition, knock and post-knock pre-ignition were detected and the ion current signal analyzed. Detailed analysis of the ion current signals, RHR and its integral showed that sporadic pre-ignition could not be predicted from the ion current or RHR of preceding cycles. Also, sporadic pre-ignition starts at different locations in the combustion chamber such as the spark plug and away from the spark plug.

## CHAPTER 9 3D CFD COMBUSTION ANALYSIS

### 9.1 Introduction

Converge 2.2, 3D CFD tool is used to investigate cycle to cycle variation in a gasoline direct injection engine. The GTDI engine model is modified considering the necessary boundary conditions and assumption to reduce the competition time. The boundary conditions of the model were the valve timing, spark timing, injection timing and duration, inlet pressure and temperature, exhaust pressure and temperature, intake and exhaust valve profiles, DI injector spray and targeting.

### 9.2 Model setup

Internal combustion engine cycle simulation includes many assumptions to set up boundary conditions to be as close as possible to the engine data from the experimental tests.

The boundary conditions used in the model are shown in table 7.5.

Setup item	Values	Remarks
Bore (mm)	86	
Stroke (mm)	86	
Connecting rod length (mm)	145.5	
Compression Ratio	9.2	
Equation of state	Redlich-Kwong	
Fuel Used	98% IC8H18 2% C7H16	The closest mixture that gives good results compared to the gasoline 87.
Initial Conditions	Intake Region	
	In-Cylinder	
	Exhaust Region	

<b>Simulation Start Time (CAD)</b>	-570	
<b>Simulation End Time (CAD)</b>	120	
<b>TDC at</b>	0	
<b>Solver time step</b>	Variable Time Step algorism provided by Converge CFD	
<b>Spray Model</b>	KH+RT	
<b>Combustion Model</b>	SAGE	
<b>Turbulence Modeling</b>	RANS	
<b>Base mesh grade</b>	4mm x 4mm x 4mm	

Table 9.1, Simulation setup data for single cylinder engine cycle simulation

### 9.3 Model convergence

For a direct injection spark ignition engine with a turbocharging engine and valve overlaps and for internal EGR control, a 720 degree full cycle simulation is needed. In addition, it is necessary to start the cycle simulation at a time before the intake valve opens to take into consideration the trapped mass for the next cycle.

The simulation time is very important in engine cycle simulation to balance the equation between model convergence and engine cycle to cycle variation. For this investigation, we tested the simulation time that would lead to model convergence. Selecting the factor that would judge the model convergence was critical, but the overall lambda of the mixture inside the cylinder at the time just before the ignition time was the closest factor to give good results rather than keeping the simulation running for a long time to get the desired IMEP.

Lambda of 1.01-1.03 was selected as the criteria that converges after the first three to four cycles and gives stable data. All the results under different operating conditions, we ran the simulation

for 8 consecutive cycles, we ignore the first four cycles (cycle No. 1, 2, 3 and 4) to make sure the simulation converged, then we take the average of the last three to four cycles (cycle No. 5, 6, 7 and 8).

For simulating the combustion process and calculating the burning velocity to compare it with the experimental data, the last four cycles for each operating condition were post processed and the average of these four cycles was taken as the average data for calculating the burning velocity.

To investigate the effect of different parameters on the cycle to cycle variation, hundred consecutive cycles was considered for which the COV % was calculated. However, this was found to be difficult because the simulation of one cycle was found to take around 48 hours, using the available high performance computer. Finally, the model for 9 consecutive cycles and considered only the last 6 cycles.

#### 9.4 Single cylinder and multi-cylinders engine modeling

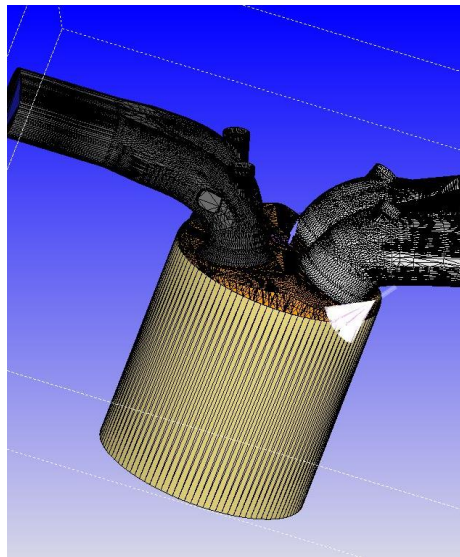


Figure 9.1 Layout of the single cylinder engine GTDI model

While simulation of a single cylinder engine does not represent some conditions in a four cylinder engine, such as engine dynamics, intake manifold pressure and temperature fluctuation, the exhaust temperature and pressure in addition to the trapped mass, the simulation in this investigation was for one cylinder in order to get the results in a reasonable period of time. Figure 9.1 shows the 3D engine model.



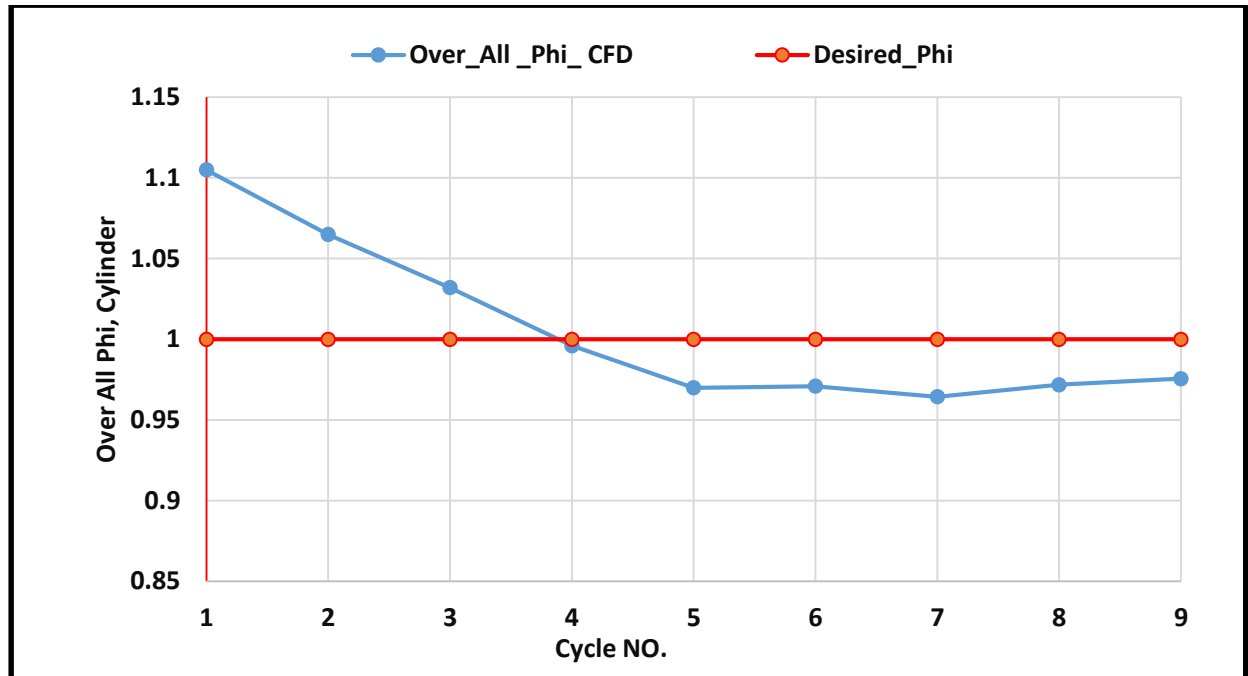


Figure 9.2 Values of the base and simulated 1.02 Lambda (Converge CFD v2.2)

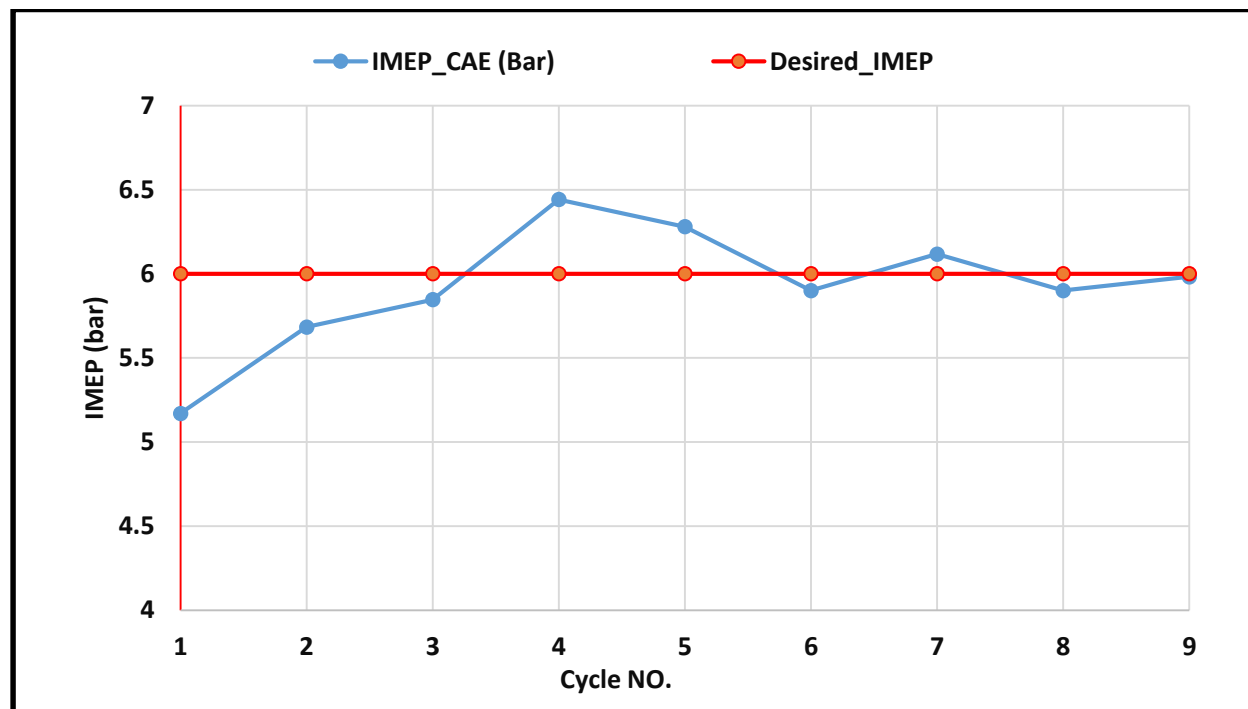


Figure 9.3 Simulated and measured IMEP around the Lambda 1.02 (Converge CFD v2.2)

Figures 9.2 and 9.3 shows the results of the CFD after calibrating the model. The desired lambda for the simulation was 1.02, and the model achieved this value after the first 4-cycles. In addition, the simulated IMEP agreed with the measured value, with.

The Pressure volume diagram of the average of the last six consecutive cycles is shown in figure 9.4. The red curve represent the P-V diagram of the average 100 consecutive cycles measured in the test cell. The blue curve represent the average of the last six consecutive cycles from the CFD simulation. The data showed a good a agreement with the experimental data.

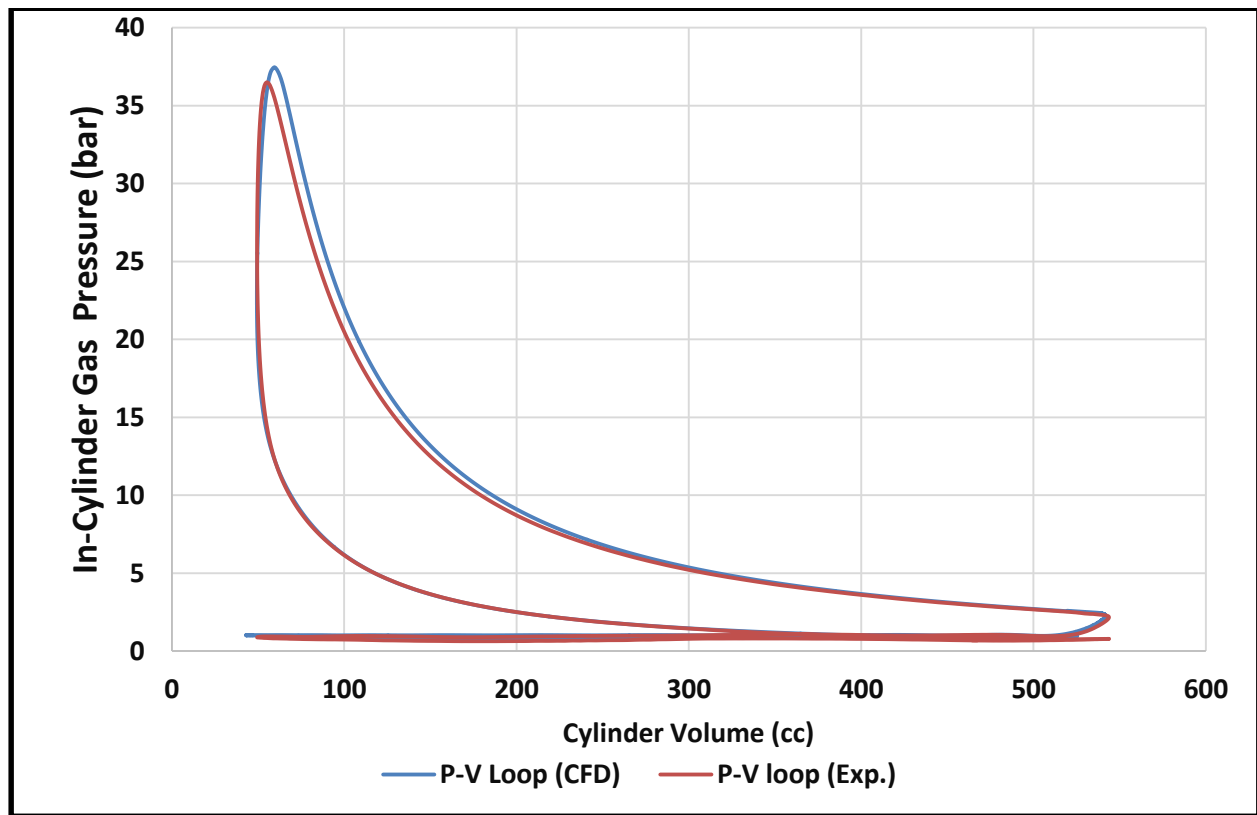


Figure 9.4 P-V diagram for the average of the last 6-consicutive cycles. (Converge CFD v2.2)

After calibrating the CFD model, the simulation ran on 1500 rpm and 15 mg of injected fuel for 10 consecutive cycles as shown in table 9.2. The first four cycles were neglected and considered to be the cycles needed for the model to adjust the boundary and initial conditions and minimize the error in the output data.

### 9.5 Boundary conditions for the 3D CFD Converge model setup.

		Spark				
	RPM	BTDC	IVO	EVC	Fuel Injected	MAP
Cycle No.	rpm	CA deg	CA deg	CA deg	kg	KPa-abs
1-10	1500	35	372	399	0.000015	85

Table 9.2 Boundary conditions for the 3D CFD Converge model setup.

The results showed that, even though the boundary conditions were the same for all the last 6 consecutive cycles, the simulation showed that the amount of air flow into the combustion chamber are not the same of each one of the 6 consecutive cycles as shown in figure 9.5. In addition, the results proved that the IMEP trend for the 6 consecutive cycles has the same trend as the amount of air flow.

Turbulence is a major factor in cycle to cycle variation because it affects the mixing between the fuel and air as well as the combustion process. Figure 9.6 shows the effect of tumble-X and tumble-Y on cycle to cycle variation. The results showed that the cycle to cycle variation in the GDI engine is related to the cycle average tumble ratio tumble ratio.

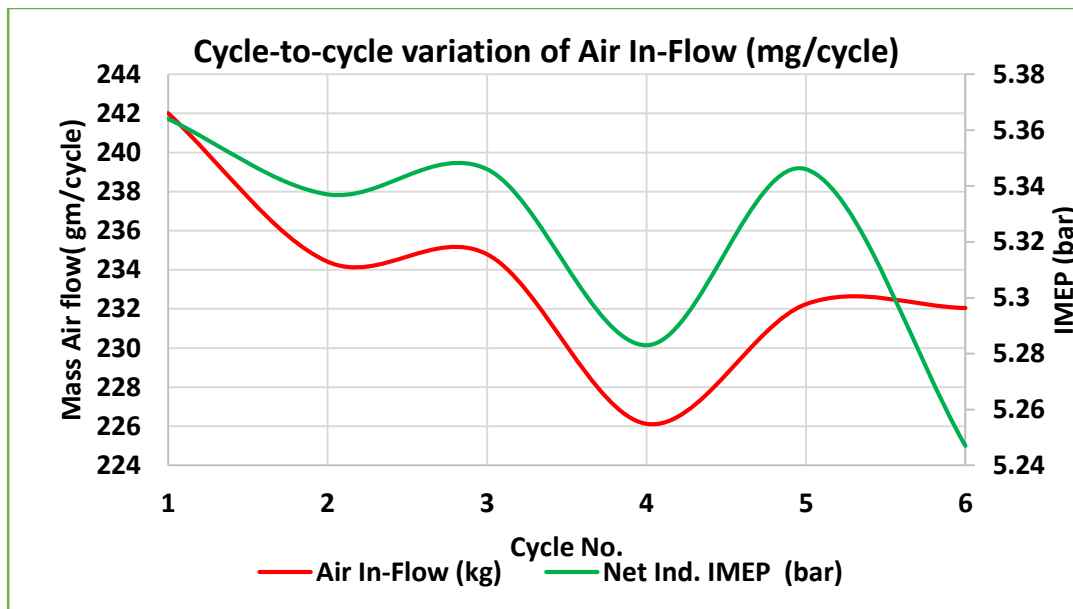


Figure 9.5 Effect of actual air flow in to cylinder on cycle to cycle variation. (Converge CFD v2.2)

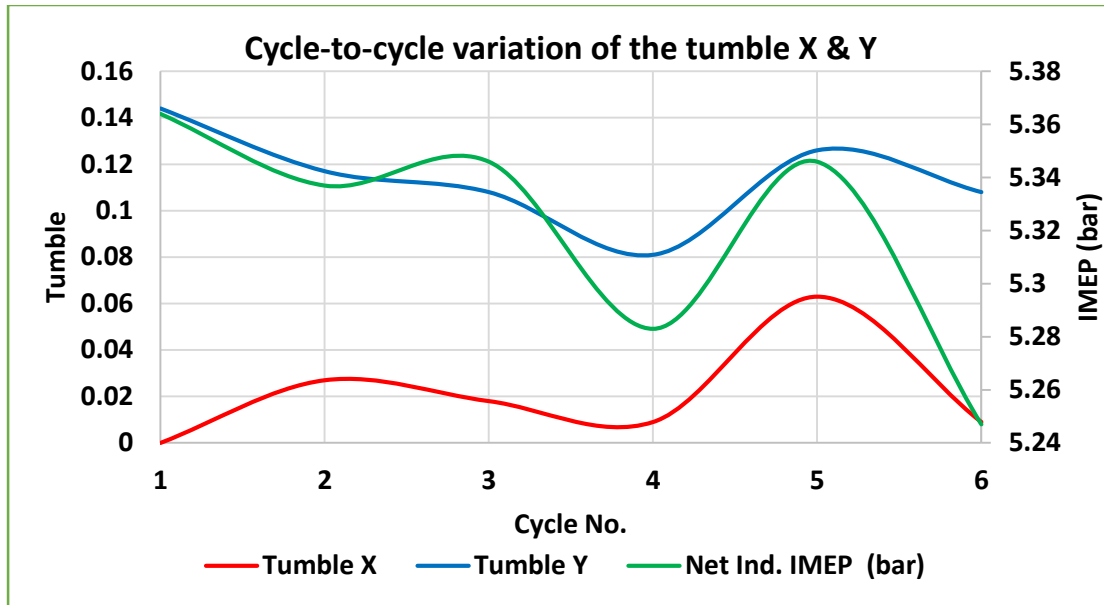


Figure 9.6 Effect of tumble-X and tumble-Y on cycle to cycle variation. (Converge CFD v2.2)

Additional simulation was conducted on a three different cases as shown in table 9.3 with different operating conditions to study the cycle to cycle variation. The results presented in Figures 9.7, 9.8 and 9.9 show the in-cylinder gas pressure trace for some consecutive cycles. These cycles taken after the first 4 consecutive cycles to make sure that any variation of the IMEP will not be due to the variation in the error of the simulation computation.

Case No.	RPM	Spark BTDC	Fuel Injected	No. Of Cycles running
	rpm	CA deg	mg	
1	1000	20	40	10
2	1250	15	20	9
3	1500	15	20	9

Table 9.3 Test matrix of three cases with different operating conditions

The variation in the peak pressure and IMEP for the three cases is due to the variation in the amount of air entering the combustion chamber and the change in turbulence from cycle to another one. The variation in mass air flow will definitely affect the overall air to fuel ratio in the cylinder. In

addition, this variation will affect the local equivalence ratio at the spark plug gap at the ignition timing. This variation in the mass air flow, is mainly due to the residuals remaining in the cylinder from the previous cycle.

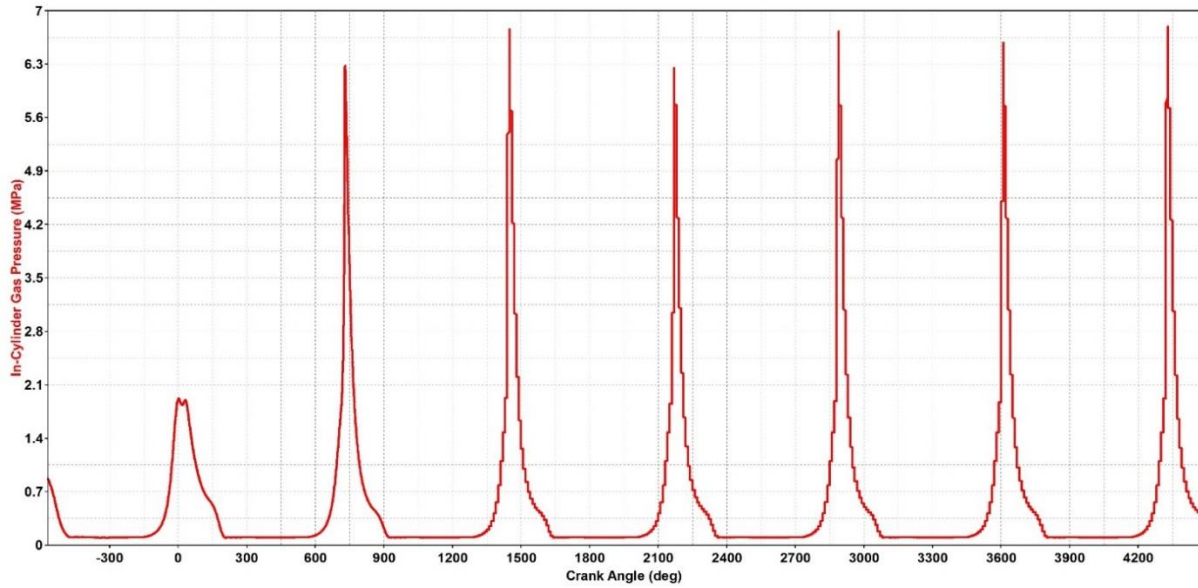


Figure 9.7 In-cylinder gas pressure (MPa) for 7 consecutive cycles for 1000 rpm, Spark 20 dBTDC and 40 mg of fuel, (Simulation done by Converge CFD v2.2)

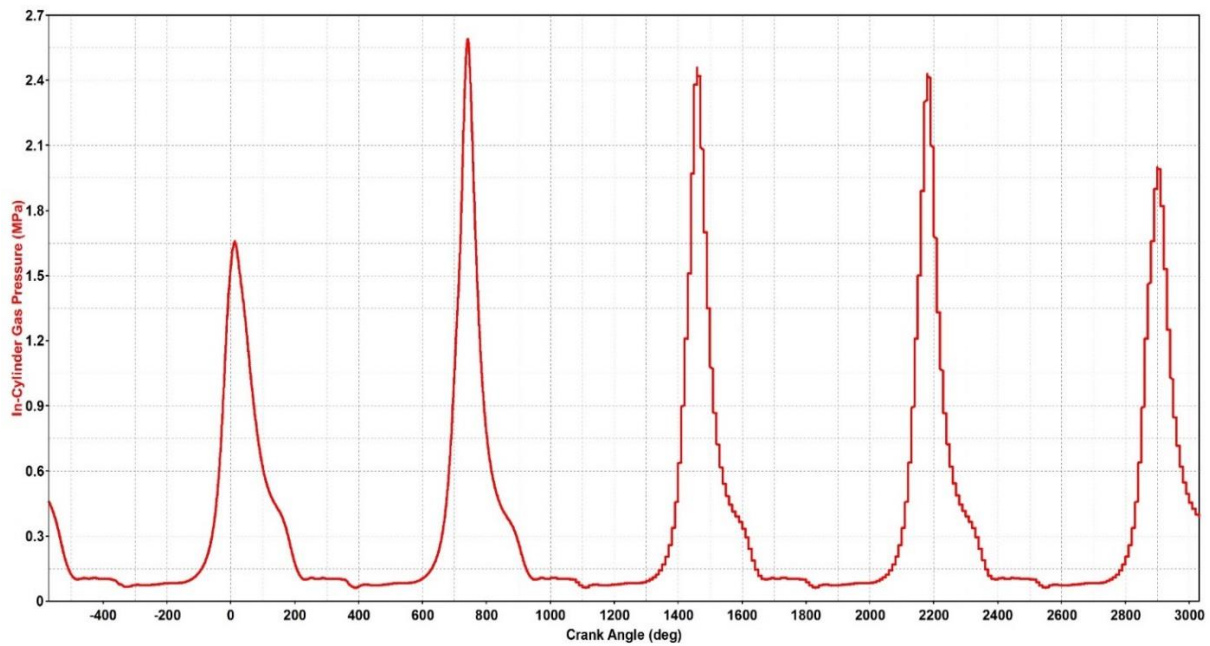


Figure 9.8 In-cylinder gas pressure (MPa) for 7 consecutive cycles for 1250 rpm, Spark 15 dBTDC and 20 mg of fuel, (Simulation conducted by Converge CFD v2.2)

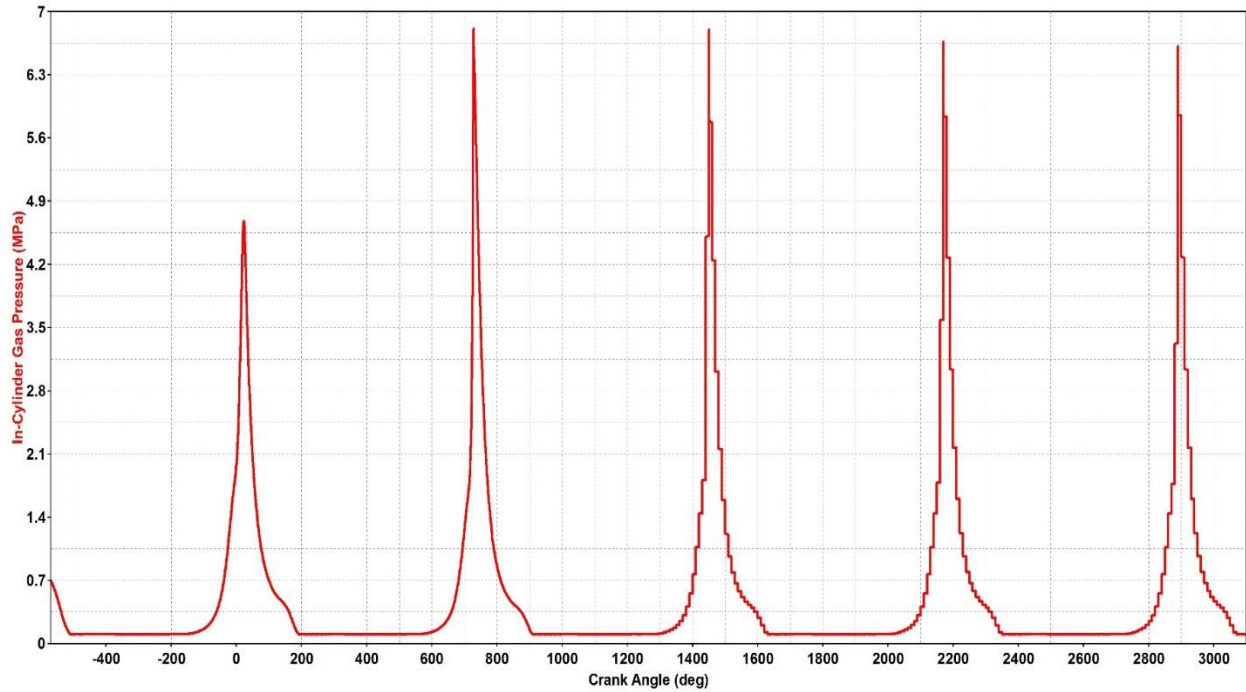


Figure 9.9 In-cylinder gas pressure (MPa) for 7 consecutive cycles for 1500 rpm, Spark 15 dBTDC and 20 mg of fuel, (Simulation conducted by Converge CFD v2.2)

### 9.6 Burning Velocity calculated from 3d CFD simulation

The burning velocity has been calculated from the ion current signals in chapter 6. This section will calculate the burning velocity using the 3D CFD simulation to support the results from the ionization measurement. A 3D CFD GDI engine model run at 1500 and 6 bar BMEP for 10 consecutive cycles. The average of the last six consecutive cycles has been taken into the consideration of calculating the burning velocity. In addition, EnSight 10.1 has been used to visualize the flame propagation in the combustion chamber.

Figure 9.10 shows the combustion chamber and the spark plug at the spark timing which was 26 degrees bTDC. The figure shows the isosurface part which shows the flame temperature. As shown in the figure, at the spark timing, there is no flame.

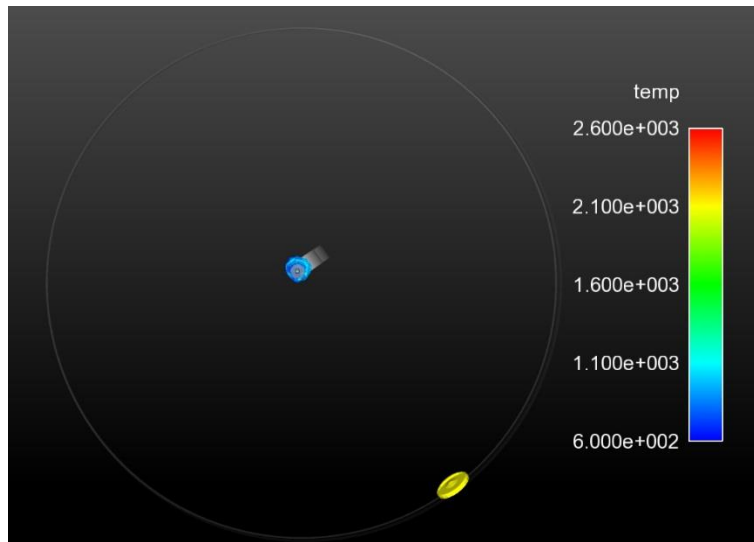


Figure 9.10 Iso Surface for the flame in the combustion chamber at the spark timing (Simulation conducted by Converge CFD v2.2)

Figure 9.11 shows the combustion chamber and the spark plug at the time when the flame starts at the spark plug gap. This occurred at 18 degrees bTDC. The figure shows the isosurface part which shows the flame temperature when the flame started. This shows that the ignition delay for this case is 8 degrees.

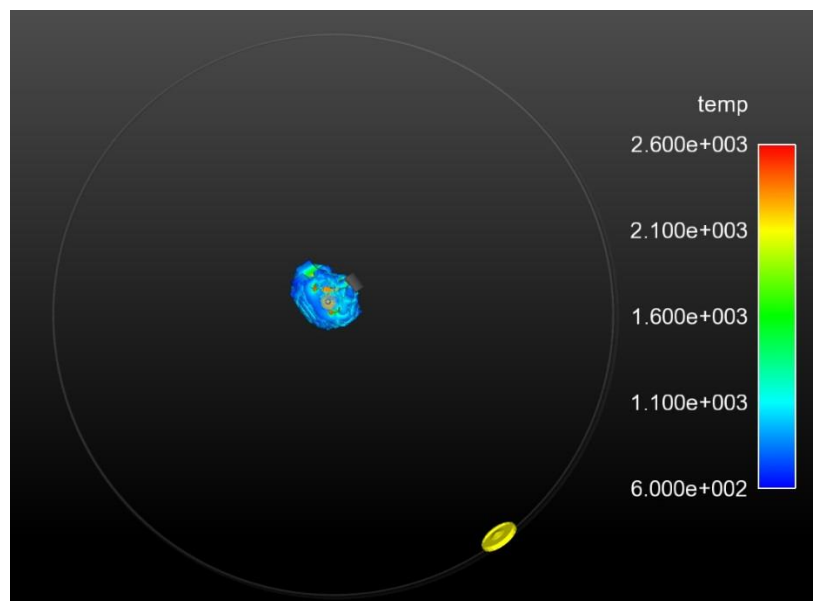


Figure 9.11 Iso Surface for the flame in the combustion chamber at the time when the flame started (Simulation conducted by Converge CFD v2.2)

Figure 9.12 shows the combustion chamber and the spark plug at the time when the flame arrived at the fuel injector. This occurred at 17 degrees aTDC. The figure shows the isosurface part which shows the flame temperature when the flame arrived at the fuel injector tip. This shows that the ignition delay for this case is 8 degrees.

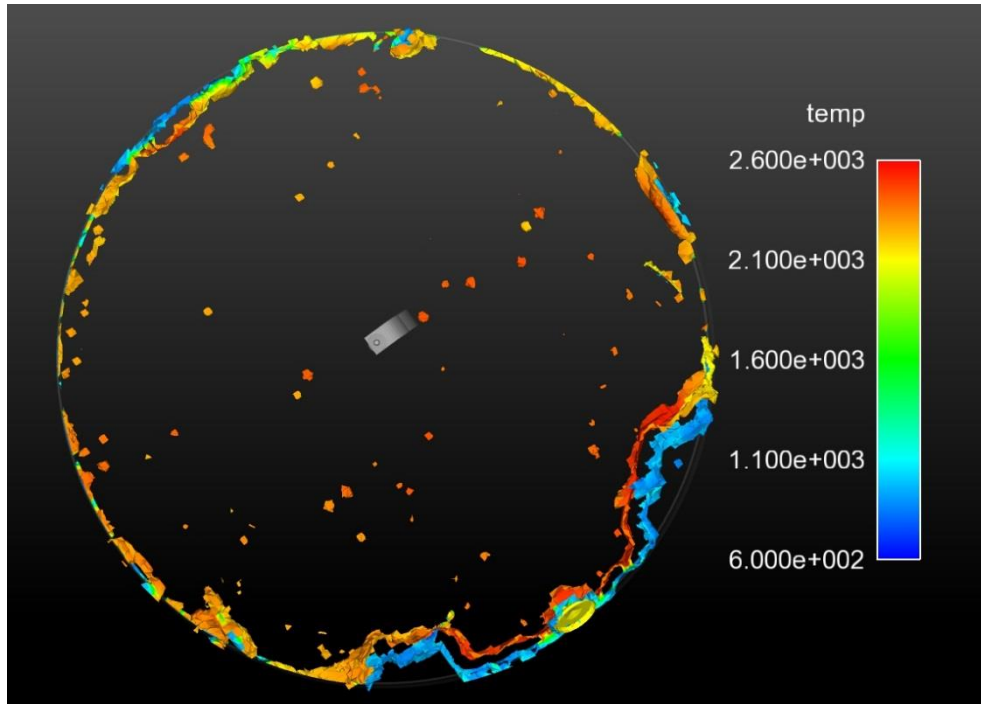


Figure 9.12 Iso Surface for the flame in the combustion chamber at the time when the flame arrived at the fuel injector (Simulation conducted by Converge CFD v2.2)

The results from the simulation showed that the flame started at 18 degrees bTDC and arrived at the fuel injector at 17 degrees aTDC. This time is around 25 degrees which represent around 3.99 msec. The distance between the spark plug central electrode and the fuel injector tip is around 41.5 mm. Using these information, the burning velocity calculation will be

$$\text{Burning velocity} = \frac{\text{Distance between the spark plug gap and fuel injector tip}}{\text{Time since the flame starts at the spark plug to the fuel injector tip}}$$

$$\text{Burning velocity} = \frac{0.0415}{0.003944} = 10.52231 \text{ m/s}$$



For this operating condition, the burning velocity calculated from the two ion current signals measured by the spark plug and fuel injector is 10.1 m/s.

$$Error = \frac{10.52331 - 10.1}{10.52331} = 4.0135 \%$$

This error between the experimental measurement and the calculation from the simulation is due to the following reasons;

- 1- The simulation using C<sub>8</sub>H<sub>18</sub> fuel in the simulation chemical mechanism which does not represent the exact fuel used in the experimental test which is gasoline 87.
- 2- The CFD did not use the crevice model. In addition, the leakage between the combustion chamber and the crank case is not considered in this case.
- 3- The CFD model does not calculate accurately the actual residuals

## 9.7 Summary

The 3D CFD model used in this investigation showed a good agreement with the experimental data for cycle to cycle variation. The GTDI 3D CFD engine model was calibrated to achieve a good agreement with the data from the engine. The experimental investigation of cycle to cycle variation showed that the fluctuation of injection pressure and injection command are major factors of cycle to cycle variation. The simulation added another factor which is the effect of turbulence and over all tumble to the factors that affecting cycle to cycle variation.

The 3D CFD combustion analysis and flame propagation visualization using simulation showed that the burning velocity calculated from the ionization agreed with the simulation results with around 4.5% error.

## CHAPTER 10 KNOCK DETECTION AND COMBUSTION DIAGNOSES USING IONIZATION

### 10.1 Introduction

Currently, the industry uses one or two knock sensors mounted on the engine block to detect engine knock from the four cylinders. Finding another technique that could be used to detect knock from each cylinder individually, this will help improve engine development and aggressively running the engine on the MBT. In addition, this could allow cycle to cycle as well as cylinder to cylinder ignition control to run each cylinder separately to obtain the MBT from each cylinder and each cycle. This chapter will explain how the ionization technique could replace the knock sensor and reduce engine cost.

In this section the signals from two ion current sensors, the fuel injector and the spark plug, and the production knock sensor are examined and compared.

### 10.2 Ion current signal from the fuel injector and spark plug

The ion current signals from the fuel injector and spark plug for normal combustion cycle without knock are shown in Figure 10.1. The in cylinder gas pressure trace in Figure 10.1 shows a normal combustion cycle without engine knock. The corresponding ion current signal from the fuel injector, the blue curve, shows a smooth trace of the ionization at the fuel injector. The ionization started at point (c) and raise gradually to the peak at point (e) and decayed gradually to the end of ionization at point (f) without fluctuation in the signal. In addition, the ion current signal from the spark plug showed a normal ionization for normal combustion without knock as shown in Figure 10.1. The ionization started at point (a), raise gradually without fluctuation to the first peak at point (b), then the second peak due to chemical and thermal ionization at point (d).

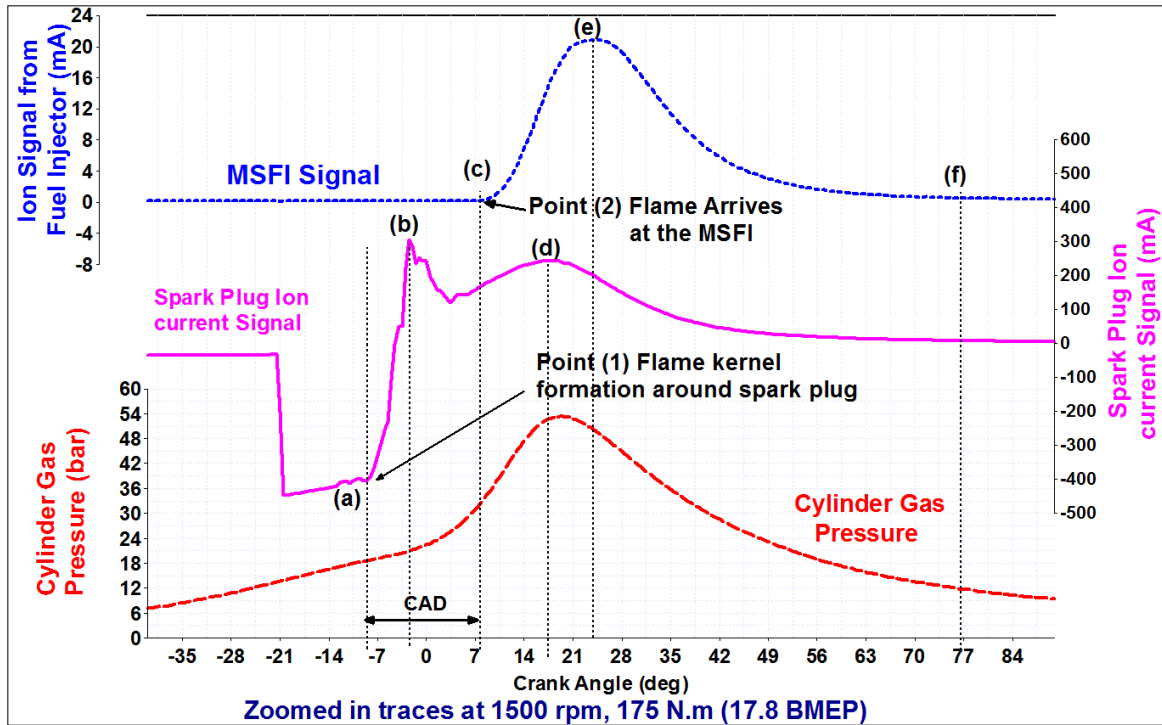


Figure 10.1 Zoomed-in traces for the two ion current signals from the spark plug and fuel injector at 1500 rpm and 175 N.m (11.0 BMEP)

### 10.3 Knock detection by the ion current signal from the fuel injector

The pressure wave occurred due to engine knock usually measured by the in-cylinder gas pressure transducer. Figure 10.2 shows zoomed-in traces for the ion current signal from the fuel injector and the in-cylinder gas pressure. The pressure trace shows that the engine is knocking and it started at 11 degrees aTDC. The corresponding ion current signal from the fuel injector detected every peak occurred on the pressure trace.

Figure 10.3 showed zoomed-in traces of Figure 10.2 for the period 10 to 20 degrees aTDC and it shows that for each peak occurred on the pressure trace due to engine knock, there is a peak detected by the ion current signal but with opposite magnitude due the way the ionization measured. In more details, positive peak on the pressure trace, showed a negative peak on the ion current signal but at the same crank angle degree with corresponding amplitude.

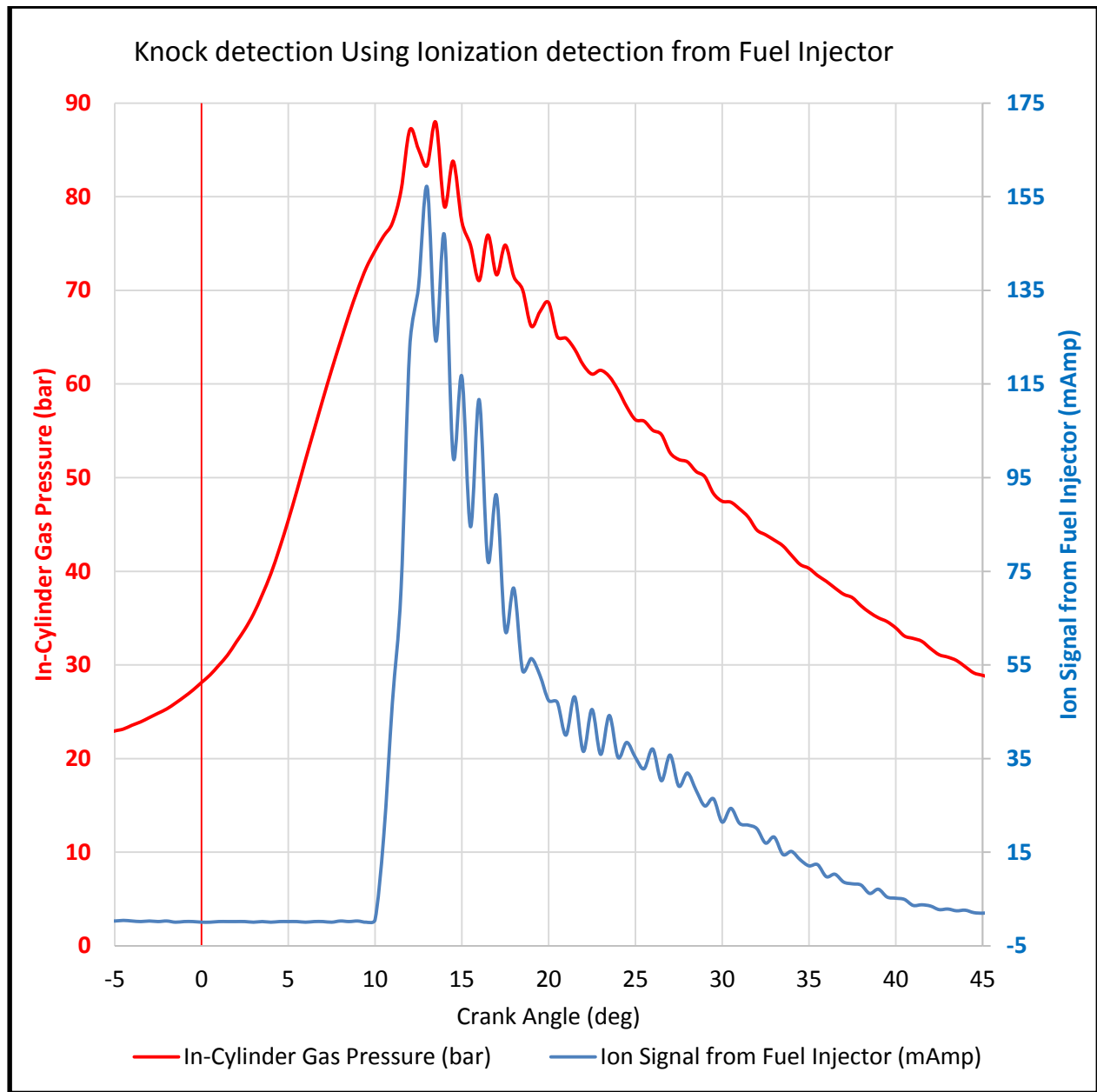


Figure 10.2 Zoomed-in traces for the ion current signal from the fuel injector and the in-cylinder gas pressure at 2000 rpm and 300 n.m

Additional information can be extracted from the ion current signal from the fuel injector which is the peak amplitude of the pressure trace. The knock intensity will cause high pressure rise with sharp peak and more fluctuation on the in-cylinder gas pressure trace. The ion current signal detected the same fluctuation occurred on the pressure trace. Precisely, the ion current signal detected each peak occurred on the pressure trace due to engine knock as it shown in more detailed signals in Figure 10.3

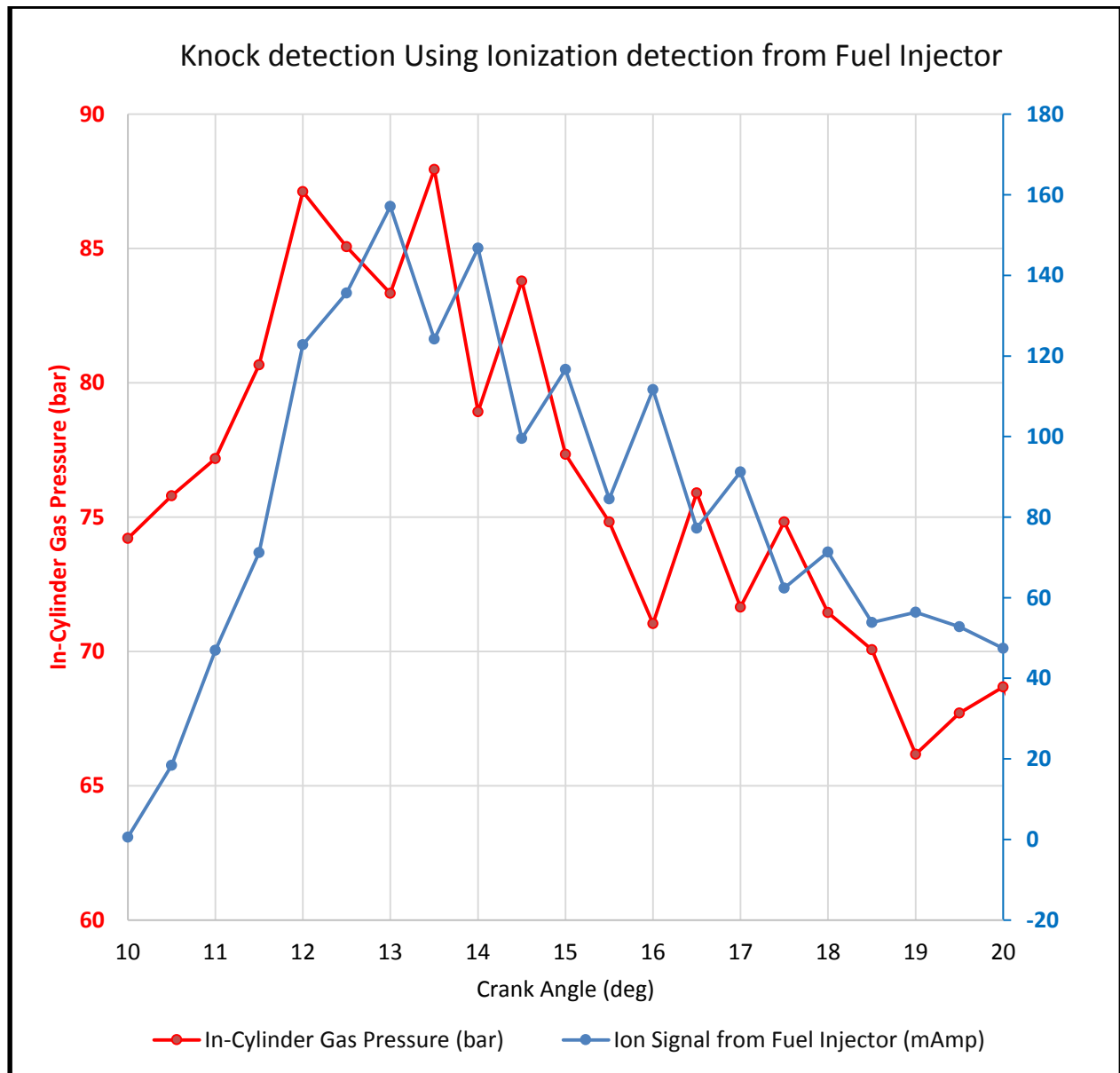


Figure 10.3 Detailed zoomed-in traces for the ion current signal from the fuel injector and the in-cylinder gas pressure for the period 10 to 20 degrees aTDC at 2000 rpm and 300 n.m

Figure 10.4 shows Knock detection using Ion current signal from fuel injector compared to signal measured by the knock sensor. The engine knock sensor has been connected to the data acquisition to record the engine knock frequency in addition to the ion current signal from the fuel injector on the same crank angle bases. The knock sensor showed no knock up till crank angle 10 degrees aTDC, then knock started at around 13.1 degrees aTDC as it shown on the signal from the knock sensor. However, according

to the pressure trace in figure 10.2, the knock started at 11.0 degrees aTDC, so, the knock sensor detected the engine knock after it occurred by 2 degrees. On the other hand, the ion current signal from the fuel injector showed that the knock started at 11.0 aTDC which is the same time the pressure transducer detected engine knock.

In addition, Figure 10.5 showed a zoomed-in traces for the knock detected by the engine knock sensor and the knock detected by the ion current signal from the fuel injector. The data showed that the ion current signal was able to detect engine knock faster than the engine knock sensor. Also, the ion signal from the fuel injector showed the time when the knock ended and agreed with the signal measured by in cylinder gas pressure transducer.

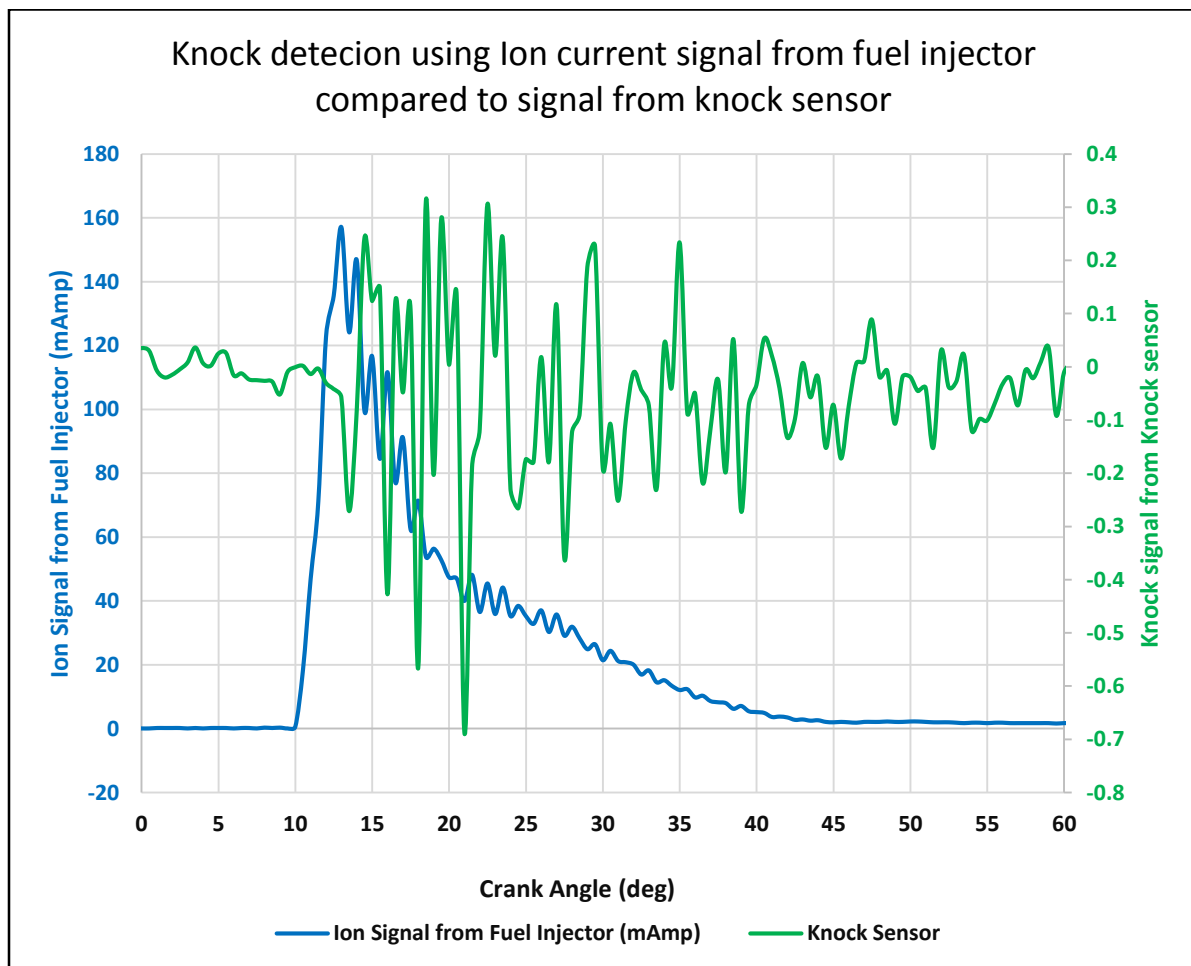


Figure 10.4 Detailed zoomed-in traces for the ion current signal from the fuel injector and the signal from the knock sensor at 2000 rpm and 300 n.m

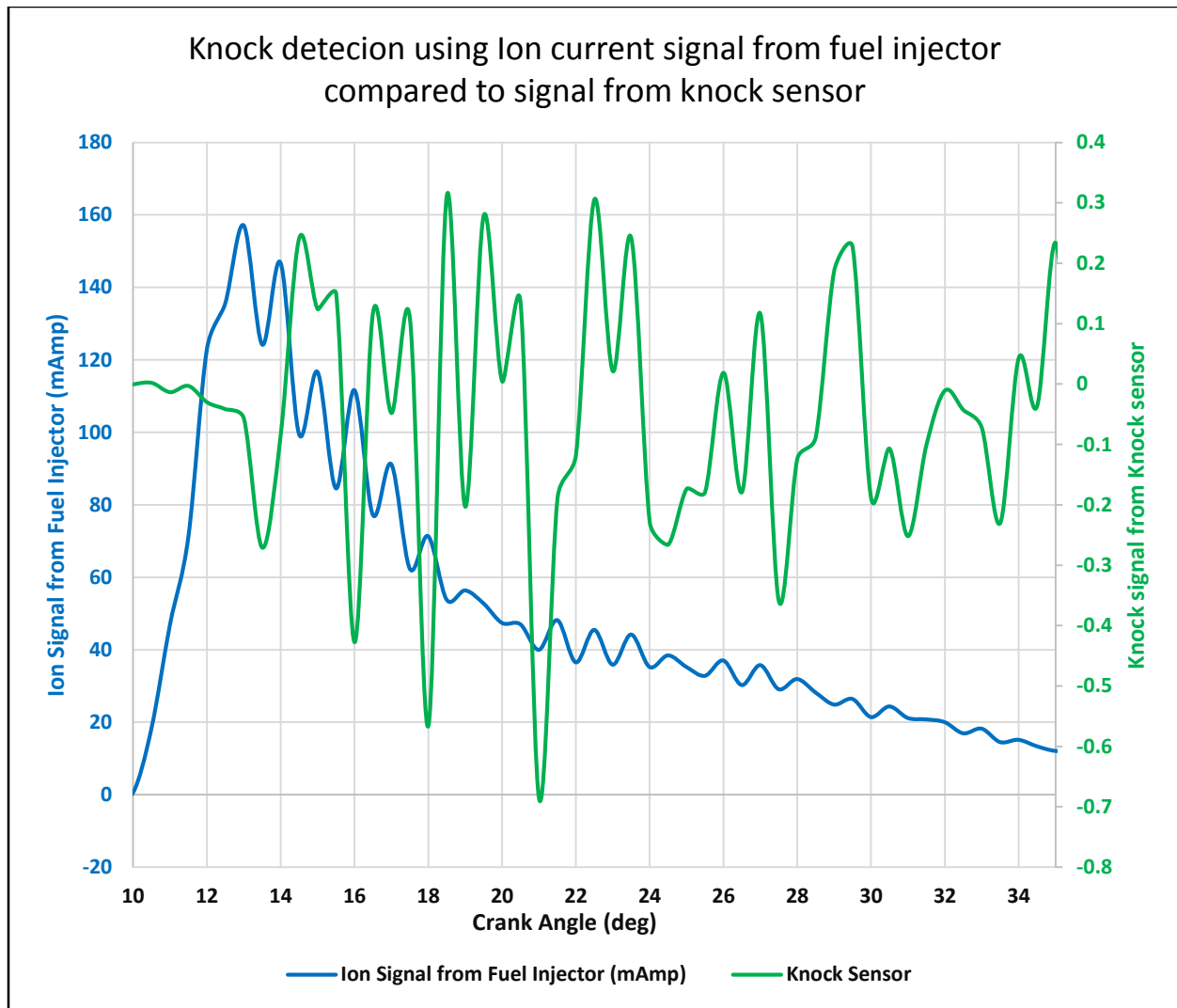


Figure 10.5 Detailed zoomed-in traces for the ion current signal from the fuel injector and the signal from the knock sensor for the period 10 to 35 degrees aTDC at 2000 rpm and 300 n.m

#### 10.4 Knock detection by the ion current signal from the spark plug

In addition to detecting engine knock from the ion current signal from the fuel injector, the ion current signal from the spark plug has been used to detect engine knock. Figure 10.6 shows the traces for in-cylinder gas pressure and the ion current signal from the spark plug while the engine is knocking for a cycle at 2000 rpm and 300 n.m. Figure 10.6 and Figure 10.7 shows the ion current signal from the spark plug and the knock signal measured from the engine knock sensor. The ion current signal from the spark plug showed that the knock started at 11.0 degrees aTDC which agreed with the data extracted from the

ion current signal from the fuel injector and from the pressure trace. The ion current signal before 11.0 degrees aTDC showed a normal ion current signal. Starting from 11.0 degrees aTDC, the knock frequency started to appear on the ion current signal from the spark plug.

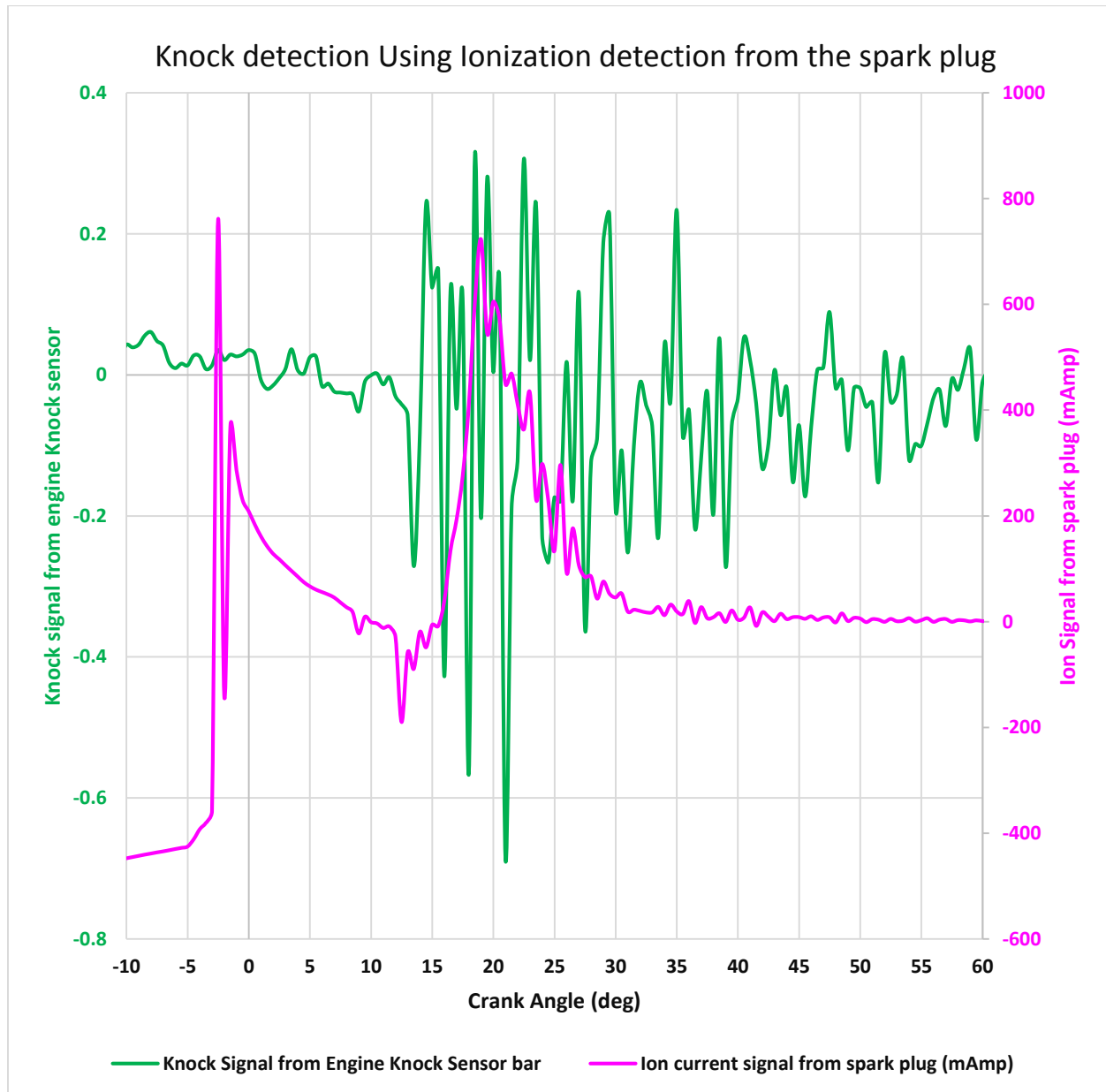


Figure 10.6 Zoomed-in traces for the ion current signal from the spark plug and the signal from the knock sensor at 2000 rpm and 300 n.m



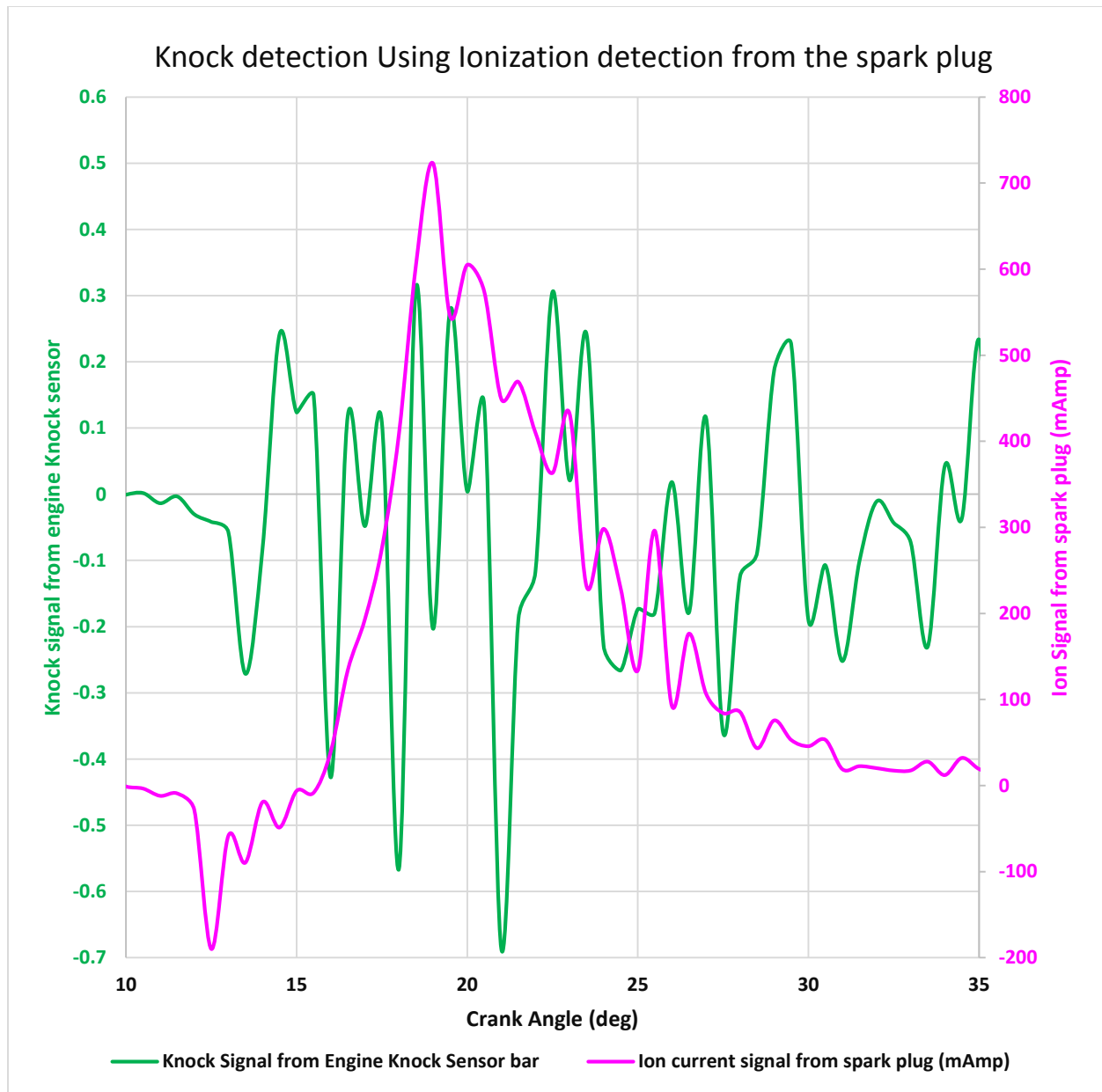


Figure 10.7 Detailed zoomed-in traces for the ion current signal from the spark plug and the signal from the knock sensor for the period 10 to 35 degrees aTDC at 2000 rpm and 300 n.m

### 10.5 Combustion diagnoses using ionization

In addition to detecting knock using the ion current signal from the spark plug and the fuel injector, the late combustion and engine misfire can be detected from the second peak of the ion signal from the spark plug. Figure 10.1, Figure 10.8 and Figure 10.9 shows the characteristics of the ion current signal from the spark plug and the fuel injector. From Figure 10.1, point (d) represents the second peak from the spark

plug and point (e) represents the peak of ionization at the fuel injector. These two peaks are due to chemical and thermal ionization which is due to the high rise in pressure and temperature. In addition point (d) is representing the peak pressure location. If the cycle has a late combustion, the two peaks location will be very late. Also, if the engine misfires, these two peaks will have a zero amplitude. Furthermore, these two peaks represent the features of the mass burned fraction. From these information, the two peak locations and amplitude can be used as a feedback signal to the engine ECU to diagnose engine misfire or the late combustion.

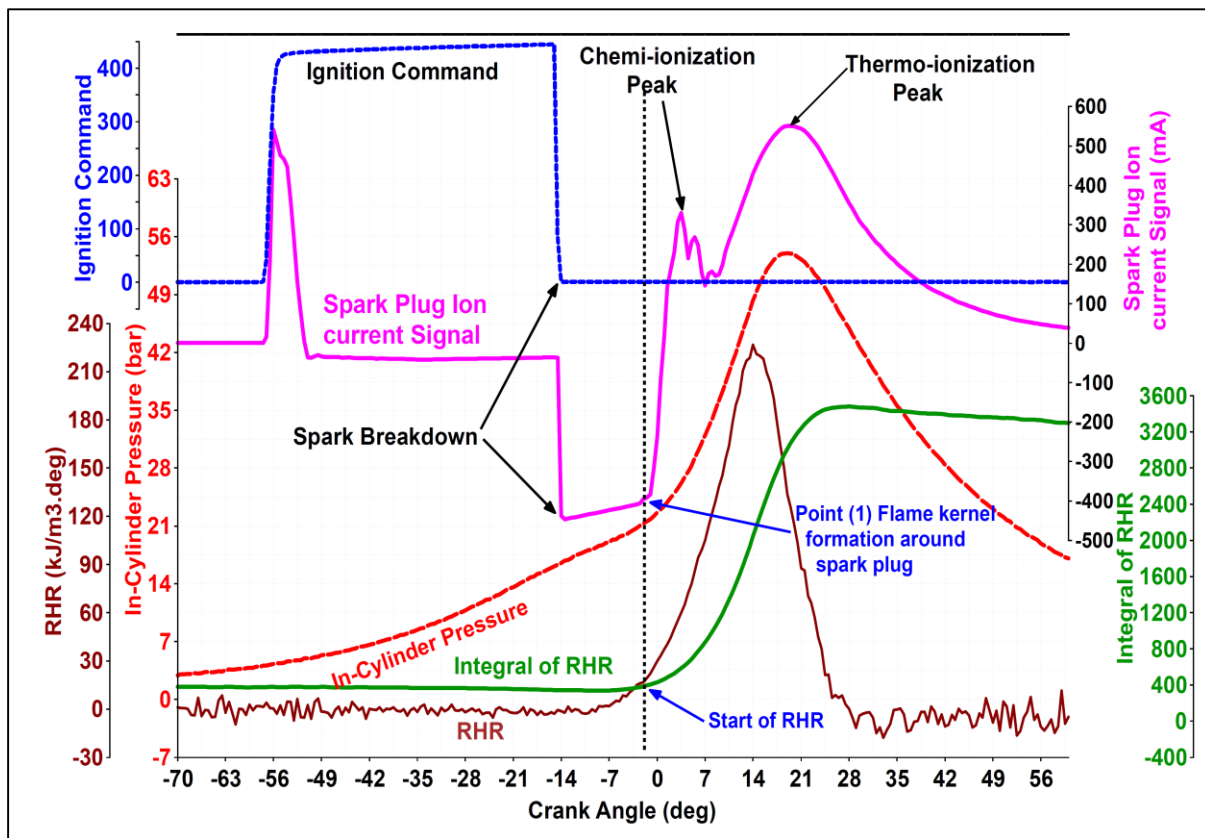


Figure 10.8 Sample of cylinder gas pressure, ignition command, and the ion current signal from the spark plug, zoomed in traces at 1500 rpm, 175 N. m (11.0 BMEP).

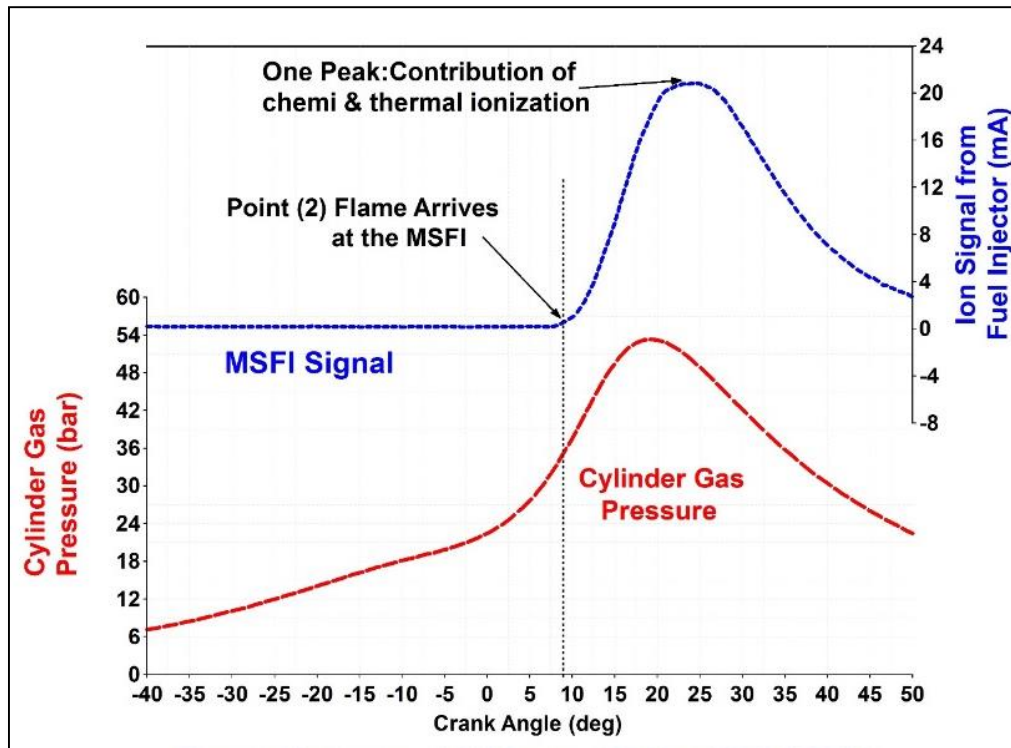


Figure 10.9 Sample of cylinder gas pressure and the ion current signal from the fuel injector. Zoomed in traces at 1500 rpm, 175 N.m (11.0 BMEP)

### 10.6 Injector functionality diagnoses using the ion current signal from the fuel injector.

Diagnosing the functionality of the fuel injectors requires a feedback signal from the fuel injector to show if the injector working probably or not. In addition, the actual opening and closing of the fuel injector requires a needle left sensor to detect the movement of the injector solenoid. Knowing the actual movement of the injector solenoid will help improve the engine development and detect the variation in the amount of fuel injected per cycle per cylinder. The ion current circuit which is connected to the fuel injector showed the electromagnetic interference when the solenoid starts to move to open and when it is fully closed. Figure 10.10 shows the ion current signal from the fuel injector and the injector command measured using the current probe. The ion signal from the fuel injector shows the opening and closing of the injector solenoid. In case the solenoid is not in a good working conditions and is not opening or closing, this ion current signal from the fuel injector will have a zero amplitude. From this information, a feedback signal from this signal can be send to the ECU to detect the functionality of the fuel injector.

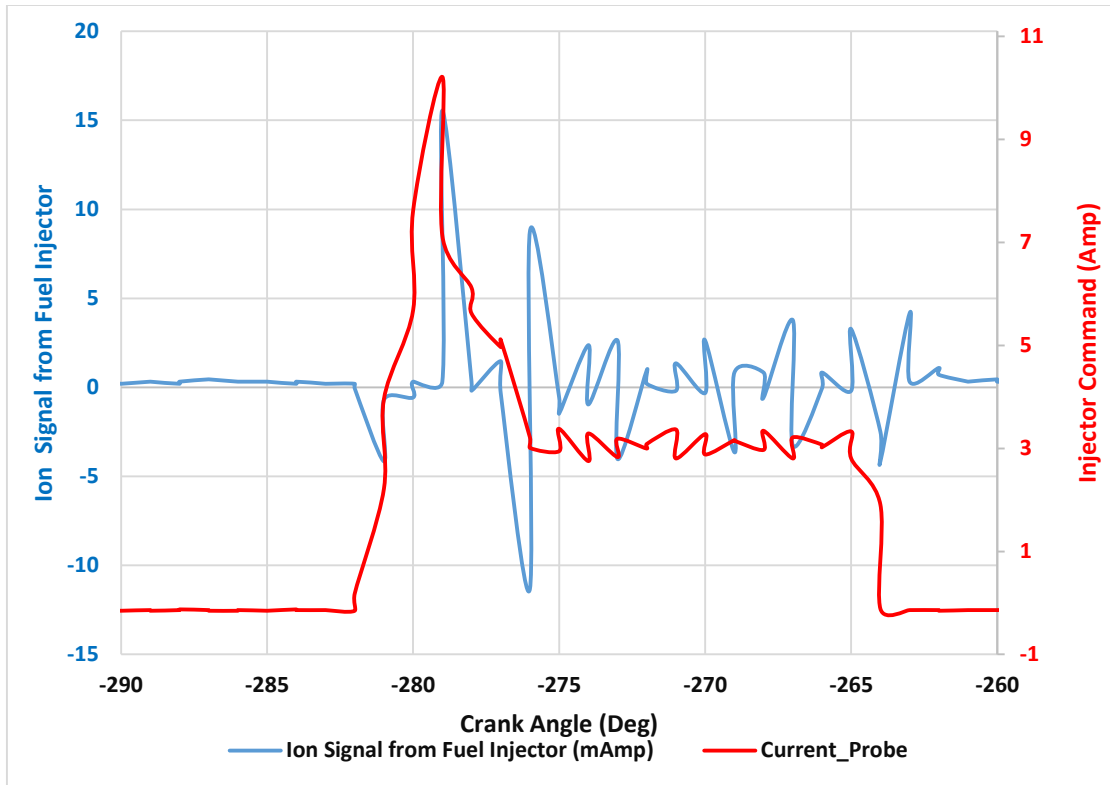


Figure 10.10 the injector command and the ion current signal from fuel injector

### 10.7 Summary

The ion current signals from the fuel injector and spark plug were able to detect the engine knock with 0.1 crank angle degree resolution. This detection compared to the data from the knock sensor. In addition, the knock detected by ionization showed a good agreement with the knock detected by the knock sensors. This results could allow the engine designers to replace the knock sensors and use the ionization technique to detect engine knock from each cylinder and allow cycle to cycle ignition control as well as cylinder to cylinder control. In addition, the knock detection using ionization showed the capability of detecting engine knock faster than the engine knock sensor.

Engine miss fire and late combustion has been detected by the ion signal from spark plug and fuel injector. In addition, the injector functionality has been monitored using the ion current signal from the

fuel injector which help understanding the actual opening and closing the of the fuel injector. Also, detecting if the injector solenoid is working

## CHAPTER 11 CONCLUSIONS

These conclusions are based on an experimental investigation and computer simulation of combustion and ionization in a 2.0 L turbocharged four cylinders gasoline direct injection (GTDI) engine, with a focus on sporadic pre-ignition. Combustion characteristics with and without pre-ignition are determined from rate of heat release calculated from cylinder gas pressure measured by a piezo quartz transducer as well as from the ion currents measured using the spark plug and the fuel injector as ion current sensors.

1. Using two ion current sensors enabled the determination of the burning velocity in the GTDI engine on cycle-by-cycle basis, and its strong dependence on engine speed, load, injection timing and spark timing. The experimental results validated results of a 3D CFD combustion simulation model. .
2. A detailed analysis of cycle-to-cycle variation, using experimental investigations and the 3D CFD combustion simulation showed that variations in fuel delivery and turbulence are major factors in the cycle to cycle variation.
3. Combustion phasing as well as abnormalities, late combustion, misfiring, knock and post-knock pre-ignition and sporadic pre-ignition are detected by the two ion current sensors as well as the pressure transducer.
4. The ion current signal from spark plug and/or the fuel injector is able to detect and characterize engine knock and can be used in the future engines to replace the knock sensors.
5. Sporadic pre-ignition initiation is very strongly dependent on the quality of the lubricating oil, less dependent on the fuel and injection strategy. It could not be detected with synthetic lubricating oil, meanwhile it was frequent with hydrocracked lubricating oil.
6. Sporadic pre-ignition results in severely high cylinder gas pressures and rates of pressure rise. It can lead to knock and after-knock pre-ignition and eventually destroy the engine.

7. The tendency to sporadic pre-ignition can be reduced by multi-event injection strategy, which reduces charge temperature due to early evaporation and by reducing fuel impingement of the cylinder walls which dilutes the lubricating oil and increase its tendency to get into the combustion chamber.
8. The ion current signal from the fuel injector used for diagnosing the functionality of the solenoid of the fuel injectors. In addition, the signal is used as a feedback signal from this signal can be send to the ECU to detect the functionality of the fuel injector.

**RECOMMENDATIONS**

1. Develop a 3D CFD simulation model for ionization in the GDI engine considering the design of the combustion chamber, location of the injector and spark plug to predict the ion current signal and its correlation with the combustion characteristics.
2. Extend the investigation of sporadic pre-ignition using different types of oil, wide range of injection strategies.
3. Consider the use of ion current sensing technology in gasoline direct injection compression ignition engines and include it in the ECU at this early state of their development.



## REFERENCES

- 1) Cao, Y. and Li, L., "A Novel Closed Loop Control based on Ionization Current in Combustion Cycle at Cold Start in a GDI Engine," SAE Technical Paper 2012-01-1339, 2012, doi:10.4271/2012-01-1339.
- 2) Abhijit, G. and Naber, J., "Correlation of Air Fuel Ratio with Ionization Signal Metrics in a Multicylinder Spark Ignited Engine," SAE Technical Paper 2009-01-0584, 2009, doi:10.4271/2009-01-0584.
- 3) Davinder Kumar, "An Ionization Current based Cylinder Gas Pressure Estimation for Knock Detection and Control in a Single Cylinder SI Engine". SAE paper 2009-32-0118.
- 4) Abdel-Rehim, A., Henein, N., and VanDyne, E., "Ion Current in a Spark Ignition Engine using Negative Polarity on Center Electrode," SAE Technical Paper 2007-01-0646, 2007, doi:10.4271/2007-01-0646.
- 5) Naoumov, V., Demin, A., Andersson, I., and Sokolov, A., "Modeling of Combustion and Non-Equilibrium Ionization in Spark Ignition Engines," SAE Technical Paper 2002-01-0009, 2002, doi:10.4271/2002-01-0009.
- 6) Moxey, B., Cairns, A., and Zhao, H., "A Study of Turbulent Flame Development with Ethanol Fuels in an Optical Spark Ignition Engine," SAE Technical Paper 2014-01-2622, 2014, doi:10.4271/2014-01-2622.
- 7) Huang, C., Lipatnikov, A., Johansen, L., and Hemdal, S., "A Study of Two Basic Issues Relevant to RANS Simulations of Stratified Turbulent Combustion in a Spray-Guided Direct-Injection Spark-Ignition Engine," SAE Technical Paper 2014-0-2572, 2014, doi:10.4271/2014-01-2572.
- 8) Young, M.B. (1981), Cyclic Dispersion in the Homogeneous-Charge Spark-Ignition Engine-A Literature Survey, SAE Paper 810020.
- 9) Ozdor, N., Dulger, M., and Sher, E. (1994), Cyclic Variability in Spark Ignition Engines A Literature Survey, SAE Paper 940987.
- 10) Matsuoka, S., Yamaguchi, T., and Umemura, Y. (1971), Factors Influencing the Cyclic Variation of Combustion of Spark Ignition Engine, SAE Paper 710586.

- 11) Pischinger, S., and Heywood, J.B. (1988), A Study of Flame Development and Engine Performance with Breakdown Ignition Systems in a Visualization Engine, SAE Paper 880518.
- 12) Pashley, N.C. (1997), Ignition Systems for Lean-Burn Gas Engines, PhD Thesis, University of Oxford.
- 13) Kuo, T.W. (1990,), What Causes Slower Flame Propagation in the Lean-Combustion Engine?, Transactions of the ASME, Journal of Engineering for Gas Turbines and Power, Vol. 112, pp. 348-356.
- 14) Shen, H., and Jiang, D. (1992), Investigation on the Flame Initiation and Early Development in a Spark Ignition Engine, SAE Paper 922239.
- 15) Lyon, D., Knock and cyclic dispersion in a spark ignition engine, Proceedings of ImechE, International Conference on Petroleum Based Fuels and Automotive Applications, 25-26 November, 1986, pp. 105-116.
- 16) Stone, C.R., Brown, A.G., and Beckwith, P. (1992), A turbulent combustion model used to give insights into cycle-by-cycle variations in spark ignition engine combustion, Proceedings of the ImechE, International Conference on Combustion in Engines, 1-3 December, 1992, pp. 47-53.
- 17) Ellison, R.J., Harrow, G.A., and Hayward, B.M. (1968), The Effect of Tetraethyl-Lead on Flame Propagation and Cyclic Dispersion in Spark-Ignition Engines, Journal of the Institute of Petroleum, Vol. 54, No. 537, pp. 243-250.
- 18) Ptterson, D.J. (1966), Cylinder Pressure Variations, a Fundamental Combustion Problem, SAE Paper 660129.
- 19) Soltau, J.P. (1960) Cylinder Pressure Variations in Petrol Engines, ImechE Conference Proceedings, July, 1960, pp. 96-116.
- 20) Grunefeld, G., Beushausen, V., Andresen, P., and Hentschel, W. (1994), a Major Origin of Cyclic Energy Conversion Variations in SI Engines: Cycle-by-Cycle Variations of the Equivalence Ratio and Residual Gas of the Initial Charge, SAE Paper 941880.

- 21) Lee, K.H., and Foster, D.E. (1995), Cycle-by-Cycle Variations in Combustion and Mixture Concentration in the Vicinity of Spark Plug Gap, SAE Paper 950814.
- 22) Berckmuller, M., Tait, N.P., and Greenhalgh, D.A. (1997), The Influence of Local Fuel Concentration on Cyclic Variability of a Lean Burn Stratified Charge Engine, SAE Paper 970826.
- 23) Brunt, M.F.J., and Pond, C.R. (1997), Evaluation of techniques for absolute cylinder pressure correction, SAE paper 970036.
- 24) Brunt, M.F.J. and Emtage, A.L. (1997), Evaluation of burn rate routines and analysis errors, SAE paper 970037.
- 25) Douglas, R., Kee, R.J., and Carberry, B.P. (1997), Analysis of In-Cylinder Pressure Data in Two-Stroke Engines, SAE Paper 972792.
- 26) Sztenderowicz, M.L., and Heywood, J.B. (1990a), Mixture Nonuniformity Effects on S.I. Engine Combustion Variability, SAE Paper 902142.
- 27) Lucas, G.G., and Brunt, M.F.J. (1982), The Effect of Combustion Chamber Shape on the Rate of Combustion in a Spark Ignition Engine, SAE Paper 820165.
- 28) Chanchaona, S., McFeaters, J.S., and Raine, R.R. (1990), Effects of High Compression Ratio and Combustion Chamber Shape on Cycle-to-Cycle Variability, SAE Paper 900385.
- 29) Sztenderowicz, M.L., and Heywood, J.B. (1990b), Cycle-to-cycle IMEP fluctuations in a stoichiometrically-fueled SI engine at low speed and load, SAE paper 902143.
- 30) Berckmuller, M., Tait, N.P., and Greenhalgh, D.A. (1997), The Influence of Local Fuel Concentration on Cyclic Variability of a Lean Burn Stratified Charge Engine, SAE Paper 970826.
- 31) Hamai, K., Kawajiri, H., Ishizuka, T., and Nakai, M. (1986), Combustion Fluctuation Mechanism Involving Cycle-to-Cycle Spark Ignition Variation due to Gas Flow Motion in S.I. Engines, 21st International Symposium on Combustion.

- 32) Lancaster, D.R., Kreiger, R.B., Sorenson, S.C., and Hull, W.L. (1976), Effects of Turbulence on Spark-Ignition Engine Combustion, SAE Paper 760160.
- 33) Cole, D.E., and Mirsky, W. (1968), Mixture Motion - Its Effect on Pressure Rise in a Combustion Bomb: New Look at Cyclic Variation, SAE Paper 680766.
- 34) LeCoz, J.F. (1992), Cycle-to-Cycle Correlations between Flow Field and Combustion Initiation in an S.I. Engine, SAE Paper 920517.
- 35) Henein, N., Bryzik, W., Abdel-Rehim, A., and Gupta, A., "Characteristics of Ion Current Signals in Compression Ignition and Spark Ignition Engines," *SAE Int. J. Engines* 3(1):260-281, 2010, doi:10.4271/2010-01-0567.
- 36) Hacohen, J., Belmont, M.R., Thurley, R.W.F., Thomas, J.C., Morris, E.L., and Buckingham, D.J. (1992), Experimental and Theoretical Analysis of Flame Development and Misfire Phenomena in a Spark-Ignition Engine, SAE Paper 920415.
- 37) Ceviz, M.A. and Yuksel, F., "Cyclic Variations on LPG and Gasoline-Fuelled LeanBurn SI Engine," *Renewable Energy*, 31, 1950-1960, 2006.
- 38) Belmont, M.R., Hacohen, J., and Carpenter, P.W. (1994), Tumble and Swirl: Are they a Mixed Blessing?, *Proceedings of the ImechE, Part D: Journal of Automobile Engineering*, Vol. 208, pp. 223-226.
- 39) Matekunas, F.A. (1983), Modes and Measures of Cyclic Combustion Variability, SAE Paper 830337.
- 40) Martin, J.K., Plee, S.L., and Remboski, D.J. (1988), Burn Modes and Prior-Cycle Effects on Cyclic Variations in Lean-Burn Spark-Ignition Engine Combustion, SAE Paper 880201.
- 41) Stevens, S.P., Shayler, P.J., and Ma, T. (1992), A basis for the predictive control of cyclic dispersion in a spark ignition engine, *Proceedings of the ImechE, International Conference on Combustion in Engines*, 1-3 December, 1992, pp. 175-182.

- 42) Stephen Samuel, Denise Morrey (2010), Combustion Characteristics and Cycle-By-Cycle Variation in a Turbocharged-Intercooled Gasoline Direct-Injected Engine, SAE 2010-01-0348.
- 43) Seungmok Choi, Joonwon Lim, Minyoung Ki, Kyoungdoug Min and Hoimyoung Choi, 2009, Analysis of Cyclic Variation and the Effect of Fuel Stratification on Combustion Stability in a Port Fuel Injection (PFI) CAI Engine, SAE 2009-01-0670.
- 44) O. Le Corre and M. Tazerout, 2001, Experimental Investigation on Cycle by Cycle Variations in a Natural Gas Fuelled Spark Ignition Engine, 2001-28-0021.
- 45) Bondi, S., and Jones, W.P., "A Combustion Model for Premixed Flames with Varying Stoichiometry," Proc. Combust. Inst. 29(2):2123-2129, 2002, doi:10.1016/S1540-7489(02)80258-9.
- 46) Polifke, W., Flohr, P., and Brandt, M. "Modeling of Inhomogeneously Premixed Combustion with an Extended TFC Model", ASME J. Eng. Gas Turbines Power, 124(1):58-65, 2002.
- 47) Domingo, P., Vervisch, L., and Bray, K.N.C., "Partially Premixed Flamelets in LES of Nonpremixed Turbulent Combustion," Combust. Theory Model. 6(4):529-551, 2002, doi:10.1088/1364-7830/6/4/301.
- 48) Nogenmyr, K.J., Petersson, P., Bai, X.S., Nauert, A., Olofsson, J., Brackman, C., Seyfried, H., Zetterberg, J., Li, Z.S., Richter, M., Dreizler A., Linne, M., and Aldén, M., "Large Eddy Simulation and Experiments of Stratified Lean Premixed Methane/Air Turbulent Flames," Proc. Combust. Inst. 31(1):1467-1475, 2007, doi:10.1016/j.proci.2006.08.038.
- 49) Nogenmyr, K.J., Fureby, C., Bai, X.S., Petersson, P., Collin, R., and Linne, M., "Large Eddy Simulation and Laser Diagnostic Studies on a Low Swirl Stratified Premixed Flame," Combust. Flame. 155(1):357-368, 2008, doi:10.1016/j.combustflame.2008.06.014.
- 50) Li, B., Baudoin, E., Yu, R., Sun, Z.W., Li, Z.S., Bai, X.S., Aldén, M., and Mansour, M.S., "Experimental and Numerical Study of a Conical Turbulent Partially Premixed Flame," Proc. Combust. Inst. 32(2):1811-1818, 2009, doi:10.1016/j.proci.2008.06.088.

- 51) Nogenmyr, K.J., Kiefer, J., Li, Z.S., Bai, X.S., and Aldén, M., "Numerical Computations and Optical Diagnostics of Unsteady Partially Premixed Methane/Air Flames," *Combust. Flame*. 157(5):915-924, 2010, doi:10.1016/j.combustflame.2009.11.012.
- 52) Ma, F., Wang, Y., Liu, H., Li, Y. et. al., "Effects of Hydrogen Addition on Cycle-By-Cycle Variations in a Lean Burn Natural Gas Spark-Ignition Engine," *International Journal of Hydrogen Energy*, 33, 823-831, 2008.
- 53) Williams, F.A., *Turbulent combustion*. In: Buckmaster J.D. (Ed.) *The Mathematics of Combustion*, SIAM, Philadelphia, pp. 97-128, 1985.
- 54) Huang, C., Yasari, E., and Lipatnikov, A., "A Numerical Study on Stratified Turbulent Combustion in a Direct-Injection Spark-Ignition Gasoline Engine Using an Open-Source Code," *SAE Technical Paper* 2014-01-1126, 2014, doi:10.4271/2014-01-1126.
- 55) Huang, C., Hung, D., Zhong, J., "Experimental Analysis of the Start of Fuel Cycle-to-Cycle Variations of Solenoid-Actuated High Pressure Injectors," *SAE Technical Paper* 2011-01-1882, 2011, doi: 10.4271/2011-01-1882
- 56) Ogink, R. and Golovitchev, V., "Gasoline HCCI Modeling: An Engine Cycle Simulation Code with a Multi-Zone Combustion Model," *SAE Technical Paper* 2002-01-1745, 2002, doi:10.4271/2002-01-1745.
- 57) 23. Huang, C., Golovitchev, V., and Lipatnikov, A., "Chemical Model of Gasoline-Ethanol Blends for Internal Combustion Engine Applications," *SAE Technical Paper* 2010-01-0543, 2010, doi:10.4271/2010-01-0543.
- 58) Huang, C. and Lipatnikov, A., "Modelling of Gasoline and Ethanol Hollow-Cone Sprays Using OpenFOAM," *SAE Technical Paper* 2011-01-1896, 2011, doi:10.4271/2011-01-1896.
- 59) Hemdal, S., Denbratt, I., Dahlander, P., and Warnberg, J., "Stratified Cold Start Sprays of Gasoline-Ethanol Blends," *SAE Int. J. Fuels Lubr.* 2(1):683-696, 2009, doi:10.4271/2009-01-1496.

- 60) Lipatnikov, A., "Fundamentals of Premixed Turbulent Combustion," CRC Press, New York, ISBN 9781466510241, 2012.
- 61) 27. Lipatnikov, A.N., and Chomiak, J., "Turbulent Flame Speed and Thickness: Phenomenology, Evaluation, and Application in Multi-Dimensional Simulations," Prog. Energy Combust. Sci., 28(1):1-73, 2002, doi:10.1016/S0360-1285(01)00007-7.
- 62) Bray K.N.C., and Moss, J.B., "A Unified Statistical Model of the Premixed Turbulent Flame," Acta Astronautica 4:291-319, 1977.
- 63) Wang, Z., Liu, H., Song, T., Xu, Y. and Wang, J-X., "Investigation on Pre-ignition and Super-Knock in Highly Boosted Gasoline Direct Injection Engines" SAE Technical Paper 2014-01-1212.
- 64) Zahdeh, A., Rothenberger, P., Nguyen, W., Anbarasu, M., Soldan, S-S., Schaefer, J. and Goebel, T. "Fundamental Approach to Investigate Pre-Ignition in Boosted SI Engines" SAE Technical Paper 2011-01-0340.
- 65) Attard, W.P., Toulson, E., Watson, H. and Hamori, F. "Abnormal Combustion including Mega Knock in a 60% Downsized Highly Turbocharged PFI Engine" SAE Technical Paper 2010-01-1456.
- 66) Okada, Y., Miyashita, S., Izumi, I. and Hayakawa, Y. "Study of Low-Speed Pre-Ignition in Boosted Spark Ignition Engine" SAE Technical Paper 2014-01-1218, SAE Int. J. Engines 7(2):2014, doi:10.4271/2014-01-1218.
- 67) Dahnz, C., Han, K-M., Spicher, U., Magar, M., Schiebl, R., und Maas, U. "Investigations on Pre-Ignition in Highly Supercharged SI Engines" SAE Technical Paper 2010-01-0355.
- 68) Haenel, P., Seyfried, P., Kleeberg, H. and Tomazic, D. "Systematic Approach to Analyze and Characterize Pre-ignition Events in Turbocharged Direct-injected Gasoline Engines" SAE Technical Paper 2011-01-0343, 2011, doi:10.4271/2011-01-0343.

- 69) Zaccardi, J-M., Duval, L. and Pagot, A. "Development of Specific Tools for Analysis and Quantification of Pre-ignition in a Boosted SI Engine" SAE Int. J. Engines 2(1):1587-1600, 2009, doi:10.4271/2009-01-1795..
- 70) Liwei Han, Tao Zhu, Haibo Qiao, Desheng Zhang, Dingyuan Fu, and Jing Zhang "Investigation of Low-Speed Pre-Ignition in Boosted Spark Ignition Engine" SAE Technical Paper 2015-01-0751, 2015, doi:10.4271/2015-01-0751.
- 71) Zhi Wang, Yunliang Qi, Hui Liu, Yan Long, and Jian-Xin Wang "Experimental Study on Pre-Ignition and Super-Knock in Gasoline Engine Combustion with Carbon Particle at Elevated Temperatures and Pressures" SAE Technical Paper 2015-01-0752, 2015, doi:10.4271/2015-01-0752.
- 72) Max Magar, Ulrich Spicher, Stefan Palaveev. "Experimental Studies on the Occurrence of Low-Speed Pre-Ignition inTurbocharged GDI Engines". SAE Int. J. Engines 8(2):2015, doi:10.4271/2015-01-0753.
- 73) Xuwei Luo, Ho Teng, Tingjun Hu, Ruigang Miao, and Liming Cao. "An Experimental Investigation on Low Speed Pre-Ignition in a Highly Boosted Gasoline Direct Injection Engine". SAE Int. J. Engines 8(2):2015, doi:10.4271/2015-01-0758.
- 74) Attard, W.P., Toulson, E., Watson, H. and Hamori, F. "Abnormal Combustion including Mega Knock in a 60% Downsized Highly Turbocharged PFI Engine" SAE Technical Paper 2010-01-1456.
- 75) Welling, Maurya, R.K. and Agarwal, A.K., "Experimental Investigation of Cycle-by-Cycle Variations in CAI/HCCI Combustion of Gasoline and Methanol Fuelled Engine," SAE Technical Paper 2009-01-1345, 2009, doi: 10.4271/2009-01-1345.
- 76) Dingle, S-F., Cairns, A., Zhao, H., Williams, J., Williams, O. and Ali, R. "Lubricant Induced Pre-Ignition in an Optical SI Engine" SAE Technical Paper 2014-01-1222.
- 77) Qi, Y., Xu, Y., Wang, Z. and Wang, X. "The Effect of Oil Intrusion on Super Knock in Gasoline Engine" SAE Technical Paper 2014-01-1224.



- 78) Sasaki, N., Nakata, K., Kawatake, K., Sagawa, S., Watanabe, M. and Sone, T. "The Effect of Fuel Compounds on Pre-ignition under High Temperature and High Pressure Condition" SAE Technical Paper 2011-01-1984.
- 79) Yang, Y., Dec,J., Dronniou, N., Sjoberg, M. and Cannella, W. "Partial Fuel Stratification to Control HCCI Heat Release Rates : Fuel Composition and Other Factors Affecting Pre-Ignition Reactions of Two-Stage Ignition Fuels" SAE Technical Paper 2011-01-1359.
- 80) Chapman, E., Davis, R., Studzinski, W. and Geng, P. "Fuel Octane and Volatility Effects on the Stochastic Pre-Ignition Behavior of a 2.0L Gasoline Turbocharged DI Engine" SAE Technical Paper 2014-01-1226, SAE Int. J. Fuels Lubr. 7(2):2014, doi:10.4271/2014-01-1226.
- 81) Amann, M., Mehta, D. and Alger, T. "Engine Operating Condition and Gasoline Fuel Composition Effects on Low-Speed Pre-Ignition in High-Performance Spark Ignited Gasoline Engines" SAE Technical Paper 2011-01-0342.
- 82) Hamilton, L.J., Rostedt, M.J., Caton, P.J. and Cowart, J.S. "Pre-Ignition Characteristics of Ethanol and E85 in a Spark Ignition Engine" SAE Int. J. Fuels Lubr. 1(1):145-154, 2009, doi:10.4271/2008-01-0321.
- 83) Amann, M., Alger, T., Westmoreland, B. and Rothmaier, A. "The Effects of Piston Crevices and Injection Strategy on Low-Speed Pre-Ignition in Boosted SI Engines" SAE Int. J. Engines 5(3):1216-1228, 2012, doi:10.4271/2012-01-1148.
- 84) Amann, M., Mehta, =====D. and Alger, T. "The Effect of EGR on Low-Speed Pre-Ignition in Boosted SI Engines" SAE Technical Paper 2011-01-0339.
- 85) Schwarz, C., Schünemann, E., Durst, B., Fischer, J. et al., "Potentials of the Spray-Guided BMW DI Combustion System," SAE Technical Paper 2006-01-1265, 2006, doi:10.4271/2006-01-1265.
- 86) Baritaud, T.A., Duglos, J.M. and Fusco, A., "Modeling Turbulent Combustion and Pollutant Formation in Stratified Charge SI Engines," Symposium (International) on Combustion, 26(2): 2627-2635, 1996, doi:10.1016/S0082-0784(96)80097-X.

- 87) Jasak, H., Weller, H., and Nordin, N., "In-Cylinder CFD Simulation Using a C++ Object-Oriented Toolkit," SAE Technical Paper 2004-01-0110, 2004, doi:10.4271/2004-01-0110.
- 88) Bradley, D., Gaskell, P.H., and Lau, A.K.C., "A Mixedness-Reactedness Flamelet Model for Turbulent Diffusion Flames," *Proc. Combust. Inst.* 23(1):685-692, 1990, doi:10.1016/S0082-0784(06)80317-6.
- 89) Bradley, D., Gaskell, P.H., and Gu, X.J., "The Mathematical Modeling of Liftoff and Blowoff of Turbulent Non-Premixed Methane Jet Flames at High Strain Rates," *Proc. Combust. Inst.* 27(1):1199-1206, 1998, doi:10.1016/S0082-0784(98)80523-7.
- 90) Müller, C.M., Morey, F., Seers, P., "Comparison of Cycle-by-Cycle Variation of Measured Exhaust-Gas Temperature and In-Cylinder Pressure Measurements," *Applied Thermal Engineering*, 30, 487-491, 2010.
- 91) Chen, M., Herrmann, M., and Peters, N., "Flamelet Modeling of Lifted Turbulent Methane/Air and Propane/Air Jet Diffusion Flames," *Proc. Combust. Inst.* 28(1):167-174, 2000, doi:10.1016/S0082-0784(00)80208-8.
- 92) Bigot, P., Champion, M., and Garréton-Bruguieres, D., "Modeling a Turbulent Reactive Flow with Variable Equivalence Ratio: Application to a Flame Stabilized by a Two-Dimensional Sudden Expansion," *Combust. Sci. and Tech.* 158:299-320, 2000.
- 93) Wallesten, J., Lipatnikov, A.N., Chomiak, J., "Modeling of Stratified Combustion in a DI SI Engine Using Detailed Chemistry Pre-Processing," *Proc. Combust. Inst.* 29(1):703-709, 2002, doi:10.1016/S1540-7489(02)80090-6.
- 94) Radwan, M., Helali, A., Elfeky, S., and Attai, Y., "An Investigation on Knock and Pre-ignition with Tumble Induced Turbulence," SAE Technical Paper 2007-01-3557, 2007, doi:10.4271/2007-01-3557.
- 95) Zhu, G., Hung, D., and Winkelman, J., "Combustion Characteristics Detection for Low Pressure Direct Injection Engines Using Ionization Signal," SAE Technical Paper 2006-01-3317, 2006, doi:10.4271/2006-01-3317.

- 96) Wallesten, J., Lipatnikov, A.N., Chomiak, J., "Modeling of Stratified Combustion in a DI SI Engine Using Detailed Chemistry Pre-Processing," Proc. Combust. Inst. 29(1):703-709, 2002, doi:10.1016/S1540-7489(02)80090-6.
- 97) Johansson, B., "Cycle to Cycle Variations in S.I. Engines - The Effects of Fluid Flow and Gas Composition in the Vicinity of the Spark Plug on Early Combustion," SAE Technical Paper 962084, 1996, doi:10.4271/962084.
- 98) Jinhua Wang, Hao Chen, Bing Liu, Zuohua Huang, "Study of cycle-by-cycle variations of a spark ignition engine fueled with natural gas–hydrogen blends". International journal of hydrogen energy 33 ( 2 0 0 8 ) 4 8 7 6 – 4 8 8 3.
- 99) Changming Gong , Kuo Huang, Yulin Chen, Jinglong Jia, Yan Su, Xunjun Liu. "Cycle-by-cycle combustion variation in a DISI engine fueled with methanol". Fuel 90 (2011) 2817–2819.
- 100) Mekhael, S., Estefanous, F., Henein, N., and Zahdeh, A., "A New Technique to Determine the Burning Velocity in a Gasoline Direct Injection Engine," SAE Int. J. Engines 7(1):339-350, 2014.
- 101) Huang, B., Hu, E., Huang, Z., Zheng, J. et. al., "Cycle-by-Cycle Variations in a Spark Ignition Engine Fueled with Natural Gas–Hydrogen Blends Combined with EGR," International Journal of Hydrogen Energy, 34, 8405-8414, 2009.

**ABSTRACT****COMBUSTION, IONIZATION AND SPORADIC PRE-IGNITION IN A TURBOCHARGED  
GASOLINE DIRECT INJECTION ENGINE**

by

**SHENOUDA MEKHAEL****May 2016****Advisor:** Dr. Naeim A. Henein**Major:** Mechanical Engineering**Degree:** Doctor of Philosophy

This research is focused on the use of ionization of combustion products in hydrocarbons-air flames to gain a better understanding of the combustion process in turbocharged gasoline direct injection engines. A GM 2.0 L Ecotec GDI-T engine is used in this investigation. The ion current is measured simultaneously by two in-cylinder combustion sensors: the spark plug and the fuel injector. The characteristics of the ion current signals produced by the two sensors are analyzed and correlated with the characteristics of the rate of heat release computed from the cylinder gas pressure. Since this is the first time for a fuel injector to be used as an ion current sensor, it was possible to determine many features of combustion in the engine which could not be determined from the spark plug signal. For example, the phase shift between the two ion current signals was used to determine the burning velocity. The results are compared with the burning velocity measured in optically accessible port injected engine in which high speed imaging techniques were used. In addition, it was possible to investigate the impact of the burning velocity on the indicated thermal efficiency and indicated mean effective pressure at different speeds and loads. Also, this research included the use of the two ion current signals for the feedback closed loop control of the engine. The engine was able to consistently operate on MBT (Maximum Brake Torque) point by adjusting the ignition and injection timings. In addition, engine knock was detected and controlled by retarding the ignition timing using the ion current signals. The findings from the

experimental investigations are supported by a 3D gasoline cycle simulation of combustion and the ion current produced at the locations of the spark plug and the injector.

The research include a detailed analysis of the factors that contribute to combustion instability and cycle-to-cycle variations. Finally, combustion ionization used to investigate the low speed sporadic pre-ignition phenomenon (LSPI) which is currently limiting the progress toward higher power density and more efficient turbocharged gasoline engines. The ionization technique used in this investigation detected the sporadic pre-ignition.

## **AUTOBIOGRAPHICAL STATEMENT**

SHENOUDA MEKHAEL

### **EDUCATION**

- 2016 PhD, Wayne State University, Detroit, Michigan, USA
- 2010 Ms.c, Cairo University, Cairo, Egypt
- 2006 Bs.c, Cairo University, Cairo Egypt

### **PROFESSIONAL APPOINTMENTS**

- 2016 Product Development Engineer, Ford Motor Company, Dearborn, Michigan, USA
- 2016 Part-Time Faculty, Wayne State University, Michigan, USA
- 2016 Part-Time Faculty, Lawrence Technological University, Southfield, USA
- 2015 Part-Time instructor, Wayne State University, Michigan, USA
- 2014 Part-Time instructor, Wayne State University, Michigan, USA
- 2012 Graduate Research Assistant, Wayne State University, Michigan, USA
- 2010 Project Coordinator, Orascom, Cairo, Egypt
- 2007 Construction Engineer, CCC, Cairo, Egypt
- 2006 Graduate Teaching and Research Assistant, Cairo University, Cairo, Egypt

### **PROFESSIONAL ASSOCIATIONS**

- 2015 National Engineering Honor Society [TAU BETA PI] Feb 2015 – Present.
- 2010 Society of Automotive Engineers [SAE] July 2010 – Present.
- 2007 American Society for Mechanical Engineering [ASME] July 2007 – Present.

### **AWARDS & COMMITTEE APPOINTMENTS**

- 2012 PhD scholarship, Wayne State University, Detroit, Michigan, USA
- 2006 Ms.c scholarship, Cairo University, Cairo, Egypt

### **PUBLICATIONS &**

- Mekhael, S., Estefanous, F., Henein, N., and Zahdeh, A., "A New Technique to Determine the Burning Velocity in a Gasoline Direct Injection Engine," SAE Int. J. Engines 7(1):339-350, 2014.
- Estefanous, F., Mekhael, S., Henein, N., and Zahdeh, A., "Multi Sensing Fuel Injector in Turbocharged Gasoline Direct Injection Engines," ASME 2013, Paper No. ICEF2013-19091, pp. V001T05A004; doi:10.1115/ICEF2013-19091

### **PATENTS**

- PCT/US2014/023245-61/776,421 "Predictive Correction In Internal combustion Engine".
- Closed loop control using ionization, patent pending.

### **PRESENTATIONS**

- SAE worl congress 2014, "A New Technique to Determine the Burning Velocity in a Gasoline Direct Injection Engine,"